N71-27871

NASA SP-232

CASE FILE COPY

ANALYSIS OF

APOLLO 10

PHOTOGRAPHY AND VISUAL OBSERVATIONS

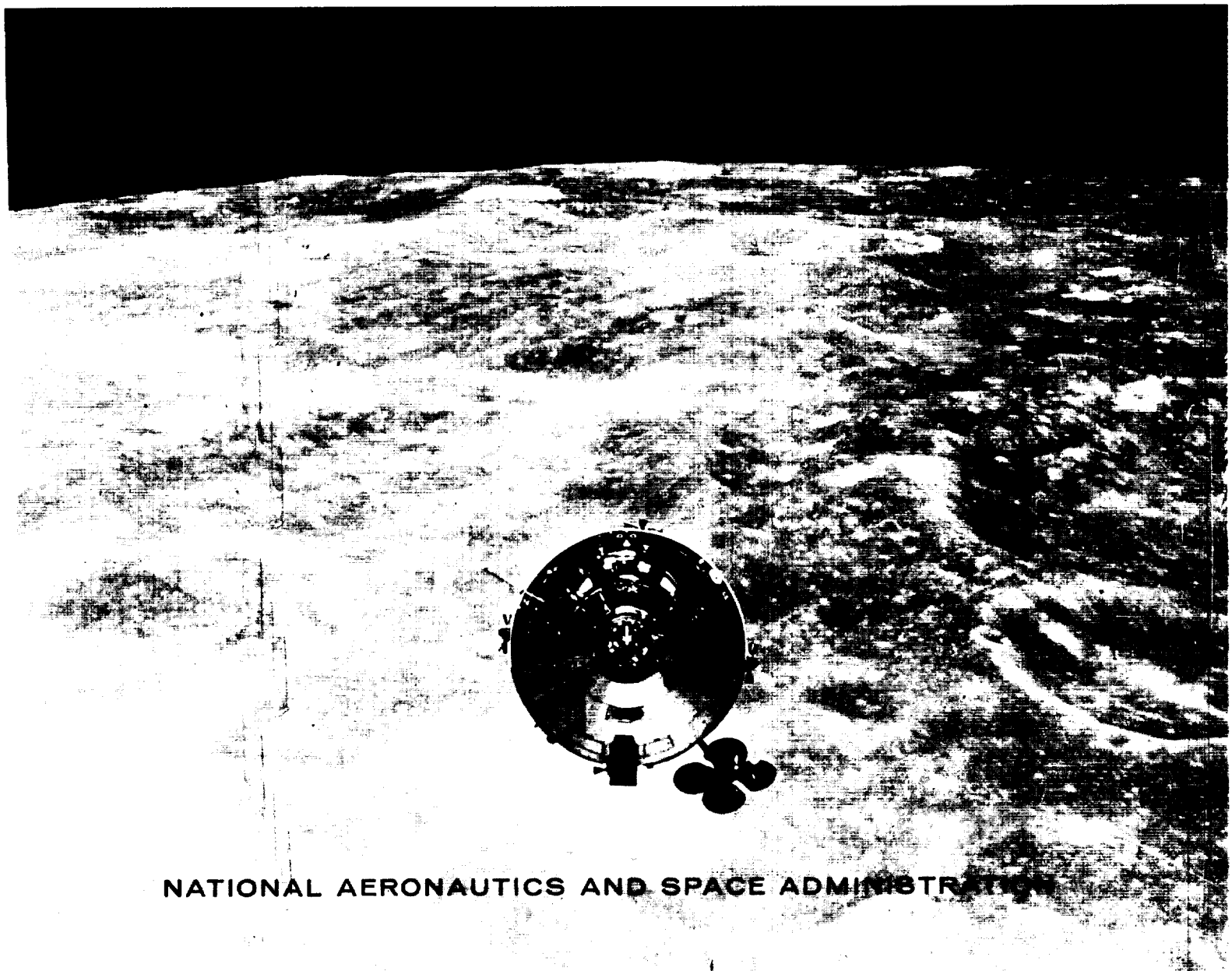

NATIONAL AERONAUTICS AND SPACE ADMINISTRATION

NASA SP-232

ANALYSIS OF APOLLO 10 PHOTOGRAPHY AND VISUAL OBSERVATIONS

COMPILED BY

NASA MANNED SPACECRAFT CENTER

Scientific and Technical Information Office 1971

NATIONAL AERONAUTICS AND SPACE ADMINISTRATION

Washington, D.C.

For sale by the Superintendent of Documents,
U.S. Government Printing Office, Washington, D.C. 20402
Price $4.25
Library of Congress Catalog Card Number 72-606239

Foreword

The Apollo 10 mission was a vital step toward the national goal of landing men on the Moon and returning them safely to Earth. This mission used the first complete Apollo spacecraft flown in lunar orbit and took men closer to the Moon than ever before. The mission clearly demonstrated that the Nation was ready to embark with the Apollo 11 crew on the voyage that has been the dream of men for thousands of years.

Each Apollo lunar mission acquires photographs of areas on the Moon never before seen in such great detail. This report provides only a small sample of the types of analysis that can be performed with this photography. Even more important, however, this report provides scientists throughout the world with a knowledge of what new lunar photography is available and how the photograph can be obtained. It is hoped that more extensive analysis of this photography will continue, and it is certain that the photographs will be used for many decades.

RICHARD J. ALLENBY
Office of Manned Space Flight

Contents

Introduction

JAMES H. SASSER

The Apollo 10 spacecraft was launched from Cape Kennedy at 12:49 p.m., e.d.t., on May 18, 1969. After the spacecraft completed 1½ revolutions of the Earth, the S-IVB was reignited to increase the speed of the spacecraft to the velocity required to escape the gravitational attraction of the Earth. Three days later, the spacecraft was placed in a 60- by 170-n.-mi. orbit around the Moon. After the spacecraft completed two revolutions of the Moon, the orbit was circularized to 60 n. mi. by a second burn of the service propulsion system.

On the fifth day of the mission, Astronauts Thomas P. Stafford and Eugene A. Cernan descended in the lunar module to an altitude of less than 47 000 ft above the Moon. At this altitude, two passes were made over the Apollo 11 landing site. The ascent and descent stages of the lunar module separated, and the astronauts in the ascent stage then completed a successful rendezvous with Astronaut John W. Young in the command module. On May 24, the service propulsion system was reignited, and the astronauts began the return journey to Earth. Splashdown occurred at 12:52 p.m. on May 26, 1969, less than 4 miles from the target point and the recovery ship.

During the mission, the astronauts obtained hundreds of still photographs and exposed many reels of motion-picture film. This photography contains much new information on those areas of the Moon that were passed over during the mission. Although some pictures were of areas that had been photographed by the Lunar Orbiter spacecraft, nearly every one that was studied revealed new detail.

This report has been limited to analyses and observations not discussed previously in NASA SP–201, "Analysis of Apollo 8 Photography and Visual Observations." The interested reader is referred to that publication for additional details on the camera and film characteristics, because the same type of equipment was used for photography in both the Apollo 8 and 10 missions. During the time that this report was in preparation, many of the participating scientists and photographic analysts were involved in planning the photographic activities for the Apollo 11 mission. This fact contributed to the brevity of this report.

1

Visual Observations

THOMAS P. STAFFORD, EUGENE A. CERNAN, AND JOHN W. YOUNG

INTRODUCTION

The flight of Apollo 10 permitted man to observe directly features on the lunar surface from an altitude of 50 000 ft, an altitude within the range of high-performance aircraft on Earth. Much of the groundtrack of Apollo 10 covered unknown parts of the Moon with observations and photographs from orbital altitudes of 60 n. mi. The color television camera permitted us to share many of the front-side observations with people on Earth.

The spacecraft remained in the vicinity of the Moon much longer than did the Apollo 8 spacecraft. This allowed more time for observations and extended coverage of a previously unphotographed segment of the Moon as the sunrise terminator moved from the vicinity of Apollo landing site 2 to the vicinity of Apollo landing site 3.

We had the advantage of the observations from the Apollo 8 crewmembers to guide the emphasis in the later phases of our training. In some areas, better Apollo 8 photographs replaced existing Lunar Orbiter coverage for preflight training and onboard charts.

COLOR

The crewmembers of Apollo 8 reported regional variations in shades of gray, with possible faint brownish hues. Our observations indicate definite brown tones on the gray lunar-surface features, except near the sunrise and sunset terminators. At such low Sun angles, the surface features were visible as variations in shades of gray.

With color television, we were able to share some of these observations in real time. At altitudes ranging from 50 000 ft to 3000 miles, the mare surface was generally brown, highland areas were tan, and the bright halos and rays around some craters were a chalky white, like gypsum.

After transearth insertion, the lunar-surface colors could be contrasted with the pitch black of space to give a color comparison. A highly significant color variation within the Sea of Serenity was described from high altitude as the area became visible. The color around the southern margin of the sea was like the mare materials observed in the equatorial seas, but the central part of the sea was a lighter shade of brown.

SURFACE TEXTURES

The variety of surface features on the Moon is amazing. Even in areas that are generally similar, differences that appear to be significant exist in the details.

Mare Areas

While Apollo 10 orbited the Moon, the near-side terminator swept from a position

in the Sea of Tranquility to a position west of the Central Bay. Long shadows near the terminator accentuate the gentle changes in slope within the mare areas; otherwise, the mare surfaces appear much like the moderate-Sun-angle Lunar Orbiter pictures of this area. When we were looking away from the Sun, numerous small, bright-halo craters could be seen near the zero-phase point. The distribution of such craters over the mare surface can be seen only at high-Sun angles. On this mission, the zero-phase point was within Smyth's Sea during the latter revolutions, so that Smyth's Sea and the eastern part of the Sea of Fertility were lighted properly for observing the bright-halo craters. During the Apollo 8 mission, near-vertical illumination occurred only in the highlands and far-side basins.

The floor of the far-side crater Tsiolkovsky, one of the few areas of marelike materials on the far side of the Moon, was not visible while Apollo 10 was in lunar orbit. After transearth insertion, the crater came into view near the horizon. The marelike floor appeared black when contrasted with the tan highland materials.

Far-Side Basins

The groundtrack of Apollo 10 was generally north of the Apollo 8 groundtrack, from the far-side terminator to the eastern limb of the Moon. The terrain we observed beneath the spacecraft generally was visible on the earlier mission only in an oblique view, often near the horizon. The basin terrain was smooth in comparison to the surrounding highlands but rougher than the surface in the near-side mare areas. Moderate-scale features such as craters, depressions, domes, benches, and cones were more common in the far-side basins. With the exception of rare irregular areas of darker deposits, the far-side basins were the tan color of the highlands.

Highland Areas

Highland areas on both the front side and far side of the Moon were illuminated at a wide range of Sun angles during the Apollo 10 mission. The front-side terminator swept the region between the Sea of Tranquility and the Central Bay, and the far-side terminator crossed rugged highland terrain west of the far-side basin XV. Both areas viewed at comparable low-Sun angles were rough. However, sharper features were observed near the front-side terminator, and boulders were more abundant in the near-side highlands. The far-side highlands are characterized by features with rounded edges less sharp than the front-side features. In both areas there are some sharp-rimmed craters, and in areas of higher Sun angles, numerous bright-halo craters were visible.

Slopes

Considerable detail was visible on slopes, both in shadow and in different degrees of illumination. The steep crater walls exhibit the wide spectrum of albedo variation under high-Sun-angle illumination that was reported by the Apollo 8 crew. In the crater Schmidt, slump near the base of the crater wall looks like tailings in a mine. Larger craters are characterized by terraces that suggest slumping of large sections of the crater wall.

Ray Patterns

Two of the more distinctive surface markings we observed on the lunar surface were the light-colored halos and the ray patterns around the many sharp craters. Extensive ray patterns extend outward from large craters in the highlands. Small sharp craters, in both the highlands and mare areas, are characterized by the rays or halos. The two long narrow rays that extend westward from Messier A were observed on many revolutions and were photographed and shown on more than one television pass. Observations from orbital altitudes and from the low-altitude pass in the lunar module indicated that the rays have no thickness.

Small Bright-Halo Craters

The high concentration of craters smaller than 1 km in diameter, with rays and bright

halos visible near the subsolar point, far exceeds that expected from pre-Apollo studies of the Lunar Orbiter photographs. We extended the Apollo 8 observations on the farside highlands into Smyth's Sea and the Sea of Fertility. Most of the craters that appear sharp and fresh within the mare areas have bright halos; therefore, we are led to assume that most of the small sharp craters near the mare landing sites will exhibit the rays and bright halos.

Large Craters

We noted that the slumping around the margin of many large craters tends to sharpen the rim. Crater diameter also is increased materially by the slump blocks in a few craters. Therefore, we question whether crater sharpness can be used as a major indicator of crater age. This process may not be pronounced in the smaller craters, but we tended to use "young" to describe craters with bright halos or rays rather than craters that were sharp.

Volcanic Terrain

The highland area between landing sites 2 and 3 includes conspicuous features that we believe to be volcanic. The crater rims appear to form cones and to be more pronounced than in other highland areas. One crater on the far side, if it were in a different setting, could be called Mount Fujiyama.

Sinuous Rilles

Sidewinder and Diamondback, two segments of a sinuous rille that crosses the approach to landing site 2, were observed from orbital altitude and from approximately 50 000 ft. We observed no deposits on the mare surface along the margin of the rille. At the low-angle illumination available during the early part of the mission, such deposits should have been visible if present. The intersection of the rille wall and mare surface appears to be rounded, and the rille floor is extremely smooth. This feature closely resembles a dry stream or arroyo like those in Arizona or New Mexico.

GENERAL LUNAR VISIBILITY

Sunshine

The observation of gentle slopes and small hills was best within a few degrees of the terminator where the long shadows accentuated the features as our training had indicated. Within the shadows, particularly in craters but also behind hills, our eyes were able to pick out details that the camera does not record. The same is true on brightly lighted crater walls where the film image is normally overexposed. In areas illuminated by a high-Sun angle, the absence of shadows made topographic features less pronounced and increased the importance of changes in albedo. From orbital altitudes, we were able to see features within a few degrees of the zero-phase point. During the lunar module approach to landing site 2, the area of washout was noticeably broader.

Earthshine

On several revolutions, we were able to observe the lunar surface lighted by earthshine. The surface appeared black until spacecraft sunset. However, after a few moments of eye adaptation, the surface appeared to be a bluish white, and peaks on the lunar horizon were clearly visible. We experienced no difficulty in recognizing major features and were able to observe a surprising amount of textural detail within the larger craters. Rays and halos were clearly visible. There is a definite earthshine terminator. As we approached this terminator, the shadows lengthened, and low slopes were accentuated just as along the sunshine terminator. Beyond the earthshine terminator, the lunar surface was black. No features could be detected by starshine, but the horizon could be seen easily as a curved line dividing the star-studded sky and absolute blackness.

ASTRONOMICAL OBSERVATIONS

Solar Corona

The solar corona was observed near the

sunrise and sunset terminators on revolutions when the spacecraft was oriented properly. Eye adaptation restricted the viewing immediately following spacecraft sunset; otherwise, the observations were symmetrical. The corona had visible ray structures during the 4- to 6-min period before sunrise or after sunset.

Dim-Light Phenomena

No specific dim-light phenomena were observed.

2

Initial Photographic Analyses

GEOLOGY

PRELIMINARY QUANTITATIVE TERRAIN-ANALYSIS RESULTS FROM THREE APOLLO 10 PHOTOGRAPHS

RICHARD J. PIKE

The elevation data from which the following results have been obtained were derived from three stereophotogrammetric models by Sherman S. C. Wu, G. Nakata, F. J. Schafer, and R. Jordan. The Fortran IV computer programs used to process the data were written by W. J. Rozema, R. H. Godson, D. K. McMacken, and G. I. Selner. The types of topography and the three profiles for which elevation data were recorded are shown in figures 2–1 to 2–3. Each profile was subdivided by gross terrain type into three or four segments. The incremental horizontal separation ($\triangle L$) of the elevations is 85 m for segments 1 to 3, 44 m for segments 4 to 7, and 35 m for the remaining three segments. The $\triangle L$ was doubled for profiles 4 to 10 so that descriptive parameters might be comparable for all 10 segments.

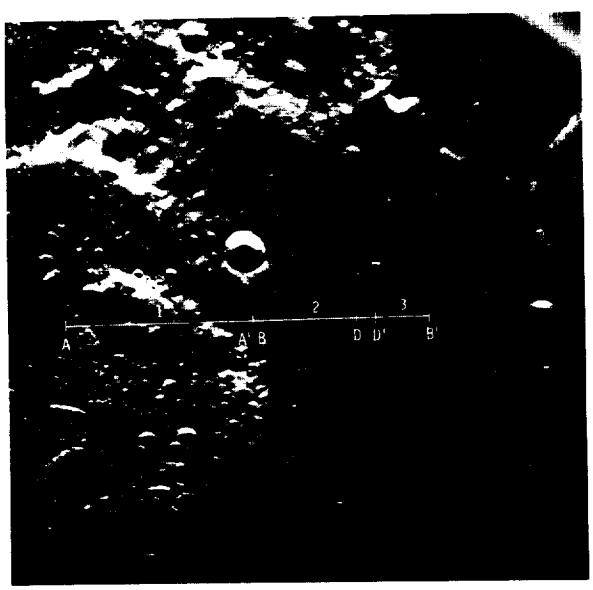

FIGURE 2–1.—Location of sample profile segments 1 to 3 and topographic profiles (fig. 2–5) A–A′; B–B′; and D–D′ across old upland crater Hypatia C (AS10–31–4541).

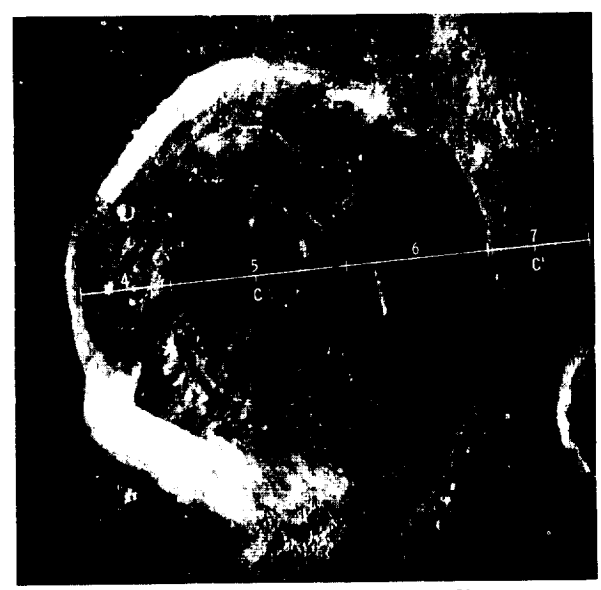

FIGURE 2–2.—Location of sample profile segments 4 to 7 and topographic profile C–C′ (fig. 2–5) across an unnamed crater 35 km in diameter, located approximately 133° E, 1° S in upland terrain (AS10–29–4199).

FIGURE 2–3.—Location of sample profile segments 8 to 10, located along same traverse as segment 4 (fig. 2–2) (AS10–28–4003).

Topographic descriptors are selected for specific purposes. These descriptors are intended to describe as completely as possible the surface roughness of the various lunar topographic units and to provide an effective quantitative discriminant among the entire spectrum of possible lunar topographic samples. Although the present emphasis is on terrain roughness, other parameters could have been added especially for topographic classification. The following terrain classification parameters were generated for the Apollo 10 topographic data:

1. Base-length slope angle:
   a. Mean (absolute value)
   b. Standard deviation (algebraic value)
   c. Maximum
2. Base-length slope curvature angle (fig. 2–4):
   a. Mean (absolute value)
   b. Standard deviation (algebraic value)
   c. Maximum
3. Total relief
4. Slope angle between slope reversals:
   a. Longest slope length
   b. Angle of longest slope
5. Number of slope reversals per kilometer of traverse

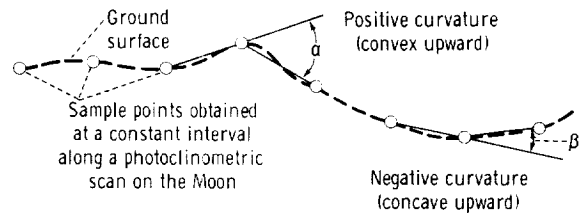

FIGURE 2–4.—Slope curvature shown diagramatically.

In addition, power spectral density (PSD) curves were computed for each of the three long profiles. The six base-length measures were generated for slopes and curvatures at a constant horizontal increment, whereas slopes measured between reversals of slope direction are variable in length. Slope-reversal frequency is a texture measure, and total relief is included for general descriptive purposes. The PSD, applicable both as a roughness parameter and as a topographic descriptor, is discussed at length by Rozema (ref. 2–1). McCauley (ref. 2–2), Rowan and McCauley (ref. 2–3), and Pike (ref. 2–4) further treat the selection of quantitative lunar terrain parameters.

The problems of apportioning the lunar surface into divisions of reasonably homogeneous topography or terrain regions are discussed in references 2–2, 2–3, and 2–4. The extent to which terrain can be subdivided by quantitative techniques depends directly upon the quantity of available topographic data. Table 2–I presents the four-part classification to which lunar terrain regionalization previously has been restricted, because of the scarcity of data, at all levels of generalization ($\triangle L$). A six-part classification, an interim objective that is being realized as increasing quantities of data have become available, would include large craters and smooth uplands. Most previous topographic data have been derived from the photoclinometric reduction of high-resolution Lunar Orbiter imagery (ref. 2–5). Because this technique is limited to smooth predominantly mare areas, few data have been generated for the rougher upland terrains or for large fresh craters. The Apollo 10 data chosen for this brief study have partially remedied this

TABLE 2–I.—*Classifications of Lunar Terrain*

Mare		Upland	
Smoother mare	Rougher mare	Hummocky upland	Rough upland
Many eastern sites Dark mare material Older subdued craters Low crater densities Craters with few blocks	Many western sites Rille, dome, and ridge areas Fresh craters High crater densities Blocky craters Secondary swarms, especially on rays Large crater rims	Older basin rim material (Fra Mauro Fm.) Older large craters Blanketed craters Older subdued crater terrain Outer rim slopes of large craters Crater floors and basin fill	Younger basin rim material (Orientale) Younger large craters Scarps Fresh crater terrain Inner rim slopes of large craters Trenches and rifts

deficiency. In the area studied, the following terrain units are included (listed in the approximate order of increasing roughness):

1. Mare—smoother segment (without rilles)
2. Mare—rougher segment (contains rilles)
3. Old upland crater and old hummocky upland surface
4. Large (351 m in diameter) fresh upland crater
5. Fresh upland crater—smoother floor
6. Fresh upland crater—outer rim slope
7. Fresh upland crater—inner rim slope
8. Fresh upland crater—rougher floor

The results are presented in tables 2–II to 2–IV and in figures 2–5 to 2–10. The four 1:1 profiles in figure 2–5 are examples of the six major terrain units for which elevations were recorded. The lettered cross sections are located on figures 2–1 and 2–2. The south wall of the Hypatia I rille is presented at a much larger scale than the other profiles. Visual inspection of the profiles in figure 2–5 anticipates some of the quantitative results summarized in table 2–II, in which the composite terrain samples are ranked in increasing order of roughness by mean absolute value of base-length slope angle. The order of the 11 terrain types is not surprising, with the exception of the exceedingly rough crater-floor unit. Inspection of the photograph (fig. 2–2) and the profile *C–C′* (fig. 2–5) does show that this particular floor is one of the roughest observed in any large fresh lunar crater. The terrain sample, "fresh upland crater," was derived by averaging the descriptive statistics of the component terrain types, including outer rim slope, inner rim slope, and rough crater floor (profile segments 4 to 7, fig. 2–2).

The data in table 2–II demonstrate the extremely rugged character of the lunar uplands (particularly of large fresh craters) when compared with the maria. At a base length of approximately 80 m, mean slope values of the roughest lunar terrains measured from Apollo 10 photographs approach mean slope values of some of the roughest terrestrial terrains measured on 1:24 000 topographic maps. Maximum slope values in the lunar uplands are sufficiently high to necessitate careful routing of all projected surface-exploration missions. Mean and maximum lunar upland slope values obtained from Apollo 8 photography and similar data for individual lunar and terrestrial craters obtained from various sources are presented in table 2–III. A study of the varying base lengths indicates that none of the slope values are inconsistent with the Apollo 10 information. Some of the lower mean slope values at a $\triangle L$ between 0.6 and 1.0 km also agree substantially with data obtained for the rough uplands by Rowan and McCauley (ref. 2–3) from terrestrially based photoclinometric data. All data in table 2–II were generated for several multiples of the initial $\triangle L$ but have been omitted for brevity. The variation of mean base-length slope and curvature

TABLE 2–III.—*Slope Means and Maxima for Lunar Uplands and Large Fresh Craters (From Previous Sources)*

Terrain type	ΔL, m	Mean slope, deg	Maximum slope, deg
Undifferentiated upland terrain, Apollo 8 data	70	15 to 20	42 to 55
	210	8 to 10	28 to 35
	350	6 to 8	19 to 31
	1050	4 to 7	13 to 17
	3500	3 to 4	7 to 15
Rim of Meteor Crater, Arizona	25	14 to 19	61
Meteor Crater, overall	61	12	52
Rim of Copernicus	600	11	39
Rim of Aristarchus	1000	7 to 10	38

TABLE 2–IV.—*Variation of Mean Slope Angle and Mean Curvature Angle With Increasing* ΔL *for 2 Lunar-Terrain Samples*

Multiple of basic ΔL	Mean (absolute value) of base-length slope angle, deg		Mean (absolute value) of base-length slope curvature angle, deg	
	Old upland crater	Fresh upland crater floor	Old upland crater	Fresh upland crater floor
1	12.2	27.2	10.7	22.9
2	10.7	24.2	9.0	26.1
4	9.3	20.7	7.6	28.2
8	8.3	16.9	6.4	29.9

trasting the three sample lunar areas photographed by Apollo 10 (figs. 2–1 to 2–3). At the ΔL at which the data are available, PSD curves do not supply an index of terrain microroughness directly applicable to vehicle design, but rather a general comparison of relative roughness and a description of topography as a time series. In this respect, the curves reveal significant differences among the three topographic samples. The PSD functions of two terrestrial topographic samples were available at the proper ΔL for

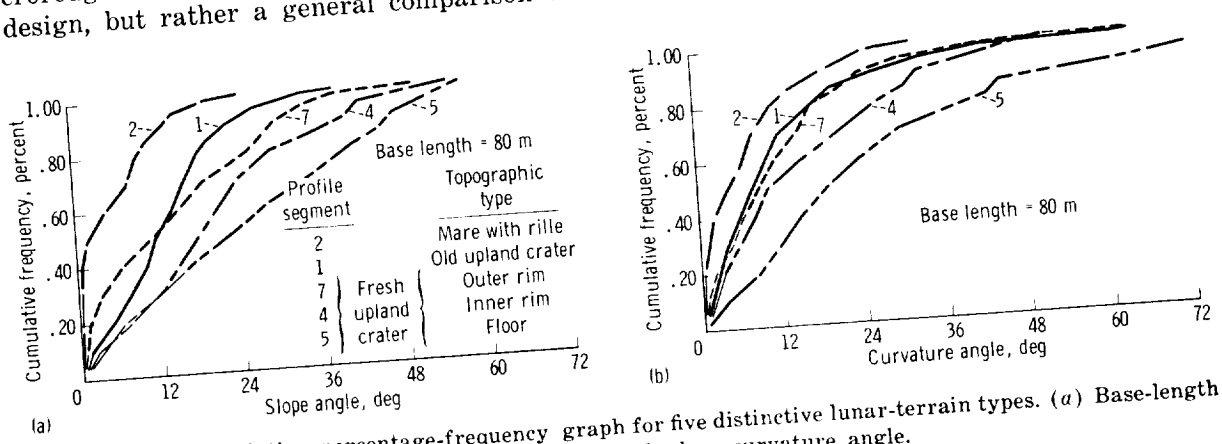

FIGURE 2–6.—Cumulative percentage-frequency graph for five distinctive lunar-terrain types. (*a*) Base-length slope angle. (*b*) Base-length slope curvature angle.

TABLE 2–I.—*Classifications of Lunar Terrain*

Mare		Upland	
Smoother mare	Rougher mare	Hummocky upland	Rough upland
Many eastern sites	Many western sites	Older basin rim material (Fra Mauro Fm.)	Younger basin rim material (Orientale)
Dark mare material	Rille, dome, and ridge areas	Older large craters	Younger large craters
Older subdued craters	Fresh craters	Blanketed craters	Scarps
Low crater densities	High crater densities	Older subdued crater terrain	Fresh crater terrain
Craters with few blocks	Blocky craters	Outer rim slopes of large craters	Inner rim slopes of large craters
	Secondary swarms, especially on rays	Crater floors and basin fill	Trenches and rifts
	Large crater rims		

deficiency. In the area studied, the following terrain units are included (listed in the approximate order of increasing roughness):

1. Mare—smoother segment (without rilles)
2. Mare—rougher segment (contains rilles)
3. Old upland crater and old hummocky upland surface
4. Large (351 m in diameter) fresh upland crater
5. Fresh upland crater—smoother floor
6. Fresh upland crater—outer rim slope
7. Fresh upland crater—inner rim slope
8. Fresh upland crater—rougher floor

The results are presented in tables 2–II to 2–IV and in figures 2–5 to 2–10. The four 1:1 profiles in figure 2–5 are examples of the six major terrain units for which elevations were recorded. The lettered cross sections are located on figures 2–1 and 2–2. The south wall of the Hypatia I rille is presented at a much larger scale than the other profiles. Visual inspection of the profiles in figure 2–5 anticipates some of the quantitative results summarized in table 2–II, in which the composite terrain samples are ranked in increasing order of roughness by mean absolute value of base-length slope angle. The order of the 11 terrain types is not surprising, with the exception of the exceedingly rough crater-floor unit. Inspection of the photograph (fig. 2–2) and the profile *C–C′* (fig. 2–5) does show that this particular floor is one of the roughest observed in any large fresh lunar crater. The terrain sample, "fresh upland crater," was derived by averaging the descriptive statistics of the component terrain types, including outer rim slope, inner rim slope, and rough crater floor (profile segments 4 to 7, fig. 2–2).

The data in table 2–II demonstrate the extremely rugged character of the lunar uplands (particularly of large fresh craters) when compared with the maria. At a base length of approximately 80 m, mean slope values of the roughest lunar terrains measured from Apollo 10 photographs approach mean slope values of some of the roughest terrestrial terrains measured on 1:24 000 topographic maps. Maximum slope values in the lunar uplands are sufficiently high to necessitate careful routing of all projected surface-exploration missions. Mean and maximum lunar upland slope values obtained from Apollo 8 photography and similar data for individual lunar and terrestrial craters obtained from various sources are presented in table 2–III. A study of the varying base lengths indicates that none of the slope values are inconsistent with the Apollo 10 information. Some of the lower mean slope values at a $\triangle L$ between 0.6 and 1.0 km also agree substantially with data obtained for the rough uplands by Rowan and McCauley (ref. 2–3) from terrestrially based photoclinometric data. All data in table 2–II were generated for several multiples of the initial $\triangle L$ but have been omitted for brevity. The variation of mean base-length slope and curvature

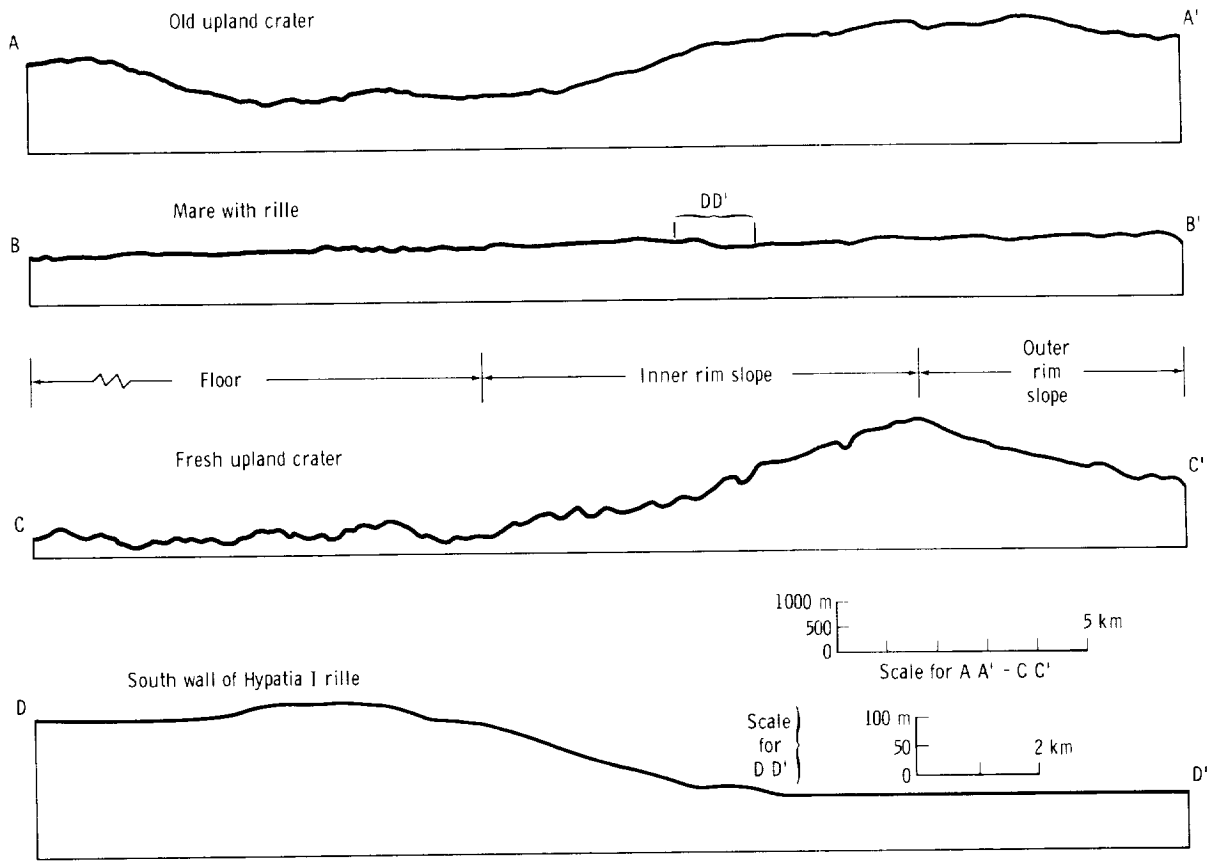

FIGURE 2–5.—Four topographic profiles showing variety of terrain for which mathematical descriptions were generated from stereophotogrammetric reduction of Apollo 10 photography.

for two different lunar upland terrains is shown in table 2–IV. A significant difference in the surface geometry of the two terrains is revealed by the increasing value of mean curvature with increasing $\triangle L$ for the rough floor of the fresh upland crater. The reverse is usually the rule. The cumulative percentage-frequency curves of base-length slope and curvature at a $\triangle L$ of 10 m for five of the terrain types listed in table 2–II are presented in figure 2–6.

Data on slopes measured not at a constant base length but between reversals in slope direction of the topographic profile are presented in figures 2–7 to 2–9. Data from profile segment 3 (fig. 2–1) are used in figure 2–7 to show how this type of information is presented most effectively. The plot of slope angle against slope length furnishes especially useful information for the engineering of lunar roving vehicles and for mission-planning purposes. The relationship between maximum slope length and frequency of slope-direction change is demonstrated in figure 2–8. Because the frequency of slope-direction change is more easily measured, the change can be used to predict the maximum slope length. A closer relationship between mean base-length slope and the angle of the longest slope measured between reversals is shown in figure 2–9. Useful but usually unavailable lunar vehicle design criteria can be predicted from two of the more common terrain classification parameters. Maximum length of slope between reversals and slope-direction changes frequently vary independently of all other roughness measures described in this report.

The five PSD functions in figure 2–10 provide a final means of comparing and con-

TABLE 2–II.—*10 Quantitative Descriptors for 11 Topographic Types Photographed by Apollo 10*

[ΔL = 80 m]

Profile segment	N[a]	Topographic unit	Base-length slope angle			Base-length slope curvature			Total relief, m	Slope between slope reversals		Slope reversal frequency, number per km
			Mean (absolute value), deg	Standard deviation (algebraic value), deg	Maximum, deg	Mean (absolute value), deg	Standard deviation (absolute value), deg	Maximum, deg		Slope of longest segment, deg	Length of longest segment, m	
3	79	Mare, smoother segment	3.2	6.3	30	4.1	7.0	35	138	9.5	518	6.8
2	189	Mare, rougher segment	4.5	7.3	24	6.4	9.5	33	251	.0	765	5.8
1	294	Upland crater, old	12.2	14.7	39	10.7	15.0	68	1626	16.0	3385	3.7
8	156	Outer rim slope, I, fresh upland crater	12.5	14.7	38	14.5	20.3	68	425	17.4	408	8.5
7	301	Outer rim slope, II, fresh upland crater	13.2	15.0	55	11.6	16.7	65	2442	14.5	2200	5.7
10	195	Smoother crater floor, fresh upland crater	14.1	14.0	35	14.0	19.2	55	1083	16.7	588	7.4
	1073	Fresh upland crater (overall)	19.2	21.1	55	17.6	23.5	69	2450	26.1	1250	6.9
4	163	Inner rim slope, I, fresh upland crater	19.7	18.6	56	15.5	20.7	52	2284	27.5	1500	5.6
9	248	Inner rim slope, II, fresh upland crater	19.7	18.8	51	19.1	24.0	70	2395	24.8	593	7.6
6	250	Inner rim slope, III, fresh upland crater	19.8	21.4	53	17.1	21.9	53	2453	26.6	663	8.4
5	359	Rougher crater floor, fresh upland crater	24.2	29.3	57	26.1	34.8	106	663	35.6	634	7.8

[a] N is number of elevations determined in each profile segment.

TABLE 2–III.—*Slope Means and Maxima for Lunar Uplands and Large Fresh Craters (From Previous Sources)*

Terrain type	ΔL, m	Mean slope, deg	Maximum slope, deg
Undifferentiated upland terrain, Apollo 8 data	70	15 to 20	42 to 55
	210	8 to 10	28 to 35
	350	6 to 8	19 to 31
	1050	4 to 7	13 to 17
	3500	3 to 4	7 to 15
Rim of Meteor Crater, Arizona	25	14 to 19	61
Meteor Crater, overall	61	12	52
Rim of Copernicus	600	11	39
Rim of Aristarchus	1000	7 to 10	38

TABLE 2–IV.—*Variation of Mean Slope Angle and Mean Curvature Angle With Increasing* ΔL *for 2 Lunar-Terrain Samples*

Multiple of basic ΔL	Mean (absolute value) of base-length slope angle, deg		Mean (absolute value) of base-length slope curvature angle, deg	
	Old upland crater	Fresh upland crater floor	Old upland crater	Fresh upland crater floor
1	12.2	27.2	10.7	22.9
2	10.7	24.2	9.0	26.1
4	9.3	20.7	7.6	28.2
8	8.3	16.9	6.4	29.9

trasting the three sample lunar areas photographed by Apollo 10 (figs. 2–1 to 2–3). At the $\triangle L$ at which the data are available, PSD curves do not supply an index of terrain microroughness directly applicable to vehicle design, but rather a general comparison of relative roughness and a description of topography as a time series. In this respect, the curves reveal significant differences among the three topographic samples. The PSD functions of two terrestrial topographic samples were available at the proper $\triangle L$ for

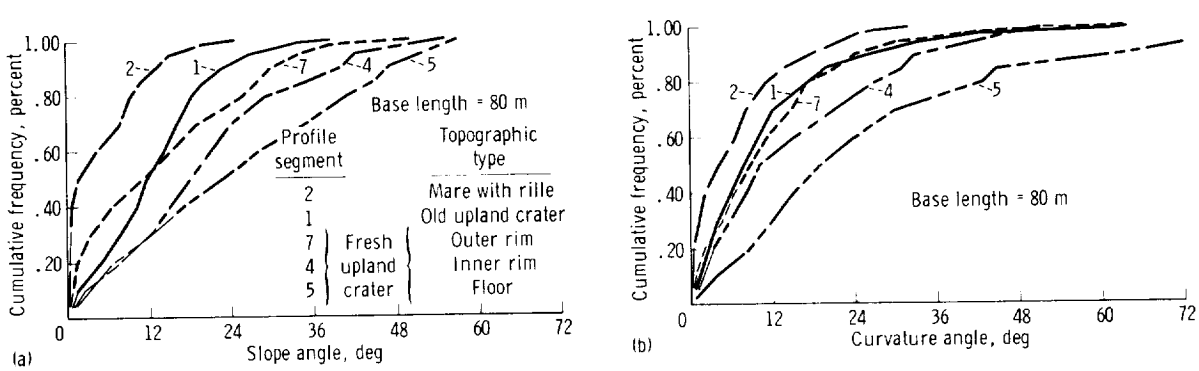

FIGURE 2–6.—Cumulative percentage-frequency graph for five distinctive lunar-terrain types. (*a*) Base-length slope angle. (*b*) Base-length slope curvature angle.

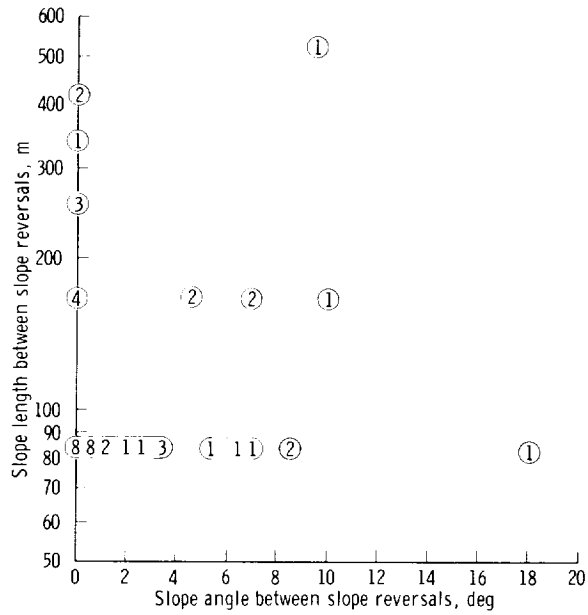

FIGURE 2–7.—Length of slope between slope reversals as a function of slope angle. Numbers represent frequency of slopes plotted at each point. (Data from table 2–II.)

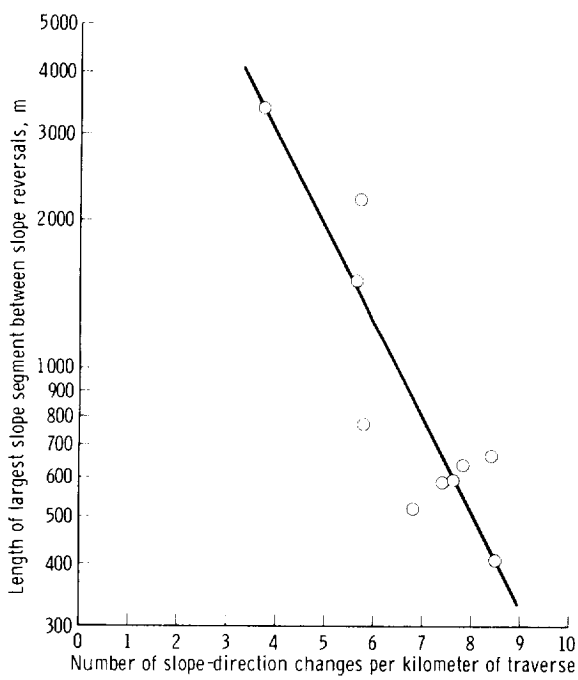

FIGURE 2–8.—Length of longest slope segment between slope reversals as a function of slope-reversal frequency. (Data from table 2–II.)

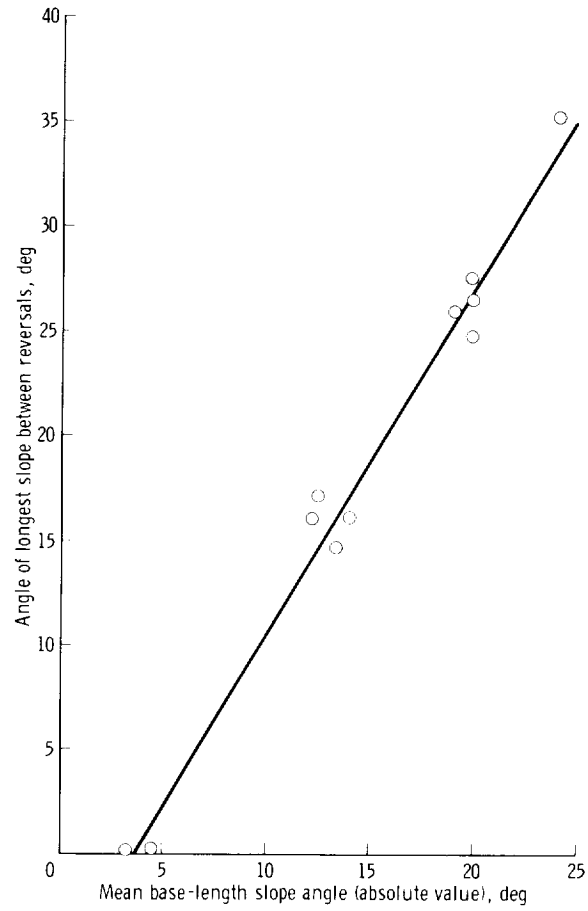

FIGURE 2–9.—Angle of longest slope between reversals as a function of mean base-length slope angle. (Data from table 2–II.)

comparison with the lunar samples. The fresh cratered basalt slopes of Kilauea Crater, Hawaii, and the steep, maturely dissected terrain of the California coast ranges at Big Sur are not generally as rough as the smoothest of the three lunar samples (fig. 2–1). Further photoclinometric reduction of Lunar Orbiter 4 imagery (nominal $\triangle L$ of 35 m) should provide numerous additional PSD curves for the comparison of lunar terrain types at this level of generalization. Apollo photographic resolution will have to be increased from 1 to 5 m if Apollo-derived quantitative surface roughness data are to be relevant to lunar exploration and mission planning.

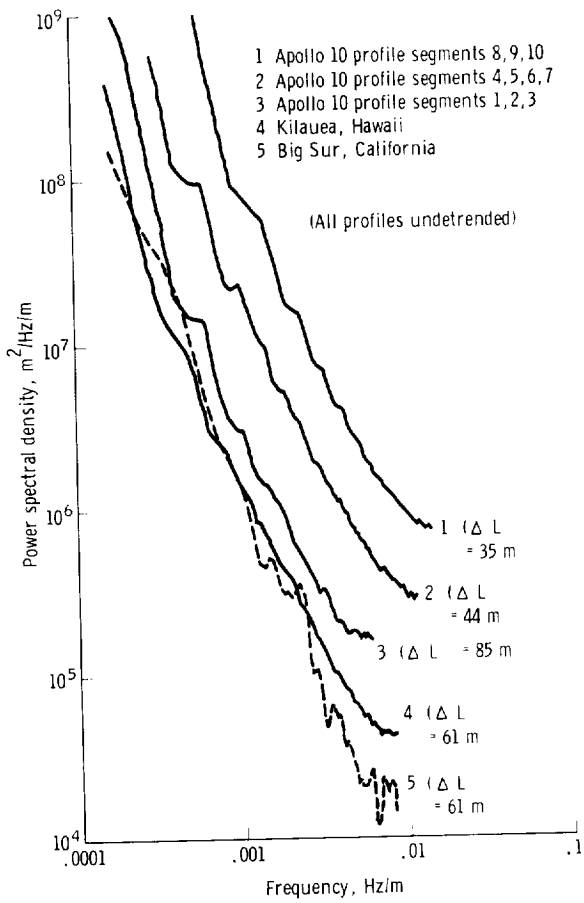

FIGURE 2-10.—Power spectral-density functions at high $\triangle L$ values for three lunar and two terrestrial terrains. These undetrended profiles cannot be compared with previously published detrended profiles.

THE APOLLO 10 LUNAR HIGHLANDS

KEITH HOWARD

With two prominent exceptions, the highlands photographed by Apollo 10 are mostly of the familiar terrain type characterized by numerous overlapping craters in varying degrees of freshness and in places by intervening light plains. One exception is in the area of Mare Marginus and to the north and east where peculiar bright surface markings much like the Reiner Gamma Formation in Oceanus Procellarum (ref. 2-6) occur on both mare and highlands over an area of 50 000 to 100 000 km². These bright markings form patches of irregular and sinuous bands and appear to have no inherent relief. The origin is not understood completely. A further discussion is in the section "An Unusual Far-Side Crater" by Strom and Whitaker. Although similar markings occur in mare material at 165° E, 35° S, the markings are not found elsewhere in the highlands. The markings in the Marginus region were observed on Lunar Orbiter and Apollo 8 photographs, but the distribution and spectacular geometric patterns are revealed clearly by Apollo 10 photographs.

A second area of unusual highland terrain occurs on the far side within the general area formerly known as the Soviet Mountains. The terrain, which has no known counterpart elsewhere on the Moon, covers approximately 1000 to 2000 km² near 119° E, 6° N, on the northwest rim of crater 211 and extends into the highlands (fig. 2-11). Young material of moderate albedo drapes over hills and collects in pools similar to lava flows. Foldlike wrinkles are common on the surface and apparently result from slow flow. In one place, the material slopes down through a narrow pass and connects a high pool with a lower one. Surface wrinkles convex to the lower pool record flow in the

FIGURE 2-11.—Crater 211 and surrounding highland terrain (AS10-30-4364).

downhill direction. If, like some pahoehoe flows, material congealed at flow fronts to form dams became ponded behind the dams, then broke through or under the dams toward lower terrain, a collapsed pond surface partly draped over underlying hills would be formed. This movement could explain the draping over some hills. Highlands covered by the material have lost the variegated brightness patterns typically seen in high-illumination oblique views and are now uniformly of moderate albedo. Bright rays of late Copernican age cover part of the material, but part of the lowest pool may postdate the rays. The material, which covers many craters, clearly flowed downhill. If the material is lava, it must have emanated from several sources, not yet discovered, that correspond to the higher elevations at which the lava is found. If the material is not lava, probably it had a solifluction or rock-glacier type of origin.

In addition to these two unusual types of terrain, dark mantling material, which perhaps is analogous to the Sulpicius Gallus Formation (ref. 2–7), was discovered in two places. One place is between two craters west of Mare Smythii (fig. 2–12); the other is on the wall of crater 211 (Apollo frame AS10–30–4364). At the second locality (discussed in the section "Terra Volcanics of the Near Side of the Moon" by Wilhelms), the dark material apparently covers late Copernican rays (Soviet Mountain system), but alternatively may represent an area of dark rocks immune to lightening by ray ejecta.

FIGURE 2–12.—An area of dark mantling material near Mare Smythii.

Apollo 10 photographs have made possible the clear recognition of two new highland geologic units on the far side. One unit is similar to the Reiner Gamma Formation, and the other is probably a viscous lava flow. The photography will be valuable in preparing geologic maps for comparing regionally the highlands of the near and far sides.

A cursory examination of other Apollo 10 photographs revealed the following features and phenomena that are of particular geologic interest. These observations are a small sample of the many that could be made by more systematic examination of the Apollo 10 material.

1. A bowl-shaped crater that is apparently part of a volcanic chain did not disrupt a large mountain ridge that extends into the crater (Apollo frame AS10–30–4327, magazine Q).

2. The central peak of the large crater Neper is a dome surrounded by a rim. This crater looks like some of the Mono Craters in California, but might instead represent concentric outcrops of hard and soft rock in a central uplift (Apollo frame AS10–30–4303, magazine Q).

3. A crater with an irregular convex to flat floor, at the center of the photograph, formed on an initial slope (the wall of a large crater), and the floor now tilts parallel to the initial slope (Apollo frame AS10–29–4177, magazine P).

4. The high-illumination views of four brightly rayed craters have asymmetric ray patterns. In each case, long radial streamers of rays extend from one side indicating the direction of oblique impact. Extending from the other side are short irregular ray loops that do not extend far from the crater (Apollo frames AS10–33–4883 to –4887, and –4890, magazine T).

5. The source crater of the Soviet Mountain rays has blocks on the rim that are as large as 250 m across. If the dark spots seen on fresh craters are individual blocks, dark patches could represent fields of blocks that are analogous to dark young aa flows where numerous small shadowed areas lower the albedo considerably (if seen from an angle). However, fields like the talus fields in the Sierra usually are bright on air photographs (Apollo frame AS10–33–4988, magazine T).

SOME PRELIMINARY INTERPRETATIONS OF LUNAR MASS-WASTING PROCESSES FROM APOLLO 10 PHOTOGRAPHY

RICHARD J. PIKE

The Apollo 10 photographs support the suggestion that mass wasting is an important degradational agent on the lunar surface. Because resolution of the 250-mm lens was only 15 to 25 m, Apollo 10 provided no new information on the types of patterned ground recognized on high-resolution Lunar Orbiter imagery. The geomorphic features and textures attributed to mass-wasting processes in this section are of larger dimensions. These features are (1) talus slopes, (2) boulder tracks and debris flows, (3) large-scale, en-bloc terracing of the inner rims of large craters (greater than 15 to 20 km in diameter), (4) small-scale terracing of crater slopes, (5) three types of earthflow textures, (6) radial channeling of predominantly small craters (smaller than 15 to 20 km in diameter), and (7) subduing of crater-rim terraces with increasing crater age. Because craters and crater-consequent geologic events create most of the steep slopes on the Moon (the surfaces that are particularly susceptible to mass wasting), most of the features discussed here occur in craters.

A talus apron at the foot of an arcuate hill (fig. 2–13) is possibly the degraded remnant of a small crater that is on the southern border of Mare Tranquillitatis near the crater Maskelyne D. The talus material covers the break in slope between the hill and the mare material and appears to be of finer texture than either subjacent unit. This apron lies at the foot of the steepest slopes on the photograph, suggesting that this narrow band of material is a talus deposit. The material has partially obscured several small shallow craters on the mare surface. The scarcity of craters on the apron material may also suggest that the material is active talus. A second talus apron is at the foot of the northern wall of the rille Ariadaeus. The breaks in slope occur between the steep rille wall or free surface, the debris slope, and the flat floor of the rille. The apron is beneath the most precipitous portion of the rille wall.

FIGURE 2–13.—Arcuate hill with talus apron located in southern Mare Tranquillitatis near the crater Maskelyne D (AS10–31–4597).

Several striking features of the unusual lunar crater in figure 2–14 are the blocks on the rim crest, the crater interior, and the outer rim slopes. Boulders apparently have rolled a short distance down the outer rim slope. Boulder tracks, if such tracks exist, are exceedingly faint. The two debris flows on the far rim of the crater are more apparent. The upper flow begins at the top of the large uppermost terrace and continues down across a series of smaller terraces approximately three-fourths of the depth of the crater. The second flow, which begins on the level at which the first flow ends, extends to

FIGURE 2–14.—Fresh unnamed crater 35 km in diameter located approximately 122° E, 5° S (AS10–28–4012).

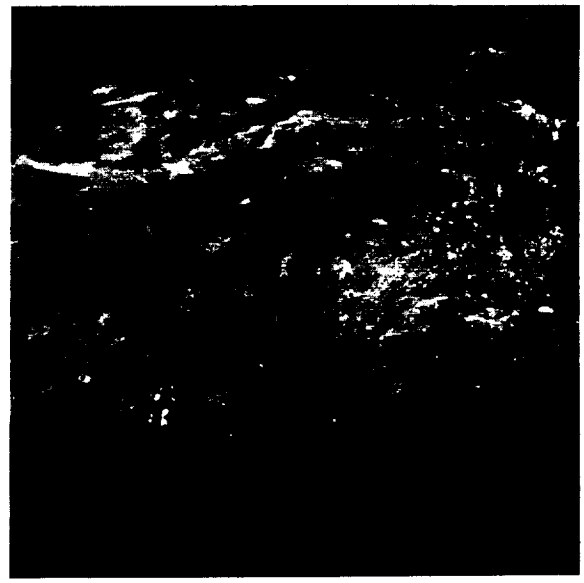

FIGURE 2–15.—Western rim of crater 211, a fresh crater 80 km in diameter located approximately 120° E, 5° N (AS10–30–4360).

the bottom of the crater and ends near the low jumble of material that comprises the central peak complex. The upper flow probably was triggered by a rockfall from the steep upper rim slope and initiated the lower flow farther down the inner slope.

The large-scale en-bloc terracing of the inner rims of large lunar craters has long been apparent from terrestrially based telescopic observation. The example of this feature (fig. 2–14) is unusual because one end of the large upper terrace has not yet broken free of the upper crater rim. Although the upper surface tilts toward the crater center with increasing proximity to the free end, this terrace appears to be one coherent faulted slice or slump block. The smaller arcuate slump blocks below this terrace all appear to be less cohesive. To the left of the major slump zone, few deposits bear any trace of the preslump configurations.

Some of the terraces in the large fresh crater shown in figure 2–15 appear to be massive faulted slices that moved downslope en bloc without much fragmentation. Although most have been mantled with loose debris, the original slip faces are still clearly recognizable. The smaller terraces within this crater are less cohesive in appearance and may have disintegrated partially during movement downslope and settling on the crater floor. The aprons of rubble can be distinguished at the foot of most of the lower terraces. At least one short debris flow appears to have distorted the shape of a subsequent meteorite impact crater as the flow moved downslope. The less cohesive terraces and slide deposits in the foreground of figure 2–15 contrast with the larger and more cohesive-appearing terraces on the far rim of the crater.

A series of well-developed nested terraces occupies most of the inner rim slope of crater 216 (fig. 2–16). The large cohesive upper terrace in the right foreground probably moved downslope en bloc from the upper rim. Such movements can cause circular craters to become acircular with time. A symmetrical meteorite crater could acquire a configuration more typical of irregularly shaped craters that commonly originate by internal processes. The irregular distribution of large continuous terraces within crater 216 is typical of many large lunar craters.

A small segment of crater IX is shown in figure 2–17. Part of the rim (right back-

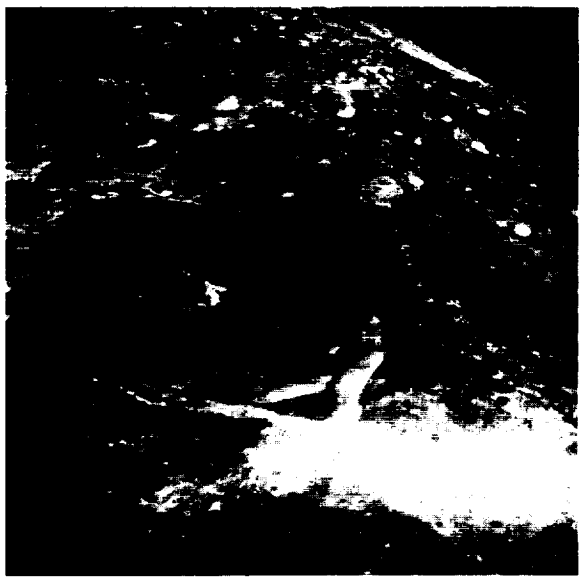

FIGURE 2–16.—Crater 216 (75 km in diameter) located approximately 134° E, 5° N (AS10–30–4467).

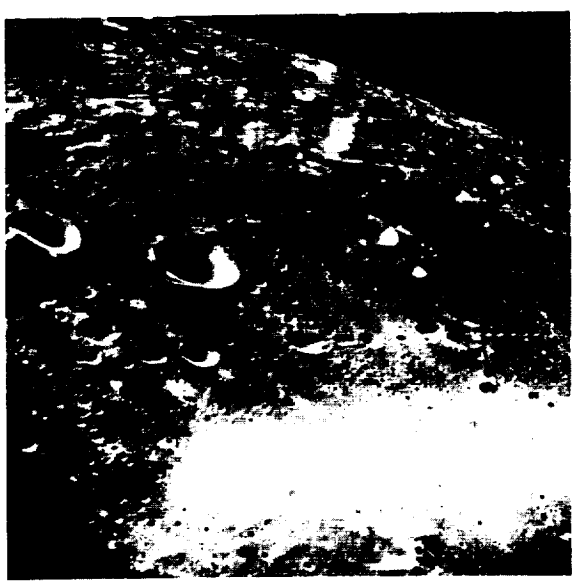

FIGURE 2–17.—Segment of crater IX, a basin 300 km in diameter, located approximately 140° E, 5° N (AS10–30–4462).

ground) has undergone little slumping; to the left, the rim has collapsed into a maze of low, broad, slump terraces. These contrasts between two types of crater-rim topography may involve irregular distributions of structural weaknesses in the lunar crust or may be due to unknown causes. Some minor mass wasting has produced small deposits of hummocky rubble at the foot of the steep escarpment shown near the right-hand edge of figure 2–17. Several ravines that may represent areas of particularly active mass wasting also are on this escarpment.

One phenomenon common to the four craters (figs. 2–14 to 2–17) is the lateral extent of the terracing and slumping. Material has moved great distances across the floors of these craters apparently without water or gas lubrication. This major problem area in lunar-surface processes should receive commensurate attention during the projected manned exploration.

Most of the craters illustrated in this section have many small arcuate terraces that are neither the large en-bloc type nor the small terracettes that are on the surface of earthflow slump deposits. These smaller slump terraces seem to be less cohesive than the largest terraces and apparently have become fragmented and deformed and lost much of the original shape. This type of terrace may be the most common type observed within lunar craters more than 15 to 20 km in diameter.

A study of craters photographed on the Apollo 10 mission and from earlier lunar spacecraft revealed that much of the mass wasting that was thought to have degraded inner rim slopes has not occurred as the slumping of discrete terraces but as earthflow. Although the large terraces are more spectacular, the earthflow deposits account for most of the volume of material displaced from the inner slopes of crater rims. This less obvious downslope movement of material results in the degradation of smaller craters (less than 15 to 20 km in diameter) and in the gradual but eventual muting of steep slopes on the larger craters.

Apollo 10 photographs of lunar craters show at least three different topographic textures attributable to small-scale mass wasting. These textures will be referred to as rapid slump, gradual slump, and sheet slump. The first two types of deposits are shown in

figures 2–14 and 2–18(*a*). Two different types of earthflow deposits are present in the crater shown in figure 2–18(*a*). The older gradual-slump unit has slipped only a short distance below the rim crest. This unit is well cratered and is characterized by a myriad of arcuate terracettes oriented nearly parallel to the rim crest. The lower portion of the unit shows some radial grooving that was possibly caused by more rapid slippage of the leading edge of the slide. However, the bulk of this unit probably moved slowly and preserved the terracettes intact. The overlying rapid-slump unit probably slipped more quickly down the inner rim. This unit appears to have been dumped in a disorganized series of hummocky piles. This interpretation is supported by the greater distance the deposit has traveled toward the center of the crater than the subjacent slump unit. The rapid-slump unit also is less heavily cratered, suggesting that the unit is younger than the underlying deposit. The slip face beneath both slump units varies significantly in albedo. The albedo is noticeably lighter behind the younger deposit. This variation was expected from previous experience in mapping units within craters.

Profiles of the two contrasting types of slump features are shown in figure 2–18(*b*). The profiles were obtained through stereo-photogrammetry of Apollo frames AS10–28–4002 and –4003 by Sherman S. C. Wu and his associates, U.S. Geological Survey. The location of the profiles is shown in figure 2–18(*a*). The shapes and relative positions of the two slides and the slip faces are apparent. Some quantitative information can be extracted from the profiles. The relative relief of the inner crater rim slope at the rapidly slumped area is 1000 m greater than the relief where the more gradual slide occurred. This difference suggests that the former slope initially may have been steeper and less stable than the latter slope. The contrast might have been sufficient to account for the occurrence of two different types of earthflow on the same crater wall. The slip face above the rapidly slumped deposit slopes approximately 29°. The slip surface inferred

(*a*)

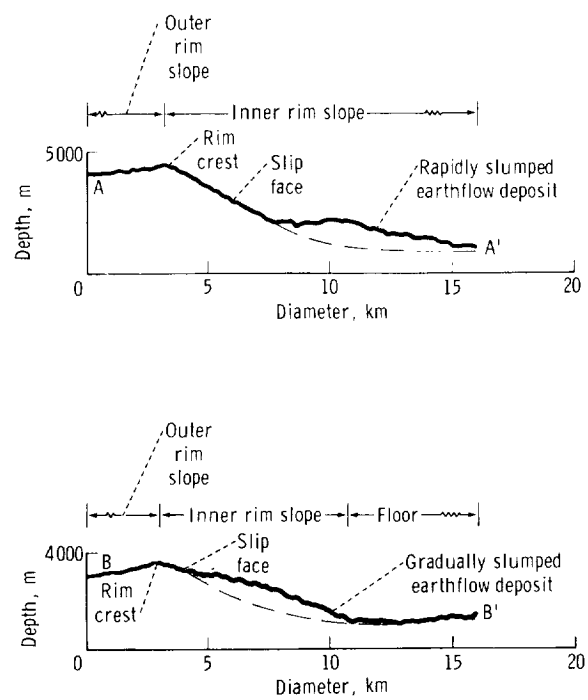

(*b*)

FIGURE 2–18.—Mass wasting in unnamed fresh crater (35 km in diameter) located approximately 133° E, 1° S. (*a*) Profiles A–A′ and B–B′ (AS10–28–4002). (*b*) Topographic profiles (1:1) showing general crater topographic divisions above each profile (S. S. C. Wu and associates, U.S. Geological Survey).

to lie beneath the gradually slumped deposit slopes approximately 25° but may actually approach 30°. No measurable significant contrast exists between the two slip faces. However, a contrast does exist between the overall surface angle of the deposits. Much of the surface of the rapidly slumped deposit lies at an inclination of approximately 11°; that of the other slide deposit, at approximately 18°. The difference suggests that the rapidly slumped material attained a more stable angle of initial deposition than did the more slowly moving slide. Activity probably has not ceased completely at this location. The numerous tension cracks in the outer rim slope on and below the crater rim crest suggest that small subsequent slides eventually will come down onto older slump deposits.

The third distinct type of small-scale mass-wasting texture observed on Apollo 10 photographs is well developed on the inner slopes of the small (8 km in diameter) post-mare crater, Messier B, in central Mare Tranquillitatis (fig. 2–19). Material appears to have moved downslope in thin sheets of poorly consolidated rock fragments. No prominent terracettes appear on the upper slopes, and no large hummocky deposits appear on the lower slopes. Some isolated blocks can be distinguished on the inner rim slope. The opposite wall of the crater shows a disconnected band of dark material that apparently has slipped downslope from directly beneath the rim crest. Parts of this band occur at varying heights above the crater floor. The portion of the wall that is partly in shadow shows some relief to the slump sheets—approximately 75 m at most. The upper rim slope is as steep as 45° (preliminary estimate), decreasing to approximately 15° at the break in slope between the rim slope and the flat floor. This juncture is remarkably distinct and has not yet been obscured by mass wasting. This indicates that mass-wasting rates are exceedingly slow on the Moon. However, the process is still sufficiently active to obliterate all craters that have impacted the inner rim slope. The occurrence of post-Messier B cratering is confirmed by the numerous craters on the outer rim slopes of Messier B. The hummocks on the floor of the crater are interpreted as remnants of the Messier B impact event. The hummocks appear to have been engulfed by particulate material eroded from the inner rim slope.

FIGURE 2–19.—Crater Messier B (8 km in diameter) in central Mare Tranquillitatis (AS10–29–4253).

General characteristics of the small fresh lunar craters are radial streaks, ravines, grooves, and bands along the inner slope. These characteristics are seen in figure 2–20 in the crater in center background and may be related to the vertical markings on slip faces behind slump blocks in much larger craters such as crater 211 (fig. 2–15). These markings probably are related to mass wasting in small craters. Another possibly related radial phenomenon in much older small craters is shown in figure 2–21. These grooves appear to have more relief than the streaks characteristic of younger craters. The relief may be the result of the development of the early markings into debris channels or of some similar feature over long periods of time. In figure 2–21, the crater densities on the inner slopes of the older craters are lower than on the flat crater floors. The crater slopes are still undergoing active mass wasting.

One surface process that probably operates on most lunar slopes is surface creep, the downslope transfer of individual grains of loose material or of thin sheets of material. The "tree-bark," parallel, and cellular patterns observed on high-resolution spacecraft imagery suggest that this mechanism is primarily responsible for degradation of gentle slopes. Therefore, creep must be an important agent on older crater surfaces. Although the Apollo 10 camera systems were unable to resolve textures produced by surface creep, smooth gentle surfaces that occupy most of the lunar highlands and older craters probably are caused in part by this mechanism. One such surface might be that shown in figure 2–22 on the far eastern limb. Micrometeoritic bombardment and impact-induced seismic shock are among the mechanisms suggested as primarily responsible for active lunar creep.

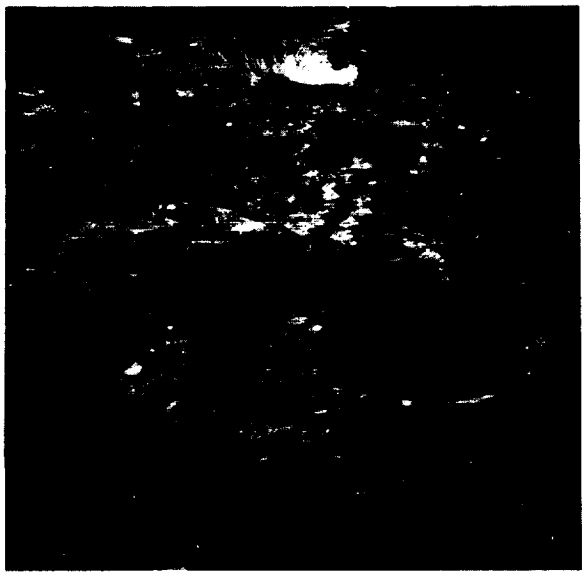

FIGURE 2–20.—Large unnamed older crater (75 km in diameter) located near craters 212 and 213 at approximately 124° E, 7° N (AS10–30–4345).

Mass wasting is an effective surface process in changing the morphology of lunar craters. A sequence that depicts craters in varying stages of modification is formed by figures 2–13, 2–16, 2–20, and 2–22. Although these craters are from approximately 35 to 100 km in diameter and are not actually comparable, the four contrasting craters portray the changes that characterize the morphologic aging of a typical large lunar impact crater. Other postformational processes, such

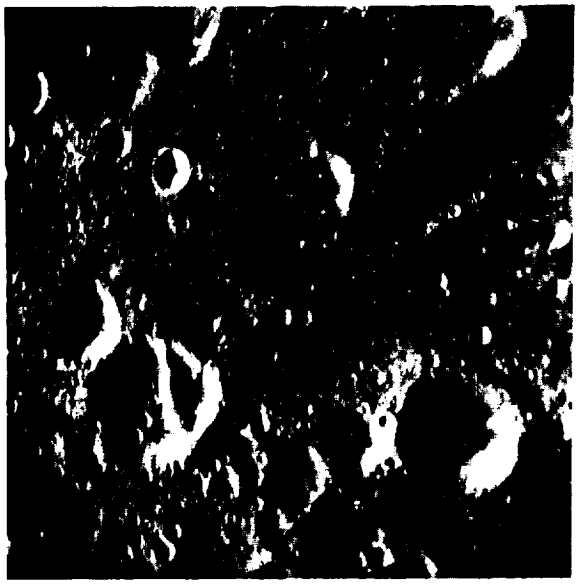

FIGURE 2–21.—Highly cratered lunar upland terrain located approximately 159° E, 1° N (AS10–28–4080).

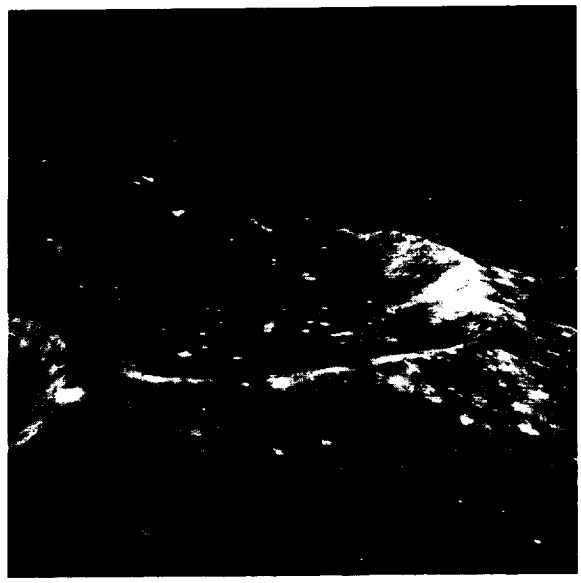

FIGURE 2–22.—The old crater Gilbert (100 km in diameter) located approximately 77° E, 1° S (AS10–29–4234).

as continuing metoritic bombardment, isostatic sinking of the rim and uplift of the floor, and lava flooding of the interior, may alter substantially the gross geometry of a crater. However, surface processes have a particularly dramatic effect.

Each of the four craters is successively more heavily cratered, and the impact-produced surface textures are gradually subdued. The initially sharp rim crest becomes increasingly rounded. The prominent slump terraces are subdued until the terraces are totally absent from the crater Gilbert (fig. 2–22). The break in slope between the foot of the inner rim slope and the flat floor gradually becomes blurred. The crater Gilbert has lost distinction from surrounding topographic features and is beginning to merge unobtrusively with the surrounding lunar landscape. Apparently, large lunar craters pass from physiographic youth through maturity to old age because of muting of the topography by gradual mass wasting of material from steeper to gentler slopes. The rate of lunar mass wasting probably is logarithmic (i.e., the rate becomes much slower as a crater ages and as the slopes become gentler and more nearly graded).

The following recommendations are offered for further study of lunar-surface processes in Apollo 10 photographs and in pictures from subsequent missions:

1. Compile a catalog of features that deserve measurement and further interpretation, especially talus slopes, debris flows, boulder tracks, and terraced crater walls.

2. Make slope measurements along profiles across slump terraces, terrace slip faces, and talus aprons to determine angles of repose and critical angles at which downslope movement may occur.

3. Conduct quantitative theoretical studies of mechanisms that could account for the ability of crater slump deposits to reach so far across the crater floors.

4. Acquire additional photography at higher resolution. Further advances in the study of lunar mass wasting will have to await 1-m-resolution photography from later Apollo missions. This resolution is mandatory for the proper study of lunar talus slopes, debris flows, boulder tracks, and slump and creep deposit textures.

CRATERS

AN UNUSUAL FAR-SIDE CRATER

R. G. Strom and E. A. Whitaker

Several Apollo 10 photographs show in detail a large crater that displays a number of unusual features. This crater is the source of a prominent but somewhat anomalous ray system on the far side of the Moon. The ray system forms part of the large bright area that was incorrectly named the Soviet Mountains. The conclusion that this area consists of two overlapping ray systems (ref. 2–8) was confirmed completely by the Apollo 8 photographs that also permitted the identification of the two source craters on Lunar Orbiter photographs (ref. 2–9).

The crater described in this section is the northernmost of the two ray centers and is different from the southern counterpart, which is also shown on Apollo 10 photographs. The craters and the general ray-covered area between the craters are shown on Lunar Orbiter photograph IM136 (fig. 2–23). A rectified and enlarged high-illumination view of the northern crater and a portion of the ray system is shown in figure 2–24.

The crater, which is approximately 90 km in diameter, is located at 5° N, 120° E, and is numbered 211 on the Lunar Farside Chart (ref. 2–10). The morphology of the crater is similar to that of the near-side rayed craters Tycho, Copernicus, and Aristarchus. The floor has a crenulated appearance with numerous linear and arcuate flow ridges that may be indicative of a solidified melt, the inner and outer walls display flowlike features, and the central peaks resemble assemblages of cones with many large boulders protruding. However, other features of this crater are not in Tycho, Copernicus, or Aristarchus and possibly may be unique.

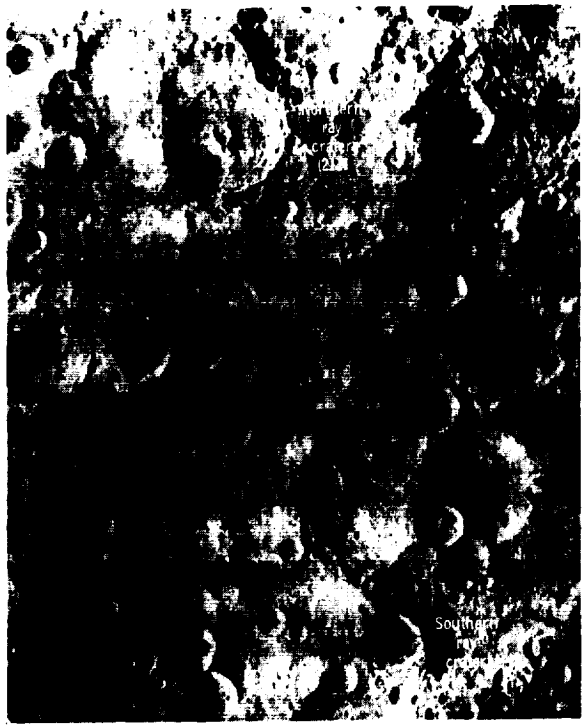

FIGURE 2–23.—Lunar Orbiter 1 photograph of ray craters producing the bright area of the Soviet Mountains.

FIGURE 2–24.—Rectified Apollo 8 photograph of northern crater and surrounding area with high illumination.

The northwestern sector of the crater and the adjoining terrain are illustrated in figures 2–25 and 2–26. A stereoscopic view of figure 2–26 indicates that area G may be an almost level dark "lake" (20 km in diameter) that has been invaded by several flows that display well-defined fronts. Most of the flows have traveled toward the lake, and three (C, D, and F) apparently have flowed onto the lake surface. This movement indicates that the flows are younger than the lake. The largest flow (A) merges with the lake and probably contributed to filling the lake when both units were fluid. Therefore, the lake and flow A are probably the same age. Flow A (approximately 15 km in length) has traveled half the length along a narrow valley and then spread out on a broad plain before merging with the lake. Flow A displays well-developed arcuate flow ridging where it emerges from the valley. Flows B, C, and D originate from small lakes on the outer slopes of the crater; flows E and F begin at ill-defined areas on the slopes of highland elevations. Flows B and E overlie flow A. Therefore, these flows are younger than flow A. The arcuate flow ridging of flow A, the large areal extent, and the fact that flow A merged with and at least partially filled lake G suggests that the flow consists of lava. Flows B, C, and D, which originate from lakes, may also consist of lava. Flow F has traveled only a short distance downslope, begins in a broad ill-defined region in the highlands, and has a surface morphology similar to the general highlands in that area. This unit may be a debris flow. Flow E could be either a debris flow or a lava flow.

Three other flows that issue from a group of low hills on the western floor of the crater are also shown in figures 2–25 and 2–26. The morphology and sources are similar to those on the eastern floor and probably have a similar origin and composition.

Area J (figs. 2–24, 2–26, and 2–27) is unusual because of the high albedo, which is

FIGURE 2–25.—Northwest sector of crater and area immediately beyond (AS10–30–4352).

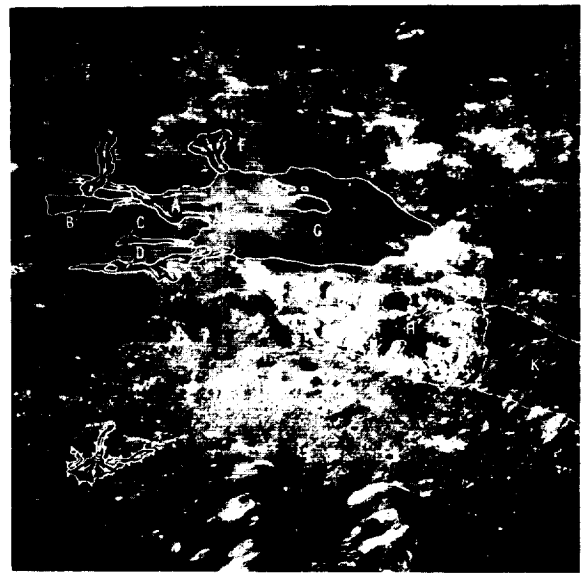

FIGURE 2–26.—Apollo 10 photograph AS10–30–4352 showing flow lines.

greater than that of the densest rays in the vicinity, and because of the abnormal morphology.

In the Apollo 8 report (ref. 2–11), evidence was presented that the bright interior slopes of craters were the result of the downslope movement of material that had exposed relatively fresh surfaces. However, this apparently is not the case for area J, because the neighboring area K displays equally steep slopes but is of considerably lower albedo.

A stereoscopic examination of area J reveals a jumbled aggregate of subconical hills. The valleys separating these hills contain darker material (similar to Tsiolkovsky), but the most unusual features are the dark narrow fingers of material that appear to have issued from the summits of some of the hills (e.g., areas L, M, and N, fig. 2–27). It is impossible to decide whether these fingers are the result of fluid flow or are talus deposits, but the fact that the fingers come from the hill summits suggests a volcanic origin. The albedo extremes are also strongly indicative of differentiation processes by long-term melting.

This high-albedo area surrounds another area (area H, figs. 2–24 and 2–26) of intermediate to low albedo that has a noticeably different morphology that resembles the general floor of the crater. Contiguous with area J on the east is an area (area K, fig. 2–26) with a different morphology. The crater wall

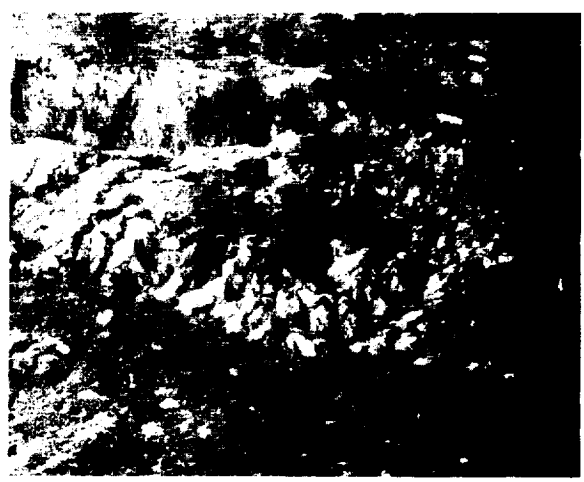

FIGURE 2–27.—Portion of Apollo 10 photograph AS10–30–4351 showing details of northwest wall of crater.

appears to have been degraded by some process that left the wall pocked with many irregular subconical craters.

On the southeastern portion of the floor is a succession of three or four flows that have different morphologies and well-defined fronts (figs. 2–28 and 2–29). These flows apparently originated from discrete portions of the lower slopes of the central peak. Flow 1 is approximately 4 km long, has a relatively smooth and slightly hummocky surface, and is clearly associated with a pair of connected craters on the lower slopes of the central peak. Flow 1 partly overlies flow 2 and, therefore, is younger. Flow 2, which is complex, has a rough surface that contains numerous arcuate and linear ridges and a high, well-defined front. This flow is approximately 12 km long and originates on the southern portion of the central peak in the vicinity of a bright-halo crater (A) that is 2 km in diameter. The head of the flow is partly obscured by bright-halo material (ejecta) from the crater. The possibility exists that this crater overlies the source of the flow and is related to the flow. Flow 2a may be a secondary flow unit that broke through the terminus of a late surge of the main flow. The rough surface texture, high flow front, and pronounced flow ridging indicate this flow was considerably more viscous than the others in the vicinity. Flow 3 is about 10 km long and has a smooth surface with a fairly low flow front that indicates a relatively low viscosity. This flow originates from an ill-defined portion of the central peak and overlies flows 2 and 2a. The different ages and surface morphologies of the flows, the lengths, the fact that one flow (flow 1) is clearly associated with a pair of craters, and the similarity between the surface morphology and the remainder of the floor strongly indicate that the flows are composed of lava.

Other parts of the central peaks display flows of a different type. Therefore, the feature P (fig. 2–29) appears to be a thin layer of darker material that has originated from the summit of the peak. The thinness suggests that either the material was deposited as a fluid melt or that it is the result of downslope movement of dark debris.

The features of area Q are deep channels carved in the flank of the peak and may be connected with the formation of the crenulated flow S. The small feature of area R appears to be identical to a slump feature formed in the cinder and ash hill that partially covers the main vent of the Kilauea Iki 1959 eruption site.

Two unusual bright surface markings, areas X and Y, which do not appear to be ray material at all but resemble the mark-

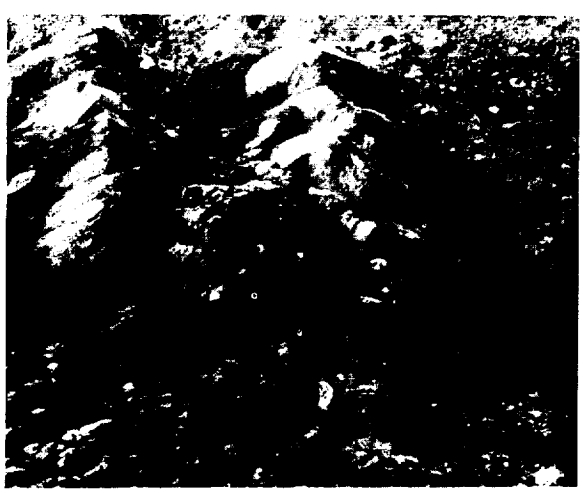

FIGURE 2–28.—Apollo 10 photograph AS10–30–4353.

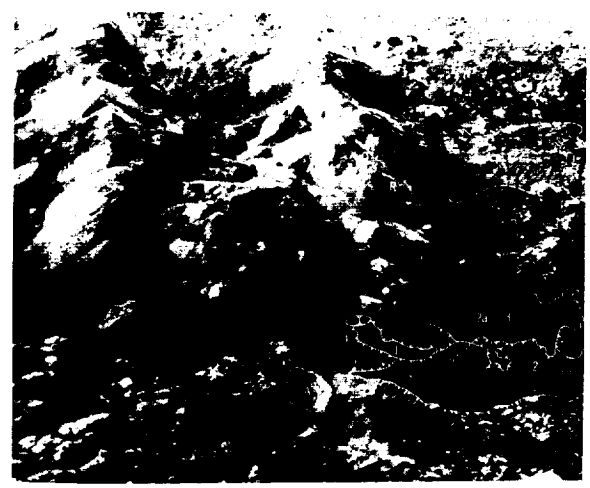

FIGURE 2–29.—Apollo 10 photograph AS10–30–4353 showing central peaks and adjoining flows.

ings near the crater Goddard on the north border of Mare Marginis, the well-known Reiner gamma marking, and a few others, are shown in figure 2–24. These markings were identified tentatively as sublimate deposits (ref. 2–9), and areas X and Y may be of similar origin. The marking at area X was photographed from the Apollo 10 command and service module, and is reproduced in figure 2–30. The swirls and curves appear to be unconnected with the topography of the region.

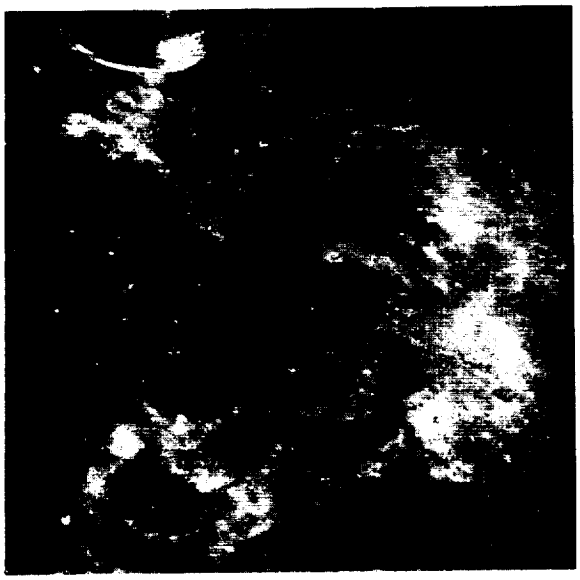

FIGURE 2–30.—Bright surface markings that do not correspond with topography (area X in fig. 2–24).

The unusual features of crater 211 make this crater one of the most interesting structures thus far photographed by any lunar mission. Although crater 211 is the center of a prominent ray system, many features of the crater and the surrounding area have close analogies in various terrestrial volcanic areas. Therefore, it is of utmost importance that this crater be photographed with higher resolution during subsequent Apollo missions when orbit and illumination conditions are favorable.

LUNAR IMPACT CRATERS

H. J. MOORE

Many lunar craters shown on Apollo 10 photographs resemble craters formed by natural and experimental impacts on Earth. Points of resemblance include rays, layering in the ejecta, and asymmetrical ejecta patterns.

One rayed lunar crater (fig. 2–31) has features common to Meteor Crater, Ariz., and to craters produced by missile impacts at White Sands Missile Range, N. Mex. Six units can be mapped in and around this lunar crater: (1) central-mound material, (2) crater-wall and floor material, (3) slump material, (4) dark upper-crater-wall material, (5) flank and rim material, and (6) ray material. Central-mound materials underlie a hummocky domed surface on the crater floor, and their reflectivities are intermediate. Crater-wall and floor materials, which are bright, underlie most of the surfaces of the lower walls, part of the upper walls, and the floor near the base of the walls. Locally, on the crater walls, these materials are raylike and form radial streaks extending downslope. A unit

FIGURE 2–31.—Apollo 10 photograph AS10–29–4207 of a rayed crater.

of dark material extends concentrically around the upper crater walls but below the crater rim. Flank and rim materials underlie the surfaces of the uppermost crater wall, the rim, and the flanks around the craters and have intermediate reflectivities except for local dark patches on the flanks. Bright rays streak from the central-mound material, up the crater walls, across the crater flanks, and beyond the mappable limits of the flank material. Not all radial bright streaks on the crater walls are rays—some are wall materials. In one place, a displaced mass of flank and rim materials and of dark upper-crater-wall materials is found at the junction of the crater wall and floor. The mass is mapped as slump material.

Observable relationships of the materials in and around this crater are consistent with those exhibited by terrestrial impact craters. For such craters, the central-mound materials represent materials from lower horizons that have been displaced upward. Bright materials of the crater walls represent talus, and where the sequence of flank and rim materials and dark material is preserved, slumping has occurred. The dark upper-crater-wall materials represent the uppermost stratigraphic horizon and ejecta. Flank and rim materials are ejecta from lower horizons. Because the reflectivity of the flank and rim materials is the same as that of the central-mound materials, they must be from the same horizon. Inverted stratigraphic relationships in the ejecta, such as those interpreted for this lunar crater, are common features of natural impact craters, missile impact craters, and small-scale laboratory impact craters in sand. Rays represent crushed and shocked materials deposited from jets of debris ejected radially outward. Rays that extend from the crater floor, up the crater wall, across the flanks, and beyond have been observed in missile impact craters. A cross section that illustrates the probable relationships between some of these units is shown in figure 2–32.

Ejecta patterns around several other lunar impact craters have counterparts in missile impact craters. For example, the bright-

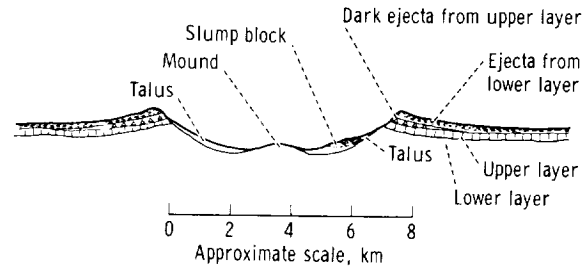

FIGURE 2–32.—Cross section of the crater shown in figure 2–31.

rayed crater shown in figure 2–33 has the same bilateral symmetry as a missile impact crater produced in water-saturated sediments at White Sands, N. Mex. (fig. 2–34) (ref. 2–12). Parallel features, such as the up-trajectory tongues of ejecta and outward gradation from a thick continuous ejecta blanket to a thin discontinuous one, to scattered rays, and to isolated secondary impacts, are also noteworthy. Other lunar craters, such as the one shown in Apollo photograph AS10–33–4889 (magazine T), also have counterparts in missile impact craters; in these, a V-shaped region on the up-trajectory side is free of ejecta.

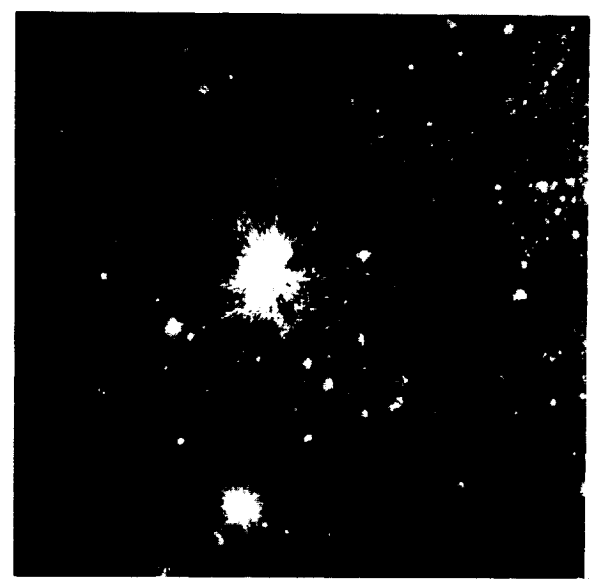

FIGURE 2–33.—Apollo 10 photograph AS10–33–4883 showing a bright-rayed crater.

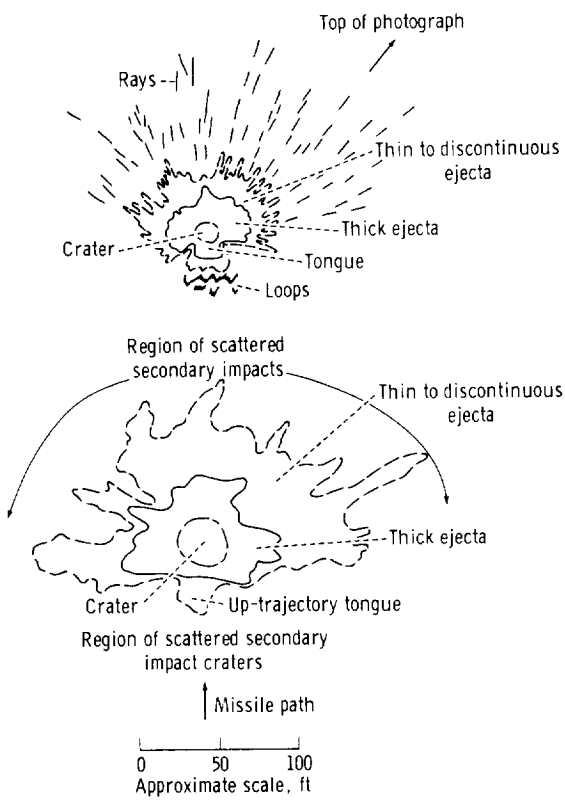

FIGURE 2–34.—A comparison of ejecta patterns of the crater shown in figure 2–33 with a missile impact crater formed in water-saturated lake beds. The lower figure was adapted from reference 2–12.

LARGE BLOCKS AROUND LUNAR CRATERS

H. J. MOORE

Additional data on the largest observable blocks around lunar craters were obtained from Apollo 10 photography. For example, blocks that are approximately 160 to 220 m across occur around the 35-km-diameter crater shown on Apollo 10 photograph AS10–33–4989 (4.8° S, 122.5° E). These blocks are larger than the blocks found around Aristarchus (40 km in diameter) on Lunar Orbiter 5 photographs (H200). The largest blocks around Aristarchus are 143 m across. Blocks around a crater that is nearly 8 km in diameter (Apollo 10 photograph AS10–28–4014) are between 84 and 100 m across. Blocks around Censorinus (Apollo 10 photograph AS10–29–4291 and Lunar Orbiter 5 photograph H63) and Mösting C (Lunar Orbiter 3 photograph H112) differ in size by a factor of nearly 2. (Both craters are approximately 3.8 km in diameter.) The blocks around Mösting C are as large as 60 m, and the blocks around Censorinus range from 25 to 45 m.

Although the scatter in the data is large, a direct relationship exists between the size of the largest observable blocks around the lunar craters and the size of the craters. Blocks that are nearly 200 m across are found around lunar craters that are 35 to 82 km in diameter, and blocks that are 25 to 100 m across occur around smaller lunar craters that are 3 to 8 km in diameter (fig. 2–35). The largest blocks around lunar craters that are 30 to 100 m in diameter range from 1 to 3 m. The largest blocks around 30- to 100-m terrestrial craters formed artificially by projectile impact and explosive charges in sparsely fractured indurated rock material are also 1 to 3 m across (fig. 2–35). Blocks around terrestrial impact craters in basalt and explosive craters in sandstone that are about 30 cm in diameter may be as large as 6 cm across.

For craters larger than 1 m, the data on limiting block sizes may be approximated by $B = KD^{2/3}$, where B is the size (centimeters) of the largest block around the crater, D is the diameter (centimeters) of the crater, and K ranges from 0.5 to 1.5.

VOLCANIC FEATURES

TERRA VOLCANICS OF THE NEAR SIDE OF THE MOON

DON E. WILHELMS

Apollo 10 photographs of certain near-side terra landforms of probable volcanic origin exceed Lunar Orbiter and Apollo 8 photographs in resolution and suitability for photogrammetric measurement of slopes and heights. Possibly, the best photographs are the stereoscopic strips taken between 44° E and the terminator. These photographs cover several features that were proposed before the Apollo 8 flight as desirable targets of

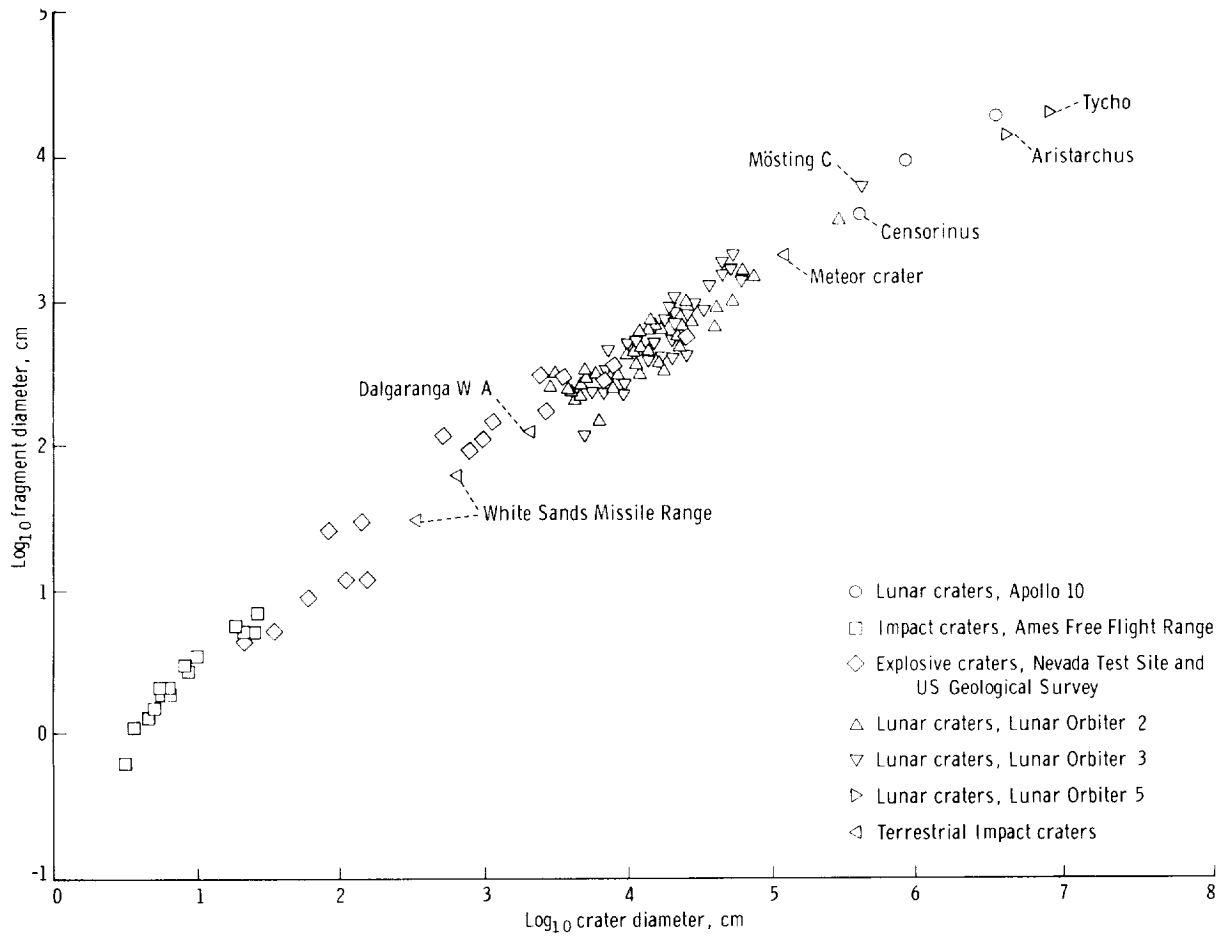

FIGURE 2–35.—Graph relating size of largest observable blocks (fragments) to diameter of crater.

opportunity. Frames AS10–32–4771 to AS10–32–4781 (magazine S), taken under good lighting conditions, show the most detail. The identification resolution is approximately 20 m, three to four times better than the Lunar Orbiter 4 photographs of the same area.

These frames show two large furrowlike craters (13 to 15 km in diameter) that are also characteristic of the Descartes area, which has been proposed for a landing mission (fig. 2–36). Terrestrial analogs tentatively suggest that such furrowlike craters, which have high to moundlike rims, were formed by eruptions of magmas with a high to intermediate content of volatiles. Smaller furrowlike or compound craters of less distinctive form also are present, mostly alined radially to the Imbrium basin (N 30° W). This alinement suggests that much volcanism in this area is controlled by the system of fractures that is radial to the Imbrium basin.

A chain of large subround craters trends transverse to the Imbrium radials (fig. 2–36). Although the shape of the individual craters is not indicative of the origin, the alinement suggests a volcanic origin. The trend of this chain indicates that fractures which are concentric to the Imbrium basin, as well as fractures that are radial to it, control volcanism.

Other probable volcanic features are small (1 to 3 km), rounded, clustered domes. Characteristics indicative of volcanism include the clustered arrangement and the presence, in at least one dome in this area and several

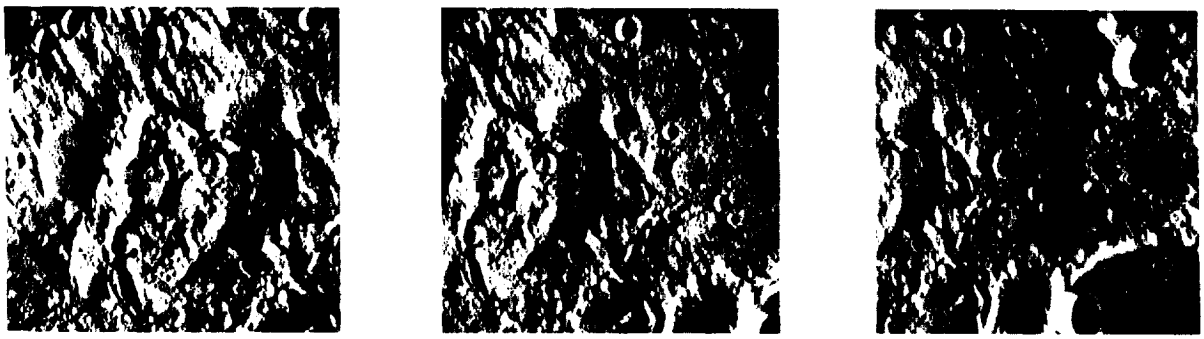

FIGURE 2–36.—Stereoscopic Apollo 10 photographs of the area between the craters Lade and Rhacticus. A chain of subround craters transverse to the Imbrium radials (upper left-hand corner of left-hand frame). One dome (upper left-hand corner of left-hand frame) has a furrowlike summit depression (AS10–32–4772, AS10–32–4773, and AS10–32–4774 from magazine S).

elsewhere, of small furrowlike summit depressions. In the Hyginus-Triesnecker region, additional examples of these features were photographed obliquely (fig. 2–37).

Additional clustered hills of probable volcanic origin, larger than those previously discussed, are in an elongate irregular depression in the rim of the crater Maskelyne A (target of opportunity 92) near Censorinus (fig. 2–38). The freshness of some of the other probable volcanic features in this area was faintly apparent in the Lunar Orbiter photographs and was confirmed by the higher resolution Apollo 10 photographs (fig. 2–39). These features are desirable targets

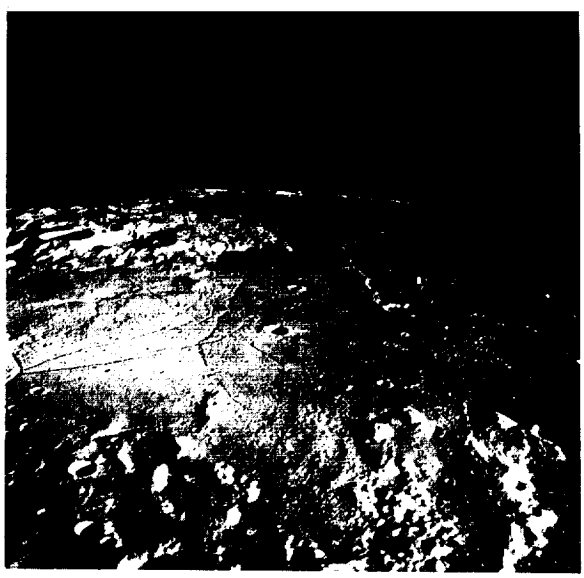

FIGURE 2–37.—Apollo 10 oblique photograph showing the Hyginus crater chain at right center; northern segment of chain is alined radially to the Imbrium basin. Clustered small domes and three furrowlike irregular craters at the summits of steep hills are in the lower right-hand corner. Crater Hyginus A (near center) is 8 km in diameter (AS10–32–4813, magazine S).

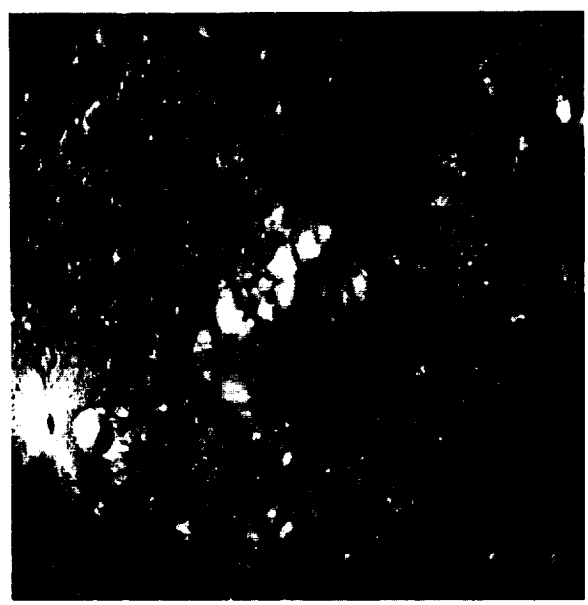

FIGURE 2–38.—Apollo 10 photograph showing large crater Maskelyne A (32 km in diameter). Sugarloaf hills in rim depression were probably formed by postcrater volcanism (AS10–28–4038, magazine O).

FIGURE 2–39.—Apollo 10 photograph showing area south of partly buried crater Maskelyne D (33 km in diameter). Sharp irregular ridges may be fresh exposures of volcanic materials (AS10–31–4258, magazine R).

for ground sampling. Lower Sun illumination at the time of photography might have brought out additional detail in the region east of Censorinus.

In summary, Apollo 10 photography has provided the best views obtained thus far of two types of volcanic landforms of the terra —furrowlike craters and clustered small domes. Also, Apollo 10 photographs have provided good views of other volcanic features.

LUNAR IGNEOUS INTRUSIONS

FAROUK EL-BAZ

Apollo 10 photographs reveal a number of igneous intrusions that include three probable dikes that crosscut the wall and floor of an unnamed 75-km crater on the far side of the Moon. These intrusions are distinguished by the setting, textures, structures, and brightness relative to the surrounding materials. Recognition of these probable igneous intrusions in the lunar highlands augments the many indications of the heterogeneity of lunar materials and the plausibility of intrusive volcanism, in addition to extrusive volcanism, on the Moon.

A number of interesting regions on the far side of the Moon were photographed during the Apollo 10 mission. Previous photographic coverage of these regions was provided by the unmanned Luna and Lunar Orbiter spacecraft. However, the resolution, Sun angle, and viewing direction of Apollo 10 photography helped to delineate features and structures that were not evident in previous photography. One of these regions includes an unnamed, generally round, partly crenulated, relatively young, large crater that is approximately 75 km in diameter. The crater is numbered 211 on the 1967 edition of the Lunar Farside Chart (LFC–1). The center of the crater is located approximately at 5° N, 120° E, and is situated in undivided highland materials in the general area previously known as the Soviet Mountains (ref. 2–13). The crater exhibits a raised, wavy, and sculptured rim and terraced interior walls that suggest an impact origin. Also, the photographs do not delineate whether the crater is rayed; the presence of an extensive ray system is believed to be a strong criterion of the impact origin of lunar craters.

The crater is a few kilometers deep, and the depth of the floor in relation to the rim crest varies with the amount of fill. The crater wall is terraced up to six levels, and the first terrace is steeper than most—a feature common to craters of a similar size. The floor of the crater displays a prominent central peak that forms a unique Y-shape (figs. 2–40 and 2–41), with the right arm trending due north.

Apollo 10 photographs of this crater are oblique views taken at high-Sun illumination with a hand-held Hasselblad camera from an altitude of approximately 110 km from the lunar surface. The 80-mm lens (frames AS10–30–4470 to AS10–30–4474) and the 250-mm lens (frames AS10–30–4349 to AS10–30–4364) were used and provided excellent stereoscopic coverage of the crater and its environs.

Distinct layering is displayed along the crater walls, where rock ledges protrude at

FIGURE 2–40.—Part of Lunar Orbiter 1 photograph (frame M–136) showing crater 211 almost in the center. Note the Y-shaped central peaks. A detail of the marked area is shown in figure 2–41.

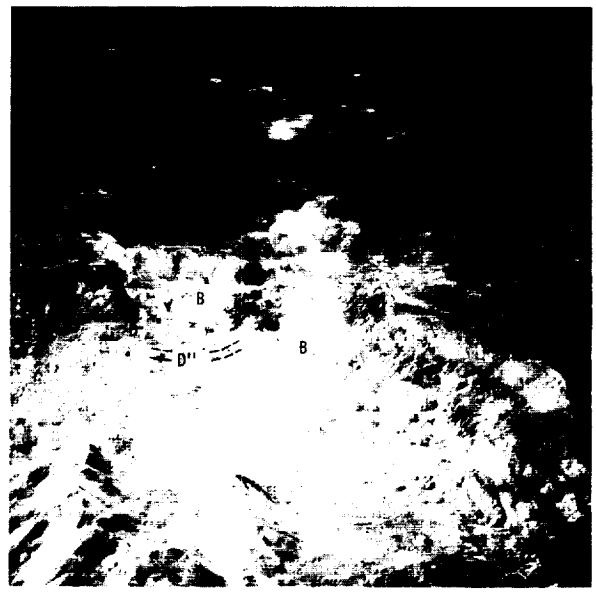

FIGURE 2–41.—Apollo 10 photograph (AS10–30–4350) showing four different types of materials: area A: mantling material that may represent lava flows of the same material in the poollike depression A′; area B: High albedo material forming domical hills that may represent part of a batholithic intrusion; area C: a segment of the crater wall typifying the character of the wall material exposed beyond the coverage of this photograph; and area D, D′, and D″: dark wall-like zones (marked with dashed lines) that may represent the outcrops of dikes.

several levels within the wall terraces. At the rim crest, the first ledge of rock can be seen along the crenulations (as in the middle of the right-hand side of fig. 2–41). At lower levels on the wall, discontinuous rock ledges could be traced for distances of approximately 10 km. These ledges indicate horizontal bedding, and the setting and textural characteristics are different from material produced by slumping and mass wasting along the walls.

In the northern segment of the crater wall, there are at least four different rock types (fig. 2–41). These rock types are distinguished by the setting, textures, structures, and relative brightness. The first rock type is exposed in area A, figure 2–41. This rock type represents a mantle of relatively young material of low albedo. This material is identical to that which could be seen in a poollike depression beyond the rim crest of the crater (area A′, fig. 2–41). The rim crest of the crater is part of an extensive unit that covers a region of several thousand square kilometers, as previously noted in the Apollo 8 photography (refs. 2–14 and 2–15). The textures and structures displayed by this unit are reminiscent of those exhibited by terrestrial lava flows. Wrinkles are common on the surface, especially at the lower parts of a given topographic level. The flow fronts are convex downslope and appear to be the result of a gentle or slow flow of molten material that has moved from higher to lower ground. Also, evidence exists of collapsed pool surfaces (upper left-hand edge of fig. 2–41). An alternative interpretation of this mantling material would be a debris flow or rock glacier. However, the aforementioned criteria that support an extrusive volcanic origin (i.e., a lava flow) are quite strong.

The second rock type (area B, fig. 2–41) is characterized by a very high albedo. The texture of this rock type is clearly different from that displayed by the rest of the crater wall. This crater wall represents a third rock type; a typical segment is shown on area C, figure 2–41. The brightest segment of the

crater wall (area B, fig. 2–41) is characterized by a great number of massive domical hills. These hills are separated by shallow furrows that are filled by darker, probably fine-grained debris material. This strongly indicates that this segment of the crater wall is made of a rock type that is dissimilar to that exposed elsewhere along the crater wall. The former may represent an exposure of intrusive, probably batholithic rock mass. This bright mass of rock displays steep contacts. The exposed portion of the rock mass appears to dip outward from the crater wall. The unusually high albedo of this material is not caused by a mantle of bright material. Bright rays from the crater Giordano Bruno (37.7° N, 102.5° E, on LFC–1 and best seen on Lunar Orbiter 5 frame M181), which were erroneously interpreted from Luna 3 photographs as the Soviet Mountains (ref. 2–13), are evident in the vicinity of the crater. The characteristics of these bright rays are easily distinguishable from the characteristics of what is interpreted here as an intrusive rock mass.

Two major zones of extremely dark rocks within the bright segment of the northern wall of the crater represent the fourth rock type. This rock type (area D, fig. 2–41) displays closely spaced discontinuous linear outcrops of rock that crosscut the wall material. The outcrops are localized in a 2-km-long zone, with an average width of approximately 0.5 km. The zone, which trends in a northwesterly direction, is texturally different and is much darker than the enclosing wall materials. By Earth analogy, this zone probably represents a dike. An alternative explanation would be that it is a segment of the layered wall material that has rotated through slumping to stand on the edge. However, the appearance and the setting of this rock support the interpretation of a dike.

Farther east, to the right of this dike, another zone of the crater wall displays a similar dark color. In this case, the first ledge from the top is nearly black. A dark zone approximately 2 km in width extends for a short distance beyond the rim crest of the crater. This zone includes a linear structure that may also represent a dike (area D′, fig. 2–41). Also, the dark layers overlying the lighter wall terrace can be seen in this area. The latter occurrence, however, probably represents a shedding from the upper rock mass.

A slightly arcuate and discontinuous line of rock outcrops within the crater floor represents a third probable dike (area D′, fig. 2–41). The outcrops are similar to the exposed rocks of the aforementioned probable intrusions. Again, the rocks are texturally different from the enclosing material. The discontinuous outcrops are raised above the surrounding terrain and appear to be much darker than the surrounding terrain.

Dark outcrops of rock are also evident on top of the central peaks, especially along the sides of the right arm of the Y-shaped chain of mountains. These occurrences of dark blocks on the central peaks may be related to the intrusive rock material. They represent either extensions of the same material or a similar rock type that was brought to the surface by the cratering event. Additional photography at higher resolutions on future Apollo missions would help to delineate these relationships.

The Flamsteed P ring in Oceanus Procellarum has been interpreted as a ring dike (ref. 2–15). A prominent zone within one of the central peaks of the crater Copernicus has also been interpreted as a possible lunar dike (ref. 2–16). The recognition of this new locality of probable igneous intrusions in the far-side highlands is strong evidence for the heterogeneity of lunar materials (ref. 2–17). It is also an additional criterion for the plausibility of intrusive volcanism, in addition to extrusive volcanism, on the Moon.

PHOTOMETRY

EVALUATION OF PHOTOMETRIC SLOPE DEVIATION

B. K. Lucchitta

Good stereoscopic-pair photography covering Apollo landing site 2 was obtained from

the Apollo 10 mission. Maps of the area can be prepared by photogrammetric methods using the stereoscopic-pair photographs. Slope profiles of the landing site were prepared by photometric methods to evaluate the precision of the photometric method, to ascertain how much detail is shown in the photometric slope profiles, and to correlate the photometric profiles and photogrammetric points so that the errors occurring in the integration of heights can be avoided.

To obtain the photometric slope derivation from Apollo 10 photographs, the computer program (ref. 2–18) used to determine slope derivation from Lunar Orbiter photographs (on 35-mm GRE film) was modified and used. Frame AS10–31–4537 (magazine R) provides a fairly accurate representation of the landing site, and the lighting conditions in frame AS10–31–4537 make the photograph suitable for photometric slope derivation. The following parameters of the viewing and lighting obtained from the scale of the stereoscopic model and the camera focal length were furnished by Sherman S. C. Wu, U.S. Geological Survey, Flagstaff, Ariz.

1. Longitude of the center of the frame: 24.3493°
2. Latitude of the center of the frame: 0.7875°
3. Longitude of the nadir point: 23.163°
4. Latitude of the nadir point: 0.3898°
5. Altitude: 122.939 km
6. Range (distance to the ground along the camera axis): 128.466 km
7. Tilt distance: 24.326 mm
8. Swing angle: 122.2595°
9. North deviation angle: 2°
10. Focal length: 80.238 mm
11. Solar elevation at the center of the frame: 19.8°
12. Scale: 1:1 532 939

The location of the initial points of the two areas scanned for this report (fig. 2–42) was measured on the Mann comparator using a coordinate system centered at the principal point. The Sun angle at the nadir point and the incidence angle at the principal point were calculated manually and established as 18.6° and 70.2°, respectively. A supporting

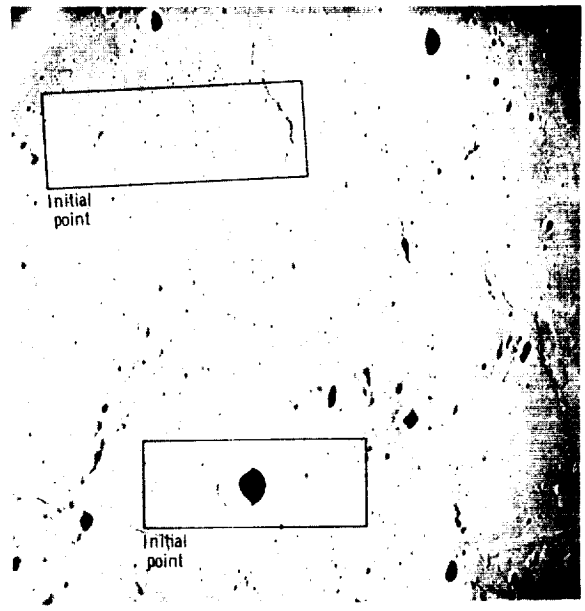

FIGURE 2–42.—Outline of scanned areas near the crater Moltke and Apollo landing site 2.

computer program gave the location of the zero-phase point with the photographic frame coordinates of the zero-phase point and the direction of the trace of the phase plane on the photograph (measured at an angle counterclockwise from the X-axis). The scan angle was given as 0.3° for the chit area covering the crater Moltke and as 1.3° for the chit area covering Apollo landing site 2. According to the parameters used, the photograph was taken on May 23 at 15 hr 2 min 24 sec, Greenwich mean time (G.m.t.).

Certain photometric quantities must be known for conversion of the film-density values to brightness values. To obtain these photometric quantities, 9 steps of the 21-step wedge at the trailing end of the film were used to calibrate the density values of the first-generation film (magazine R) with the exposure values of type 3400 film. The exposure values, density values, and brightness values are given in table 2–V. The two chit areas selected were scanned on the Joyce-Loebl microdensitometer, and the density values were coded on a minitape in 168 steps of binary-coded decimal. The machine parameters are given in table 2–VI. Each chit area is approximately 20 mm by 8 mm (20

TABLE 2–V.—*Gray-Scale Calibration Values (Positive, Magazine R)*

Step	Relative density values	Relative brightness values	Exposure values
1	2.0807	5.1329	0.0162
2	1.8949	13.1930	.0417
3	1.5481	20.9082	.0661
4	1.1518	30.2215	.0955
5	.7431	44.7152	.1413
6	.3220	63.1646	.1996
7	.1858	100.0949	.3163
8	.1329	166.1076	.5249
9	.0869	302.2152	.9550

TABLE 2–VI.—*Joyce-Loebl MK CS Microdensitometer Parameters*

Condenser, mm	32
Optical magnification	20×
Mechanical magnification	10×
Vertical aperture, mm	1.5
Horizontal aperture, mm	1.5
Spot size, mm	0.075 by 0.075
Wedge	F–362
Wedge range, density units	0 to 2.4
Encoder, levels	1 to 168

mm along the trace of the phase plane) and was covered by 15 scans 0.6 mm apart. The phase angle ranged from 72° to 89° for the landing site and from 73° to 90° for the crater site. The computer program (ref. 2–18) was processed on the IBM 360/30 computer in Flagstaff, Ariz., and the slopes, heights, and distances of all the points along each scan were calculated. The heights were printed out on cards, and this output was converted into a format acceptable to the *XYZ* plotter in Flagstaff, Ariz. The plots were compiled at a scale of 1:100 000 with a vertical exaggeration of 5×.

The profiles across crater Moltke are shown in figure 2–43. The crater has a maximum depth of 1200 m below the rim crest and a rim height of 100 to 200 m above the mare surface. The derived shape of the crater is affected by the shadow, which covers the bottom of the crater and obscures

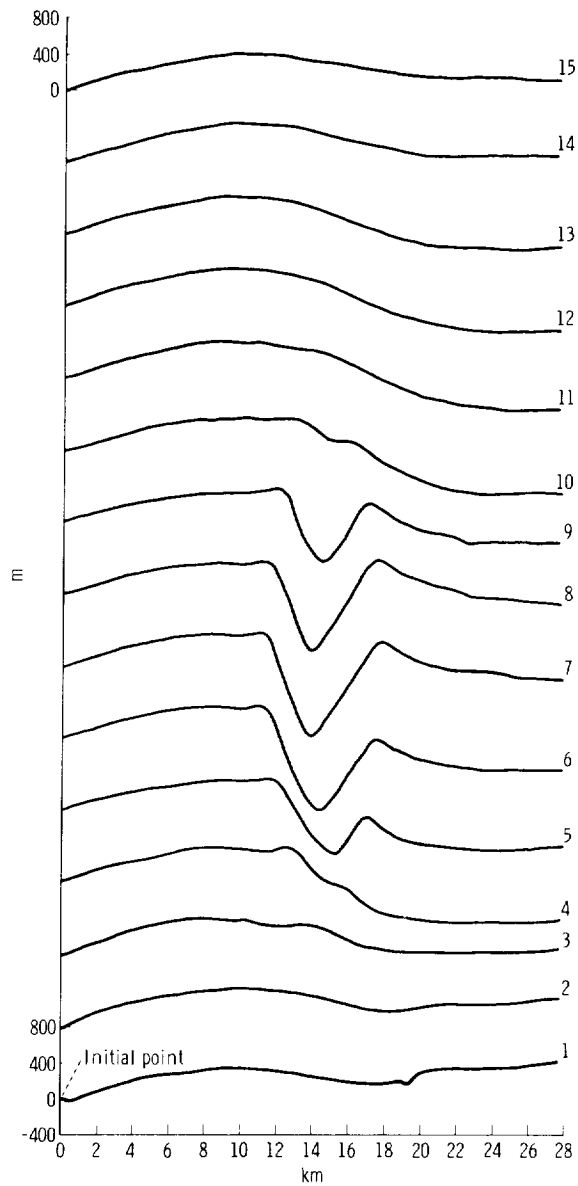

FIGURE 2–43.—Photometric profiles across the crater Moltke.

detail in the crater. The mare surface surrounding the crater is convex upward west of the crater and concave upward east of the crater. This effect may be attributed to albedo changes between the mare, the crater, and the crater halo. Because the computer program assumes that albedo is uniform and that the average brightness reflects a level surface, the mare surface with its relatively

low albedo will not be interpreted as level. The upward slopes on the west side of the crater reflect the lower albedo of the mare, and the downward slopes on the east side of the crater coincide with rays of higher albedo emanating from Moltke. Because of the low albedo of the dark halo (fig. 2–43, scan 1), the small dark halo crater east of Moltke appears to be surrounded by upward slopes.

Fifteen scans across Apollo landing site 2 are shown in figure 2–44. The area is smooth, without many noticeable craters. Apparently, the surface is not level. Inspection of the photograph and frame AS10–32–4754 (magazine S), which shows the landing site at low-phase angle, shows three rays crossing the area in a northerly direction. These rays

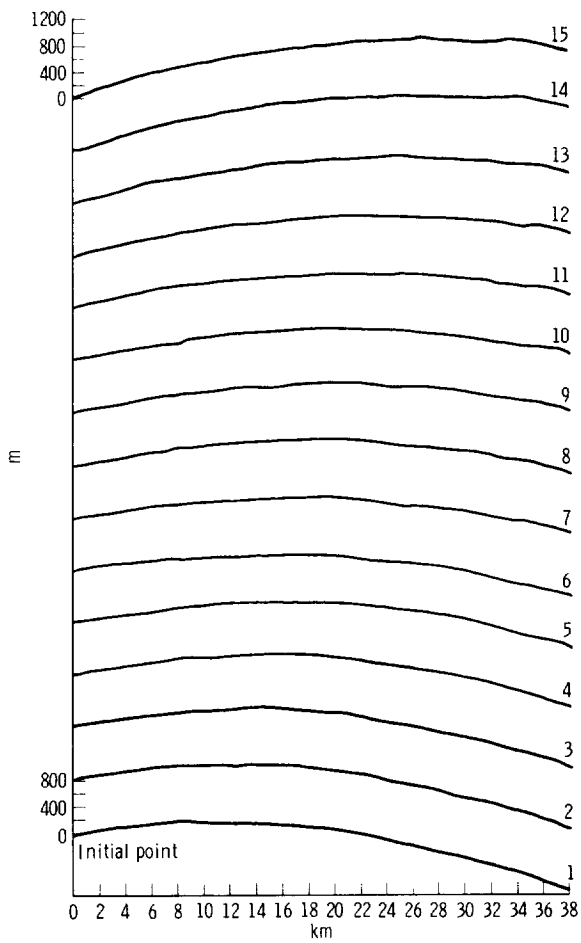

FIGURE 2–44.—Photometric profiles across Apollo landing site 2.

increase the average brightness; thus, the definition for a level surface is affected in such a way that the relatively dark mare surface will appear to be an upward slope. The middle ray is especially obvious where the southern scans cross the area. Hence, the southern scans are upward on the west side of the crater and downward on the east side of the crater, where the middle ray is most prominent. The mare ridge east of the landing site is bounded by a scarp approximately 60 m high.

The crater profiles obtained photogrammetrically are compared to profiles obtained photoclinometrically and adjusted to tie points every 5 km in figure 2–45. In the photogrammetric profile, crater Moltke is approximately 1200 m deep, with a rim height greater than 200 m. The surrounding surface is rough. The landing site appears rougher in the photogrammetric profiles (fig. 2–46) than in the photoclinometric profiles.

At the scale of the photograph (1:1 532 939), the scanning spot covers an area of 115 m by 115 m on the ground. No small features appear on the profiles. At this scale (1:1 532 939), the photogrammetric profiles apparently give better results. Much more detailed profiles could be achieved with a high-quality enlargement of the photograph used to construct the profile or with a reduced spot size and greater frequency of points along the scan line. However, the reduced signal-to-noise ratio of the photomultiplier tube at low light levels may render the latter method unsuitable.

The photometric profiles will show prominent topographic features. However, because of albedo changes, the precision of the photometric profiles is greatly reduced if large ground areas are covered. To obtain better results from the photometric profiles, care should be taken to scan only areas of uniform albedo or to make corrections for each albedo change.

If photogrammetric tie points are available, the photometric profiles will give a fair representation of the topography. Use of the photometric profiles of an area could be helpful when stereoscopic-pair coverage of the

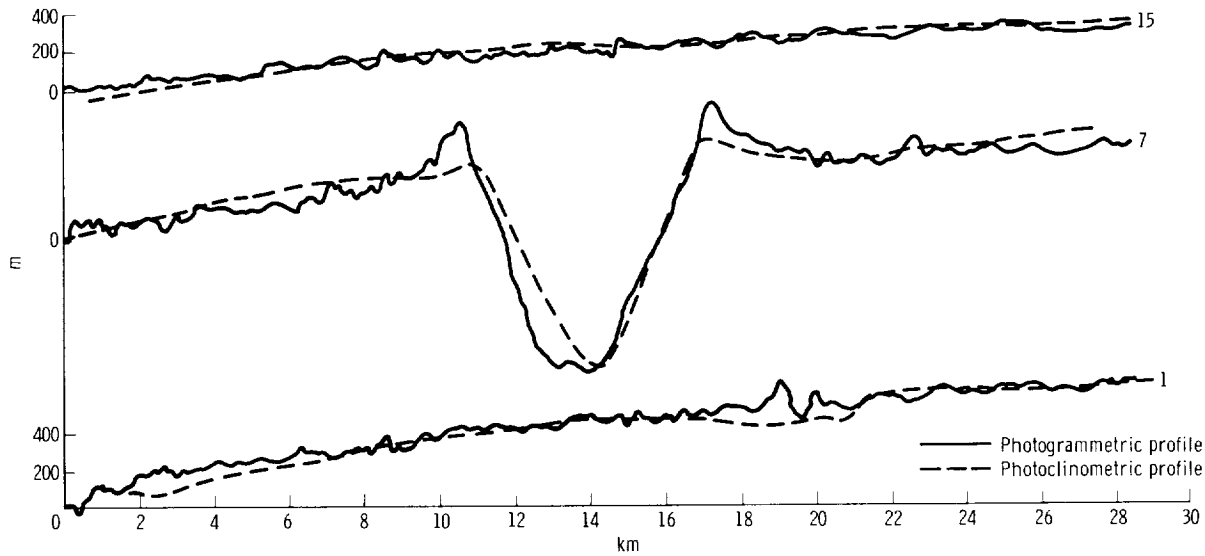

FIGURE 2-45.—Photogrammetric and adjusted photoclinometric profiles across the crater Moltke.

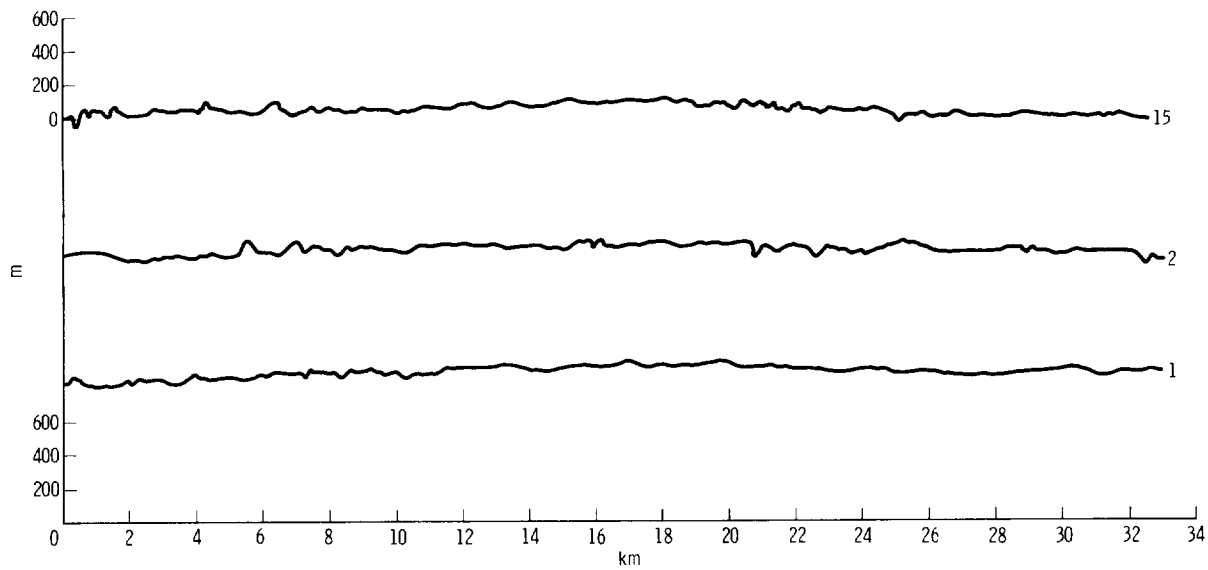

FIGURE 2-46.—Photogrammetric profiles across Apollo landing site 2.

same area is presented at a small scale and monoscopic coverage at a large scale.

THE NORMAL ALBEDO OF THE APOLLO 11 LANDING SITE AND INTRINSIC DISPERSION IN THE LUNAR HEILIGENSCHEIN

ROBERT L. WILDEY AND HOWARD A. POHN

A search of the photographic data collected from lunar orbit during the Apollo 10 mission revealed that the Apollo 11 landing site approximately corresponded to the zero-phase point in frame AS10-32-4753. By combining photographic photometry near the heiligenschein with Earth-based photoelectric-photographic photometry, it has been possible to make an accurate determination of the normal albedo in the immediate vicinity of the landing site. Accordingly, the following steps were taken. Using lunar features common to both the Apollo 10 frame and the U.S. Geological Survey map of the

normal albedo of the Moon (ref. 2–19), especially the crater Moltke, the position of the Apollo 11 landing site was identified on the albedo map. The normal albedo read directly from the map was 0.096. Furthermore, the phase angle of that particular point of the map corresponding to the epoch of acquisition of the map data was determined to be 1.5°. This point of the map was identified with a projected circular area 2 km in diameter in the Apollo 10 frame (the resolution element of the albedo map). Over this area, the Apollo frame appeared fairly homogeneous in normal albedo. The brightness over this area was averaged. The brightness was read from an isodensitracing of frame with conversion from density to relative brightness as deduced by use of the step-wedge imprint and step-wedge parameters provided with the film magazine print. Although the albedo map was given a nominal blanket correction to zero phase based on previous Earth-based work (ref. 2–20), it was desirable to remove this correction and replace it with one not only based on an observed rather than an extrapolated result but based on the local photometric function rather than on a function corresponding to either a "mean" Moon or a different lunar region such as was obtained from Apollo 8 photography (ref. 2–21). Thus, the original 5-percent brightness correction was removed, and a normalized specific intensity was obtained at $g = 1.5°$ of 0.915 (g = phase angle).

To obtain a new correction to $g = 0$, the isodensitracings of the Apollo 10 frame were analyzed, and the ratio of the original brightnesses in object space at $g = 0°$ and $g = 1.5°$ was evaluated by a method previously reported (ref. 2–21). This correction to zero phase thus deduced was +7.2 percent, which resulted in a new normal albedo of 0.098. This still refers to a circular region 2 km in diameter. From the Apollo 10 photograph, a further correction must be deduced that gives the ratio of brightness at the landing site to the average brightness of the surrounding 3 km^2. This correction, at the resolution limit of the 80-mm camera, is estimated to be between +1 and +2 percent, implying a final value of 0.099 to 0.100 for the normal albedo of the Apollo 11 landing site.

Of greater physical significance is the fact that the brightness surge from $g = 1.5°$ to $g = 0°$ at Tranquility Base as found in the present study is only 7 percent. The results of previous heiligenschein photometry (ref. 2–21) indicated that the magnitude of this phenomenon was 19 percent. This cannot be an effect produced by the greater obliquity of the terrain view in the Apollo 10 frame over that of the Apollo 8 frame, for reasons previously discussed. The results represent a true measurement of the cosmic dispersion in the lunar photometric function. Unfortunately few heiligenschein frames show sufficient homogeneity in normal albedo (and, of less significance, topography) for such dispersion to be correlated comprehensively with lunar morphology. However, the present study was carried out in maria, whereas the Apollo 8 measurement was of a region of plains in the lunar highlands. Further investigation may show that the magnitude of the zero-phase brightness surge can be correlated with fundamental lithologic properties.

PHOTOGRAPHS OF APOLLO LANDING SITE 3

N. J. Trask

Apollo 10 photographs AS10–27–3905 to AS10–27–3908 (magazine N) show Apollo landing site 3 with the lowest Sun angles (2° to 3°) yet obtained. Numerous low-relief positive features are apparent under this illumination. However, at the western edge of landing site 3, the smoothest part of the site, few low-relief positive features are observed. Some features are shown on the 1:100 000- and 1:25 000-scale geologic maps of the site (refs. 2–22 and 2–23). Other features were recognized for the first time on Apollo 10 photographs. Most of the newly observed features appear to be branches of the irregular east-west ridge system that lies north of the site. A broad plateaulike area (2 km wide) is present in the southeast part of the site. The ridges in the east-west ridge system

range from 200 to 400 m in width and are estimated to be from 2 to 5 m higher than the local surroundings. The angle of most slopes on the ridges is less than the Sun angle; the slopes do not appear to be serious hazards to landing.

Outside the landing site, but included in the area mapped at 1:100 000 (ref. 2–22), are several broad, low ridges and scarps trending generally north to south. West of the area mapped at 1:100 000 (ref. 2–22) an interesting, narrow, gently symmetrical trough is observed.

All of these gentle features—the plateau-like area, the ridges, the scarps, and the trough—suggest that mild vertical movements affected large parts of the mare material after emplacement of the material. Rectification of frames AS10–27–3905 to AS10–27–3908 may permit photogrammetric study of the low-relief positive features observed in the area of Apollo landing site 3.

PHOTOGRAMMETRY

PHOTOGRAMMETRY FROM APOLLO 10 PHOTOGRAPHY

SHERMAN S. C. WU

Except for a few segments of continuous strips of photographs, most of the photographs from the Apollo 10 mission are oblique. The quality of the vertical photography is not as good as the quality of the oblique photography, but is satisfactory for photogrammetry. For a preliminary scientific evaluation of the photogrammetric and geologic applications of the Apollo 10 photographs, it was originally planned to set up nine models in the U.S. Geological Survey analytical plotter/computer (AP/C) in Flagstaff, Ariz. The nine models would include parts of each of the seven magazines with two different focal lengths. One model would be in color. The landing sites and outstanding geological features were given first consideration in selecting the location of the models.

The lack of time and photographic supporting data precluded setting up more than six models. The three uncompleted models are of high-oblique photography that presents geometric situations that are troublesome on the AP/C, either in the relative orientation mode or in the absolute orientation mode.

The models that have been completed on the AP/C are in three different modes. They include vertical, convergent, and oblique photographs from magazines O, P, R, and S. All the photographs were taken with Hasselblad cameras, using Kodak 70-mm film (Estar Thin Base type 3400, Panatomic X aerial film). Camera focal lengths of 80 and 250 mm were used. Photographs selected from magazines P, R, and S were taken with the 80-mm-lens camera. One model taken with the 250-mm-lens camera (magazine O) was completed. For this evaluation, second-generation positive transparencies were used. No camera calibration data were available for this testing; and no data were available for computing control, except for scaling data obtained from the unmanned Lunar Orbiter photographs.

Four contour maps have been compiled from the models on the AP/C. The map of landing site 2, which was compiled from a model of magazine S, has a 200-m contour interval at a scale of 1:200 000. The map of landing site 2, which was compiled from a model of magazine R, has a 170-m contour interval at a scale of 1:100 000. The other two maps were compiled from models of magazines P and R and have 200-m contour intervals at scales of 1:100 000 and 1:200 000, respectively.

Eleven profiles were measured for geologic interpretation in four of the models. Some of the profiles were measured by using an equal incremental distance, so that statistical data can be computed for surface-roughness studies.

Most of the photographs, except for the photographs taken in color and those taken in the high-oblique mode, can possibly be used in stereopairs for establishing photogrammetric models, provided that an index of camera calibration data is available. Fur-

thermore, a system of control coordinates can be established by means of strip aerotriangulation by using the five strips of continuous photography, a total of 219 photographs.

Photographs of the Apollo 10 mission have varying scales because they were taken from the main spacecraft during orbit and from the lunar module during its approach to the lunar surface. Because the AP/C can be read to within 1μ, repeated measurements on the plotter of a specific image point in the model have produced good results from three different AP/C operators. Using a transparency (scale of approximately 1:554 000) from magazine O (taken with the 250-mm-lens camera), the standard deviations of horizontal-position pointings and elevation readings (using five readings each from the three operators) are ±3.1, ±3.3, ±5.7, and ±2.7 m; and ±9.5 and ±8.5 m, respectively. This test was also made of a model from magazine R photograph (taken with the 80-mm-lens camera) at an approximate scale of 1:1 265 000. The standard deviations of position and elevation from five repetitions by the three operators are ±6.9, ±19.3, ±10.4, and ±6.2 m; and ±14.6 and ±18.3 m, respectively.

Convergent photographs AS10–29–4199 and AS10–29–4200 (fig. 2–47), which were taken from the lunar module with the 80-mm-lens camera, were selected so that east-west and north-south profiles across a large crater could be measured. The original black-and-white photographs have a scale of 1:815 000. The model coverage is a large crater located at 133° E, 0.2° N.

The contour map of this model is shown in figure 2–48. The model was scaled by measuring the distance between similar images (H1 and H2) identified on Lunar Orbiter 1 frame M136. Leveling of this model was performed by selecting arbitrarily three points on the map (V1, V2, and V3) that appear to be approximately at the same elevation. The model scale is 1:888 495. This scale was magnified 8.8885 times to obtain the map and profile scale of 1:100 000. Parameters from the output of the AP/C for the relative and the absolute orientations are listed in table 2–VII where BX, BY, and BZ are base components and κ, ω, and ϕ are rotation components.

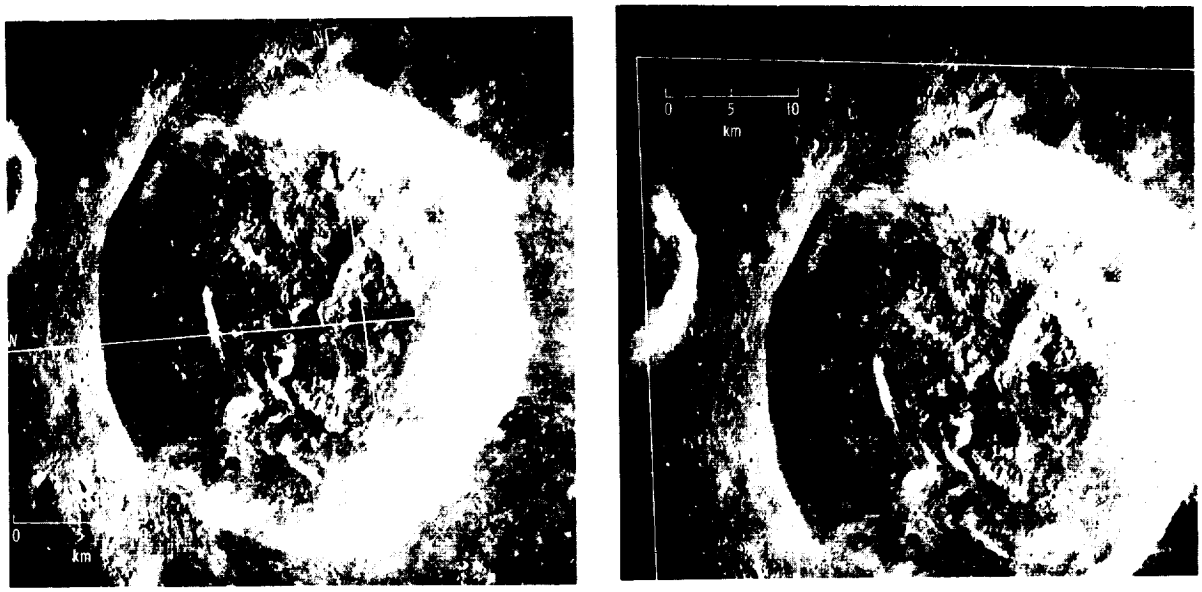

(a) (b)

FIGURE 2–47.—Photographs used in the model of convergent photography from magazine P. (a) AS10–29–4199. (b) AS10–29–4200.

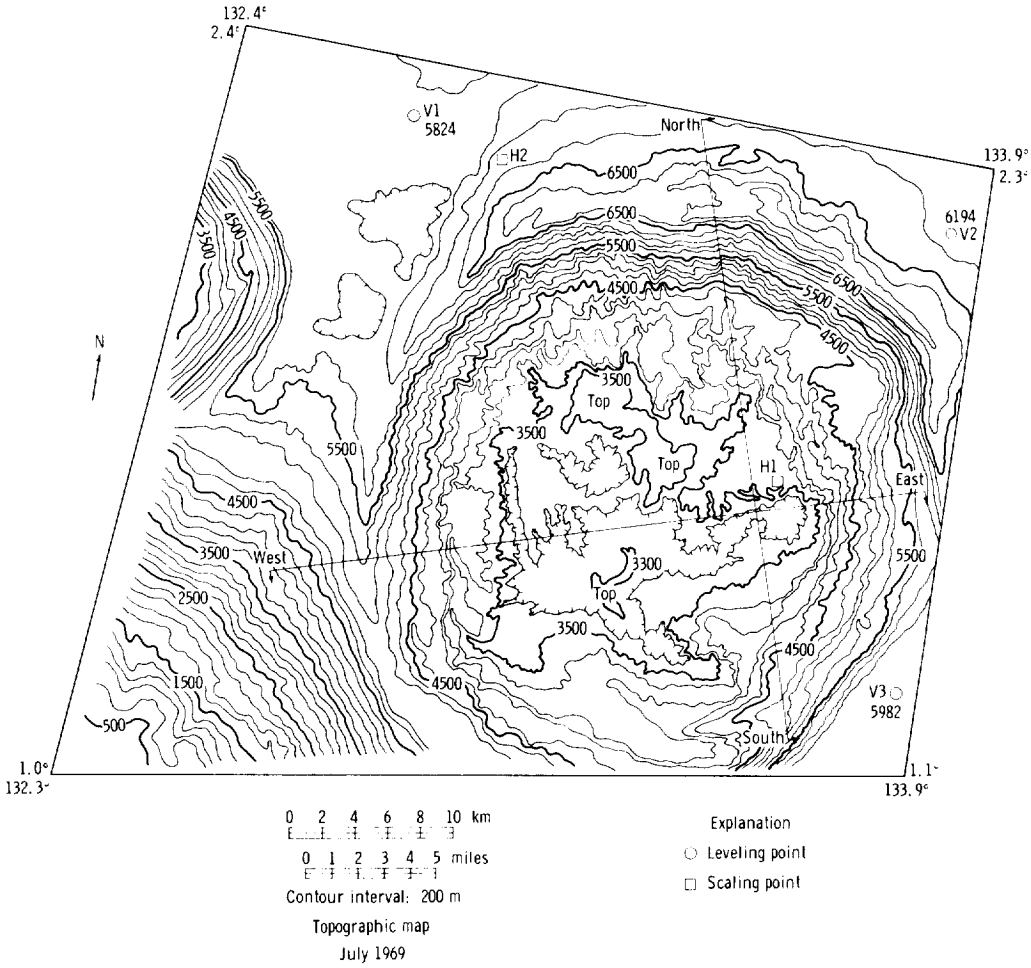

FIGURE 2-48.—Contour map of a large crater at 133° E, 0.2° N. Model was taken from photographs AS10-29-4199 and AS10-29-4200.

TABLE 2-VII.—*Parameters of Orientations for Model of Photographs AS10-29-4199 and AS10-29-4200*

Parameters	Relative orientation		Absolute orientation	
	Photograph AS10-29-4199	Photograph AS10-29-4200	Photograph AS10-29-4199	Photograph AS10-29-4200
Focal length, mm	80.283	80.283	80.283	80.283
BX, mm	−20.761	−15.781	−23.957	−18.426
BY, mm	−13.634	−15.907	−12.273	−15.374
BZ, mm	74.711	73.947	73.988	73.397
κ, deg	−4.5786	−8.3582	−4.3020	−8.1290
ω, deg	6.0732	2.5278	5.2068	2.4017
ϕ, deg	−16.6918	−16.0656	−19.2470	−18.1811

Profiles A and B (fig. 2–49) were plotted directly from the AP/C, as indicated in figure 2–47. Profile C was measured at the same location as profile B; but profile C was measured by using an equal incremental distance of 44 m, was computed on the IBM 360 computer, and then was plotted on the *XYZ* plotter. This provides the geologist with information for statistical analysis of surface roughness.

Oblique photographs AS10–28–4002 and AS10–28–4003 (fig. 2–50) of magazine O were selected because this model covers a part of the crater of the previous model at a larger scale. These photographs were taken with the 250-mm-lens camera; the original

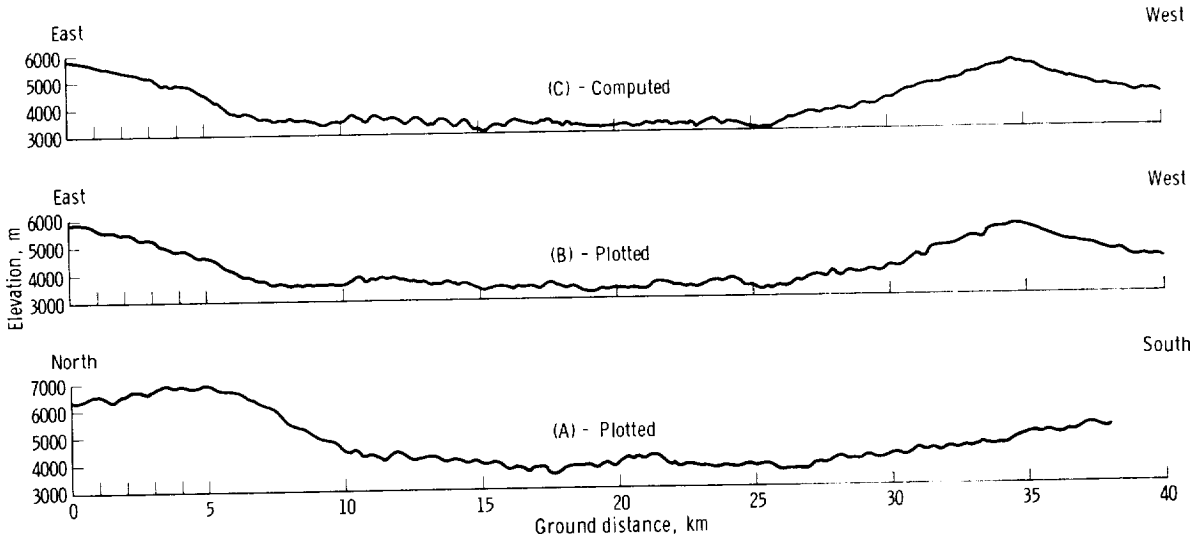

FIGURE 2–49.—Profiles from model AS10–29–4199 and AS10–29–4200, magazine P.

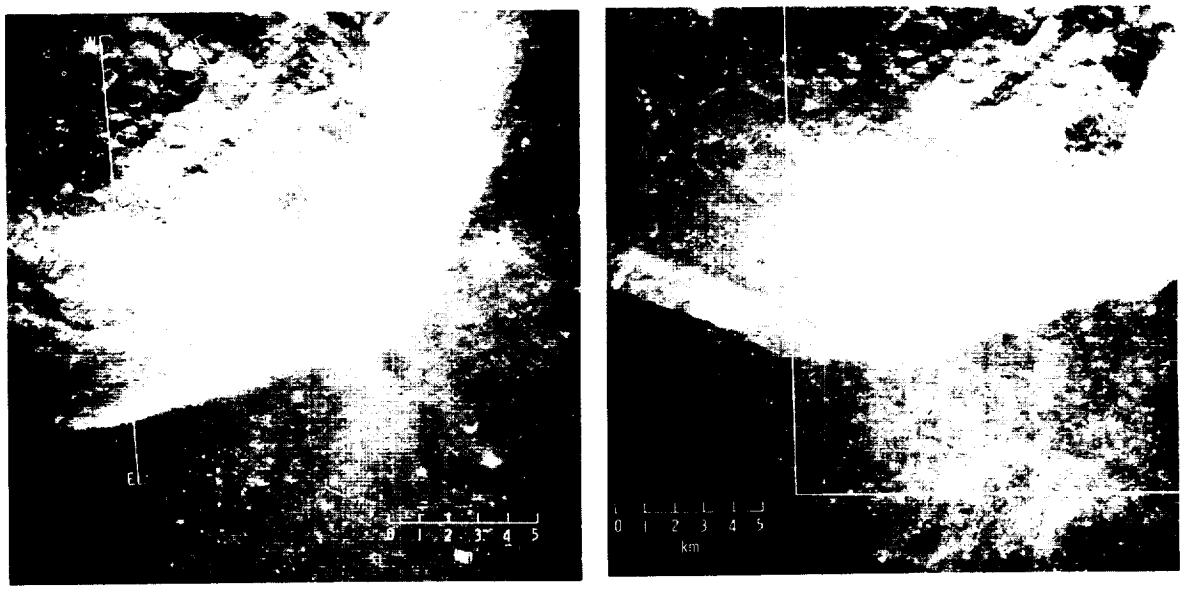

(*a*) (*b*)

FIGURE 2–50.—Photographs used in the model of oblique photography from magazine O. (*a*) AS10–28–4002. (*b*) AS10–28–4003.

photograph scale is 1:554 000. Because the model covers part of the previous model, which had a slightly larger scale of 1:585 934, absolute orientation was obtained by reading control points from the previous model.

Only two profiles were measured and plotted (fig. 2–51). These profiles provide the geologist with data for surface-roughness studies at a different scale from a different magazine. The repeatability of observations obtained from this model shows that good resolution can be obtained with the 250-mm-lens camera.

Parameters from the output of the AP/C, after relative and absolute orientations of this model, are listed in table 2–VIII.

Vertical photographs AS10–32–4848 and AS10–32–4849 (fig. 2–52) were selected because they cover the entire landing site 2. The photographs were taken with the 80-mm-lens camera with the S magazine.

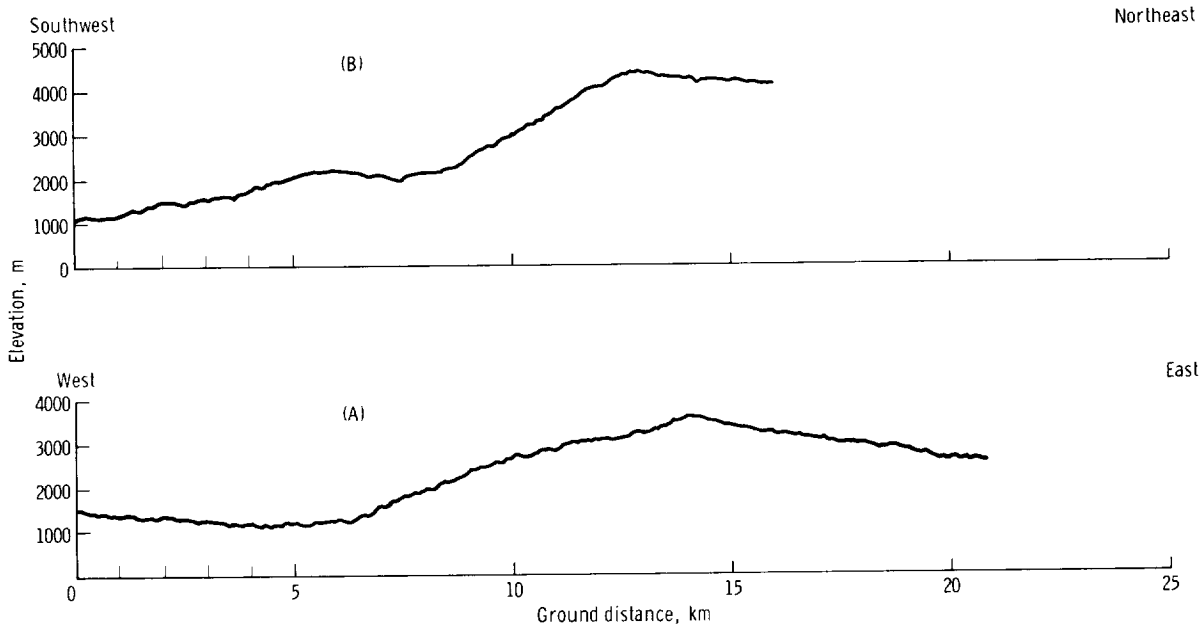

FIGURE 2–51.—Profiles from model AS10–28–4002 and AS10–28–4003, magazine O.

TABLE 2–VIII.—*Parameters of Orientations for Model of Photographs AS10–28–4002 and AS10–28–4003*

Parameters	Relative orientation		Absolute orientation	
	Photograph AS10–28–4003	Photograph AS10–28–4002	Photograph AS10–28–4003	Photograph AS10–28–4002
Focal length, mm	248.662	248.662	248.662	248.662
BX, mm	−16.864	4.760	−82.965	−56.318
BY, mm	1.980	−1.958	6.811	1.256
BZ, mm	248.083	242.515	234.306	235.891
κ, deg	.5136	−.0630	.3555	1.3512
ω, deg	−.4774	4.9710	−1.7899	4.1313
ϕ, deg	−3.8621	4.4630	−19.4450	−9.7062

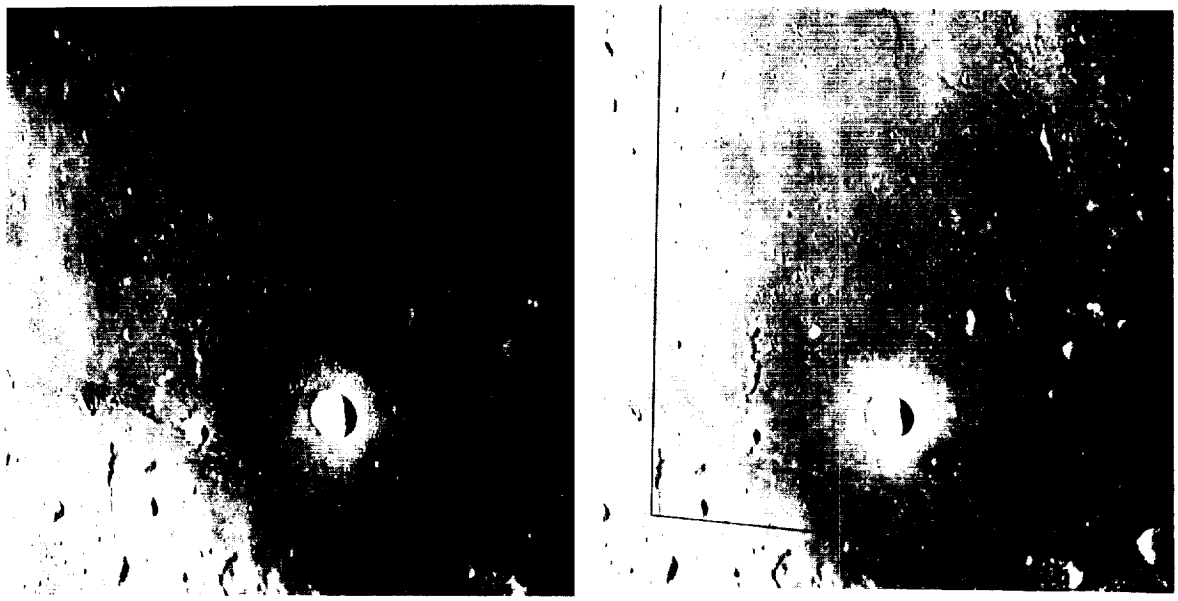

(*a*) (*b*)

FIGURE 2–52.—Photographs used in the model of vertical photography from magazine S. (*a*) AS10–32–4848. (*b*) AS10–32–4849.

For controlling this model, a model of Lunar Orbiter 2 frames M79 and M80 was set up on the AP/C to obtain both horizontal and vertical control points. The model of the Lunar Orbiter photography was oriented so that both the X- and Y-tilt angles were made equal to the two corresponding components of the original tilt angle, as given in the supporting data. Also, this model was scaled by using the coordinates of the principal point of each photograph, as given in the supporting data.

From the Apollo 10 model, a contour map (fig. 2–53) was compiled with a contour interval of 200 m at a scale of 1:200 000. To obtain this scale, the original model scale of 1:896 032 was magnified 4.4802 times. The map covers the area of Apollo landing site 2 and much more.

Elements from the output of the AP/C, after relative and absolute orientations of the model, are listed in table 2–IX.

After the absolute orientation was made by using the control from the model of Lunar Orbiter photographs, the tilt angles were 6° to 8° in the Y-direction and 25° to 30° in the X-direction (table 2–IX). These values differ from those in the NASA preliminary photographic index which described these as 1:1 375 000. A scale of 1:810 950 was calcu- vertical photographs and listed the scale as lated in this study. The leveling was rechecked by arbitrarily selecting three points (V1, V2, and V3) that appeared to be at approximately the same elevation (fig. 2–53). Both X- and Y-tilt angles were found to be even larger than on the first leveling.

The model shown in figure 2–54 was selected because it covers the Sabine area, which is located in the western part of landing site 2. The photographs were taken obliquely with the 80-mm-lens camera at a scale of 1:1 308 000.

A profile (fig. 2–55) that includes three sections for covering different ground features (fig. 2–54) was measured in the north-south direction, using an equal ground distance of 85 m. Statistical data were also computed for geological interpretation. A contour map (fig. 2–56) was compiled at a scale of 1:200 000 with a 200-m contour interval. This scale was magnified 7.0965 times over the model scale of 1:1 419 305.

For absolute orientation, this model was

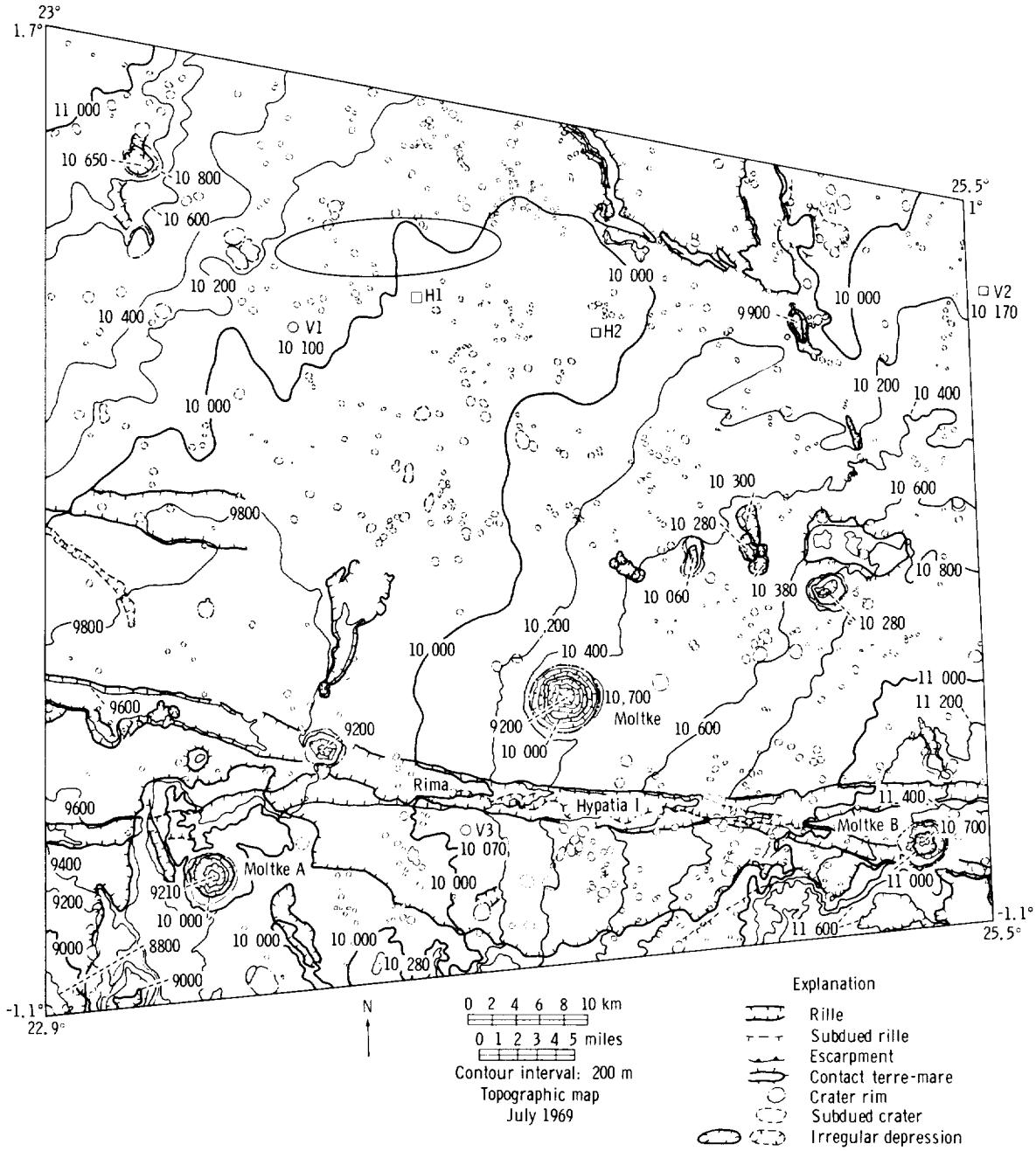

FIGURE 2–53.—Contour map taken from model AS10–32–4848 and AS10–32–4849, magazine S.

scaled by using a measured distance between image points appearing on the Lunar Orbiter frame M68, indicated as H1 and H2 on the map (fig. 2–56). This model was leveled by arbitrarily selecting three points in the model that appear approximately at the same elevation as V1, V2, and V3 (as marked on the map). An elevation of 10 000 m was assigned.

Parameters for both relative and absolute orientations from the output of the AP/C are listed in table 2–X.

TABLE 2–IX.—*Parameters of Orientations for Model of Photographs AS10–32–4848 and AS10–32–4849*

Parameters	Relative orientation		Absolute orientation	
	Photograph AS10–32–4849	Photograph AS10–32–4848	Photograph AS10–32–4849	Photograph AS10–32–4848
Focal length, mm	80.238	80.238	80.238	80.238
BX, mm	.0	14.009	31.311	46.910
BY, mm	.0	1.777	14.063	13.737
BZ, mm	80.238	86.121	72.568	72.669
κ, deg	.0	2.2830	−.4228	.0838
ω, deg	.0	1.5544	−11.1314	−8.5964
ϕ, deg	.0	4.9497	22.9327	28.1316

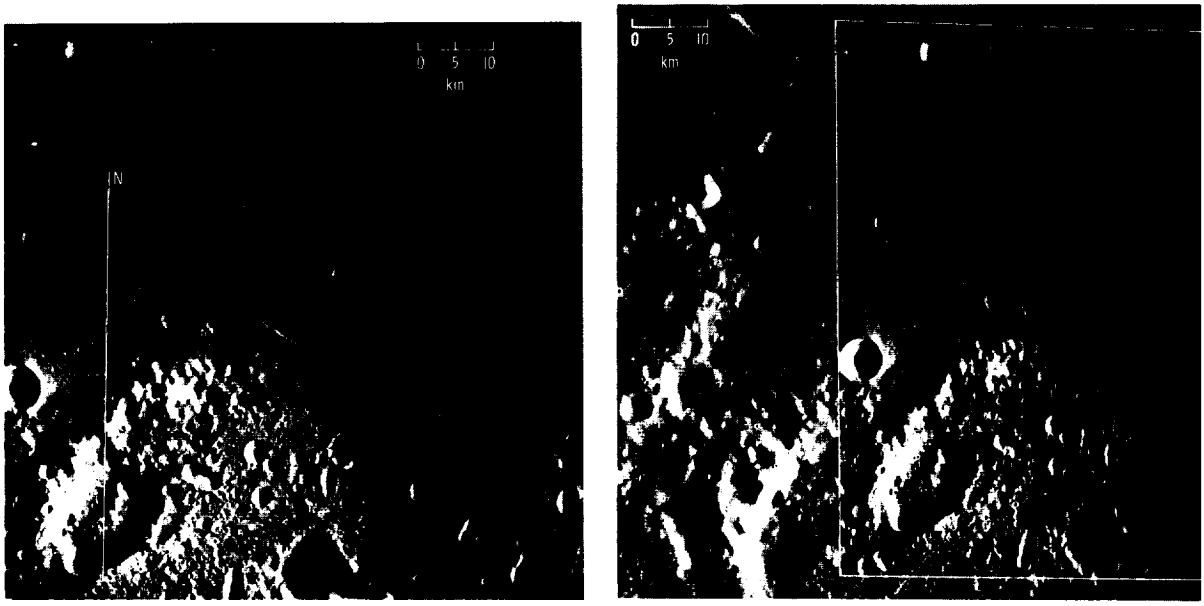

(*a*) (*b*)

FIGURE 2–54.—Oblique photographs of western part of Apollo landing site 2. (*a*) AS10–31–4540. (*b*) AS10–31–4541.

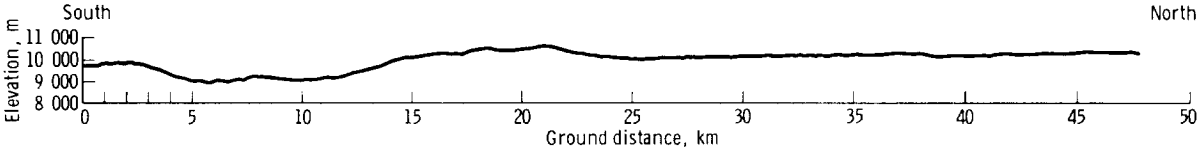

FIGURE 2–55.—Profile from model AS10–31–4540 and AS10–31–4541, magazine R.

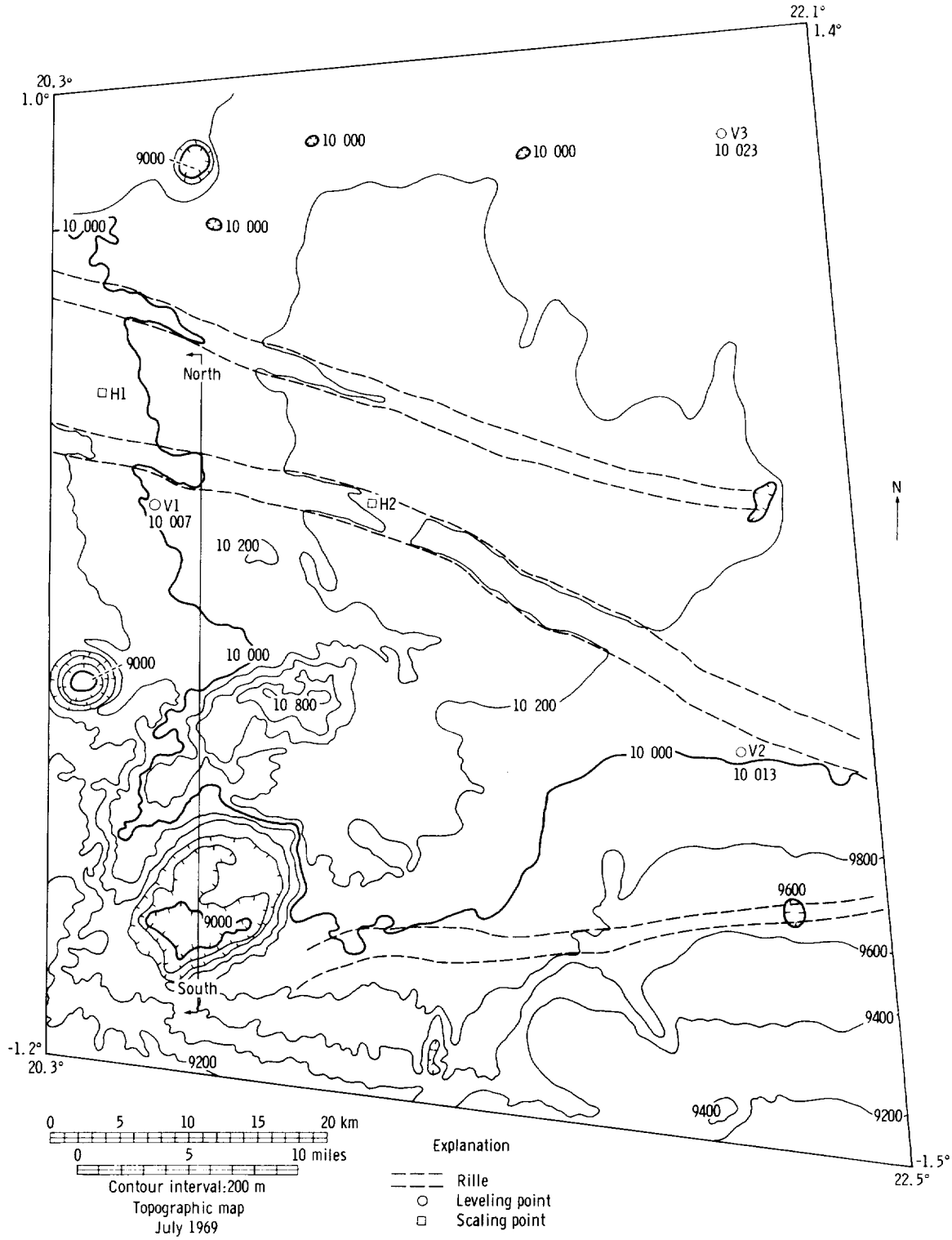

FIGURE 2-56.—Contour map taken from model AS10-31-4540 and AS10-31-4541, magazine R.

TABLE 2–X.—*Parameters of Orientations for Model of Photographs AS10–31–4540 and AS10–31–4541*

Parameters	Relative orientation		Absolute orientation	
	Photograph AS10–31–4541	Photograph AS10–31–4540	Photograph AS10–31–4541	Photograph AS10–31–4540
Focal length, mm	80.238	80.238	80.238	80.238
BX, mm	.0	21.552	−31.093	−7.967
BY, mm	.0	.047	8.399	8.399
BZ, mm	80.238	71.998	73.491	74.384
κ, deg	.0	−.0871	−.0191	.0767
ω, deg	.0	.7961	−6.4845	−5.6031
ϕ, deg	.0	3.1909	−22.8012	−19.5242

The landing site 2 was covered in the oblique photographs AS10–31–4527 and AS10–31–4528 (fig. 2–57) at an approximate original scale of 1:1 265 000. These photographs were taken with an 80-mm-lens camera with the R magazine.

The scale of this model was obtained from measurements made on Lunar Orbiter 2 frame M35. Leveling of this model was also done by arbitrarily selecting three points (V1, V2, and V3) (fig. 2–58).

A contour map was compiled at a scale of 1:100 000 with a 170-m contour interval. The scale was magnified 14.0972 times over the model scale of 1:1 409 717.

The repeatability of measurements from this model, as described in the introduction to this section, was not as good as that obtained from the photography taken at a relatively larger scale with the 250-mm-lens camera.

Parameters from the output of the AP/C,

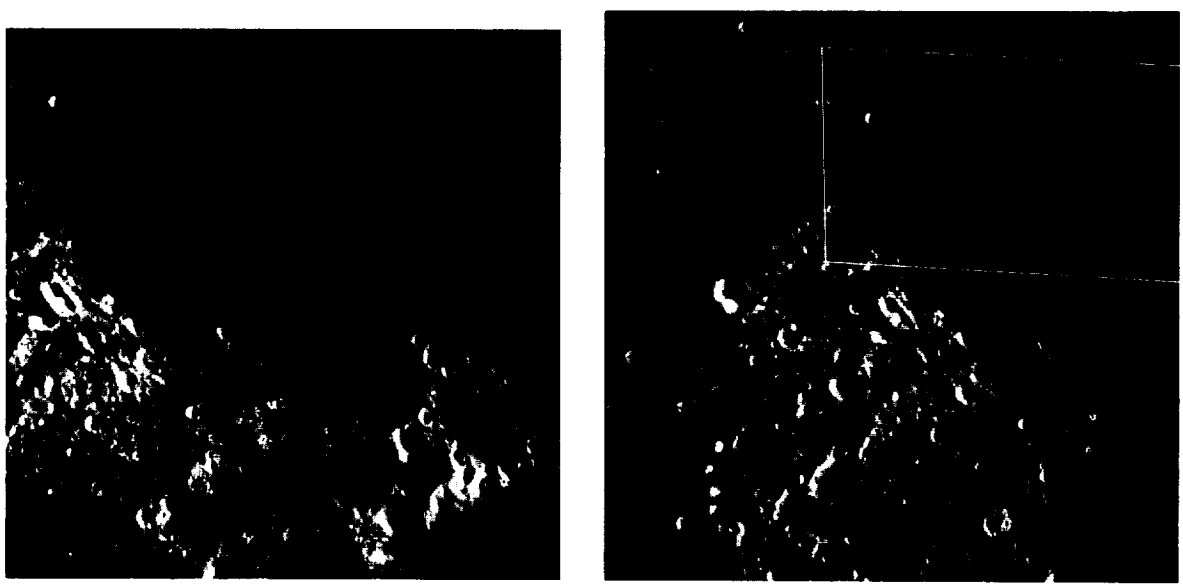

(*a*) (*b*)

FIGURE 2–57.—Apollo landing site 2. (*a*) AS10–31–4527. (*b*) AS10–31–4528.

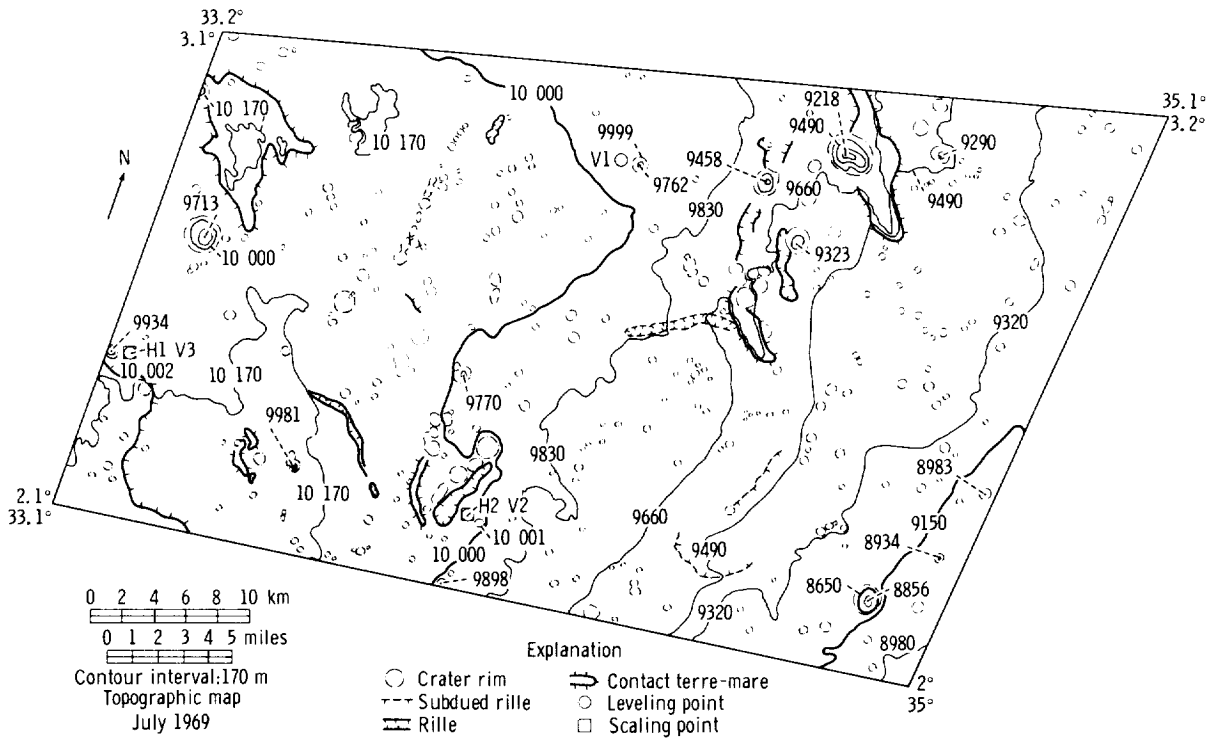

FIGURE 2–58.—Contour map of Apollo landing site 2.

after orientation of this model, are listed in table 2–XI.

According to the photographic index issued by NASA, photographs AS10–31–4537 and AS10–31–4538 (fig. 2–59) are vertical. Because this combination of photographs covers landing site 2, it was specially selected for plotting profiles to control the slope of similar profiles obtained from the isodensitracer.

Control used for this model was obtained from a model of Lunar Orbiter 2 frames M79

TABLE 2–XI.—*Parameters of Orientations for Model of Photographs AS10–31–4527 and AS10–31–4528*

Parameters	Relative orientation		Absolute orientation	
	Photograph AS10–31–4527	Photograph AS10–31–4528	Photograph AS10–31–4527	Photograph AS10–31–4528
Focal length, mm	80.238	80.238	80.238	80.238
BX, mm	.0	22.982	−24.786	−.820
BY, mm	.0	−1.394	−25.427	−26.939
BZ, mm	80.238	73.418	71.953	72.069
κ, deg	.0	−.0596	.0169	−.0152
ω, deg	.0	.0898	19.4554	19.5593
ϕ, deg	.0	2.3381	−17.9948	−15.6441

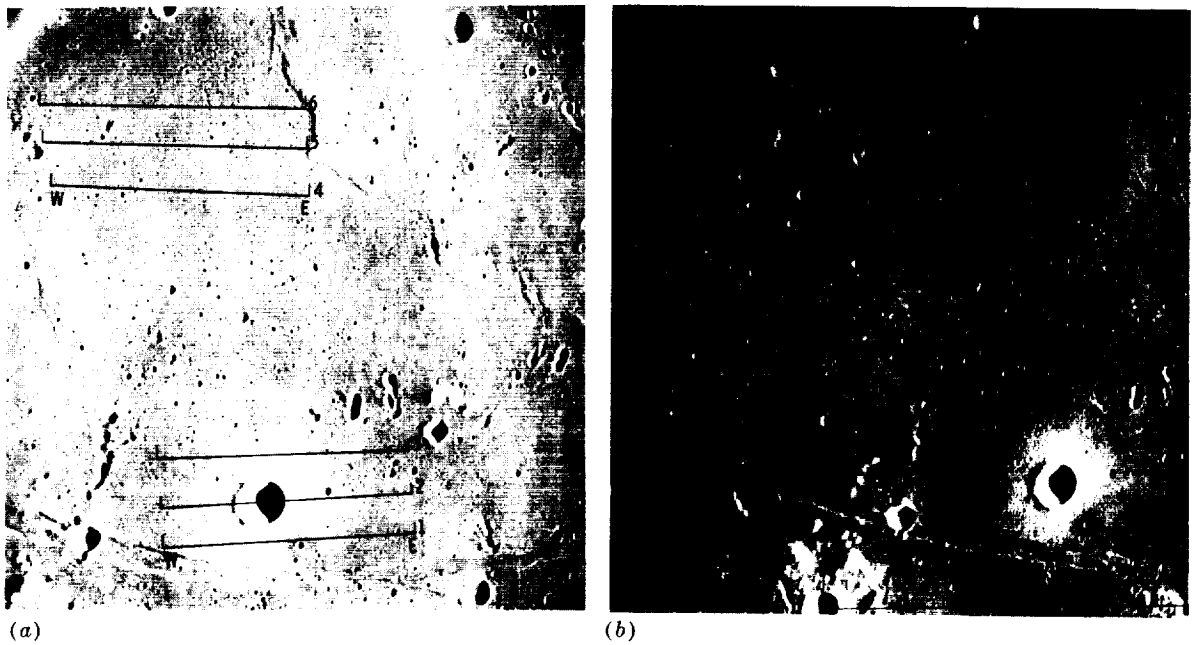

(a) (b)

FIGURE 2–59.—Vertical photographs of Apollo landing site 2. (a) AS10–31–4537. (b) AS10–31–4538.

and M80. However, there was no way to make the absolute orientation of this model so that both X- and Y-tilt angles would approach zero. It was concluded that the frames were tilted 16° to 19° in the flight direction. Based on the judgment of the operator, after the absolute orientation was established, the parameters necessary for processing photograph AS10–31–4537 on the isodensitracer are as follows:

Focal length, mm	80.238
Flight height, km	103.737
Photograph scale	1:1 293 000
Tilt angle	16°52′
Tilt distance, mm	24.326
Swing angle	192°16′
North deviation, deg	272
Sun angle, deg	19.8
Longitude of principal point	24°21′ E
Latitude of principal point	0°11′ N
Longitude of nadir point	23°10′ E
Latitude of nadir point	0°23′ N

Six profiles were plotted directly from the AP/C at a horizontal scale of 1:100 000 and a vertical scale of 1:20 000 from two different areas (fig. 2–59). The plotting scales were magnified 13.9235 times and 69.600 times, respectively, for the horizontal and vertical directions, over a model scale of 1:1 392 354.

Profiles 1, 2, and 3 (fig. 2–60) were measured from the vicinity of the crater Moltke; and profiles 4, 5, and 6 (fig. 2–60) were measured at the potential landing area of Apollo 11. These six profiles were used to control the slope of scans 1, 7, and 15 of each area from the isodensitracer. Profiles from the isodensitracer, after adjusting to the profiles from the AP/C, are shown in figure 2–61.

Unlike Apollo 8 photography, almost all of the models from Apollo 10 photographs that have been set up on the AP/C have large residuals in their relative orientation. This probably is caused by the geometric problems inherent in oblique photography and by the occurrence of very significant distortions, especially along the edges and the corners of the photographs.

The three unsuccessful models took almost as much time to process in the plotter as did the six completed models. The model of photographs AS10–34–5156 and AS10–34–5157 (magazine M, photographs in color), one model of photographs AS10–30–4334 and

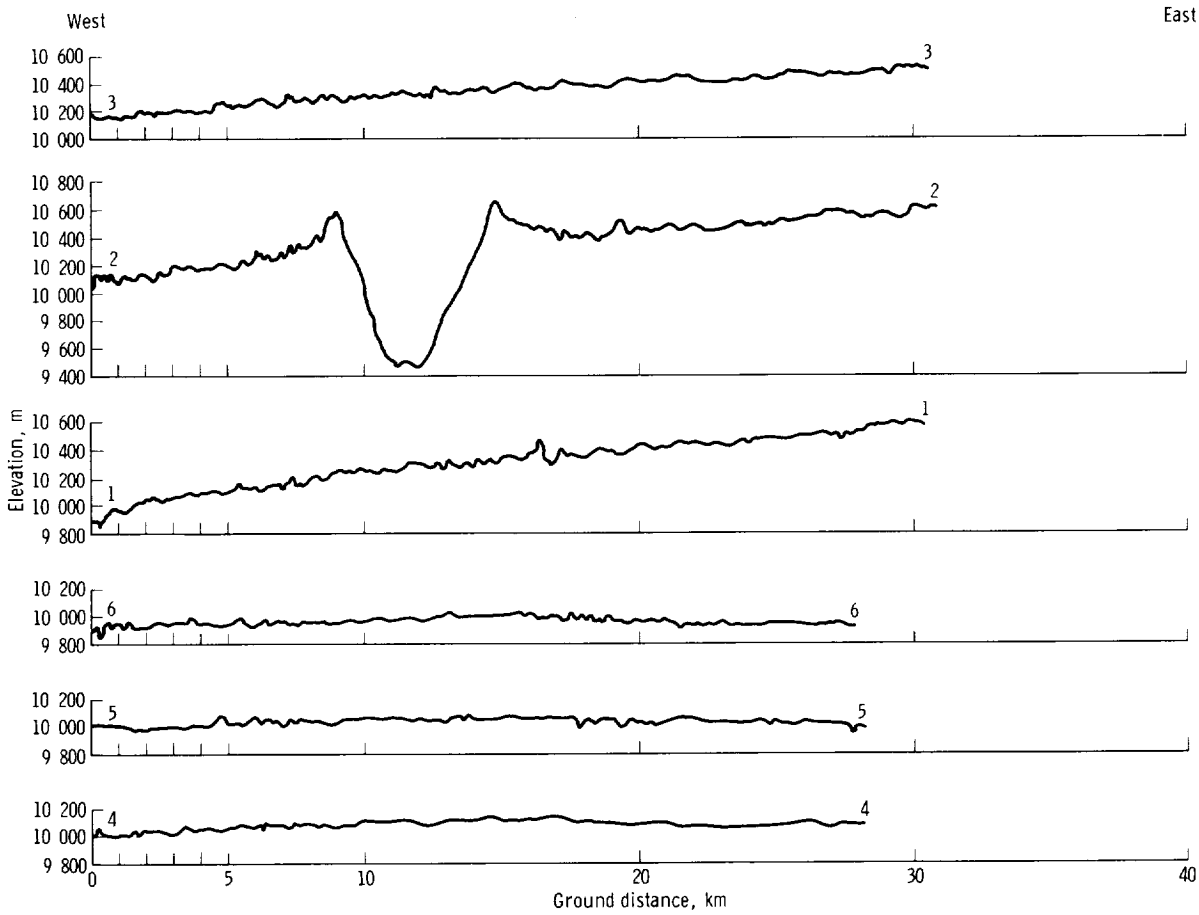

FIGURE 2-60.—Profiles from model AS10-31-4537 and AS10-31-4538, magazine R.

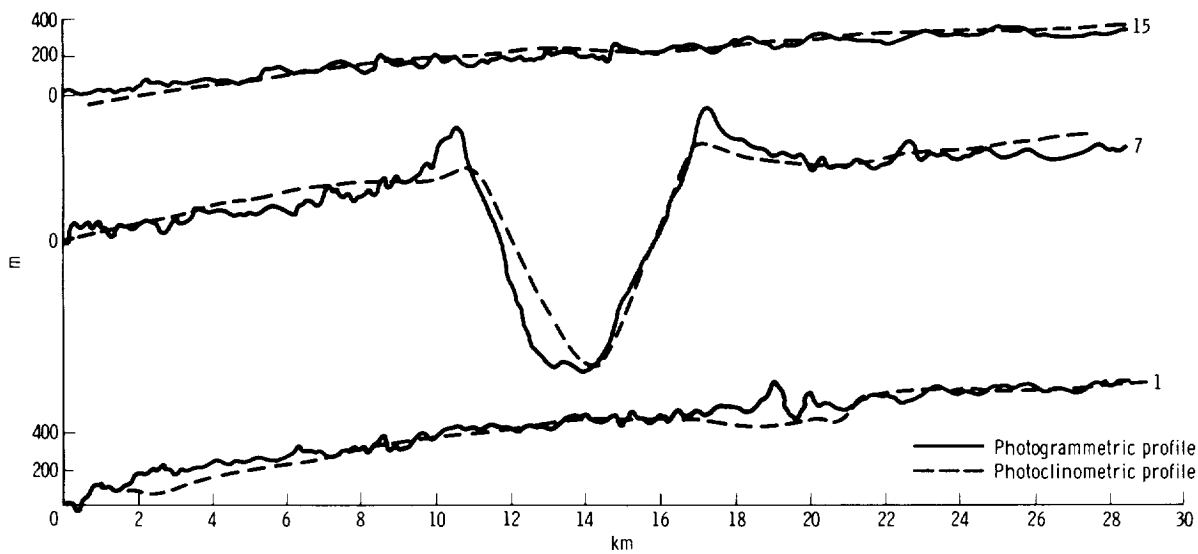

FIGURE 2-61.—Profiles for comparison between methods of photogrammetry and photoclinometry.

AS10–30–4335 (magazine Q), and the model selected from magazine T were set up carefully. However, no acceptable level of convergence in the relative orientation was obtained. All of these photographs were taken with the 250-mm-lens camera.

Although the model of photographs AS10–33–4848 and AS10–33–4849 (covering landing site 2) was set up and a contour map compiled, the model pattern was strange to the compilers. This may prove further that serious distortions occurred in the photographs.

For the six models from which satisfactory results were obtained, camera calibration data were not available; only curvature correction has been applied. The scale of each model may be slightly in error because the only source for the measurement was Lunar Orbiter photography, which also may be affected by serious distortion and tilt-angle problems.

It is recommended that, after applying corrections for the camera calibration data and avoiding the use of peripheral parts of the photographs, the strips of continuous photographs listed in table 2–XII may be used for strip triangulation by analytical solutions.

Because real-time communications do not exist with most SAO stations, predictions were generated for each station at intervals of 10 min throughout the period when the spacecraft was visible from the station. The stations were instructed to photograph the spacecraft at all times as if the waste-water dumps were occurring and to use a special procedure. The stations were also instructed to report all successful observations, to give a full description of any unusual images as soon as possible, and to forward all film by the fastest means.

The special procedure to be followed on all routine Apollo 10 photography is quoted as follows:

1. Take three frames at 32-sec cycle. Take two additional frames at same cycle but with differing filter on camera.
2. Repeat step 1 but using zero transport, shutter-latched time exp. at 32-sec cycle for one rev of gross shutter dial.
3. Repeat step 2 but for two rev of gross shutter dial. Report successful obs with full description of any unusual images asap. Forward all film via fastest means.

Copies of the predictions and instructions were sent directly to the U.S. Air Force Baker-Nunn stations.

A number of Baker-Nunn films, taken during periods when waste-water dumps were scheduled, have been examined by photoreduction with negative results. The limiting magnitude of the film taken under the most optimum conditions was estimated as approximately +10 to +11.

OPTICAL TRACKING OF APOLLO 10 FROM EARTH

EDWARD H. JENTSCH

The operational aspects of the Smithsonian Astrophysical Observatory (SAO) ef-

TABLE 2–XII.—*Continuous Photographs for Strip Triangulation*

Magazine	Photograph no.[a]	Focal length, mm	Longitude coverage, deg E	Latitude coverage, deg N
O	AS10–28–4030 to 4049	80	26 to 43	0
	AS10–28–4057 to 4163	80	180 to 76	1
Q	AS10–30–4327 to 4337	250	138 to 134	4 to 6
R	AS10–31–4500 to 4558	80	62 to 4	1
S	AS10–32–4762 to 4788	80	18 to 00	0

[a] Total photographs equal 219.

forts during the recent Apollo 10 mission are summarized in this paper. Efforts were made to obtain Baker-Nunn photographs of waste-water dumps from the spacecraft environmental control system and of liquid-oxygen dumps. The efforts for the entire mission are listed in table 2–XIII.

During the Apollo 10 mission, the major effort of SAO tracking support was aimed toward obtaining Baker-Nunn photographs of waste-water dumps from the spacecraft environmental control system. The dumps, involving approximately 50 lb of water dumped over a timespan of approximately 1½ hr, were scheduled to take place at approximately 24-hr intervals. The actual time of the dumps was decided 1 to 2 hr prior to the dump procedure.

Successful observations were reported by the stations in Argentina and India. Neither of these observations coincides with waste-water-dump times supplied by Bellcomm, Inc., to SAO. Photoreduction has confirmed that Argentina recorded 10 images of the outbound spacecraft or of the S-IVB. India obtained six images of the spacecraft a few hours prior to splashdown. These images will be checked against the actual positions of the spacecraft as soon as the necessary state vectors are obtained.

Approximately 2 hr and 12 min after translunar injection, a liquid-oxygen (LOX) dump, similar to the Apollo 8 dump photographed by the Spain station, was made. However, because of the difference in light conditions between the Apollo 8 and Apollo 10 missions, all Baker-Nunn stations that were in a position to view the LOX dump were in daylight. Previous calculations had shown that daylight photography was marginal. The Mount Hopkins staff had formulated a technique for daylight photography with the Baker-Nunn camera. Two stations, Mount Hopkins and Hawaii, were requested to attempt the daylight photography of the Apollo 10 S-IVB fuel dump. The stations were requested to obtain images by using suitable neutral-density filter combinations, exposure times, and so forth. Neither attempt was successful.

At two other stations, Peru and Florida, sunset occurred within 40 min and within 2 hr, respectively, of the LOX dump initiation. Peru was requested to search visually for the LOX cloud prior to sunset; however, they were to delay photographing until after sunset, which would improve the lighting conditions. Photographic instructions were as follows:

1. Take 4 frames at 8-sec cycle rate. Take two additional frames with diffuser filter in place.
2. Repeat step 1 using 32-sec cycle rate.
3. Repeat step 1 but for each frame make exposure using 16-sec cycle rate; zero transport with shutter-latch on for one rev of gross shutter dial.
4. Repeat step 3 but for 3 rev of gross shutter dial for each frame.

   Steps 1 through 4 should be repeated until LOX cloud disappears. Twice during cloud's existence take sequence of photographs using polarizing filter at orientations of 0, 30, 60, 90, 150, and 180 degrees. At each orientation take two time exposures using 32-sec cycle, zero transport, and shutter-latch for one rev of shutter dial.

The Peru station subsequently reported that the dump was detected neither visually nor photographically. (The U.S. Air Force Baker-Nunn station in Florida was completely clouded over during the LOX dump; therefore, no photography was attempted.)

The Townsville, Australia, Moonwatch team used predictions sent by the SAO Moonwatch Headquarters to successfully photograph the translunar injection burn of the S-IVB booster. Twenty-nine black-and-white photographs were taken with a 35-mm camera equipped with a 200-mm telephoto lens. The film is available at SAO for analysis. Some of the photographs of the translunar injection burn are shown in figures 2–62 and 2–63. The SAO also received two excellent reports of the Apollo 10 command module reentry.

TABLE 2–XIII.—*Summary of SAO Support of Apollo 10, May 18 to 26, 1969*

[All times are given in Greenwich mean time]

Event, date time	Station[a]	Prediction period, date time	Observation period, date/time	Range, mm	Results
Earth parking orbit		None			No visibilities at SAO Baker-Nunn sites.
Translunar injection, 18 19:27	Townsville	18 19:27	18/19:26 to 18/19:29		29 photographs using 35-mm camera, 200-mm lens (Moonwatch).
Liquid oxygen dump, 18 21:40	Britain				Visual observations reported (Moonwatch).
Liquid oxygen dump, 18 21:40	9012	18 21:22 to 19 00:15	18 21:22 to 18 22:18	38 to 68	Photographed; visual search; not found; daylight and clouds.
Liquid oxygen dump, 18 21:40	9021	18 21:22 to 19 00:15			Photographed; visual search; not found; daylight (clear sky).
Liquid oxygen dump, 18 21:40	9007	18/22:18 to 19/00:39		48 to 78	Photographed; visual search; not found; twilight and low elevation.
Liquid oxygen dump, 18 21:40	9110	18/23:58 to 19/00:42	None		No photography; clouds and rain.
Water dump, 19 00:46	9021	19/00:46 to 19/01:46	19/00:43 to 19/01:41		Photographed; not found, daylight.
Water dump, 19 00:46	9110	19/00:46 to 19/01:46	None		No photography; clouds and rain.
Midcourse correction, 19/02:27	9021	19/02:27	19/02:10 to 19/02:32	88 to 92	Photographed; not found, bright sky.
Translunar coast	9021	19/03:14	None		No photography, power failure.
Translunar coast	9012	19 05:48 to 19/06:09	None	122	No photography, clouds.
Translunar coast	9117	19/06:36 to 19/07:06		125 to 130	No report.
Translunar coast	9023	19/08:58 to 19/09:52	None	144 to 146	No photography, clouds.
Translunar coast	9025	19/10:48 to 19/11:21	None	156 to 160	No photography, clouds.
Translunar coast	9006	19/14:26 to 19/15:09	None	178 to 184	No photography, clouds.
Water dump, 19 16:30	9002	19/16:19 to 19/17:03	19/16:18 to 19/17:14	190 to 195	Photographed; not found, bright sky.
Water dump, 19 16:30	9028	19 16:20 to 19 17:40	19/16:19 to 19/17:37	190 to 196	Photographed; not found, reason unknown.
Translunar coast	9091	19/18:37 to 19/19:20	19/18:37 to 19/19:24	202 to 214	Photographed; not found, reason unknown.
Translunar coast	9004	19/20:31 to 19/21:25	19/20:32 to 19/21:15	213 to 219	Photographed; not found, reason unknown.
Translunar coast	9029	19/20:59 to 19/21:53	None	216 to 221	No photography, clouds.
Translunar coast	9031	19/22:16 to 19/22:47	19/22:15 to 19/22:48	224 to 227	Photographed; successful, 10 images.
Translunar coast	9007	19 23:10 to 19/23:54		227 to 231	Photographed, not found.
Translunar coast	9110	20/00:58 to 20/02:03		235 to 242	No report.
Translunar coast	9021	20 03:10 to 20/04:09		246 to 252	No report.

Translunar coast	9113	20/03:53 to 20/04:47		250 to 255	No report.
Translunar coast	9114	20/05:28		259	No report.
Translunar coast	9012	20/05:49 to 20/06:53	20/06:03 to 20/07:06	258 to 264	Photographed; not found, reason unknown.
Translunar coast	9117	20/06:33 to 20/07:38		262 to 268	No report.
Translunar coast	9023	20/08:58 to 20/09:52	None	274 to 278	No photography, clouds.
Translunar coast	9025	20/10:49 to 20/11:43		281 to 285	No report.
Translunar coast	9006	20/14:27 to 20/15:32	20/14:27 to 20/15:39	295 to 301	Photographed; not found, bright sky.
Translunar coast	9002	20/16:19 to 20/17:24	None	304 to 309	No photography, clouds.
Translunar coast	9028	20/16:25 to 20/17:41	20/16:25 to 20/16:31	303 to 309	Photographed, not found.
Translunar coast	9091	20/18:38 to 20/19:42	20/18:48 to 20/19:51	312 to 317	Photographed, not found.
Water dump, 20/20:34	9004	20/20:33 to 20/21:38	20/20:33 to 20/21:45	319 to 324	Photographed, not found.
Translunar coast	9029	20/20:59 to 20/22:15	None	320 to 326	No photography, clouds.
Translunar coast	9031	20/22:14 to 20/22:57	None	327 to 330	No photography, clouds.
Translunar coast	9007	20/23:10 to 20/23:43		329 to 331	Photographed; not found, clouds.
Translunar coast	9007	21/00:04 to 21/00:26	None	332 to 334	No photography, predictions received late.
Translunar coast	9110	21/01:00 to 21/02:15		334 to 340	No report.
Translunar coast	9021	21/03:16 to 21/04:21		343 to 347	No report.
Translunar coast	9113	21/03:54 to 21/04:59		345 to 350	No report.
Translunar coast	9114	21/05:31		352	No report.
Translunar coast	9012	21/05:49 to 21/07:05	21/06:22 to 21/07:03	351 to 356	Photographed; not found.
Translunar coast	9117	21/06:34 to 21/07:49		353 to 359	No report.
Translunar coast	9023	21/08:57 to 21/10:13	21/09:08 to 21/10:24	363 to 367	Photographed; not found.
Translunar coast	9025	21/10:49 to 21/11:54		365 to 380	No report.
Translunar coast	9006	21/14:28 to 21/15:43	21/14:27 to 21/15:47	378 to 383	Photographed; not found, bright sky.
Translunar coast	9002	21/16:19 to 21/17:35	None	385 to 389	No photography, clouds.
Translunar coast	9028	21/16:26 to 21/17:52	21/16:26 to 21/18:00	384 to 389	Photographed; not found, bright sky.
Translunar coast	9091	21/18:39 to 21/19:44		391 to 395	No report.
Translunar coast	9004	21/20:33 to 21/21:38	21/20:34 to 21/21:41	396 to 400	Photographed; not found.
Translunar coast	9029	21/20:59 to 21/21:42	None	397 to 400	No photography, clouds.
Lunar orbit, 21/21:44 to 24/11:18		None.			
Transearth coast	9029	24/20:11 to 25/01:31		339 to 315	No report.
Transearth coast	9091	24/20:11 to 25/22:11	24/20:12 to 24/21:32	341 to 333	Photographed; not found.
Water dump, 25/02:19	9031	24/21:11 to 25/02:31	None	336 to 309	No photography, clouds.
Water dump, 25/02:19	9007	25/00:11 to 25/03:51		318 to 302	Photographed; not found, bright sky.
Water dump, 25/02:19	9110	25/00:11 to 25/04:51		317 to 296	No report.
Water dump, 25/02:19	9021	25/02:19 to 25/07:11	None	304 to 284	Station closed.
Water dump, 25/02:19	9113	25/02:19 to 25/07:31		303 to 281	No report.
Transearth coast	9114	25/03:51 to 25/07:11		301 to 283	No report.

[a] See note following table for station locations.

TABLE 2–XIII.—*Summary of SAO Support of Apollo 10, May 18 to 26, 1969*—Concluded

[All times are given in Greenwich mean time]

Event, date/time	Station*	Prediction period, date time	Observation period, date/time	Range, mm	Results
Transearth coast	9012	25 05:11 to 25 09:51	None	289 to 268	No photography, clouds.
Transearth coast	9117	25 05:51 to 25 10:51		286 to 262	No report.
Transearth coast	9023	25 08:11 to 25 13:31	25 08:36 to 25 10:41	275 to 246	Photographed; not found.
Transearth coast	9006	25 13:31 to 25 18:31	25 14:12 to 25 18:34	241 to 228	Photographed; not found, bright sky.
Transearth coast	9002	25 15:31 to 25 21:11		230 to 196	Photographed; not found, bright sky.
Transearth coast	9028	25 15:51 to 25 20:51	25 17:11 to 25 17:52	226 to 198	Photographed; not found, bright sky.
Transearth coast	9091	25 17:31 to 25 22:11	25 19:32 to 25 21:43	216 to 189	Photographed; not found, bright sky.
Transearch coast	9004	25 19:31 to 26 00:11	25 20:32 to 26 23:38	203 to 175	Photographed; not found, bright sky.
Transearth coast	9029	25 20:11 to 26 01:15	None	199 to 163	No photography, clouds.
Transearth coast	9031	25 21:11 to 26 03:11	None	194 to 153	No photography, clouds.
Transearth coast	9007	25 22:31 to 26 04:11		182 to 173	Photographed; not found, bright sky and clouds.
Transearth coast	9110	26 00:11 to 26 05:11		170 to 136	No report.
Transearth coast	9021	26 02:31 to 26 07:11		153 to 119	No report.
Transearth coast	9113	26 02:51 to 26 07:51		151 to 113	No report.
Transearth coast	9114	26 03:31 to 26 07:11		147 to 120	No report.
Transearth coast	9012	26 05:11 to 26 10:11	26 07:16 to 26 10:29	131 to 88	Photographed; not found.
Transearth coast	9117	26 05:51 to 26 11:31		127 to 77	No report.
Transearth coast	9023	26 08:11 to 26 16:31	26 11:51 to 26 13:14 26 16:10 to 26 16:34	107 to 53	Photographed; not found.
Transearth coast	9025	26 09:51 to 26 14:51		91 to 35	No report.
Transearth coast	9006	26 13:31 to 26 15:31	26 14:51 to 26 16:25	50 to 11	Photographed; successful, 6 images.
Transearth coast	9002	26 15:31 to 26 15:51		23 to 17	No report.
Transearth coast	9028	26 15:51		17	No report.
Reentry	Aircraft		26 16:40		Visual observations by 2 pilots (Moonwatch).

NOTE: Station locations:

9002	South Africa	9012	Hawaii	9028	Ethiopia	9110	Florida
9004	Spain	9021	Arizona	9029	Brazil	9113	California
9006	India	9023	Australia	9031	Argentina	9114	Canada
9007	Peru	9025	Japan	9091	Greece	9117	Johnston Island

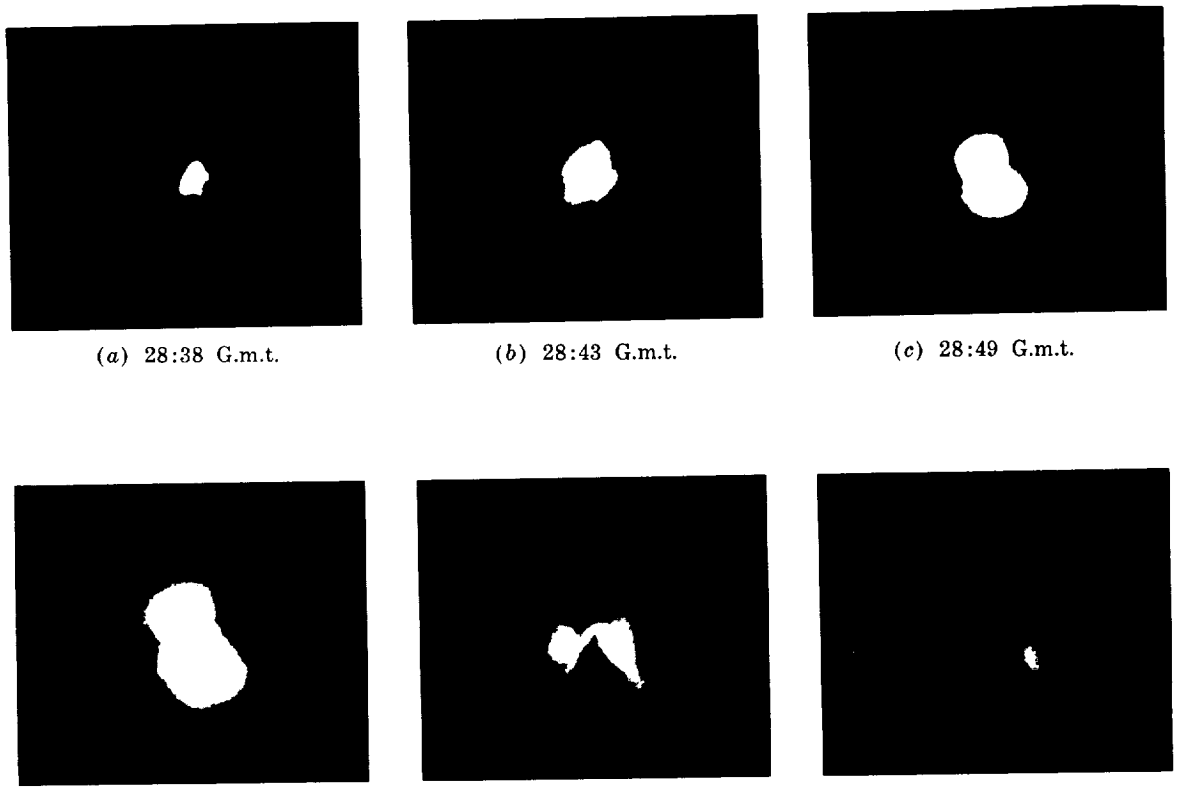

(*a*) 28:38 G.m.t. (*b*) 28:43 G.m.t. (*c*) 28:49 G.m.t.

(*d*) 28:54 G.m.t. (*e*) 29:01 G.m.t. (*f*) 29:07 G.m.t.

FIGURE 2-62.—Translunar injection burn photographs taken by the Townsville, Australia, Moonwatch team on May 19, 1969 (print 1).

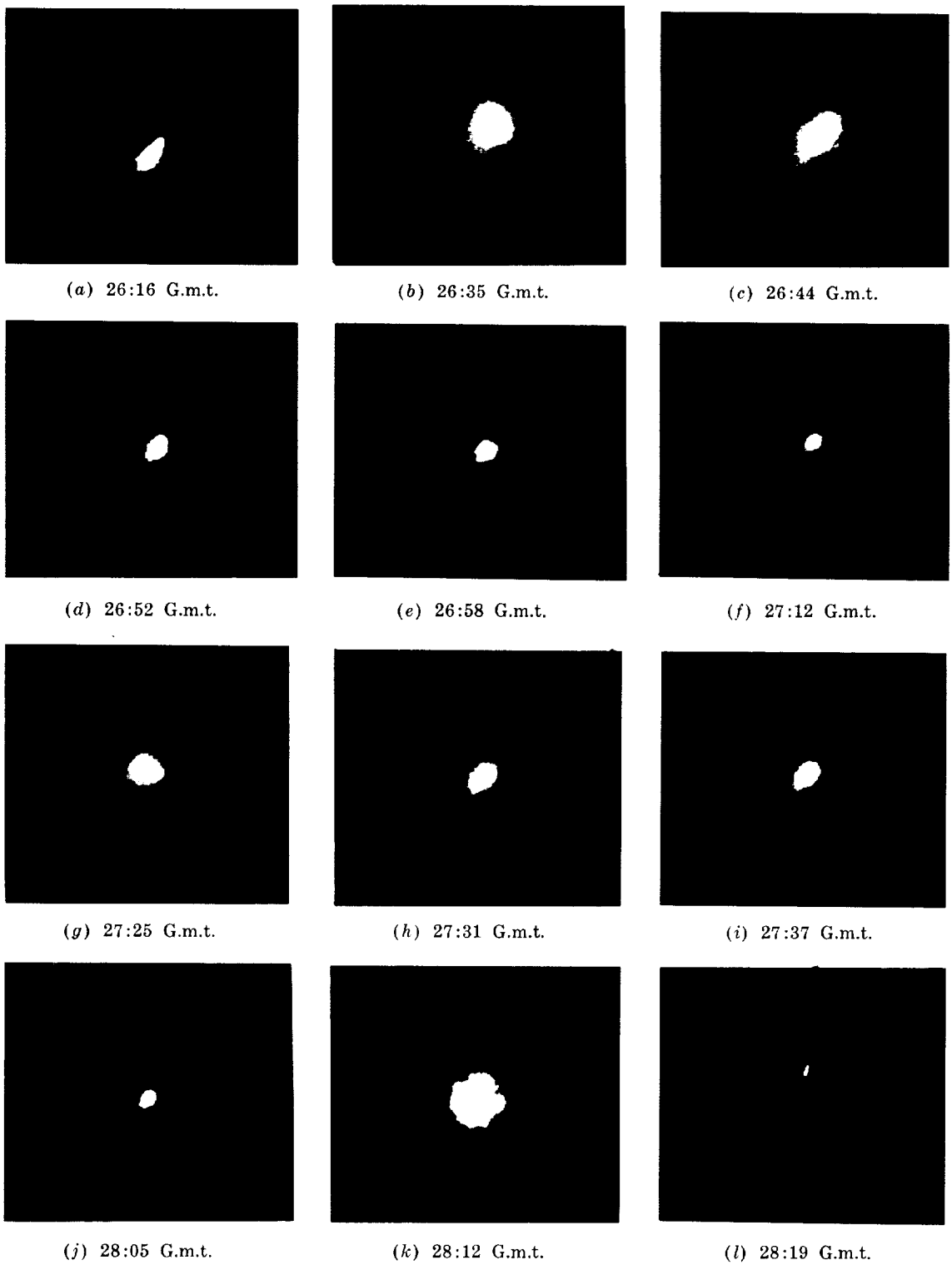

FIGURE 2–63.—Translunar injection burn photographs taken by the Townsville, Australia, Moonwatch team on May 19, 1969 (print 2).

REFERENCES

2–1. ROZEMA, W. J.: The Use of Spectral Analysis in Describing Lunar Surface Roughness. U.S. Geol. Survey Open-File Rept. (Interagency Report: Astrogeology 12), 1968.

2–2. MCCAULEY, J. F.: Terrain Analysis of the Lunar Equatorial Belt. U.S. Geol. Survey Open-File Rept., 1964.

2–3. ROWAN, L. C.; AND MCCAULEY, J. F.: Lunar Terrain Analysis. Lunar Orbiter—Image Analysis Studies Report, May 1, 1965, to January 31, 1966. U.S. Geol. Survey Open-File Rept., 1966, pp. 89–129.

2–4. PIKE, R. J.: Lunar Surface Geometry. Lunar Terrain and Traverse Data for Lunar Roving Vehicle Design Study. Prelim. U.S. Geol. Survey Rept., 1969, pp. B1–B46.

2–5. LAMBIOTTE, J. J.; AND TAYLOR, G. R.: A Photometric Technique for Deriving Slopes From Lunar Orbiter Photography. Use of Space Systems for Planetary Geology and Geophysics Conf. Paper, Boston, Mass., May 25–27, 1967.

2–6. MCCAULEY, J. F.: Geologic Map of the Hevelius Region of the Moon. U.S. Geol. Survey Misc. Geol. Inv. Map I–491, 1967.

2–7. CARR, M. H.: Geologic Map of the Mare Serenitatis Region of the Moon. U.S. Geol. Survey Misc. Geol. Inv. Map I–489, 1966.

2–8. WHITAKER, E. A.: Evaluation of the Russian Photographs of the Moon's Far Side. Comm. Lunar and Planetary Lab., Univ. of Arizona, vol. 1, no. 13, May 18, 1962, pp. 67–71.

2–9. WHITAKER, E. A.: Discussion of Named Features. Analysis of Apollo 8 Photography and Visual Observations, NASA SP–201, 1969, pp. 11–12.

2–10. ANON.: Lunar Farside Chart (LFC–1), second ed., Oct. 1967. (Air Force Chart and Information Center, St. Louis.)

2–11. STROM, R. G.: Preliminary Comparison of Apollo 8 and Lunar Orbiter Photography. Analysis of Apollo 8 Photography and Visual Observations, NASA SP–201, 1969, pp. 12–16.

2–12. MOORE, H. J.; and LUGN, R. V.: A Missile Impact in Water-Saturated Sediments. Astrogeologic Studies Ann. Prog. Rept., July 1, 1964–July 1, 1965, pt. B. U.S. Geol. Survey Open-File Rept., pp. 101–126.

2–13. WHITAKER, E. A.: Comparison with Luna III Photographs. Analysis of Apollo 8 Photography and Visual Observations, NASA SP–201, 1969, pp. 9–10.

2–14. EL-BAZ, FAROUK; and WILSHIRE, H. G.: Possible Volcanic Features—Landforms. Analysis of Apollo 8 Photography and Visual Observations, NASA SP–201, 1969, pp. 32–33.

2–15. WILHELMS, D. E.; STUART-ALEXANDER, D. E.; AND HOWARD, K. A.: Preliminary Interpretations of Lunar Geology. Analysis of Apollo 8 Photography and Visual Observations, NASA SP–201, 1969, pp. 16–18.

2–16. O'KEEFE, J. A.; LOWMAN, P. D., JR.; AND CAMERON, W. S.: Science, vol. 155, no. 3758, 1967, pp. 77–79.

2–17. EL-BAZ, FAROUK: Geologic Characteristics of the Nine Lunar Landing Mission Sites Recommended by the Group for Lunar Exploration Planning. Bellcomm TR–68–340–1, 1968.

2–18. LAMBIOTTE, J. J.; AND TAYLOR, G. R.: A Photometric Technique for Deriving Slopes From Lunar Orbiter Photography. Use of Space Systems for Planetary Geology and Geophysics Conf. Paper, Boston, Mass., May 25–27, 1967.

2–19. POHN, H. A.; and WILDEY, R. L.: A Photoelectric-Photographic Study of the Normal Albedo of the Moon. U.S. Geol. Survey Prof. Paper 599E, 1969.

2–20. WILDEY, R. L.; AND POHN, H. A.: Detailed Photoelectric Photometry of the Moon. Astron. J., vol. 69, 1964, pp. 619–634.

2–21. POHN, H. A.; RADIN, H. W.; AND WILDEY, R. L.: The Moon's Photometric Function Near Zero Phase Angle from Apollo 8 Photography. Astrophys. J., vol. 157, part 2, Sept. 1969, pp. L193–L197.

2–22. ROWAN, L. C.: Geologic Map of Lunar Orbiter Site II P–8 (Scale 1:100,000). U.S. Geol. Survey Open-File Rept., 1968.

2–23. TRASK, N. J.: Geologic Map of the Ellipse Central One Area (Scale 1:25,000). U.S. Geol. Survey Open-File Rept., 1968.

APPENDIX A

Data Availability

This appendix contains a nearly complete index of Apollo 10 photographic coverage. Included are tables that list pertinent information about each photographic frame. This information includes the frame number; the latitude and longitude of the principal point of the frame (given only when that point intercepts the lunar surface), the mode (whether an oblique or vertical view), the direction (the approximate direction the camera was aimed), the Sun angle at the principal point, and the remarks as to the region shown in the photograph, the lens used, and so forth.

Six lunar charts depict the areal coverage of the 70-mm lunar photography and the strip coverage of the 16-mm sequence camera and are included in the cover pocket of this report. The charts were prepared by the U.S. Air Force Aeronautical Chart and Information Center (ACIC) from information supplied by the NASA Manned Spacecraft Center Mapping Sciences Laboratory. These charts, when used in conjunction with the tables, make it possible to locate fairly accurately the area covered by a frame of photography. Photography of targets of opportunity (T/O) is outlined on one of the charts, covering 70-mm magazines S, T, and Q and 16-mm magazine F. Each block of grid on these charts is 5° to the side. The scale of these Mercator projections is 1:7 500 000 at the equator.

This appendix is concluded with black-and-white contact-print reproductions of all 70-mm Apollo 10 photography.

Tables A–I(*a*) to A–I(*h*) contain detailed information on the 70-mm photography. Each table represents one film magazine with consecutively numbered frames.

Magazine M (frames AS10–34–5009 to 5173) contains high-altitude views of the Earth and Moon taken during the translunar coast. There are several shots showing the extraction of the lunar module (LM) from the S-IVB, including one view of the LM and S-IVB prior to extraction. This magazine has many good shots of the lunar surface including shots of landing sites 1 and 2 and targets of opportunity 67, 74, 75, 78a, 114, 69a, 120, 128. There are many crew-select targets. There are sequence shots showing the LM in free flight, as well as a very good sequence of the LM approach and rendezvous over the far-side lunar surface.

Magazine N (frames AS10–27–3855 to 3987) contains high-altitude Earth and Moon shots taken during the translunar coast. There is an interesting sequence showing the earthrise over the lunar horizon. This magazine has three very good shots of the approach to landing site 3. There are several shots of the Earth as seen from lunar orbit. Also, there is a sequence of shots of the command and service module (CSM) as seen from the LM during the flyby maneuver showing the lunar surface in the background.

Magazine O (frames AS10–28–3988 to 4163) contains two near-vertical passes. One pass was recorded over site 2 and the other was taken on the central far side of the Moon. The 80-mm lens was used on both passes.

There are individual 250-mm vertical shots taken over the far-side lunar surface. The

targets of opportunity that are covered are 29, 33, 41, 43, 45, 78a, 112, 113, and 114. In addition, site 2 is covered with oblique photography.

Magazine P (frames AS10–29–4164 to 4326) contains photographs taken from the LM during the descent approach to landing site 2 (just missing the site). It also includes several shots of the CSM. Most of the photographs are oblique views of crew-select targets. The following targets of opportunity are at least partially covered: 29, 30, 46, 55, 57, 67, 75, 78a, and 112.

All photos were taken with an 80-mm lens. There are three excellent low-altitude obliques of Censorinus.

Magazine Q (frames AS10–30–4327 to 4499) contains an oblique sequence of landing sites 1 and 2. The following targets of opportunity are at least partially covered: 16a, 30, 34, 46, 55, 59, 67, 69a, 70, 74, 75, 76, 78, 112, 113, 114, and 123. Several crew-select oblique views are present.

Magazine R (frames AS10–31–4500 to 4674) contains a near-vertical pass from site 1 to site 2. The following areas of interest and named crater regions were photographed: Sea of Fertility, Foaming Sea, Sea of Tranquility, Maskelyne, Sabine, Delambre, and Taruntius G and K. There are far-side photographs of craters IX, 218, and 221. The following targets of opportunity (at an oblique angle) are imaged: 67, 70, 74, 76, 78a, 107, 112, 114, 116a, 123, and 128. Most of the areas were photographed with the 250-mm lens and were exposed under a high degree of Sun angle.

Magazine S (frames AS10–32–4675 to 4856) contains high-altitude photographs of the lunar surface. Both the 80- and the 250-mm lens were used.

There are sequences of vertical, near-vertical, and oblique overlapping photographs covering sites 1, 2, and 3 and targets of opportunity 29, 59, 78a, 104, 112, 114, 123, 128, and 142. Also, there are numerous crew-select targets of both Earth-side and far-side areas.

Magazine T (frames AS10–33–4857 to 5008) contains targets of opportunity, crew-select targets, and a series of obliques in the Sea of Tranquility. The following targets of opportunity were photographed: 29, 33, 34, 41, 45, 46, 55, 59, 75, 78, 114, 120, and 128.

Magazine U containing special color film was not available for screening.

Table A–II contains information on the 15 magazines of Apollo 10 16-mm sequence photography, which used SO–368 (CEX) and SO–168 (CIN) film. Eleven of these magazines contain plottable scenes of the lunar surface. Four magazines contain photographs of intravehicular activity (IVA), docking, and reentry. A review of the film in the magazines indicates that very good lunar-surface detail was obtained from high and low obliques and near-vertical sequences, as well as in many panoramic views. Most exposures were good except near the subsolar point when the rendition of scene was poor.

This index has been compiled for the benefit of those groups and individuals who wish to obtain photographic prints for further study. Inquiries should be directed to the following address:

National Space Science Data Center
Goddard Space Flight Center
Code 601
Greenbelt, Md. 20771

The 70-mm photographs can be obtained either as positive or negative film copies on 70-mm black-and-white film or as 8- by 10-in. black-and-white paper prints. The 16-mm sequence films are available as 16-mm positive or negative copies. Although the Apollo 10 mission included color photography, only black-and-white copies of these films are generally available from the Data Center.

Limited quantities of black-and-white reproductions can often be furnished without charge to researchers performing studies that require the photographs. Color reproductions or reproductions in nonstandard formats will be made available at cost to qualified users. Scientists requiring photographic data for research should inform the Data Center of their needs and identify the nature of their study; their affiliation with any sci-

entific organization, university, or company; and any contracts they may have with the Government for the performance of the investigation.

Requests for photographs should include the following information, which can be found in the charts and tables that comprise this index:

1. Mode (stereoscopic strips, sequence photography, or targets of opportunity)
2. Frame number of 70-mm photography, including letter designation of magazine
3. Magazine designation of 16-mm sequence photography
4. Format of photography (positive or negative, films or prints)

Requests for Apollo 10 photography from outside the United States should be directed to the following address:

World Data Center A for Rockets and Satellites
Goddard Space Flight Center
Code 601
Greenbelt, Md. 20771

Many general-interest requests may be satisfied with materials available in printed form. Requests of this type should be directed to the following address:

Office of Public Affairs
Goddard Space Flight Center
Code 202
Greenbelt, Md. 20771

Inquiries or requests regarding the pictures of the Earth taken from Apollo 10 should be directed to the following address:

Technology Application Center
University of New Mexico
Albuquerque, N. Mex. 87106

Prints of the Apollo 10 photography may be viewed at the National Space Science Data Center at the Goddard Space Flight Center in Greenbelt, Md. The Data Center also will supply requesters with copies of the charts published in this appendix.

The following abbreviaions are used in the 70-mm and 16-mm tables:

CSM	command and service module
FL	focal length
F/OL	forward overlap
IP	identification point
IVA	intravehicular activity
lat	latitude
LM	lunar module
long	longitude
med	medium
obliq	oblique
PP	principal point
TEI	transearth injection
TLI	translunar injection
T/O	target of opportunity
vert	vertical
VHF	very high frequency

TABLE A–I.—*Apollo 10 Hasselblad Photography*

(*a*) Magazine N, film SO–368

[Available in color]

Frame no. AS10–27–	Description	FL, mm	Vert	Obliq	Principal point		Sun angle			Photo quality	Remarks
					Long, deg	Lat, deg	High	Med	Low		
3855	CSM from LM with limb of Moon	250		X	(PP on CSM)		X			Poor	LM flyby sequence
3856	CSM from LM with limb of Moon	250		X	(PP on CSM)		X			Poor	LM flyby sequence
3857	CSM from LM with limb of Moon	250		X	(PP on CSM)		X			Good	LM flyby sequence
3858	CSM from LM with limb of Moon	250		X	(PP on CSM)		X			Good	LM flyby sequence
3859	CSM from LM with limb of Moon	250		X	(PP on CSM)		X			Good	LM flyby sequence
3860	CSM from LM with limb of Moon	250		X	(PP on CSM)		X			Good	LM flyby sequence
3861	CSM from LM with limb of Moon	250		X	(PP on CSM)					Good	LM flyby sequence
3862	CSM from LM with limb of Moon	250		X	(PP on CSM)					Good	LM flyby sequence
3863	CSM from LM with limb of Moon	250		X	(PP on CSM)		X			Good	LM flyby sequence
3864	CSM from LM with limb of Moon	250		X	(PP on CSM)					Good	LM flyby sequence
3865	CSM from LM with limb of Moon.	250		X	(PP on CSM)					Good	LM flyby sequence
3866	CSM from LM with limb of Moon	250		X	(PP on CSM)					Good	LM flyby sequence
3867	CSM from LM with limb of Moon	250		X	(PP on CSM)					Good	LM flyby sequence
3868	CSM from LM with limb of Moon	250		X	(PP on CSM)		X			Good	LM flyby sequence
3869	CSM from LM; craters 275, 207	250		X	(PP on CSM)		X			Good	LM flyby sequence
3870	CSM from LM; craters 275, 207	250		X	(PP on CSM)		X			Good	LM flyby sequence
3871	CSM from LM; craters 275, 207	250		X	(PP on CSM)		X			Good	LM flyby sequence

3872	CSM from LM; craters 275, 207	250		X	(PP on CSM)	X			Good	LM flyby sequence
3873	CSM from LM; crater 270	250		X	(PP on CSM)	X			Good	LM flyby sequence
3874	CSM from LM; northeast corner, Smyth's Sea	250		X	(PP on CSM)		X		Good	LM flyby sequence
3875	CSM from LM; northeast corner, Smyth's Sea	250		X	(PP on CSM)		X		Good	LM flyby sequence
3876	CSM from LM; northeast corner, Smyth's Sea	250		X	(PP on CSM)		X		Good	LM flyby sequence
3877	CSM from LM; northern region, Smyth's Sea	250		X	(PP on CSM)		X		Good	LM flyby sequence
3878	CSM from LM; northern region, Smyth's Sea	250		X	(PP on CSM)	X			Good	LM flyby sequence
3879	CSM from LM; northwest corner, Smyth's Sea	250		X	(PP on CSM)	X			Good	LM flyby sequence
3880	CSM from LM; northwest corner, Smyth's Sea	250		X	(PP on CSM)	X			Good	LM flyby sequence
3881	CSM from LM; northwest corner, Smyth's Sea	250		X	78 E | 0.5 S	X			Good	LM flyby sequence
3882	CSM from LM; northwest corner, Smyth's Sea	250		X	(PP on CSM)					LM flyby sequence
3883	CSM from LM; northwest corner, Smyth's Sea	250		X	(PP on CSM)					LM flyby sequence
3884	Crater 192	250		X	96.4 E | 3.8 N					LM flyby sequence
3885	Earthrise	250		X	(PP in space)					Lunar-Earth sequence
3886	Earthrise	250		X	(PP in space)					Lunar-Earth sequence
3887	Earthrise	250		X	(PP in space)	X			Good	Lunar-Earth sequence
3888	Earthrise	250		X	(PP in space)	X			Good	Lunar-Earth sequence
3889	Earthrise	250		X	(PP in space)	X			Good	Lunar-Earth sequence
3890	Earthrise	250		X	(PP in space)	X			Good	Lunar-Earth sequence
3891	Earthrise	250		X	(PP in space)	X			Good	Lunar-Earth sequence
3892	Earthrise	250		X	(PP in space)	X			Good	Lunar-Earth sequence
3893	Earthrise	250		X	(PP in space)	X			Good	Lunar-Earth sequence
3894	Earthrise	250		X	(PP in space)	X			Good	Lunar-Earth sequence
3895	Earthrise	250		X	(PP in space)	X			Good	Lunar-Earth sequence
3896	Earthrise	250		X	(PP in space)	X			Good	Lunar-Earth sequence
3897	Earthrise	250		X	(PP in space)	X			Good	Lunar-Earth sequence
3898	Earth	250			(PP in space)				Good	Lunar-Earth sequence
3899	Earth	250			(PP in space)				Good	Lunar-Earth sequence
3900	Earth	250			(PP in space)				Good	Lunar-Earth sequence
3901	Earth	250			(PP in space)				Good	Lunar-Earth sequence
3902	Earth	250			(PP in space)				Good	Lunar-Earth sequence
3903	Earth	250			(PP in space)				Good	Lunar-Earth sequence
3904	Earth	250			(PP in space)				Good	Lunar-Earth sequence
3905	Site 3	80		X	4.3 E | 1.1 N			X	Good	Lunar-Earth sequence

TABLE A-I.—*Apollo 10 Hasselblad Photography*—Continued

(*a*) Magazine N, film SO-368—*Continued*

[Available in color]

Frame no. AS10-27-	Description	FL, mm	Vert	Obliq	Principal point		Sun angle			Photo quality	Remarks
					Long, deg	Lat, deg	High	Med	Low		
3906	Site 3	80		X	0.4 E	1.4 N			X	Good	Lunar-Earth sequence
3907	Site 3	80		X	1.0 E	1.4 N			X	Good	Lunar-Earth sequence
3908	Site 3	80		X	1.0 E	1.0 N			X	Good	Lunar-Earth sequence
3909	Tycho	250			TEI					Poor	TEI
3910	Tycho	250			TEI					Poor	TEI
3911	Foaming Sea	250			TEI					Poor	TEI
3912	Foaming Sea	250			TEI					Poor	TEI
3913	Tycho	250			TEI					Poor	TEI
3914	Tycho	250			TEI					Poor	TEI
3915	Smyth's Sea	250			88 E	3 S	X			Fair	TEI
3916	Tycho; Ptolemaeus	250									
3917	Tycho; Ptolemaeus	250			TEI					Poor	TEI
3918	Smyth's Sea	250			90 E	5 S				Poor	TEI
3919	Tycho				TEI					Poor	TEI
3920	Mare Crisium	250			TEI					Poor	TEI
3921	Smyth's Sea; Langrenus	250			TEI					Poor	TEI
3922	Sea of Moscow; Sea of Waves	250			TEI					Fair	TEI
3923	Sea of Moscow; Sea of Waves	250			TEI					Poor	TEI
3924	Mare Crisium	250			TEI					Fair	TEI
3925	Mare Crisium; Cleomedes	250			TEI					Fair	TEI
3926	Mare Crisium; Langrenus	250			TEI					Fair	TEI
3927	Langrenus; Sea of Moscow	250			TEI					Fair	TEI
3928	Langrenus; Sea of Moscow	250			TEI					Fair	TEI
3929	Smyth's Sea; Sea of Moscow	250			TEI					Fair	TEI
3930	Langrenus; Sea of Moscow	250			TEI					Fair	TEI
3931	Langrenus; Mare Crisium	250			TEI					Fair	TEI
3932	Sea of Tranquility; Sea of Crises	250			TEI					Fair	TEI
3933	Sea of Nectar; Sea of Serenity	250			TEI					Fair	TEI
3934	Langrenus; Sea of Nectar	250			TEI					Good	TEI
3935	Sea of Nectar; Sea of Crises	250			TEI					Good	TEI
3936	Sea of Nectar; Border Sea	250			TEI					Good	TEI
3937	Langrenus; Humboldt	250			TEI					Good	TEI
3938	Sea of Nectar; Sea of Crises	250			TEI					Good	TEI

3939	Sea of Waves; Sea of Nectar	250			TEI				Good	TEI
3940	Sea of Nectar; Smyth's Sea	250			TEI				Good	TEI
3941	Sea of Serenity; Smyth's Sea	250			TEI				Good	TEI
3942	Mare Australe; Smyth's Sea	250			TEI				Good	TEI
3943	Mare Australe; Sea of Nectar	250			TEI				Good	TEI
3944	Mare Australe; Sea of Nectar	250			TEI				Good	TEI
3945	Mare Australe; Sea of Nectar	250			TEI				Good	TEI
3946	Sea of Nectar; Sea of Crises	250			TEI				Good	TEI
3947	Sea of Nectar; Endymion	250			TEI				Good	TEI
3948	Sea of Nectar; Endymion	250			TEI				Good	TEI
3949	Sea of Nectar; Endymion	250			TEI				Good	TEI
3950	Sea of Nectar; Endymion	250			TEI				Fair	TEI
3951	Southern Sea; Sea of Tranquility	250			TEI				Fair	TEI
3952	Earth	250			TEI (PP in space)				Fair	TEI
3953	Earth	250			TEI (PP in space)				Fair	TEI
3954	Lunar	250			TEI (PP in space)				Poor	TEI
3955	Lunar	250			TEI (PP in space)				Good	TEI
3956	Lunar	250			TEI (PP in space)				Good	TEI
3957	Lunar	250			TEI (PP in space)				Good	TEI
3958	Lunar	250			TEI (PP in space)				Good	TEI
3959	Lunar	250			TEI (PP in space)				Good	TEI
3960	Lunar	250			TEI (PP in space)				Good	TEI
3961	Lunar	250			TEI (PP in space)				Good	TEI
3962	Inside CSM	250			Inside CSM				Poor	TEI
3963	Inside CSM	250			Inside CSM				Poor	TEI
3964	Inside CSM	250			Inside CSM				Poor	TEI
3965	Inside CSM	250			Inside CSM				Poor	TEI
3966	Lunar	250			TEI (PP in space)				Fair	TEI
3967	Lunar	250			TEI (PP in space)				Good	TEI
3968	Lunar	250			TEI (PP in space)				Good	TEI
3969	Lunar	250			TEI (PP in space)				Good	TEI
3970	Earth	250			TEI (PP in space)				Good	TEI
3971	Lunar	250			TEI (PP in space)				Good	TEI
3972	Lunar	250			TEI (PP in space)				Good	TEI
3973	Lunar	250			TEI (PP in space)				Good	TEI
3974	Lunar	250			TEI (PP in space)				Good	TEI
3975	Lunar	250			TEI (PP in space)				Good	TEI
3976	Lunar	250			TEI (PP in space)				Good	Arabian Peninsula
3977	Lunar	250			TEI (PP in space)				Good	TEI
3978	Lunar	250			TEI (PP in space)				Good	TEI
3979	Earth	250			TEI (PP in space)				Good	Cloud cover
3980	Earth	250			TEI (PP in space)				Good	Cloud cover
3981	Earth	250			TEI (PP in space)				Good	Cloud cover
3982	Earth	250			TEI (PP in space)				Good	Cloud cover

TABLE A-I.—*Apollo 10 Hasselblad Photography*—Continued

(*a*) Magazine N, film SO-368—*Concluded*

[Available in color]

Frame no. AS10-27-	Description	FL, mm	Vert	Obliq	Principal point		Sun angle			Photo quality	Remarks
					Long, deg	Lat, deg	High	Med	Low		
3983	Earth	250			TEI (PP in space)					Good	Cloud cover
3984	Earth	250			TEI (PP in space)					Good	Cloud cover
3985	Earth	250			TEI (PP in space)					Good	Cloud cover
3986	Earth	250			TEI (PP in space)					Good	Cloud cover
3987	Earth	250			TEI (PP in space)					Good	Cloud cover

(*b*) Magazine O, film 3400

Frame no. AS10-28-	Description	FL, mm	Vert	Obliq	Principal point		Sun angle			Photo quality	Remarks
					Long, deg	Lat, deg	High	Med	Low		
3988	Craters 299, 297	250		X	Above horizon		X			Poor	High oblique
3989	Craters 299, 297	250		X	Above horizon		X			Poor	High oblique
3990	Craters 299, 297	250		X	Above horizon		X			Poor	High oblique
3991	Crater 297	250		X	149.0 E	4.2 S	X			Good	High oblique
3992	T/O 292	250		X	141.2 E	4.4 S	X			Good	
3993	Crater 297	250		X	148.8 E	1.8 S	X			Good	
3994		250		X	139.6 E	1.6 S	X			Good	
3995		250		X	137.4 E	1.9 S	X			Good	
3996		250	X		See Remarks		X			Good	1:420 000; not plotted; locate on magazine O frames AS10-28-4099 and AS10-28-4100
3997	T/O 33	250			138.3 E	4.2 S	X			Good	
3998		250			134.1 E	1.7 S	X			Good	Start of sequence
3999		250			134.8 E	2.2 S	X			Good	
4000		250			140.4 E	2.6 S	X			Good	End of sequence
4001	Near crater 217	250			133.0 E	0.7 S	X			Good	Start of sequence
4002	Near crater 217	250			133.2 E	0.8 S				Good	Start of sequence
4003	Near crater 217	250		X	133.5 E	0.6 N	X			Good	Start of sequence; 1:420 000
4004	Near crater 217	250	X		132.5 E	1.1 N	X			Good	30 percent F/OL with AS10-28-4001; end of sequence

4005	Craters 287, 288	250		X	132.0 E	5.8 S	X			Good	
4006	Craters 288, 290	250		X	133.7 E	7.7 S	X			Good	High oblique
4007	Craters 284, 286	250		X	130.4 E	4.8 S	X			Good	
4008	Crater 286	250		X	129.2 E	2.7 S	X			Good	
4009	Crater 290	250		X	134.0 E	5.4 S	X			Good	30 percent F OL with AS10-28-4005, AS10-28-4006; high oblique
4010	T O 41	250		X	127.5 E	4.4 S	X			Good	
4011		250		X	127.6 E	1.8 S	X			Good	
4012	T O 45	250		X	122.5 E	4.8 S	X			Good	
4013	T O 43	250		X	123.6 E	2.8 S	X			Good	
4014		250	X		See Remarks		X			Good	1:420 000; not plotted; locate on magazine O frames AS10-28-4116, AS10-28-4117, and AS10-28-4118
4015	T O 45	250		X	122.3 E	4.6 S	X			Good	
4016	T O 45	250		X	123.7 E	5.8 S	X			Good	
4017	Crater 279	250		X	118.7 E	6.2 S	X			Good	
4018		250		X	120.2 E	5.5 S	X			Good	
4019		250	X		See Remarks		X			Good	1:420 000; not plotted; locate on magazine O frames AS10-28-4121, AS10-28-4122, and AS10-28-4123
4020	Crater 277	250			114.5 E	2.2 S	X			Good	
4021	Crater 277	250			114.3 E	3.7 S	X			Good	
4022		250	X		See Remarks		X			Good	1:420 000 not plotted; locate on magazine O frames AS10-28-4126, AS10-28-4127
4023		250	X		See Remarks		X			Good	1:420 000 not plotted; locate on magazine O frame AS10-28-4217
4024		250	X		See Remarks		X			Good	1:420 000 not plotted; locate on magazine O frame AS10-28-4217
4025	Crater 273	250			109.8 E	5.1 S	X			Good	
4026	Crater 202	250			107.8 E	0.1 S	X			Good	
4027	Crater 270	250			104.4 E	4.2 S	X			Good	
4028											Not plottable
4029	T O 78a	80	X		43.0 E	0.4 S		X		Fair	1:1 345 000; near-vertical approach into and over site 2
4030	T O 78a	80	X		42.0 E	0.5 S		X		Fair	1:1 322 000
4031	T O 78a	80	X		41.0 E	0.4 S		X		Fair	1:1 328 000
4032	T O 78a	80	X		40.0 E	0.4 N		X		Fair	1:1 311 000; near-vertical approach into and over site 2

TABLE A–I.—*Apollo 10 Hasselblad Photography*—Continued

(*b*) **Magazine O, film 3400**

Frame no. AS10–28–	Description	FL, mm	Vert	Obliq	Principal point		Sun angle			Photo quality	Remarks
					Long, deg	Lat, deg	High	Med	Low		
4033	T/O 78a	80	X		39.1 E	0.4 N		X		Fair	1:1 311 000; near-vertical approach into and over site 2
4034	T/O 78a	80	X		38.0 E	0.4 N		X		Fair	1:1 311 000; near-vertical approach into and over site. 2
4035	T/O 78a	80	X		37.1 E	0.3 N		X		Fair	1:1 311 000; near-vertical approach into and over site 2
4036	T/O 78a	80	X		36.0 E	0.3 N		X		Fair	1:1 311 000; near-vertical approach into and over site 2
4037	T/O 78a	80	X		35.0 E	0.3 N		X		Fair	1:1 311 000; near-vertical approach into and over site 2
4038	T/O 78a	80	X		34.5 E	0.3 N		X		Fair	1:1 311 000; near-vertical approach into and over site 2
4039	T/O 78a	80	X		32.9 E	0.3 N		X		Fair	1:1 311 000; near-vertical approach into and over site 2
4040	T/O 78a	80	X		31.8 E	0.4 N		X		Fair	1:1 311 000; near-vertical approach into and over site 2
4041	T/O 78a	80	X		31.1 E	0.4 N		X		Fair	1:1 311 000; near-vertical approach into and over site 2
4042	T/O 78a	80	X		29.8 E	0.3 N		X		Fair	1:1 311 000; near-vertical approach into and over site 2
4043	T/O 78a	80	X		28.8 E	0.3 N		X		Fair	1:1 311 000; near-vertical approach into and over site 2
4044	T/O 78a	80	X		27.9 E	0.4 N		X		Fair	1:1 311 000; near-vertical approach into and over site 2
4045	T/O 78a	80	X		27.5 E	0.4 N		X		Fair	Vertical photograph over site 2
4046	T/O 78a	80	X		27.5 E	0.4 N		X		Fair	Vertical photograph over site 2
4047	T/O 78a	80	X					X		Fair	Near-vertical photograph over site 2
4048	Sea of Tranquility	80	X		26.6 E	0.7 N		X		Fair	1:1 328 000; near-vertical over site 2
4049	Sea of Tranquility	80	X		25.9 E	0.8 N		X		Fair	1:1 396 000; near-vertical over site 2
4050	Sea of Tranquility	80		X	25.6 E	0.9 N		X		Fair	Low oblique over site 2
4051	Sea of Tranquility	80		X	25.6 E	0.9 N		X		Fair	Low oblique over site 2

4052	Sea of Tranquility	80		X	26.1 E	0.8 N		X		Fair	High oblique over site 2
4053	T O 122	80		X	27.0 E	0.4 N		X		Fair	High oblique over site 2
4054	T O 122	80		X	Above horizon			X		Poor	High oblique over site 2
4055		80		X	Above horizon			X		Poor	High oblique over site 2
4056		80		X	Above horizon			X		Poor	End of sequence
4057	Start of sequence along 0° Lat (4057 to 4163).	80	X		178.8 W	0.1 S	X			Good	1:1 320 000; start of near-vertical sequence; long shadows
4058		80	X		179.8 W	0.1 N	X			Good	1:1 320 000; start of near-vertical sequence; long shadows
4059		80	X		179.4 E	0.1 N	X			Good	1:1 320 000; start of near-vertical sequence; long shadows
4060		80	X		178.5 E	0.1 N	X			Good	1:1 345 000; start of near-vertical sequence; long shadows
4061		80	X		177.7 E	0.2 N	X			Good	1:1 320 000; start of near-vertical sequence; long shadows
4062		80	X		176.7 E	0.3 N	X			Good	1:1 295 000; near-vertical pass
4063		80	X		175.9 E	0.2 N	X			Good	1:1 295 000; near-vertical pass
4064		80	X		174.9 E	0.3 N	X			Good	1:1 395 000; near-vertical pass
4065	Crater 225	80	X		173.9 E	0.3 N	X			Good	1:1 345 000; near-vertical pass
4066	Crater 225	80	X		172.8 E	0.4 N	X			Good	1:1 345 000; near-vertical pass
4067	Crater 225	80	X		171.9 E	0.4 N	X			Good	1:1 345 000; near-vertical pass
4068	Crater 225	80	X		170.9 E	0.5 N	X			Good	1:1 345 000; near-vertical pass
4069	Crater 225	80	X		169.8 E	0.5 N	X			Good	1:1 345 000; near-vertical pass
4070		80	X		168.9 E	0.5 N	X			Good	1:1 345 000; near-vertical pass
4071		80	X		167.7 E	0.6 N	X			Good	1:1 395 000; near-vertical pass
4072		80	X		166.8 E	0.5 N	X			Good	1:1 395 000; near-vertical pass
4073		80	X		165.7 E	0.6 N	X			Good	1:1 444 000; near-vertical pass
4074	Crater 303	80	X		164.7 E	0.5 N	X			Good	1:1 395 000; near-vertical pass
4075	Crater 303	80	X		163.7 E	0.5 N	X			Good	1:1 395 000; near-vertical pass
4076	Crater 303	80	X		162.7 E	0.5 N	X			Good	1:1 395 000; near-vertical pass
4077	Crater 303	80	X		161.6 E	0.5 N	X			Good	1:1 395 000; near-vertical pass
4078		80	X		160.6 E	0.5 N	X			Good	1:1 395 000; near-vertical pass
4079		80	X		159.7 E	0.5 N	X			Good	1:1 395 000; near-vertical pass
4080		80	X		158.9 E	0.5 N	X			Good	1:1 420 000; near-vertical pass
4081		80	X		158.2 E	0.6 N	X			Good	1:1 444 000; near-vertical pass
4082		80	X		157.4 E	0.6 N	X			Good	1:1 444 000; near-vertical pass
4083		80	X		156.3 E	0.7 N	X			Good	1:1 470 000; near-vertical pass
4084		80	X		155.2 E	0.7 N	X			Good	1:1 470 000; near-vertical pass
4085		80	X		154.4 E	0.7 N	X			Good	1:1 420 000; near-vertical pass
4086		80	X		153.5 E	0.7 N	X			Good	1:1 420 000; near-vertical pass
4087		80	X		152.4 E	0.8 N	X			Good	1:1 420 000; near-vertical pass
4088		80	X		151.4 E	0.8 N	X			Good	1:1 470 000; near-vertical pass
4089		80	X		150.4 E	0.8 N	X			Good	1:1 395 000; near-vertical pass
4090		80	X		149.0 E	0.9 N	X			Good	1:1 395 000; near-vertical pass
4091		80	X		148.2 E	0.9 N	X			Good	1:1 420 000; near-vertical pass

TABLE A-I.—*Apollo 10 Hasselblad Photography*—Continued

(*b*) Magazine O, film 3400—*Concluded*

Frame no. AS10-28-	Description	FL, mm	Vert	Obliq	Principal point		Sun angle			Photo quality	Remarks
					Long, deg	Lat, deg	High	Med	Low		
4092		80	X		147.0 E	0.8 N	X			Good	1:1 376 000; near-vertical pass
4093		80	X		146.0 E	0.9 N	X			Good	1:1 395 000; near-vertical pass
4094		80	X		144.9 E	0.8 N	X			Good	1:1 395 000; near-vertical pass
4095		80	X		143.8 E	0.9 N	X			Good	1:1 395 000; near-vertical pass
4096		80	X		142.7 E	0.9 N	X			Good	1:1 370 000; near-vertical pass
4097		80	X		141.6 E	0.8 N	X			Good	1:1 345 000; near-vertical pass
4098		80	X		140.5 E	0.7 N	X			Good	1:1 345 000; near-vertical pass
4099		80	X		139.4 E	0.7 N	X			Good	1:1 320 000; near-vertical pass
4100		80	X		138.4 E	0.7 N	X			Good	1:1 320 000; near-vertical pass
4101		80	X		137.1 E	0.7 N	X			Good	1:1 395 000; near-vertical pass
4102		80	X		136.2 E	0.6 N	X			Good	1:1 370 000; near-vertical pass
4103		80	X		135.5 E	0.6 N	X			Good	1:1 320 000; near-vertical pass
4104		80	X		134.4 E	0.6 N	X			Good	1:1 395 000; near-vertical pass
4105		80	X		133.7 E	0.9 N	X			Good	1:1 375 000; near-vertical pass
4106		80	X		132.6 E	0.9 N	X			Good	1:1 370 000; near-vertical pass
4107		80	X		131.4 E	1.0 N	X			Good	1:1 370 000; near-vertical pass
4108		80	X		130.2 E	1.0 N	X			Good	1:1 370 000; near-vertical pass
4109		80	X		129.2 E	1.0 N	X			Good	1:1 370 000; near-vertical pass
4110	Crater 282	80	X		127.9 E	1.1 N	X			Good	1:1 370 000; near-vertical pass
4111	Crater 282	80	X		127.0 E	1.0 N	X			Good	1:1 370 000; near-vertical pass
4112	Crater 282	80	X		126.0 E	1.0 N	X			Good	1:1 370 000; near-vertical pass
4113	Crater 282	80	X		124.8 E	1.0 N	X			Good	1:1 370 000; near-vertical pass
4114		80	X		123.7 E	1.0 N	X			Good	1:1 395 000; starts washing out because of high-Sun angle
4115		80	X		122.7 E	1.1 N	X			Good	1:1 420 000; high-Sun angle
4116		80	X		121.6 E	1.0 N	X			Good	1:1 420 000; high-Sun angle
4117		80	X		120.7 E	1.0 N	X			Good	1:1 370 000; high-Sun angle
4118		80	X		119.8 E	1.1 N	X			Good	1:1 370 000; high-Sun angle
4119		80	X		118.8 E	1.0 N	X			Good	1:1 370 000; high-Sun angle
4120		80	X		117.8 E	1.0 N	X			Good	1:1 370 000; high-Sun angle
4121		80	X		116.8 E	0.9 N	X			Good	1:1 370 000; high-Sun angle
4122		80	X		115.9 E	0.8 N	X			Good	1:1 345 000; high-Sun angle
4123		80	X		115.1 E	0.9 N	X			Good	1:1 345 000; high-Sun angle
4124		80	X		114.2 E	0.7 N	X			Good	1:1 345 000; high-Sun angle
4125	Craters 206, 207	80	X		113.2 E	0.8 N	X			Good	1:1 345 000; high-Sun angle

4126	Crater 207	80	X		112.2 E	0.9 N	X			Good	1:1 345 000; near-vertica l pass
4127	Crater 207	80	X		111.3 E	1.0 N	X			Good	1:1 345 000; near-vertical pass
4128		80	X		110.2 E	1.1 N	X			Good	1:1 345 000; near-vertical pass
4129	Crater 202	80	X		109.3 E	1.1 N	X			Good	1:1 345 000; near-vertical pass
4130	Crater 202	80	X		108.2 E	1.1 N	X			Good	1:1 345 000; near-vertical pass
4131	Crater 202	80	X		107.2 E	1.2 N	X			Good	1:1 345 000; near-vertical pass
4132	Crater 202	80	X		106.1 E	1.3 N	X			Good	1:1 345 000; near-vertical pass
4133		80	X		105.0 E	1.2 N	X			Good	1:1 345 000; near-vertical pass
4134		80	X		103.6 E	1.2 N	X			Good	1:1 345 000; near-vertical pass
4135		80	X		102.8 E	1.3 N	X			Good	1:1 345 000; near-vertical pass
4136		80	X		102.1 E	1.3 N	X			Good	1:1 345 000; near-vertical pass
4137		80	X		101.1 E	1.3 N	X			Good	1:1 345 000; near-vertical pass
4138		80	X		99.8 E	1.3 N	X			Good	1:1 345 000; near-vertical pass
4139		80	X		98.8 E	1.2 N	X			Good	1:1 345 000; near-vertical pass
4140	Crater 192	80	X		97.5 E	1.2 N	X			Good	1:1 345 000; near-vertical pass
4141	Crater 192	80	X		96.5 E	1.2 N	X			Good	1:1 345 000; near-vertical pass
4142	Crater 192	80		X	95.6 E	1.0 N	X			Good	Start of 180° roll maneuver
4143		80		X	94.1 E	0.7 N	X			Good	
4144		80		X	93.0 E	0.1 N	X			Good	
4145	Smyth's Sea	80		X	92.6 E	0.1 N	X			Good	
4146	Smyth's Sea	80		X	91.8 E	0.5 S	X			Good	
4147	Smyth's Sea	80		X	91.0 E	0.2 S	X			Good	End of 180° roll maneuver
4148	Smyth's Sea	80	X		90.0 E	0.2 N	X			Good	1:1 245 000; near-vertical pass
4149	Smyth's Sea	80	X		90.3 E	0.0	X			Good	1:1 245 000; near-vertical pass
4150	Smyth's Sea	80	X		89.6 E	0.1 N	X			Good	1:1 245 000; near-vertical pass
4151	Smyth's Sea	80	X		88.8 E	0.1 N	X			Good	1:1 295 000; near-vertical pass
4152	Smyth's Sea	80	X		88.1 E	0.2 N	X			Good	1:1 295 000; near-vertical pass
4153	Smyth's Sea	80	X		86.6 E	0.1 S	X			Good	1:1 345 000; near-vertical pass
4154	Smyth's Sea	80	X		85.5 E	0.3 N	X			Good	1:1 345 000; near-vertical pass
4155	Smyth's Sea	80	X		84.7 E	0.2 N	X			Good	1:1 345 000; near-vertical pass
4156	Smyth's Sea	80	X		83.7 E	0.3 N	X			Good	1:1 345 000; near-vertical pass
4157	Smyth's Sea	80	X		83.7 E	0.0	X			Good	1:1 345 000; near-vertical pass
4158	Smyth's Sea	80	X		81.9 E	0.1 S	X			Good	1:1 295 000; near-vertical pass
4159	Smyth's Sea	80	X		80.6 E	0.5 S	X			Good	1:1 295 000; near-vertical pass
4160	Schubert	80	X		79.9 E	0.4 S	X			Good	1:1 295 000; near-vertical pass
4161	Schubert	80	X		78.5 E	0.9 S	X			Good	1:1 295 000; near-vertical pass
4162	Schubert	80	X		77.5 E	1.1 S	X			Good	1:1 295 000; near-vertical pass
4163	Schubert	80	X		76.1 E	1.2 S	X			Good	1:1 295 000; near-vertical pass

TABLE A–I.—*Apollo 10 Hasselblad Photography*—Continued

(*c*) Magazine P (from LM), film 3400

Frame no. AS10–29–	Description	FL, mm	Vert	Obliq	Principal point		Sun angle			Photo quality	Remarks
					Long, deg	Lat, deg	High	Med	Low		
4164	Unusable	80		X			X			Poor	Shows window frame; ⅛ of frame shows lunar surface
4165	Eastern Sea of Tranquility	80	X		39 E	0.5 N		X		Fair	Eastern Sea of Tranquility; shows CSM; 1:1 309 000
4166	Eastern Sea of Tranquility	80	X		39.5 E	0.7 N		X		Fair	Shows CSM; 1:1 309 000
4167	Eastern Sea of Tranquility	80	X		38.7 E	0.7 N		X		Fair	Shows CSM; 1:1 309 000
4168	Eastern Sea of Tranquility	80	X		31.1 E	1 N		X		Fair	Shows CSM; 1:1 309 000
4169	Eastern Sea of Tranquility	80	X		30.8 E	1 N		X		Fair	Shows CSM; 1:1 309 000
4170	Eastern Sea of Tranquility	80	X		30 E	0.9 N		X		Fair	Shows CSM; 1:1 309 000
4171	Eastern Sea of Tranquility	80	X		29.5 E	0.9 N		X		Fair	Shows CSM; 1:1 309 000
4172	Eastern Sea of Tranquility	80	X		28.7 E	1 N		X		Fair	Shows CSM; 1:1 309 000
4173	Eastern Sea of Tranquility	80	X		28.2 E	1.2 N		X		Fair	Shows CSM; 1:1 309 000
4174	Eastern Sea of Tranquility	80	X		26.4 E	1.4 N		X		Fair	Shows CSM; 1:1 309 000
4175	Crater 303	80		X	161.7 E	1 S		X		Fair	
4176	Crater 301	80		X	157.5 E	6 S		X		Fair	
4177	Crater 301	80		X	156.4 E	8 S		X		Fair	
4178	Crater 301	80		X	157.5 E	3 S		X		Fair	
4179	Crater 297; T/O 29	80			(PP above horizon)			X		Fair	
4180	Crater 297; T/O 29	80		X	149 E	7.5 S		X		Good	
4181	Crater 297	80		X	151 E	8.2 S		X		Fair	
4182	South of sea IX; near T/O 30	80		X	142.5 E	1.6 N	X			Fair	
4183	South of sea IX; near T/O 30	80		X	142.5 E	1.6 N	X			Fair	
4184	South of crater 218; near T/O 30.	80		X	141.5 E	0.6 N	X			Fair	
4185	South of crater 218; near T/O 30.	80		X	145 E	1.2 N	X			Fair	
4186	Crater 217; near T/O 30	80		X	136.7 E	0.2 N	X			Fair	
4187	South of sea IX; near T/O 30	80		X	142.5 E	0.2 N	X			Fair	
4188	South of sea IX; near T/O 30	80		X	142.2 E	1.2 N	X			Fair	
4189	T/O 30	80		X	139 E	2.5 N	X			Fair	
4190	South of sea IX; near T/O 30	80		X	138.1 E	2.2 N	X			Fair	
4191	South of sea IX; near T/O 30	80		X	136.5 E	2.2 N	X			Fair	
4192	South of sea IX; near T/O 30	80		X	138.7 E	1 N	X			Fair	
4193	South of sea IX; near T/O 30	80		X	137.9 E	1 N	X			Fair	
4194	T/O 30	80		X	136.4 E	3.5 N	X			Fair	
4195	Crater 217; near T/O 30	80		X	136.2 E	1.2 N	X			Fair	

4196	Crater 217; near T/O 30	80	X		136 E	1.5 N	X			Fair	
4197	Not plotted	80	X							Fair	
4198	Large crater south of crater 216.	80		X	133.2 E	0.2 N	X			Fair	IP
4199	Large crater south of crater 216.	80	X		133.2 E	0.2 N	X			Fair	IP
4200	Large crater south of crater 216.	80		X	133.2 E	0.2 N	X			Fair	IP
4201	Near T/O 43	80		X	123 E	1.5 S	X			Fair	
4202	South of crater 211; near T/O 46.	80		X	118.7 E	0.5 S	X			Fair	
4203	South of crater 211; near T/O 46.	80		X	119.5 E	0.5 S	X			Fair	
4204	South of crater 211; near T/O 46.	80		X	119.5 E	0.5 S	X			Fair	
4205	South of crater 211; near T/O 46.	80		X	119.2 E	0.0	X			Fair	
4206	South of crater 211; near T/O 46.	80		X	119.5 E	0.5 N	X			Fair	
4207	South of crater 211; near T/O 46.	80		X	119.5 E	0.5 N	X			Fair	
4208	Crater 211; T/O 46	80		X	120 E	5 N	X			Fair	
4209	Crater 211; T/O 46	80		X	120 E	5.5 N	X			Fair	
4210	East of crater 206	80		X	116 E	1.5 N	X			Fair	
4211	East of crater 206	80		X	116.5 E	1.5 N	X			Fair	
4212	Images of crater 206 near horizon.	80		X	112 E	1.5 N	X			Fair	
4213	South of crater 208	80		X	116 E	7 N	X			Fair	
4214	East of crater 207	80		X	117 E	1.5 N	X			Fair	
4215	East of crater 207	80		X	116.3 E	1 N				Fair	
4216	Not plotted	80		X			X			Fair	
4217	East of crater 202	80		X	110.5 E	0	X			Fair	
4218	South of crater 201	80		X	106.5 E	3 N	X			Fair	
4219	Crater 201; near T/O 55	80		X	107.5 E	5.5 N	X			Fair	
4220	Crater 201; near T/O 55	80		X	107.5 E	5.5 N	X			Fair	
4221	South of crater 199; near T/O 55.	80		X	101.2 E	1.7 N	X			Fair	
4222	Near T/O 55	80		X	99 E	4 N	X			Fair	
4223	South of crater 199	80		X	101.5 E	1 N	X			Fair	
4224	West of crater 199; T/O 55	80		X	100 E	3.5 N	X			Fair	
4225	Crater 199; T/O 55	80		X	97.5 E	5 N	X			Fair	
4226	North of crater 269	80		X	97 E	1.5 N	X			Fair	
4227	North of crater 269	80		X	97 E	1.5 N	X			Fair	
4228	Crater 189; near T/O 55	80		X	93.5 E	3 N	X			Fair	
4229	Near T/O 59	80		X	80 E	1.5 S	X			Fair	

TABLE A-I.—*Apollo 10 Hasselblad Photography*—Continued

(*c*) Magazine P (from LM), film 3400—*Continued*

Frame no. AS10-29-	Description	FL, mm	Vert	Obliq	Principal point		Sun angle			Photo quality	Remarks
					Long, deg	Lat, deg	High	Med	Low		
4230	Near T/O 59	80		X	81.5 E	1 S	X			Fair	
4231	Near T/O 59	80		X	78 E	1 S	X			Fair	
4232	Near T/O 59	80		X	79.2 E	2.5 S	X			Fair	
4233	Near T/O 59	80		X	77.7 E	1 S	X			Fair	
4234	Gilbert	80		X	77.5 E	0.5 S	X			Fair	
4235	Gilbert	80		X	77 E	0.5 S	X			Fair	
4236	Gilbert	80	X		77.5 E	0.5 S	X			Fair	
4237	Not plotted	80	X				X			Fair	
4238	Near Mare Undarum	80		X	72 E	0.2 S	X			Fair	
4239	Near Mare Undarum	80		X	70 E	0	X			Fair	
4240	Mare Spumans	80		X	67.5 E	1.3 N	X			Fair	
4241	Mare Spumans	80		X	67.5 E	0.5 N	X			Fair	
4242	Mare Spumans	80		X	67.5 E	0.5 N	X			Fair	
4243	Mare Spumans	80		X	64.5 E	0.5 N	X			Fair	
4244	T/O 67	80		X	64 E	3 N	X			Fair	Southern rim of Sea of Crises
4245	T/O 67	80		X	62.5 E	2.5 N	X			Fair	Southern rim of Sea of Crises
4246	Near T/O 69a	80		X	57 E	0	X			Fair	
4247	Near T/O 69a	80		X	56 E	1 N	X			Fair	
4248	Near T/O 69a	80		X	54.7 E	1 S	X			Fair	
4249	Near T/O 69a	80		X	53 E	1 N	X			Fair	
4250	Near T/O 69a	80		X	50.7 E	0.2 N		X		Good	
4251	Near T/O 69a	80		X	51.2 E	0.5 N		X		Good	
4252	Near T/O 69a	80		X	50 E	0.2 S		X		Good	
4253	Near T/O 75	80		X	48 E	1 S		X		Good	
4254	Near T/O 75	80		X	48 E	1 S		X		Good	
4255	Near T/O 75	80		X	48 E	0.5 S		X		Good	
4256	Near T/O 75	80		X	47 E	3 S		X		Good	
4257	Near T/O 75	80		X	47.2 E	0.5 N	X			Fair	
4258	Near T/O 75	80		X	47.3 E	0.5 N		X		Good	
4259	Near T/O 75	80		X	46.6 E	0.2 E		X		Good	
4260	Near T/O 75	80		X	46 E	0.5 N		X		Fair	
4261	Near T/O 75	80		X	45.2 E	0		X		Good	
4262	Near T/O 75	80		X	43.5 E	0.7 N		X		Fair	
4263	Near T/O 75	80		X	43.5 E	1 N		X		Fair	
4264	T/O 78a	80		X	42.5 E	0.5 S		X		Good	
4265	T/O 78a	80		X	42.5 E	0.5 N		X		Good	

4266	T/O 78a	80		X	41.7 E	0.7 N		X		Good	Highlands between Sea of Fertility and Sea of Tranquility
4267	T/O 78a	80		X	40 E	0.2 N		X		Fair	Sea of Tranquility
4268	T/O 78a	80		X	40.5 E	0.2 S		X		Fair	Pyrenees Mountains
4269	T/O 78a	80		X	40 E	0.5 N		X		Fair	Sea of Tranquility
4270	T/O 78a	80		X	39.5 E	0.5 N		X		Fair	
4271	T/O 78a	80		X	39.5 E	0.7 N		X		Fair	
4272	T/O 78a	80		X	39 E	0.5 N		X		Fair	
4273	T/O 78a	80		X	38.5 E	0.0		X		Fair	
4274	T/O 78a	80		X	38.5 E	0.7 N		X		Fair	
4275	T/O 78a	80		X	38.5 E	0.5 N		X		Fair	
4276	T/O 78a	80		X	38 E	0.5 N		X		Good	
4277	T/O 78a	80		X	37.5 E	0.5 N		X		Good	
4278	T/O 78a	80		X	37 E	0.2 N		X		Fair	
4279	T/O 78a	80		X	36.2 E	0.5 N		X		Good	
4280	T/O 78a	80		X	35.5 E	0.4 N		X		Good	
4281	T/O 78a	80		X	35.5 E	0.2 N		X		Fair	
4282	T/O 78a	80		X	35.2 E	0.5 N		X		Fair	
4283	T/O 78a	80		X	34.2 E	0.5 N		X		Fair	Pyrenees Mountains
4284	T/O 78a	80		X	34 E	0.2 N		X		Fair	
4285	T/O 78a	80	X		34.2 E	0.5 N		X		Good	1:260 000
4286	T/O 78a	80	X		34.2 E	0.5 N		X		Good	1:260 000
4287	T/O 78a	80		X	32.6 E	2.4 N		X		Fair	Sea of Tranquility
4288	T/O 78a	80		X	(PP above horizon)			X		Fair	
4289	T/O 78a	80		X	32.7 E	2.2 N		X		Fair	
4290	T/O 78a	80		X	32.2 E	0.3 S		X		Good	Censorinus
4291	T/O 78a	80		X	32.7 E	0.2 S		X		Good	Censorinus
4292	T/O 78a	80		X	32.7 E	0.2 S		X		Good	Censorinus
4293	T/O 78a	80		X	32.2 E	0.7 S		X		Good	Sea of Tranquility
4294	T/O 78a	80		X	31 E	0.6 N		X		Fair	
4295	T/O 78a	80		X	30.7 E	0.5 N		X		Fair	
4296	Maskelyne	80		X	30.5 E	2 N		X		Fair	
4297	Sea of Tranquility	80		X	28.5 E	0.3 N		X		Fair	
4298	Sea of Tranquility	80		X	28 E	0.4 N		X		Fair	
4299	Sea of Tranquility	80		X	28 E	0.2 N		X		Fair	
4300	Sea of Tranquility	80		X	28.1 E	0.2 S		X		Good	
4301	Sea of Tranquility	80		X	28.2 E	0.2 N		X		Good	
4302	Sea of Tranquility	80		X	28.1 E	0.5 N		X		Good	
4303	Sea of Tranquility	80		X	27.4 E	1.2 N		X		Good	
4304	Sea of Tranquility	80		X	26.6 E	1.7 N		X		Good	
4305	Sea of Tranquility	80		X	(PP above horizon)			X		Fair	
4306	Sea of Tranquility	80		X	(PP above horizon)			X		Fair	
4307	Sea of Tranquility	80		X	26.1 E	1.7 N		X		Fair	
4308	Sea of Tranquility	80		X	26.5 E	0.4 N		X		Fair	

TABLE A-I.—*Apollo 10 Hasselblad Photography*—Continued

(*c*) Magazine P (from LM), film 3400—*Concluded*

Frame no. AS10-29-	Description	FL, mm	Vert	Obliq	Principal point		Sun angle			Photo quality	Remarks
					Long, deg	Lat, deg	High	Med	Low		
4309	Sea of Tranquility	80	------	X	26.5 E	0.5 N	------	X	------	Fair	
4310	Sea of Tranquility	80	------	X	26.4 E	0.5 N	------	X	------	Fair	
4311	Sea of Tranquility	80	------	X	25.7 E	0.5 N	------	X	------	Fair	
4312	Sea of Tranquility	80	------	X	25.5 E	0.5 N	------	X	------	Fair	
4313	Sea of Tranquility	80	------	X	25.5 E	0.5 N	------	X	------	Fair	
4314	Sea of Tranquility	80	------	X	25.2 E	0.2 N	------	X	------	Fair	
4315	Sea of Tranquility	80	------	X	25.2 E	0.2 N	------	X	------	Good	
4316	Sea of Tranquility	80	------	X	25 E	0.5 N	------	X	------	Fair	
4317	Sea of Tranquility	80	------	X	24.9 E	0.5 N	------	X	------	Fair	
4318	Sea of Tranquility	80	------	X	24.9 E	0.5 N	------	X	------	Fair	
4319	Sea of Tranquility	80	------	X	24.8 E	0.5 N	------	X	------	Fair	
4320	Sea of Tranquility	80	------	X	24.7 E	0.5 N	------	X	------	Fair	
4321	Sea of Tranquility	80	------	X	24.7 E	0.6 N	------	X	------	Fair	
4322	Sea of Tranquility	80	------	X	24.7 E	0.5 N	------	X	------	Good	
4323	Sea of Tranquility	80	------	X	24.7 E	0.5 N	------	X	------	Good	
4324	T/O 112	80	------	X	24.2 E	0.3 S	------	X	------	Good	
4325	Sea of Tranquility	80	X	------	24 E	0.2 N	------	X	------	Good	1:300 000
4326	Sea of Tranquility	80	X	------	23.9 E	0.2 N	------	X	------	Good	1:300 000

(*d*) **Magazine Q, film 3400**

Frame no. AS10-30-	Description	FL, mm	Vert	Obliq	Principal point		Sun angle			Photo quality	Remarks
					Long, deg	Lat, deg	High	Med	Low		
4327	Crater IX; T/O 34	250	------	X	138.5 E	6.0 N	------	X	------	Good	First frame of a 10-frame sequence
4328	Crater IX; T/O 34	250	------	X	138.0 E	6.0 N	------	X	------	Good	Low-oblique photography of crater floor and western rim
4329	Crater IX; T/O 34	250	------	X	138.0 E	6.0 N	------	X	------	Good	Low-oblique photography of craterfloor and western rim
4330	Crater IX; T/O 34	250	------	X	137.5 E	6.0 N	------	X	------	Good	Low-oblique photography of crater floor and western rim

4331	Crater IX; T O 34	250		X	137.0 E	6.0 N		X		Good	Low-oblique photography of crater floor and western rim
4332	Crater IX; T O 34	250		X	136.5 E	5.5 N		X		Good	Low-oblique photography of crater floor and western rim
4333	Crater IX; T O 34	250		X	136.0 E	5.5 N		X		Good	Low-oblique photography of crater floor and western rim
4334	Crater IX; T O 34	250		X	135.5 E	5.5 N		X		Good	Low-oblique photography of crater floor and western rim
4335	Crater IX; T O 34	250		X	135.0 E	5.5 N		X		Good	Low-oblique photography of crater floor and western rim
4336	Crater IX; T O 34	250		X	135.0 E	5.5 N		X		Good	Low-oblique photography of crater floor and western rim
4337	Crater IX; T O 34	250		X	134.5 E	5.0 N		X		Good	End of 10-frame sequence
4338	Crater 216	250		X	134.5 E	4.0 N		X		Good	End of 10-frame sequence
4339	Crater 216	250		X	133.0 E	4.5 N		X		Good	Floor and central peak of crater 216
4340	Crater 216	250		X	132.5 E	4.5 N		X		Good	Floor and central peak of crater 216
4341	Crater 216	250		X	132.5 E	4.5 N		X		Good	Floor and central peak of crater 216
4342	Crater 216	250		X	132.5 E	4.5 N		X		Good	Floor and central peak of crater 216
4343	Crater near craters 212, 213	250		X	124.5 E	7.0 N		X		Good	Medium-size crater with high central peak
4344	Crater near craters 212, 213	250		X	124.0 E	7.0 N		X		Good	Medium-size crater with high central peak
4345	Crater near craters 212, 213	250		X	124.0 E	7.0 N		X		Good	Medium-size crater with high central peak
4346	Crater near craters 212, 213	250		X	124.0 E	7.0 N		X		Good	Medium-size crater with high central peak
4347	Crater 212	250		X	123.5 E	10.0 N		X		Good	Large smooth-floored crater
4348	Crater 212	250		X	123.5 E	10.0 N		X		Good	Large smooth-floored crater
4349	Crater 211; T O 46	250		X	119.0 E	5.0 N		X		Good	Large rough-rimmed crater with massive central peak
4350	Crater 211; T O 46	250		X	119.0 E	5.0 N		X		Good	Large rough-rimmed crater with massive central peak
4351	Crater 211; T O 46	250		X	119.0 E	5.0 N		X		Good	Large rough-rimmed crater with massive central peak
4352	Crater 211; T O 46	250		X	119.0 E	5.0 N		X		Good	Large rough-rimmed crater with massive central peak
4353	Crater 211; T O 46	250		X	119.5 E	4.5 N		X		Good	Large rough-rimmed crater with massive central peak
4354	Crater 211; T O 46	250		X	119.5 E	4.5 N		X		Good	Large rough-rimmed crater with massive central peak

TABLE A-I.—*Apollo 10 Hasselblad Photography*—Continued

(*d*) Magazine Q, film 3400—*Continued*

Frame no. AS10-30-	Description	FL, mm	Vert	Obliq	Principal point		Sun angle			Photo quality	Remarks
					Long, deg	Lat, deg	High	Med	Low		
4355	Crater 211; T/O 46	250	------	X	119.5 E	4.5 N	------	X	------	Good	Large rough-rimmed crater with massive central peak
4356	Crater 211; T/O 46	250	------	X	119.0 E	4.5 N	------	X	------	Good	Large rough-rimmed crater with massive central peak
4357	Crater 211; T/O 46	250	------	X	119.0 E	4.5 N	------	X	------	Good	Large rough-rimmed crater with massive central peak
4358	Crater 211; T/O 46	250	------	X	119.0 E	4.5 N	------	X	------	Good	Large rough-rimmed crater with massive central peak
4359	Crater 211; T/O 46	250	------	X	119.0 E	4.5 N	------	X	------	Good	Large rough-rimmed crater with massive central peak
4360	Crater 211; T/O 46	250	------	X	118.5 E	4.5 N	------	X	------	Good	Large rough-rimmed crater with massive central peak
4361	Crater 211; T/O 46	250	------	X	118.5 E	4.5 N	------	X	------	Good	Large rough-rimmed crater with massive central peak
4362	Crater 211; T/O 46	250	------	X	119.5 E	5.0 N	------	X	------	Good	Large rough-rimmed crater with massive central peak
4363	Crater 211; T/O 46	250	------	X	119.5 E	5.0 N	------	X	------	Good	Large rough-rimmed crater with massive central peak
4364	Crater 211; T/O 46	250	------	X	119.5 E	5.0 N	------	X	------	Good	Large rough-rimmed crater with massive central peak
4365	Near crater 206	250	------	X	115.0 E	5.0 N	------	X	------	Fair	Unusual surface configuration
4366	Near crater 206	250	------	X	115.0 E	5.0 N	------	X	------	Fair	Unusual surface configuration
4367	Near crater 206	250	------	X	115.0 E	5.0 N	------	X	------	Fair	Unusual surface configuration
4368	Near crater 206	250	------	X	115.0 E	5.0 N	------	X	------	Fair	Unusual surface configuration
4369	Near crater 206	250	------	X	115.0 E	5.0 N	------	X	------	Fair	Unusual surface configuration
4370	Near crater 206	250	------	X	115.0 E	5.0 N	------	X	------	Fair	Unusual surface configuration
4371	Near crater 202	250	------	X	107.0 E	0.0	------	X	------	Good	Double impact-type crater
4372	Near crater 199; T/O 55	250	------	X	100.0 E	4.5 N	------	X	------	Fair	Bright Copernican crater with extensive ray system
4373	Near crater 199; T/O 55	250	------	X	100.0 E	4.5 N	------	X	------	Fair	Bright Copernican crater with extensive ray system
4374	Near crater 199; T/O 55	250	------	X	100.0 E	4.5 N	------	X	------	Good	Bright Copernican crater with extensive ray system
4375	Near crater 199; T/O 55	250	------	X	100.0 E	4.5 N	------	X	------	Good	Bright Copernican crater with extensive ray system

4376	Near Jansky; T/O 55.4	250		X	92.0 E	7.5 N		X		Good	29-frame sequence over Jansky and Neper
4377	Near Jansky; T/O 55	250		X	91.5 E	7.0 N		X		Good	Overlapping obliques
4378	Near Jansky; T/O 55	250		X	91.0 E	7.0 N		X		Good	Overlapping obliques
4379	Near Jansky; T/O 55	250		X	91.0 E	7.0 N		X		Good	Overlapping obliques
4380	Near Jansky; T/O 55	250		X	90.5 E	7.0 N		X		Good	Overlapping obliques
4381	Near Jansky; T/O 55	250		X	90.5 E	7.0 N		X		Good	Overlapping obliques
4382	Near Jansky; T/O 55	250		X	90.0 E	7.0 N		X		Good	Overlapping obliques
4383	Near Jansky; T/O 55	250		X	90.0 E	7.0 N		X		Good	Overlapping obliques
4384	Near Jansky; T/O 55	250		X	90.0 E	7.0 N		X		Good	Overlapping obliques
4385	Near Jansky; T/O 55	250		X	90.0 E	7.0 N		X		Good	Overlapping obliques
4386	Near Jansky; T/O 55	250		X	90.0 E	7.0 N		X		Good	Overlapping obliques
4387	Near Jansky; T/O 55	250		X	89.5 E	7.0 N		X		Good	Overlapping obliques
4388	Jansky	250		X	89.0 E	7.0 N		X		Good	Overlapping obliques
4389	Jansky	250		X	88.5 E	6.5 N		X		Good	Overlapping obliques
4390	Jansky	250		X	88.0 E	6.5 N		X		Good	
4391	Jansky	250		X	87.5 E	6.5 N		X		Good	Overlapping obliques
4392	Jansky	250		X	87.5 E	6.5 N		X		Good	Overlapping obliques
4393	Jansky	250		X	86.5 E	6.0 N		X		Good	Overlapping obliques
4394	Near Jansky	250		X	86.5 E	6.0 N		X		Good	Overlapping obliques
4395	Near Jansky	250		X	85.5 E	6.0 N		X		Good	Overlapping obliques
4396	Neper	250		X	85.5 E	6.0 N		X		Good	Overlapping obliques
4397	Neper	250		X	85.5 E	6.0 N		X		Good	Overlapping obliques
4398	Neper	250		X	85.5 E	6.0 N		X		Good	Overlapping obliques
4399	Neper	250		X	85.0 E	6.5 N		X		Good	Overlapping obliques
4400	Neper	250		X	84.5 E	7.0 N		X		Good	Overlapping obliques
4401	Neper	250		X	84.5 E	7.0 N		X		Good	Overlapping obliques
4402	Neper	250		X	84.5 E	7.0 N		X		Good	Overlapping obliques
4403	Neper	250		X	84.0 E	7.0 N		X		Good	Overlapping obliques
4404	Neper	250		X	84.0 E	7.0 N		X		Good	Overlapping obliques
4405	Neper	250		X	83.5 E	7.0 N		X		Good	Overlapping obliques
4406	Neper	250		X	83.5 E	7.0 N		X		Good	Overlapping obliques
4407	Neper	250		X	83.5 E	7.0 N		X		Good	Overlapping obliques
4408	Neper	250		X	83.0 E	7.0 N		X		Good	Overlapping obliques
4409	Neper	250		X	83.0 E	7.0 N		X		Good	Overlapping obliques
4410	Neper	250		X	83.0 E	7.0 N		X		Good	Overlapping obliques
4411	Not located	250		X							Unable to locate
4412	Not located	250		X							Unable to locate
4413	Not located	250		X							Unable to locate
4414	Mare Crisium; T/O 70	250		X	57.0 E	12.0 N	X			Good	High oblique of floor and rim of Mare Crisium
4415	Mare Crisium; T/O 70	250		X	57.0 E	12.0 N	X			Good	High oblique of floor and rim of Mare Crisium
4416	Mare Crisium; T/O 70	250		X	56.0 E	11.5 N	X			Good	High oblique of floor and rim of Mare Crisium

TABLE A–I.—*Apollo 10 Hasselblad Photography*—Continued

(*d*) Magazine Q, film 3400—*Continued*

Frame no. AS10-30-	Description	FL, mm	Vert	Obliq	Principal point		Sun angle			Photo quality	Remarks
					Long, deg	Lat, deg	High	Med	Low		
4417	Mare Crisium; T O 70	250		X	55.0 E	11.5 N	X			Good	High oblique of floor and rim of Mare Crisium
4418	Mare Crisium; T O 70	250		X	54.5 E	11.0 N	X			Good	High oblique of floor and rim of Mare Crisium
4419	Mare Crisium; T O 70	250		X	54.0 E	11.0 N	X			Good	High oblique of floor and rim of Mare Crisium
4420	Mare Crisium; T O 70	250		X	53.5 E	10.5 N	X			Good	High oblique of floor and rim of Mare Crisium
4421	Picard; T O 70	250		X	55.0 E	14.0 N	X			Good	High oblique of floor and rim of Mare Crisium
4422	Messier; T O 75	250		X	46.5 E	2.0 S	X			Good	High oblique of Messier and Messier A
4423	Messier; T O 75	250		X	46.5 E	2.0 S	X			Good	High oblique of Messier and Messier A
4424	Secchi	250		X	44.0 E	3.0 N	X			Good	High oblique of Secchi
4425	Secchi	250		X	44.0 E	2.0 N	X			Good	High oblique of Secchi
4426	Near Taruntius; T O 74	250		X	50.0 E	7.0 N	X			Fair	Obliques of western rim of Mare Crisium
4427	Near Taruntius; T O 74	250		X	48.5 E	8.5 N	X			Fair	Obliques of western rim of Mare Crisium
4428	Near Taruntius; T O 74	250		X	48.0 E	9.0 N	X			Fair	Obliques of western rim of Mare Crisium
4429	Near Taruntius; T O 74	250		X	48.0 E	9.0 N	X			Fair	Obliques of western rim of Mare Crisium
4430	Near Taruntius; T O 76	250		X	47.0 E	9.0 N	X			Fair	Obliques of western rim of Mare Crisium
4431	Near Taruntius; T O 76	250		X	46.5 E	8.5 N	X			Fair	Obliques of western rim of Mare Crisium
4432	Near Taruntius; T O 76	250		X	45.5 E	9.5 N	X			Fair	Palus Somni
4433	Near Taruntius; T O 76	250		X	45.0 E	9.0 N	X			Fair	Palus Somni
4434	Taruntius	250		X	47.0 E	5.5 N	X			Fair	Rim and floor of Taruntius
4435	Taruntius	250		X	46.0 E	5.5 N	X			Fair	Rim and floor of Taruntius
4436	T O 78	250		X	37.5 E	1.0 N	X			Good	Sea of Tranquility
4437	T O 78	250		X	37.5 E	1.5 N	X			Good	Sea of Tranquility
4438	Sea of Tranquility	250		X	35.5 E	4.0 N	X			Good	High oblique

4439	Sea of Tranquility; Maskelyne	250		X	35.0 E	1.0 N	X			Good	High oblique of Maskelyne
4440	Sea of Tranquility; Maskelyne	250		X	34.0 E	2.0 N	X			Good	High oblique of Maskelyne
4441	Sea of Tranquility; T/O 112, 113	250		X	25.5 E	1.0 S		X		Fair	Landing site 2
4442	Sea of Tranquility; T/O 112, 113	250		X	25.5 E	1.0 S		X		Fair	Landing site 2
4443	Sea of Tranquility; T/O 114	250		X	25.5 E	1.0 N		X		Fair	Landing site 2
4444	Sea of Tranquility; T/O 114	250		X	25.5 E	1.0 N		X		Fair	Landing site 2
4445	Sea of Tranquility; T/O 114	250		X	25.0 E	1.0 N		X		Fair	Landing site 2
4446	Sea of Tranquility; T/O 114	250		X	25.0 E	1.0 N		X		Fair	Landing site 2
4447	Sea of Tranquility; T/O 114	250		X	24.5 E	1.0 N		X		Fair	Landing site 2
4448	Sea of Tranquility; T/O 114	250		X	24.5 E	1.0 N		X		Fair	Landing site 2
4449	Rima Ariadaeus; T/O 123	250		X	17.5 E	5.0 N		X		Good	High forward oblique of Rima Ariadaeus
4450	Rima Ariadaeus; T/O 123	250		X	17.5 E	5.0 N		X		Good	High forward oblique of Rima Ariadaeus
4451	Sabine; Ritter	250		X	21.0 E	1.0 N		X		Good	Rim and floor of Sabine; Ritter
4452	Craters 227, 226; T/O 16a	80		X	173.0 E	9.5 N			X	Good	High oblique with low-Sun angle
4453	Craters 221, 223	80		X	168.0 E	5.0 N			X	Good	High oblique with low-Sun angle
4454	Crater 218	80		X	146.5 E	5.0 N			X	Good	Long overlapping oblique sequence looking north
4455	Crater 218	80		X	145.0 E	5.0 N			X	Good	Long overlapping oblique sequence looking north
4456	Crater 218	80		X	144.0 E	4.5 N			X	Good	Long overlapping oblique sequence looking north
4457	Crater IX	80		X	143.0 E	4.5 N			X	Good	Long overlapping oblique sequence looking north
4458	Crater IX; T/O 30, 34	80		X	141.5 E	4.0 N			X	Good	Long overlapping oblique sequence looking north
4459	Crater IX; T/O 30, 34	80		X	141.0 E	5.0 N			X	Good	Long overlapping oblique sequence looking north
4460	Crater IX; T/O 30, 34	80		X	141.0 E	5.0 N			X	Good	Long overlapping oblique sequence looking north
4461	Crater IX; T/O 30, 34	80		X	140.0 E	5.0 N			X	Good	Long overlapping oblique sequence looking north
4462	Crater IX; T/O 30, 34	80		X	138.5 E	5.5 N			X	Good	Long overlapping oblique sequence looking north
4463	Crater IX; T/O 30, 34	80		X	137.0 E	5.0 N			X	Good	Long overlapping oblique sequence looking north
4464	Crater IX; T/O 30, 34	80		X	137.0 E	5.0 N			X	Good	Long overlapping oblique sequence looking north

TABLE A-I.—*Apollo 10 Hasselblad Photography*—Continued

(*d*) Magazine Q, film 3400—*Continued*

Frame no. AS10-30-	Description	FL, mm	Vert	Obliq	Principal point		Sun angle			Photo quality	Remarks
					Long, deg	Lat, deg	High	Med	Low		
4465	Craters 216, 217; T O 34	80		X	135.0 E	4.5 N			X	Good	Long overlapping oblique sequence looking north
4466	Craters 216, 217	80		X	135.5 E	5.0 N			X	Good	Long overlapping oblique sequence looking north
4467	Crater 216	80		X	134.0 E	5.0 N			X	Good	Long overlapping oblique sequence looking north
4468	Crater 216	80		X	133.0 E	5.5 N			X	Good	Long overlapping oblique sequence looking north
4469	Crater 216	80		X	131.0 E	4.5 N			X	Good	Long overlapping oblique sequence looking north
4470	Crater 211; T O 46	80		X	121.5 E	4.5 N			X	Good	Long overlapping oblique sequence looking north
4471	Crater 211; T O 46	80		X	120.0 E	4.5 N			X	Good	Long overlapping oblique sequence looking north
4472	Crater 211; T O 46	80		X	120.0 E	4.5 N			X	Good	Long overlapping oblique sequence looking north
4473	Crater 211; T O 46	80		X	120.0 E	4.5 N			X	Good	Long overlapping oblique sequence looking north
4474	Crater 211; T O 46	80		X	120.0 E	4.5 N			X	Good	Long overlapping oblique sequence looking north
4475	Mare Smythii; T O 59	80		X	84.5 E	0.0	X			Fair	Long forward-looking oblique sequence over Mare Smythii with Earth in background
4476	Mare Smythii; T O 59	80		X	82.5 E	0.0	X			Fair	Long forward-looking oblique sequence over Mare Smythii with Earth in background
4477	Mare Smythii; T O 59	80		X	81.0 E	0.0	X			Fair	Long forward-looking oblique sequence over Mare Smythii with Earth in background
4478	Mare Smythii; T O 59	80		X	80.0 E	0.0	X			Fair	Long forward-looking oblique sequence with Mare Smythii with Earth in background
4479	Mare Smythii; T O 59	80		X	79.0 E	0.0	X			Fair	Long forward-looking oblique sequence over Mare Smythii with Earth in background

4480	Mare Smythii; T/O 59	80		X	78.0 E	0.0	X			Fair	Long forward-looking oblique sequence over Mare Smythii with Earth in background
4481	Mare Smythii; T/O 59	80		X	77.5 E	0.0	X			Fair	Long forward-looking oblique sequence over Mare Smythii with Earth in background
4482	Mare Smythii; T/O 59	80		X	75.5 E	0.5 N	X			Fair	Long forward-looking oblique sequence over Mare Smythii with Earth in background
4483	Mare Smythii; T/O 59	80		X	74.5 E	0.5 N	X			Fair	Long forward-looking oblique sequence over Mare Smythii with Earth in background
4484	Mare Smythii; T/O 59	80		X	72.5 E	1.0 N	X			Fair	Long forward-looking oblique sequence over Mare Smythii with Earth in background
4485	Mare Smythii; T/O 59	80		X	71.5 E	1.0 N	X			Fair	Long forward-looking oblique sequence over Mare Smythii with Earth in background
4486	Mare Smythii; T/O 59	80		X	69.5 E	1.0 N	X			Fair	Long forward-looking oblique sequence over Mare Smythii with Earth in background
4487	Mare Smythii; T/O 59	80		X	68.5 E	1.0 N	X			Fair	Long forward-looking oblique sequence over Mare Smythii with Earth in background
4488	Mare Smythii; T/O 59	80		X	67.0 E	1.0 N	X			Fair	Long forward-looking oblique sequence over Mare Smythii with Earth in background
4489	Mare Smythii; T/O 59	80		X	67.0 E	1.0 N	X			Fair	Long forward-looking oblique sequence over Mare Smythii with Earth in background
4490	Mare Smythii; T/O 59	80		X	66.0 E	1.0 N	X			Fair	Long forward-looking oblique sequence over Mare Smythii with Earth in background
4491	Mare Smythii; T/O 59	80		X	65.0 E	1.0 N	X			Fair	Long forward-looking oblique sequence over Mare Smythii with Earth in background
4492	Mare Smythii; T/O 59	80		X	64.0 E	1.0 N	X			Fair	Long forward-looking oblique sequence over Mare Smythii with Earth in background
4493	Mare Smythii; T/O 59	80		X	On horizon		X			Fair	Long forward-looking oblique sequence over Mare Smythii with Earth in background
4494	Mare Spumans	80		X	On horizon		X			Fair	Long forward-looking oblique sequence over Mare Smythii with Earth in background

TABLE A-I.—*Apollo 10 Hasselblad Photography*—Continued

(*d*) Magazine Q, film 3400—*Concluded*

Frame no. AS10-30-	Description	FL, mm	Vert	Obliq	Principal point		Sun angle			Photo quality	Remarks
					Long, deg	Lat, deg	High	Med	Low		
4499	Mare Spumans; T O 69a, 67	80		X	On horizon		X			Fair	Long forward-looking oblique sequence over Mare Smythii with Earth in background
4495	Mare Spumans	80		X	On horizon		X			Fair	Long forward-looking oblique sequence over Mare Smythii with Earth in background
4496	Mare Spumans	80		X	On horizon		X			Fair	Long forward-looking oblique sequence over Mare Smythii with Earth in background
4497	Mare Spumans; T O 69a, 67	80		X	On horizon		X			Fair	Long forward-looking oblique sequence over Mare Smythii with Earth in background
4498	Mare Spumans; T O 69a, 67	80		X	On horizon		X			Fair	Long forward-looking oblique sequence over Mare Smythi with Earth in background

(*e*) Magazine R, film 3400

Frame no. AS10-31-	Description	FL, mm	Vert	Obliq	Principal point		Sun angle			Photo quality	Remarks
					Long, deg	Lat, deg	High	Med	Low		
4500	T O 67	80	X		62.4 E	0.6 N	X			Good	1:1 440 000; pass over sites 1 and 2
4501	T O 67	80	X		60.3 E	1.1 N	X			Good	1:1 440 000; Crater Apollonius
4502	Foaming Sea	80	X		58.9 E	1.9 N	X			Good	1:1 440 000
4503	Foaming Sea	80	X		58.0 E	2.0 N	X			Good	1:1 440 000
4504		80	X		57.3 E	2.1 N	X			Good	1:1 440 000
4505		80	X		56.4 E	1.6 N	X			Good	1:1 440 000
4506	Sea of Fertility	80	X		55.9 E	1.7 N	X			Good	1:1 440 000
4507	Sea of Fertility	80	X		54.9 E	1.6 N	X			Good	1:1 440 000
4508	Sea of Fertility	80	X		54.1 E	1.5 N	X			Good	1:1 440 000

4509	Sea of Fertility	80	X		53.7 E	1.6 N	X			Good	1:1 420 000
4510	Taruntius K	80	X		51.7 E	1.6 N	X			Good	1:1 420 000
4511	Taruntius G	80	X		50.9 E	1.5 N	X			Good	1:1 420 000
4512	Taruntius G	80	X		49.6 E	1.5 N	X			Good	1:1 420 000
4513	Sea of Fertility	80	X		48.3 E	1.5 N	X			Good	1:1 330 000
4514	Sea of Fertility	80	X		47.2 E	1.4 N	X			Good	1:1 330 000
4515	Sea of Fertility	80	X		46.0 E	1.2 N	X			Good	1:1 330 000
4516	Secchi	80		X	44.8 E	1.0 N	X			Good	
4517	Secchi	80		X	43.8 E	1.1 N	X			Good	
4518	Secchi	80		X	43.2 E	1.1 N	X			Good	
4519	Lubbock S	80		X	42.1 E	1.1 N	X			Good	
4520	Lubbock S	80		X	41.2 E	1.2 N	X			Good	
4521	Lubbock S	80		X	40.1 E	1.5 N	X			Good	
4522	Site 1 approach	80		X	39.4 E	1.4 N	X			Good	
4523	Site 1 approach	80		X	38.2 E	1.3 N	X			Good	
4524	Site 1 approach	80		X	37.5 E	1.6 N	X			Good	
4525	Site 1 approach	80		X	36.4 E	1.5 N	X			Good	
4526	Site 1	80		X	35.6 E	1.8 N	X			Good	
4527	Site 1	80		X	34.4 E	1.7 N	X			Good	
4528	Site 1	80		X	33.4 E	1.7 N	X			Good	
4529		80		X	32.5 E	1.4 N	X			Good	
4530	Maskelyne	80		X	31.8 E	1.0 N	X			Good	
4531	Maskelyne	80	X		30.4 E	0.5 N	X			Good	1:1 330 000
4532	Maskelyne	80	X		29.5 E	0.5 N		X		Good	1:1 330 000
4533		80	X		28.4 E	0.5 N		X		Good	1:1 330 000
4534		80	X		27.4 E	0.6 N		X		Good	1:1 330 000
4535	T/O 112	80	X		26.8 E	0.3 N		X		Good	1:1 330 000
4536	T/O 112	80	X		25.9 E	0.0		X		Good	1:1 330 000
4537	Site 2	80	X		24.6 E	0.2 S		X		Good	1:1 330 000
4538	T/O 114; site 2	80	X		23.8 E	0.3 S		X		Good	1:1 330 000
4539	T/O 114	80	X		22.8 E	0.4 S		X		Good	1:1 330 000
4540	T/O 114	80		X	22.0 E	0.4 S		X		Good	1:1 330 000
4541	Sabine	80		X	21.0 E	0.3 S		X		Good	1:1 330 000
4542	Sabine	80		X	20.0 E	0.4 S		X		Good	1:1 330 000
4543		80		X	19.1 E	0.4 S		X		Good	1:1 330 000
4544	Delambre	80		X	18.5 E	0.5 S			X	Good	1:1 330 000
4545	Delambre	80		X	16.9 E	0.4 S			X	Good	1:1 330 000
4546		80		X	16.2 E	0.3 S			X	Good	1:1 330 000
4547		80		X	15.3 E	0.4 S			X	Good	1:1 330 000
4548		80		X	14.2 E	0.3 S			X	Good	
4549		80		X	13.3 E	0.4 S			X	Good	
4550		80		X	12.3 E	0.0			X	Good	
4551	T/O 128	80		X	11.2 E	0.2 N			X	Good	
4552	T/O 128	80		X	10.1 E	0.2 N			X	Good	
4553	T/O 128	80		X	9.4 E	0.2 N			X	Good	

TABLE A-I.—*Apollo 10 Hasselblad Photography*—Continued

(*e*) Magazine R, film 3400—*Continued*

Frame no. AS10-31-	Description	FL, mm	Vert	Obliq	Principal point		Sun angle			Photo quality	Remarks
					Long, deg	Lat, deg	High	Med	Low		
4554		80		X	8.2 E	0.3 N			X	Fair	
4555		80		X	7.0 E	0.3 N			X	Fair	
4556		80		X	6.1 E	0.4 N			X	Fair	
4557		80		X	5.2 E	0.5 N			X	Poor	
4558		80		X	4.1 E	0.8 N			X	Poor	End of pass over sites 1 and 2
4559		80		X					X	Poor	
4560	T/O 70	250		X	Above horizon		X			Good	
4561	T/O 67	250		X	60.6 E	4.8 N	X			Good	Apollonius P, F
4562	Palus Somni	250		X	46.0 E	20.0 N	X			Good	
4563	T/O 74	250		X	50.4 E	7.2 N	X			Good	Taruntius A
4564	T/O 76	250		X	45.1 E	11.4 N	X			Good	
4565	Palus Somni	250		X	Horizon		X			Good	
4566	Taruntius	250		X	46.4 E	5.7 N	X			Good	
4567	Taruntius	250		X	45.9 E	6.3 N	X			Good	
4568	T/O 76	250		X	Horizon		X			Good	Palus Somni
4569	T/O 74	250		X	46.8 E	5.8 N	X			Good	Taruntius
4570	Taruntius	250		X	45.6 E	5.2 N	X			Good	
4571	T/O 76	250		X	43.2 E	13.2 N	X			Good	
4572	T/O 78a	250		X	33.2 E	0.3 S	X			Fair	
4573		250		X	43.5 E	5.9 N	X			Good	
4574	Taruntius E, F	250		X	40.5 E	5.5 N	X			Good	
4575	T/O 78a	250		X	33.3 E	0.3 S	X			Fair	
4576	T/O 78a	250		X	33.3 E	0.3 S	X			Fair	
4577	T/O 76	250		X	39.4 E	7.9 N		X		Good	Cauchy
4578	T/O 76	250		X	38.5 E	7.8 S		X		Good	Cauchy
4579	T/O 78a	250		X	31.7 E	0.4 S	X			Fair	
4580	Near site 1	250		X	35.5 E	3.7 N	X			Good	
4581	Near site 1	250		X	36.0 E	2.9 N	X			Good	
4582	Near site 1	250		X	35.7 E	2.8 N	X			Good	
4583	Near site 1	250		X	35.7 E	2.8 N	X			Good	
4584	Near site 1	250		X	35.5 E	2.6 N	X			Good	
4585	Near site 1	250		X	36.3 E	2.6 N	X			Good	End of vertical pass over sites 1 and 2
4586	Site 1	250		X	34.7 E	2.8 N	X			Good	
4587	T/O 78a	250		X	24.6 E	0.9 S	X			Good	
4588	Sea of Tranquility	250		X	33.2 E	2.8 N	X			Good	

4589	Sea of Tranquility	250		X	33.1 E	3.0 N	X			Good	
4590	T/O 76	250		X	33.7 E	5.0 N	X			Good	
4591	Site 1	250		X	32.8 E	2.7 N	X			Fair	
4592	Site 1	250		X	32.7 E	2.7 N	X			Fair	
4593	Maskelyne H	250		X	32.4 E	2.7 N	X			Fair	
4594	Maskelyne H	250		X	33.3 E	2.8 N	X			Fair	
4595	Maskelyne H	250		X	33.2 E	2.7 N	X			Fair	
4596	Maskelyne H	250		X	32.9 E	2.7 N	X			Fair	
4597	Maskelyne H	250		X	32.9 E	2.7 N	X			Fair	
4598	North edge of Sea of Tranquility	250		X	30.1 E	10.5 N	X			Good	
4599	T/O 107	250		X	24.8 E	14.8 N	X			Good	Plinius on the horizon
4600	Maskelyne M	250		X	28.5 E	5.2 N	X			Good	
4601	T/O 112	250		X	24.5 E	0.8 S	X			Good	
4602	T/O 114	250		X	24.2 E	0.5 N	X			Good	Site 2
4603	T/O 114	250		X	24.2 E	0.5 N	X			Good	Site 2
4604	T/O 114	250		X	24.1 E	0.5 N	X			Good	Site 2
4605	T/O 114	250		X	24.1 E	0.5 N	X			Good	Site 2
4606	T/O 114	250		X	24.0 E	0.5 N	X			Good	Site 2
4607	T/O 114	250		X	24.0 E	0.5 N	X			Good	Site 2
4608	T/O 114	250		X	23.9 E	0.5 N	X			Good	Site 2
4609	T/O 114	250		X	23.7 E	0.5 N	X			Good	Site 2
4610	T/O 114	250		X	23.5 E	0.5 N	X			Good	Site 2
4611	T/O 114	250		X	23.4 E	0.0	X			Good	Site 2
4612	T/O 114	250		X	23.3 E	0.0	X			Good	Site 2
4613	Site 2 area	250		X	23.1 E	0.0	X			Good	
4614	Site 2 area	250		X	23.0 E	0.0	X			Good	
4615	Site 2 area	250		X	22.9 E	0.0	X			Good	
4616	Site 2 area	250		X	22.7 E	0.0	X			Good	
4617	Site 2 area	250		X	22.6 E	0.0	X			Good	
4618	Site 2 area	250		X	22.4 E	0.0	X			Good	
4619	Site 2 area	250		X	22.3 E	0.0	X			Good	
4620	Site 2 area	250		X	22.1 E	0.0	X			Good	
4621	Site 2 area	250		X	22.0 E	0.0	X			Good	
4622	Site 2 area	250		X	21.9 E	0.0	X			Good	
4623	Site 2 area	250		X	21.7 E	0.0	X			Good	
4624	Sea of Tranquility	250		X	24.8 E	3.5 N		X		Good	
4625	Sea of Tranquility	250		X	24.6 E	2.6 N		X		Good	
4626	Sea of Tranquility	250		X	24.6 E	5.9 N		X		Good	
4627	Sabine	250		X	21.0 E	0.4 N		X		Good	
4628	Sabine	250		X	20.7 E	0.5 N		X		Good	
4629	Sabine, Ritter	250		X	19.4 E	0.9 N		X		Good	
4630	T/O 116a	250		X	22.0 E	5.9 N	X			Good	Arago
4631	T/O 116a	250		X	23.0 E	7.1 N	X			Good	
4632	T/O 116a	250		X	22.8 E	5.4 N	X			Good	Arago

TABLE A-I.—*Apollo 10 Hasselblad Photography*—Continued

(*e*) Magazine R, film 3400—*Concluded*

Frame no. AS10-31-	Description	FL, mm	Vert	Obliq	Principal point		Sun angle			Photo quality	Remarks
					Long, deg	Lat, deg	High	Med	Low		
4633	T O 116a	250		X	22.6 E	4.7 N	X			Good	Arago
4634	Sea of Tranquility	250		X	22.8 E	2.5 N		X		Good	
4635	Sea of Tranquility	250		X	22.7 E	2.4 N		X		Good	
4636	T O 116a	250		X	22.4 E	3.2 N		X		Good	
4637	T O 116a	250		X	22.3 E	3.5 N		X		Good	
4638	T O 123	250		X	17.1 E	5.5 N		X		Good	Ariadaeus rille
4639	T O 123	250		X	16.8 E	5.7 N		X		Good	Ariadaeus rille
4640	T O 123	250		X	16.2 E	5.8 N		X		Good	Ariadaeus rille
4641	T O 123	250		X	16.1 E	5.9 N		X		Good	
4642	T O 123	250		X	14.7 E	6.6 N		X		Good	
4643	T O 123	250		X	14.6 E	6.6 N		X		Good	
4644	T O 123	250		X	14.5 E	6.6 N		X		Good	
4645	T O 123	250		X	14.4 E	6.7 N		X		Good	
4646	T O 123	250		X	13.3 E	7.1 N		X		Good	
4647	T O 128	250		X	10.6 E	2.1 N		X		Good	Godin
4648	Hyginus rille	250		X	8.5 E	7.9 N			X	Fair	
4649	Hyginus rille	250		X	8.1 E	8.0 N			X	Fair	
4650	Hyginus rille	250		X	7.6 E	8.1 N			X	Fair	
4651	Hyginus rille	250		X	7.1 E	8.2 N			X	Fair	
4652	Hyginus rille	250		X	6.6 E	8.5 N			X	Fair	
4653	Crater 221	250		X	164.3 E	10.2 N		X		Fair	
4654	Crater 221	250		X	164.1 E	10.0 N		X		Fair	
4655	Crater 221	250		X	163.9 E	10.0 N		X		Fair	
4656	Crater 221	250		X	163.6 E	10.0 N		X		Fair	
4657	Crater 221	250		X	163.2 E	9.8 N		X		Fair	
4658	Crater 221	250		X	163.0 E	9.6 N		X		Fair	
4659	Crater 218	259		X	146.6 E	6.6 N	X			Fair	
4660	Crater 218	250		X	146.2 E	6.1 N	X			Good	
4661	Crater 218	250		X	145.6 E	6.4 N	X			Good	
4662	Crater 218	250		X	144.8 E	6.9 N	X			Good	
4663	Basin IX	250		X	143.8 E	7.0 N	X			Good	
4664	Basin IX	250		X	143.5 E	7.0 N	X			Good	
4665	Basin IX	250		X	143.1 E	7.1 N	X			Good	
4666	Basin IX	250		X	142.6 E	7.0 N	X			Good	
4667	Basin IX	250		X	142.1 E	7.0 N	X			Good	
4668	Basin IX	250		X	141.9 E	7.0 N	X			Good	

4669	Basin IX	250		X	141.7 E	7.0 N	X			Good	
4670	Basin IX	250		X	141.1 E	7.0 N	X			Good	
4671	Basin IX	250		X	140.8 E	7.0 N	X			Good	
4672	Basin IX	250		X	140.5 E	7.0 N	X			Good	
4673	Basin IX	250		X	140.1 E	7.0 N	X			Good	
4674	Basin IX	250		X	139.8 E	7.0 N	X			Good	

(*f*) **Magazine S, film 3400**

Frame no. AS10-32-	Description	FL, mm	Vert	Obliq	Principal point		Sun angle			Photo quality	Remarks
					Long, deg	Lat, deg	High	Med	Low		
4675	Langrenus	250		X	61.1 E	9.4 S		X		Good	
4676	Langrenus	250		X	63.1 E	8.6 S		X		Good	
4677	Langrenus	250		X	62.2 E	8.7 S		X		Good	
4678	Langrenus	250		X	59.2 E	7.5 S		X		Good	
4679	Langrenus	250		X	59.2 E	7.5 S		X		Good	
4680	Langrenus	250		X	59.3 E	9.0 S		X		Good	
4681	Langrenus	250		X	59.4 E	10.0 S		X		Good	
4682	Sea of Fertility; Taruntius H, K, P	250		X	54.1 E	0.0		X		Good	
4683	Sea of Fertility; Taruntius H, K, P	250		X	53.0 E	0.3 N		X		Good	
4684	Sea of Fertility; Taruntius K, H, G	250		X	52.5 E	0.5 N		X		Good	
4685	Taruntius G	250		X	50.0 E	0.3 N		X		Good	
4686	Sea of Fertility	250		X	50.7 E	1.8 N		X		Good	
4687	Sea of Fertility; Taruntius H, K, P	250		X	49.5 E	1.0 N		X		Good	
4688	Taruntius G	250		X	47.9 E	0.3 N		X		Good	
4689	Sea of Fertility	250		X	47.0 E	1.1 N		X		Good	
4690	Secchi	250		X	46.0 E	1.1 N		X		Good	
4691	Secchi	250		X	44.2 E	2.0 N		X		Good	Hatch window shadow
4692	Lubbock S	250		X	43.3 E	0.7 N		X		Good	
4693	Near T/O 78a; Lubbock S	250		X	42.6 E	0.8 N		X		Good	
4694	Near T/O 78a; Lubbock S	250		X	42.2 E	0.6 N		X		Good	
4695	Near T/O 78a; Lubbock S	250		X	41.6 E	0.6 N		X		Good	
4696	Near T/O 78a; Lubbock S	250		X	41.1 E	0.7 N		X		Good	
4697	Near T/O 78a; Lubbock S	250		X	40.4 E	1.1 N		X		Good	
4698	Near T/O 78a; Lubbock S	250		X	40.4 E	1.2 N		X		Good	
4699	Near T/O 78a; Lubbock S	250		X	40.6 E	0.2 N		X		Poor	Blurred (blocked view of CSM window)

TABLE A–I.—*Apollo 10 Hasselblad Photography*—Continued

(*f*) Magazine S, film 3400—*Continued*

Frame no. AS10-32-	Description	FL, mm	Vert	Obliq	Principal point		Sun angle			Photo quality	Remarks
					Long, deg	Lat, deg	High	Med	Low		
4700	Near T O 78a; Lubbock S	250		X	40.1 E	1.1 N		X		Good	
4701	Near T O 78a; Lubbock S	250		X	39.7 E	1.2 N		X		Good	
4702	Sea of Tranquility	250		X	39.4 E	1.1 N		X		Good	
4703	Sea of Tranquility	250		X	39.0 E	1.1 N		X		Good	
4704	Site 1	250		X	37.8 E	1.4 N		X		Good	
4705	Site 1	250		X	36.9 E	1.6 N		X		Good	
4706	Site 1	250		X	34.6 E	2.1 N		X		Good	
4707	Site 1	250		X	35.1 E	2.0 N		X		Good	
4708	Site 1	250		X	35.1 E	2.2 N		X		Good	
4709	T O 78a; Maskelyne	250		X	33.5 E	2.2 N		X		Good	Hand-held obliques blocked view (CSM window)
4710	T O 78a; Maskelyne	250		X	33.2 E	2.3 N		X		Good	Hand-held obliques blocked view (CSM window)
4711	T O 78a; Maskelyne	250		X	31.3 E	1.6 N		X		Good	Hand-held obliques blocked view (CSM window)
4712	T O 78a; Maskelyne	250		X	30.4 E	1.4 N		X		Good	Hand-held obliques blocked view (CSM window)
4713	T O 78a; Maskelyne	250		X	29.5 E	1.3 N		X		Good	Hand-held obliques blocked view (CSM window)
4714	T O 78a; Maskelyne	250		X	28.6 E	1.3 N		X		Good	Hand-held obliques blocked view (CSM window)
4715	Sea of Tranquility	250		X	27.8 E	1.1 N		X		Good	Hand-held obliques blocked view (CSM window)
4716	T O 104; Theophilus	250		X	25.3 E	12.5 S		X		Good	
4717	T O 104; Theophilus	250		X	25.7 E	12.8 S		X		Good	
4718	T O 104; Theophilus	250		X	24.3 E	11.9 S		X		Good	
4719	Near T O 114; site 2	250		X	26.3 E	0.2 N		X		Good	
4720	Near T O 114; site 2	250		X	25.9 E	0.4 N		X		Good	
4721	Near T O 114; site 2	250		X	25.2 E	0.1 N		X		Good	
4722	Near T O 114; site 2	250		X	24.5 E	0.1 N		X		Good	
4723	Near T O 114; site 2	250		X	23.4 E	0.1 N		X		Good	
4724	Near T O 114; site 2	250		X	24.1 E	0.8 S		X		Good	
4725	Sabine	250		X	23.9 E	0.4 N		X		Good	
4726	Sabine	250		X	23.5 E	0.4 N			X	Good	Hand-held obliques
4727	T O 114; Sabine; Ritter	250		X	23.0 E	0.4 N			X	Good	Hand-held obliques
4728	T O 114; Sabine; Ritter	250		X	22.5 E	0.5 N			X	Good	Hand-held obliques

4729	T O 114; Sabine; Ritter	250		X	22.0 E	0.4 N			X	Good	Hand-held obliques
4730	T O 114; Sabine; Ritter	250		X	21.4 E	0.5 N			X	Good	Hand-held obliques
4731	T O 114; Sabine; Ritter	250		X	20.6 E	0.5 N			X	Good	Hand-held obliques
4732	Delambre	250		X	Above horizon				X	Good	Hand-held obliques
4733	Delambre	250		X	17.2 E	2.5 S			X	Good	Hand-held obliques
4734	Central Bay; Triesnecker; T O 123	250		X	1.0 W	5.0 N			X	Good	Looking into darkness
4735	T O 142; Oppolzer	250		X	In darkness				X	Good	Looking into darkness
4736	Albategnius	250		X	Above horizon				X	Good	Looking into darkness
4737	T O 142; Oppolzer	250		X	In darkness				X	Good	Looking into darkness
4738	T O 142; Blagg	250		X	3.0 W	2.4 S			X	Good	Looking into darkness
4739	T O 78a; mare near Lubbock S	80	X		43.1 E	0.8 N		X		Good	1:1 451 625
4740	T O 78a; mare near Lubbock S	80	X		42.2 E	0.6 N		X		Good	1:1 451 625
4741	T O 78a; Lubbock S	80	X		40.7 E	0.6 N		X		Good	1:1 451 675
4742	Sea of Tranquility; T O 78a	80	X		39.3 E	0.5 N		X		Good	
4743	Sea of Tranquility	80	X		37.8 E	0.5 N		X		Good	
4744	Sea of Tranquility	80		X	36.1 E	0.5 N		X		Good	
4745	Censorinus A; Maskelyne; T O 78	80		X	35.0 E	0.5 N		X		Good	
4746	Censorinus A; Maskelyne; T O 78	80		X	32.1 E	0.7 N		X		Good	
4747	Censorinus A; Maskelyne; T O 78	80		X	30.3 E	0.7 N		X		Good	
4748	Maskelyne	80		X	28.2 E	0.8 N		X		Good	
4749	Site 2; T O 112	80		X	27.0 E	0.8 N		X		Good	
4750	Site 2; T O 112, 114	80		X	25.3 E	0.6 N		X		Good	
4751	Site 2; T O 112, 114	80		X	25.0 E	0.6 N		X		Good	
4752	Site 2; T O 112, 114	80		X	24.6 E	0.5 N		X		Good	
4753	Site 2; T O 112, 114	80		X	23.7 E	0.5 N		X		Good	
4754	Site 2; T O 112; Sabine; Ritter	80		X	23.3 E	0.5 N		X		Good	
4755	Site 2; T O 114	80		X	22.6 E	0.5 N		X		Good	
4756	Site 2; T O 114	80		X	22.0 E	0.5 N		X		Good	
4757	Site 2; T O 114; Sabine; Ritter	80		X	21.3 E	0.4 N		X		Good	
4758	Dionysius; T O 114; Sabine; Ritter	80		X	20.5 E	0.4 N		X		Good	
4759	Dionysius; T O 114; Sabine; Ritter	80		X	20.0 E	0.4 N		X		Good	
4760	Sabine; Ritter	80		X	19.2 E	0.3 N		X		Good	
4761	Sabine; Ritter; Delambre	80		X	18.5 E	0.2 N		X		Good	
4762	Delambre	80		X	17.6 E	0.1 N		X		Good	
4763	Theon Senior	80		X	16.9 E	0.1 N		X		Good	

TABLE A–I.—*Apollo 10 Hasselblad Photography*—Continued

(*f*) Magazine S, film 3400—*Continued*

Frame no. AS10-32-	Description	FL, mm	Vert	Obliq	Principal point		Sun angle			Photo quality	Remarks
					Long, deg	Lat, deg	High	Med	Low		
4764	Theon Senior	80		X	16.1 E	0.1 N		X		Good	
4765	Theon Senior	80		X	15.2 E	0.0		X		Good	
4766	Theon Senior	80	X		14.4 E	0.1 N		X		Good	1:1 300 000
4767	Theon Senior	80	X		13.6 E	0.1 N		X		Good	1:1 300 000
4768	Lade	80	X		12.6 E	0.1 N		X		Good	1:1 300 000
4769	Lade	80	X		11.9 E	0.1 N		X		Good	1:1 300 000
4770	Lade	80	X		10.9 E	0.2 N		X		Good	1:1 300 000
4771	Lade	80	X		10.1 E	0.1 N		X		Good	1:1 300 000
4772	Lade	80	X		9.4 E	0.0			X	Good	1:1 300 000
4773	Lade	80	X		9.85 E	0.0			X	Good	1:1 300 000
4774	Highlands	80	X		7.6 E	0.0			X	Good	1:1 300 000
4775	Highlands	80	X		6.7 E	0.0			X	Good	1:1 300 000
4776	Highlands	80	X		5.9 E	0.0			X	Good	1:1 300 000
4777	Central Bay; highlands	80	X		5.1 E	0.3 N			X	Good	1:1 300 000
4778	Central Bay; highlands	80	X		4.4 E	0.3 N			X	Good	1:1 300 000
4779	Central Bay; highlands	80	X		4.1 E	0.3 N			X	Good	1:1 300 000
4780	Central Bay; highlands	80	X		3.6 E	0.4 N			X	Good	1:1 300 000
4781	Central Bay; highlands	80	X		3.2 E	0.4 N			X	Good	1:1 350 000
4782	Central Bay; Blagg; Bruce; site 3	80	X		3.1 E	0.5 N			X	Good	1:1 500 000
4783	T O 142	80		X	03.0 E	0.6 N			X	Poor	Bad glare
4784	T O 142	80		X	2.6 E	0.5 N			X	Poor	Bad glare
4785	Central Bay; Blagg; T O 142	80		X	1.2 E	0.4 N			X	Poor	Bad glare
4786	T O 142	80		X	0.1 W	0.3 N			X	Poor	Bad glare
4787	T O 142	80		X	1.2 W	0.2 N			X	Poor	Bad glare into terminator
4788	T O 142; Oppolzer	80		X	2.5 W	0.0			X	Poor	Bad glare into terminator
4789	T O 142; highlands	80		X	3.9 W	0.2 S			X	Poor	Bad glare into terminator
4790	T O 29; crater 302	80		X	161.2 E	13.2 S		X		Good	
4791	T O 29; crater 302	80		X	159.1 E	14.2 S		X		Good	
4792	Crater 300; T O 29	80		X	157.0 E	7.1 S		X		Good	
4793	Crater 300; T O 29	80		X	Above horizon			X		Good	
4794	T O 29; crater 297	80		X	149.5 E	6.2 S		X		Good	
4795	T O 29; crater 297	80		X	149.1 E	13.2 S		X		Good	
4796	T O 29; crater 297	80		X	146.0 E	10.1 S		X		Good	
4797	T/O 29; crater 297	80		X	147.4 E	5.0 S		X		Good	
4798	T/O 29; crater 297	80		X	144.1 E	11.4 S		X		Good	

4799	Unknown	80		X	Above horizon		X			Fair	Unable to locate
4800	Unknown	80		X	Above horizon		X			Fair	Unable to locate
4801	Unknown	80		X	Above horizon		X			Fair	Unable to locate
4802	Smyth's Sea; T/O 59	80		X	Above horizon		X			Fair	
4803	Smyth's Sea; T/O 59	80		X	Above horizon		X			Fair	
4804	Smyth's Sea; T/O 59	80		X	Above horizon		X			Fair	
4805	Crater 263	80		X	Above horizon		X			Fair	
4806	Crater 263; Kastner R	80		X	Above horizon		X			Fair	
4807	Crater 263; Kastner R	80		X	Above horizon		X			Fair	
4808	Earth; Gilbert M, N	80		X	Above horizon		X			Fair	
4809	T/O 123; Hyginus Rille	80		X	6.5 E	9.0 N		X		Good	
4810	T/O 123; Hyginus Rille	80		X	5.2 E	9.5 N		X		Good	
4811	Hyginus Rille; T/O 123	80		X	7.4 E	7.2 N			X	Good	
4812	Central Bay	80		X	1.2 W	1.4 N			X	Good	
4813	Hyginus; T/O 123; Hyginus Rille	80		X	5.3 E	8.2 N			X	Good	
4814	Hyginus; T/O 123; Hyginus Rille	80		X	5.2 E	7.4 N			X	Good	
4815	Hyginus; T/O 123; Hyginus Rille	80		X	5.1 E	7.2 N			X	Good	
4816	Triesnecker; T/O 123; Central Bay	80		X	2.3 E	8.2 N			X	Good	
4817	Triesnecker; T/O 123; Central Bay	80		X	4.1 E	4.5 N			X	Good	
4818	Central Bay	80		X	3.1 W	1.3 N			X	Good	
4819	Triesnecker; T/O 123; Central Bay	80		X	4.3 E	5.2 N			X	Good	
4820	Triesnecker; T/O 123; Central Bay	80		X	0.2 W	10.4 N			X	Good	
4821	Triesnecker; T/O 123; Central Bay	80		X	0.5 W	8.3 N			X	Good	
4822	Triesnecker; T/O 123; Central Bay	80		X	Above horizon				X	Good	
4823	T/O 28; crater 302	80		X	162.2 E	10.1 S			X	Good	
4824	T/O 28; crater 302	80		X	161.2 E	9.3 S			X	Good	
4825	North of (adjacent to) crater 299; T/O 29	80		X			X			Good	
4826	Crater 299; T/O 29	80		X	156.0 E	2.0 S	X			Good	
4827	Crater 299; T/O 29	80		X	148.1 E	4.1 N	X			Good	
4828	T/O 29; crater 295	80		X	146.5 E	4.1 S	X			Good	
4829	T/O 59; Smyth's Sea	80		X	82.3 E	1.1 S	X			Good	
4830	T/O 59; Smyth's Sea	80	X		82.2 E	0.2 N	X			Good	1:1 202 775
4831	North of (adjacent to) Gilbert M	80	X		76.2 E	1.5 S	X			Good	1:1 202 775

TABLE A–I.—*Apollo 10 Hasselblad Photography*—Continued

(*f*) Magazine S, film 3400—*Concluded*

Frame no. AS10–32–	Description	FL, mm	Vert	Obliq	Principal point		Sun angle			Photo quality	Remarks
					Long, deg	Lat, deg	High	Med	Low		
4832	North of (adjacent to) Gilbert M	80	X		75.0 E	3.0 S	X			Good	1:1 202 775
4833		80	X		72.0 E	4.0 S	X			Good	1:1 202 775
4834	Maclaurin	80		X	69.4 E	1.5 S	X			Good	
4835	Maclaurin	80		X	69.4 E	1.4 N	X			Good	
4836	Maclaurin	80		X	69.0 E	1.1 N	X			Good	
4837	Maclaurin	80		X	66.5 E	1.2 N	X			Good	
4838	T O 67	80		X	62.0 E	2.5 N	X			Good	
4839		80		X	66.0 E	5.0 S	X			Good	
4840		80		X	84.2 E	1.0 S	X			Good	
4841	T O 78a	80		X	36.3 E	3.4 S	X			Good	
4842	T O 78a	80		X	38.4 E	0.5 S	X			Good	
4843	Censorinus A	80	X		33.4 E	1.0 S	X			Good	1:1 587 000
4844	Censorinus A	80	X		33.0 E	0.3 S	X			Good	1:1 463 000
4845	Censorinus A	80	X		32.2 E	0.4 S	X			Good	1:1 375 000; hatch frame window
4846	Sea of Tranquility	80	X		28.2 E	0.2 N		X		Good	1:1 375 000; hatch frame window
4847	T O 112; Moltke	80	X		25.4 E	1.2 S		X		Good	1:1 148 213; hatch frame window
4848	T O 112; Moltke	80	X		24.4 E	0.2 S		X		Good	1:1 375 000; hatch frame window
4849	T O 112; Moltke	80	X		23.3 E	0.3 S		X		Good	1:1 375 000; hatch frame window
4850	Near T O 113	80		X	14.5 E	0.4 N		X		Good	
4851	Near T O 113	80		X	14.3 E	0.5 N		X		Fair	
4852	Near T O 113	80		X	13.4 E	0.5 N		X		Fair	
4853	T O 128; Lade; Godin	80		X	8.0 E	0.1 N		X		Fair	
4854	Central Bay; T O 142; Blagg; Bruce	80		X	6.0 E	0.4 N		X		Fair	
4855	Central Bay; T O 142; Blagg; Bruce	80		X	5.0 E	0.4 N			X	Fair	
4856	Central Bay; T O 142; Blagg; Bruce	80		X	2.5 E	0.3 N			X	Fair	

(*g*) Magazine T, film 3400

Frame no. AS10-33-	Description	FL, mm	Vert	Obliq	Principal point		Sun angle			Photo quality	Remarks
					Long, deg	Lat, deg	High	Med	Low		
4857	Near crater 220	250		X	159.5 E	3.5 N	X			Poor	
4858	Near crater 220	250		X	158.5 E	2.0 N	X			Poor	
4859	Near crater 220	250		X	157.5 E	3.5 N	X			Poor	
4860	Crater 220	250		X	159.5 E	4.0 N	X			Poor	
4861	Crater 220	250		X	160.0 E	5.0 N	X			Poor	
4862	Near crater 220	250		X	158.5 E	2.0 N	X			Poor	
4863	Near crater 301	250		X	160.0 E	3.5 S	X			Poor	
4864		250		X	156.5 E	1.0 N	X			Poor	
4865	Crater 297	250		X	151.0 E	4.5 S	X			Poor	
4866	Crater 297	250		X	152.0 E	5.0 S	X			Poor	
4867	Removed	250		X	152.0 E	5.0 S	X			Poor	
4868	Crater 297	250		X	152.0 E	5.0 S	X			Poor	
4869	Crater 217	250		X	134.5 E	1.5 N	X			Poor	
4870	Near crater 217	250		X	134.0 E	0.0	X			Poor	
4871	Near crater 217	250		X	131.0 E	0.0	X			Poor	
4872	Near crater 286	250		X	130.0 E	2.0 S	X			Poor	
4873	T/O 45	250		X	122.0 E	5.5 S	X			Poor	
4874	T/O 45	250		X	122.0 E	5.5 S	X			Poor	
4875	T/O 45	250		X	122.0 E	6.5 S	X			Poor	
4876	Not used										
4877	Not used										
4878	Not used										
4879	T/O 45	250		X	122.0 E	5.5 S	X			Poor	
4880	Crater 273	250		X	109.0 E	6.0 S	X			Poor	
4881	Crater 273	250		X	110.5 E	4.0 S	X			Poor	
4882	Crater 273	250		X	110.5 E	4.0 S	X			Poor	
4883	Not used										
4884	Not used										
4885	T/O 59	250		X	90.0 E	2.0 S	X			Poor	
4886	Mare Smythii	250		X	88.0 E	3.0 N	X			Poor	
4887	T/O 59	250		X	90.0 E	2.0 S	X			Poor	
4888		250		X	89.5 E	6.0 S	X			Poor	
4889	Near crater 266	250		X	89.5 E	6.0 S	X			Poor	
4890	T/O 59	250		X	90.0 E	2.0 S	X			Poor	
4891		250		X	86.5 E	7.0 S	X			Poor	
4892	Near Mare Spumans	250		X	66.0 E	3.0 S	X			Poor	
4893		250		X	61.5 E	3.0 S	X			Poor	
4894		250		X	61.5 E	3.0 S	X			Poor	

TABLE A–I.—*Apollo 10 Hasselblad Photography*—Continued

(*g*) Magazine T, film 3400—*Continued*

Frame no. AS10–33–	Description	FL, mm	Vert	Obliq	Principal point		Sun angle			Photo quality	Remarks
					Long, deg	Lat, deg	High	Med	Low		
4895		250		X	63.0 E	3.0 S	X			Poor	
4896		250		X	56.0 E	2.5 S	X			Fair	
4897		250		X	56.5 E	3.0 S	X			Fair	
4898		250		X	56.5 E	3.0 S	X			Fair	
4899	Sea of Fertility	80	X		53.8 E	1.6 S		X		Fair	1:1 250 000
4900	Sea of Fertility	80	X		53.9 E	2.1 S		X		Fair	1:1 250 000
4901	Sea of Fertility	80	X		53.6 E	2.6 S		X		Fair	1:1 250 000
4902	Sea of Fertility	80	X		52.2 E	0.7 N		X		Good	1:1 700 000
4903	Sea of Fertility	80	X		52.3 E	0		X		Good	1:1 700 000
4904	Sea of Fertility	80		X	49.9 E	2.1 N		X		Good	
4905	Sea of Fertility	80	X		44.3 E	1.3 N		X		Fair	1:1 000 000
4906	T O 75	80	X		48.1 E	1.6 S		X		Fair	1:1 000 000
4907	West of Censorinus	80	X		38.2 E	2.3 S		X		Fair	1:1 000 000
4908	Gutenberg	80		X	40.4 E	6.6 S			X	Fair	
4909	West of Maskelyne	80	X		27.5 E	3.6 S			X	Poor	1:1 000 000
4910	Theophilus	80		X	25.9 E	10.9 S	X			Poor	
4911	Crater 227	80		X	174.4 E	7.1 N	X			Good	
4912	Crater 226	80		X	173.4 E	12.2 N	X			Good	
4913	East of crater 221	80		X	166.4 E	5.4 N	X			Good	
4914	T O 34	250		X	139.4 E	7.1 N	X			Poor	
4915	T O 34	250		X	130.8 E	5.5 N	X			Poor	
4916	West of T O 34	250		X	128.3 E	7.3 N	X			Poor	
4917	Crater 212	250		X	124.4 E	11.0 N	X			Poor	
4918	T O 46	250		X	120.0 E	6.6 N	X			Poor	
4919	T O 55	250		X	100.2 E	4.8 N	X			Poor	
4920	Neper	250		X	84.7 E	8.7 N	X			Poor	
4921	Neper	80		X	85.3 E	8.7 N	X			Poor	
4922	Oblique strip; Sea of Tranquility including T O 78, 114, 120	80		X	37.5 E	0.7 N	X			Poor	
4923	Oblique strip; Sea of Tranquility including T O 78, 114, 120	80		X	39.0 E	0.8 N	X			Poor	
4924	Oblique strip; Sea of Tranquility including T O 78, 114, 120	80		X	39.0 E	0.2 N	X			Poor	

4925	Oblique strip; Sea of Tranquility including T O 78, 114, 120	80		X	30.6 E	1.3 N	X			Poor
4926	Oblique strip; Sea of Tranquility including T O 78, 114, 120	80		X	32.7 E	1.4 N	X			Poor
4927	Oblique strip; Sea of Tranquility including T O 78, 114, 120	80		X	32.6 E	1.2 N	X			Poor
4928	Oblique strip; Sea of Tranquility including T O 78, 114, 120	80		X	31.0 E	0.9 N	X			Poor
4929	Oblique strip; Sea of Tranquility including T O 78, 114, 120	80		X	30.7 E	0.9 N	X			Poor
4930	Oblique strip; Sea of Tranquility including T O 78, 114, 120	80		X	30.5 E	0.9 N	X			Poor
4931	Oblique strip; Sea of Tranquility including T O 78, 114, 120	80		X	29.6 E	1.1 N	X			Poor
4932	Oblique strip; Sea of Tranquility including T O 78, 114, 120	80		X	29.0 E	0.9 N	X			Poor
4933	Oblique strip; Sea of Tranquility including T O 78, 114, 120	80		X	27.1 E	1.0 N	X			Poor
4934	Oblique strip; Sea of Tranquility including T O 78, 114, 120	80		X	26.9 E	0.9 N	X			Poor
4935	Oblique strip; Sea of Tranquility including T O 78, 114, 120	80		X	25.1 E	0.8 N	X			Poor
4936	Oblique strip; Sea of Tranquility	80		X	24.5 E	0.8 N	X			Poor
4937	Oblique strip; Sea of Tranquility	80		X	23.3 E	0.5 N	X			Poor
4938	Oblique strip; Sea of Tranquility	80		X	21.5 E	0.5 N	X			Poor
4939	Oblique strip; Sea of Tranquility	80		X	20.1 E	0.6 N	X			Poor
4940	Oblique strip; Sea of Tranquility	80		X	19.1 E	0.5 N	X			Poor
4941	Oblique strip; Sea of Tranquility	80		X	18.5 E	0.6 N	X			Poor

TABLE A–I.—*Apollo 10 Hasselblad Photography*—Continued

(*g*) **Magazine T, film 3400**—*Concluded*

Frame no. AS10–33–	Description	FL, mm	Vert	Obliq	Principal point		Sun angle			Photo quality	Remarks
					Long, deg	Lat, deg	High	Med	Low		
4942	Oblique strip; Sea of Tranquility	80		X	18.0 E	0.5 N	X			Poor	
4943	Oblique strip; Sea of Tranquility	80		X	17.7 E	0.6 N	X			Poor	
4944	Oblique strip; Sea of Tranquility	80		X	16.6 E	0.5 N	X			Poor	
4945	Oblique strip; Sea of Tranquility	80		X	16.0 E	0.5 N	X			Poor	
4946	T O 128	80	X		6.3 E	1.2 N			X	Good	1:1 000 000
4947	T O 128	80	X		6.0 E	1.3 N			X	Good	1:1 000 000
4948	T O 128	80	X		5.7 E	1.4 N			X	Good	1:1 000 000
4949	Rhaeticus	80		X	6.7 E	1.5 N			X	Poor	
4950	Rhaeticus	80		X	6.2 E	1.6 N			X	Poor	
4951	Sinus Medii	80		X	4.6 E	1.4 N			X	Poor	
4952	Sinus Medii	80		X	3.3 E	1.4 N			X	Poor	
4953	Sinus Medii	80		X	1.5 E	1.5 N			X	Poor	
4954	Craters 302, 305	80		X	Over horizon				X	Good	
4955	Craters 302, 305	80		X	167.9 E	11.4 S			X	Good	
4956	Craters 302, 305	80		X	166.3 E	12.0 S			X	Good	
4957	Craters 302, 305	80		X	166.0 E	11.8 S			X	Good	
4958	Craters 302, 305	80		X	165.0 E	11.5 S			X	Good	
4959	Craters 302, 305	80		X	164.4 E	11.5 S			X	Good	
4960	Craters 302, 305	80		X	163.7 E	11.9 S			X	Good	
4961	Craters 302, 305	80		X	162.9 E	11.9 S		X		Good	
4962	Craters 302, 305	80		X	162.0 E	11.9 S		X		Good	
4963	Craters 302, 305	80		X	Over horizon			X		Good	
4964	Craters 302, 305	80		X	Over horizon			X		Good	
4965	Crater 297	250		X	152.0 E	5.4 S	X			Good	
4966	T O 29	250		X	146.4 E	5.2 S	X			Fair	
4967	T O 29	250		X	146.4 E	4.4 S	X			Fair	
4968	T O 29	250		X	146.2 E	4.9 S	X			Fair	
4969	T O 29	250		X	146.4 E	5.7 S	X			Fair	
4970	T O 29	250		X	146.2 E	5.7 S	X			Fair	
4971	Craters 292, 293	250		X	140.4 E	6.0 S	X			Fair	
4972	Craters 292, 293	250		X	140.1 E	6.0 S	X			Fair	
4973	Craters 292, 293	250		X	140.1 E	5.9 S	X			Fair	

4974	Craters 292, 293	250		X	139.4 E	6.3 S	X			Fair
4975	Craters 292, 293	250		X	139.4 E	5.7 S	X			Fair
4976	T O 33	250		X	136.8 E	4.2 S	X			Fair
4977	T O 33	250		X	137.2 E	3.5 S	X			Fair
4978	T O 41	250		X	129.3 E	4.6 S	X			Fair
4979	T O 41	250		X	128.9 E	4.7 S	X			Fair
4980	T O 41	250		X	127.8 E	6.0 S	X			Fair
4981	T O 41	250		X	127.5 E	5.0 S	X			Fair
4982	T O 41	250		X	127.3 E	5.7 S	X			Fair
4983	T O 41	250		X	126.7 E	5.3 S	X			Fair
4984	T O 41	250		X	125.7 E	6.0 S	X			Poor
4985	T O 41	250		X	124.9 E	6.5 S	X			Poor
4986	T O 41	250		X	124.0 E	6.8 S	X			Poor
4987	T O 45	250		X	122.4 E	6.4 S	X			Poor
4988	T O 45	250		X	122.4 E	5.3 S	X			Poor
4989	T O 45	250		X	122.3 E	5.0 S	X			Poor
4990	T O 45	250		X	122.1 E	5.2 S	X			Poor
4991	Crater 279	250		X	119.2 E	11.2 S	X			Poor
4992	Crater 279	250		X	117.9 E	10.6 S	X			Poor
4993	Crater 279	250		X	117.2 E	11.0 S	X			Poor
4994	Unused									
4995	Unused									
4996	T O 59	250		X	85.9 E	0.3 S	X			Poor
4997	T O 59	250		X	83.6 E	0.5 S	X			
4998	T O 59	250		X	80.1 E	3.9 S	X			
4999	T O 59	250		X	82.1 E	1.0 S	X			Poor
5000	T O 59	250		X	82.0 E	0.7 S	X			Poor
5001	T O 59	250		X	79.5 E	1.6 S	X			Poor
5002	T O 59	250		X	78.9 E	1.6 S	X			Poor
5003	T O 59	250		X	78.6 E	1.4 S	X			Poor
5004	T O 59	250		X	78.1 E	1.2 S	X			Poor
5005	T O 59	250		X	77.8 E	0.7 S	X			Poor
5006	T O 59	250		X	77.8 E	0.7 S	X			Poor
5007	T O 59	250		X	77.8 E	0.7 S	X			Poor
5008	T O 59	250		X	77.2 E	0.7 S	X			Poor

TABLE A–I.—*Apollo 10 Hasselblad Photography*—Continued

(*h*) Magazine M, film SO–368

[Available in color]

Frame no. AS10–34–	Description	FL, mm	Vert	Obliq	Principal point		Sun angle			Photo quality	Remarks
					Long, deg	Lat, deg	High	Med	Low		
5009	Earth	80			TLI (PP in space)					Good	Cloud cover
5010	Earth	80			TLI (PP in space)					Good	Cloud cover
5011	LM in S–IVB	80			TLI (PP in space)					Good	
5012	Earth	80			TLI (PP in space)					Good	Cloud cover
5013	Earth	80			TLI (PP in space)					Good	Western U.S.; Mexico; stereo pair
5014	Earth	80			TLI (PP in space)					Good	Western U.S.; Mexico; stereo pair
5015	Earth	80			TLI (PP in space)					Good	Western U.S.; Mexico; stereo pair
5016	Earth	80			TLI (PP in space)					Good	Western U.S.; Mexico; stereo pair
5017	Earth	80			TLI (PP in space)					Good	Southwest U.S.; Mexico; stereo
5018	Earth	80			TLI (PP in space)					Good	Southwest U.S.; Mexico; stereo
5019	Earth	80			TLI (PP in space)					Good	Southwest U.S.; Mexico; stereo
5020	Earth	80			TLI (PP in space)					Good	North Africa to Sinai
5021	Earth	80			TLI (PP in space)					Good	North Africa to Sinai
5022	Earth	80			TLI (PP in space)					Good	North Africa to Sinai
5023	Earth	80			TLI (PP in space)					Good	North Africa to Sinai
5024	Earth	80			TLI (PP in space)					Good	North Africa to Sinai
5025	Overexposed										No imagery
5026	Earth	250			TLI (PP in space)					Good	North Africa; Sinai
5027	Earth	250			TLI (PP in space)					Good	North Africa; Sinai
5028	Earth	250			TLI (PP in space)					Good	North Africa
5029	Earth	250			TLI (PP in space)					Fair	Earth almost missed
5030	Earth	250			TLI (PP in space)					Good	North Africa
5031	Earth	250			TLI (PP in space)					Good	North Africa
5032	Earth	250			TLI (PP in space)					Good	Stereo pair; North Africa
5033	Earth	250			TLI (PP in space)					Good	Stereo pair; North Africa
5034	Earth	250			TLI (PP in space)					Good	North and South America

5035	Earth	250			TLI (PP in space)					Good	North and South America
5036	Earth	250			TLI (PP in space)					Good	North and South America
5037	Earth	250			TLI (PP in space)					Good	North America
5038	Earth	250			TLI (PP in space)					Good	North America
5039	Earth	250			TLI (PP in space)					Good	North America
5040	Earth	250			TLI (PP in space)					Good	North America
5041	Earth	250			TLI (PP in space)					Good	North America
5042	Earth	250			TLI (PP in space)					Good	Africa and Mideast
5043	Earth	250			TLI (PP in space)					Good	Africa-Mideast
5044	Earth	250			TLI (PP in space)					Good	Africa-Mideast
5045	Earth	250			TLI (PP in space)					Good	Africa-Mideast
5046	Earth	250			TLI (PP in space)					Good	Africa-Mideast
5047	Earth	250			TLI (PP in space)					Good	Africa-Mideast
5048	Earth	250			TLI (PP in space)					Good	Africa-Mideast
5049	Earth	250			TLI (PP in space)					Good	Northwest Africa
5050	Earth	250			TLI (PP in space)					Good	Northwest Africa to U.S. coast
5051	Earth	250			TLI (PP in space)					Good	Northwest Africa to U.S. coast
5052	Earth	250			TLI (PP in space)					Good	Northwest Africa to U.S. coast
5053	LM	80			TLI (PP in space)					Good	VHF antenna array
5054	Earth	250			TLI (PP in space)					Good	U.S. and Mexico
5055	Earth	250			TLI (PP in space)					Good	U.S. and Mexico
5056	LM	80			TLI (PP in space)					Good	LM high-gain antenna
5057	LM	80			TLI (PP in space)					Good	LM high-gain antenna
5058	LM	80			TLI (PP in space)					Good	LM high-gain antenna
5059	LM	80			TLI (PP in space)					Good	LM high-gain antenna
5060	LM	80			TLI (PP in space)					Good	VHF antenna and attitude nozzle
5061	LM	80			TLI (PP in space)					Good	VHF antenna and attitude nozzle
5062	LM	80			TLI (PP in space)					Good	Docking target
5063	LM	80			TLI (PP in space)					Good	Rendezvous window
5064	LM	80			TLI (PP in space)					Good	Attitude nozzles
5065	LM	80			TLI (PP in space)					Good	Rendezvous window
5066	LM	80			TLI (PP in space)					Good	Rendezvous window
5067	LM	80			TLI (PP in space)					Good	Attitude nozzles
5068	Earth	250			TLI (PP in space)					Good	Western U.S. and Mexico
5069	Earth	250			TLI (PP in space)					Good	Western U.S. and Mexico
5070	Earth	250			TLI (PP in space)					Good	Western U.S. and Mexico
5071	Earth	250			TLI (PP in space)					Good	Northwest Africa
5072	Earth	250			TLI (PP in space)					Good	Africa to the Americas
5073	Moltke; Moltke B; Rima Hypatia I	80		X	24.2 E	0.6 N			X	Good	Africa to the Americas

TABLE A-I.—*Apollo 10 Hasselblad Photography*—Continued

(*h*) Magazine M, film SO-368—*Continued*

[Available in color]

Frame no. AS10-34-	Description	FL, mm	Vert	Obliq	Principal point		Sun angle			Photo quality	Remarks
					Long, deg	Lat, deg	High	Med	Low		
5074											Washed out
5075											Washed out
5076											Washed out
5077											Washed out
5078											Not located
5079											Not located
5080	Sea of Tranquility	80		X	35.2 E	2.0 N			X	Fair	
5081	Neper	80		X	85.0 E	4.0 N	X			Good	
5082	LM	80			(PP in space)					Good	Reflections on window
5083	LM				(PP in space)					Good	Reflections on window
5084	LM	80			(PP in space)					Good	Reflections on window
5085	LM	80			(PP in space)					Good	Reflections on window
5086	LM	80			(PP in space)					Good	Reflections on window
5087	LM	80			(PP in space)					Good	Reflections on window
5088	LM	80			(PP in space)					Good	Reflections on window
5089	LM	80			(PP in space)					Good	Reflections on window
5090	LM	80			(PP in space)					Good	Reflections on window
5091	LM	80			(PP in space)					Good	Reflections on window
5092	LM	80			(PP in space)					Good	Reflections on window
5093	Crater Webb and Foaming Sea	80		X	65.0 E	1.5 N			X	Good	Reflections on window
5094	Crater Webb and Foaming Sea	80		X	58.5 E	1 S		X		Good	
5095	Sea of Crises; Picard and Lick	80		X	54.0 E	9.5 N		X		Good	
5096	Sea of Crises; Picard and Lick	80		X	50.0 E	11 N		X		Good	
5097	Sea of Crises; Picard and Lick	80		X	50.0 E	6 N		X		Good	
5098	Taruntius A and U	80		X	50.0 E	5 N			X	Good	
5099	Moltke and landing site 2	80		X	27.2 E	0.7 N	X			Good	Overlap with AS10-34-5100
5100	Moltke and landing site 2	80		X	26.2 E	0.7 N	X			Fair	Overlap with AS10-34-5099
5101		80		X	151 E	1 N	X			Good	

5102		80		X	150 E	1.16N	X			Good	
5103		80		X	147.5 E	1 N	X			Good	
5104		80		X	148 E	0.5 N	X			Good	
5105		80		X	146.5 E	0.5 N	X			Good	
5106	Crater 217	80		X	134.5 E	2.5 N	X			Good	LM approaching CSM
5107		80		X	131 E	0.5 N	X			Fair	LM approaching CSM
5108		80		X	130.0 E	1.0 N	X			Good	LM approaching CSM
5109		80		X	129.5 E	1 N	X			Good	LM approaching CSM
5110	Crater 282	80		X	128.5 E	1.2 N	X			Good	LM approaching CSM
5111	Crater 282	80		X	127.5 E	1.5 N	X			Good	LM approaching CSM
5112	Crater 282	80		X	126 E	2 N	X			Good	LM approaching CSM
5113		80		X	122.5 E	2 N	X			Good	LM approaching CSM
5114		80		X	122 E	2 N	X			Good	LM approaching CSM
5115		80		X	121.5 E	2 N	X			Good	LM approaching CSM
5116		80		X	117 E	2 N	X			Good	LM approaching CSM
5117	LM docking	80		X	117.5 E	2 N	X			Good	
5118	Censorinus X and V; Maskelyne P	80		X	37 E	1 N	X			Fair	Overexposed
5119	Censorinus	80		X	33.2 E	0.5 N	X			Fair	Overexposed
5120	Censorinus	80		X	32.5 E	0.5 S			X	Good	Near terminator
5121	Terminator	80		X	22 E	1.5 N			X	Poor	
5122	Sabine; Ritter; Schmidt	80		X	18.5 E	1.5 N			X	Poor	
5123	Godin	80		X	85 E	2.2 N			X	Good	
5124	Dembowski	80		X	7 E	3 N			X	Good	Terminator
5125	Underexposed									Poor	No imagery
5126	Dubiago	80		X	71.5 E	1.5 N				Good	
5127	Sea of Waves; Firmicus	80		X	67.2 E	3.5 N	X			Good	
5128	West edge, Foaming Sea	250		X	64.5 E	1 N	X			Good	
5129	West edge, Foaming Sea	250		X	64.5 E	1 N	X			Good	
5130	West edge, Foaming Sea	250		X	64 E	1 N	X			Good	
5131	Apollonius	250		X	61 E	4 N	X			Good	
5132	Apollonius A	250		X	60 E	2.5 N	X			Good	
5133	Sea of Fertility	250		X	53 E	0.5 N	X			Good	75 percent overlap
5134	Taruntius K and P	250		X	52.2 E	0.5 N	X			Good	75 percent overlap
5135	Taruntius K and P	250		X	52 E	0.5 N	X			Good	75 percent overlap
5136	Taruntius H	250		X	50 E	0.5 N	X			Good	75 percent overlap
5137	Messier A and B	250		X	48 E	1 S	X			Good	50 percent side lap
5138	Messier A and B	250		X	47.5 E	2 S	X			Good	50 percent side lap
5139	Messier A, B, D, E	250		X	45.5 E	3 S	X			Good	
5140	Secchi X	250			45.5 E	0.0	X			Good	
5141	Sea of Fertility	250			47 E	2 N	X			Good	
5142	Lubbock S	250			45 E	1 N				Good	50 percent overlap
5143	Lubbock S	250		X	41.5 E	1 N	X			Good	75 percent overlap
5144	Lubbock S	250			41.2 E	1 N	X			Good	75 percent overlap
5145	Taruntius F	250		X	40.5 E	3.5 N	X			Good	

TABLE A–I.—*Apollo 10 Hasselblad Photography*—Concluded

(*h*) Magazine M, film SO–368—*Concluded*

[Available in color]

Frame no. AS10–34–	Description	FL, mm	Vert	Obliq	Principal point		Sun angle			Photo quality	Remarks
					Long, deg	Lat, deg	High	Med	Low		
5146	Near site 1	250		X	35 E	2.2 N		X		Good	95 percent overlap
5147	Near site 1	250		X	35 E	2.2 N		X		Good	95 percent overlap
5148	Near site 1	250		X	35 E	2.2 N		X		Good	95 percent overlap
5149	Near site 1	250		X	35 E	2.2 N		X		Good	95 percent overlap
5150	Near site 1	250	X		35 E	2.2 N		X		Good	95 percent overlap (1:440 000)
5151	Maskelyne	250	X		30 E	2.2 N		X		Good	1:440 000
5152	Maskelyne Y	250		X	27.5 E	1.5 N		X		Good	
5153	Maskelyne G; Rima Maskelyne I	250		X	27 E	2.5 N		X		Good	
5154	Maskelyne G; Rima Maskelyne I	250		X	27 E	3 N		X		Good	40 percent overlap
5155	Near Maskelyne G	250		X	27 E	3.5 N		X		Good	
5156	Landing site 2	250		X	24 E	1 N		X		Good	
5157	Landing site 2	250		X	24 E	1 N		X		Good	90 percent overlap
5158	Landing site 2	250		X	23.7 E	0.7 N		X		Good	60 percent overlap
5159	Landing site 2	250	X		23.7 E	1 N		X		Fair	70 percent overlap (1:440 000)
5160	Ritter	250		X	19 E	2 N			X	Good	
5161	Schmidt	250		X	19.75 E	1 N			X	Good	
5162	Schmidt	250		X	19.7 E	0.7 N			X	Good	
5163	Godin area	250		X	12.5 E	2 N			X	Good	
5164	Godin	250		X	10 E	2.2 N			X	Good	
5165	Godin	250		X	10 E	2.2 N			X	Good	
5166	Godin	250		X	9 E	2.5 N			X	Good	50 percent overlap
5167	Godin C	250	X		8 E	2 N			X	Good	1:440 000
5168	Rhaeticus B	250		X	7 E	1.5 N			X	Good	
5169	Rhaeticus B	250	X		7.2 E	1.5 N			X	Good	1:440 000
5170	Craters 221, 223	80		X	165 E	4.5 N		X		Good	Light reflection
5171	Crater 302	80		X	161.5 E	5 S		X		Good	
5172	Craters 300, 302	80		X	158 E	6 S		X		Good	
5173	Craters 300, 301	80		X	157.5 E	9 S		X		Good	

TABLE A–II.—*Apollo 10 Sequence Photography (16 mm)*

Frames	Location	Description	Remarks
Magazine A, film SO–368			
----------	----------	Docking; no scene	Not plotted
Magazine AA, film SO–168			
----------	----------	IVA	Not plotted
Magazine B, film SO–168			
----------	----------	IVA	Not plotted
Magazine C, film SO–368			
1–1120	Not located	Underexposed; window glare; scene not identifiable	Not plotted
1121–4376	Sequence from 117° W to 15° E	Continuous near-vertical sequence from lunar far side across Sea of Tranquility	Plotted
4377–4666	Sequence from 33° E to 18° E	Continuous high-oblique sequence over Maskelyne, Sabine, and Ritter	Plotted
4667–5414	8° S, 15° E (approximate center of sequence)	Panoramic high obliques over Delambre and Theon Junior	Plotted
Magazine D, film SO–368			
1–1407	2° S, 86° E (approximate center of sequence)	High-oblique sequence of earthrise over Smyth's Sea; poor scene rendition	Plotted
1408–2265	Sequence from 46° E to 4° E	Continuous high- to low-oblique sequence from edge of Sea of Fertility near Secchi, over sites 1 and 2, Sabine and Ritter; stops at margin of Central Bay	Plotted
2666–2671	----------	Blank	

TABLE A-II.—*Apollo 10 Sequence Photography (16 mm)*—Continued

Magazine D, film SO-368—*Concluded*

Frames	Location	Description	Remarks
2672-3089	1° S, 83° E (approximate center of sequence)	High-oblique sequence of earthrise over Smyth's Sea; poor scene rendition	Plotted
3090-3121			Not plottable at map scale
3122-3175		Entire Moon	
3176-3195			Not plotted
3196-5732		Earth view	

Magazine F, film SO-368

Frames	Location	Description	Remarks
1-973	5° S, 168° W (approximate center of sequence)	High-oblique sequence of lunar far-side craters	Plotted
974-1043	1° S, 163° E (approximate center of sequence)	Near-vertical sequence of lunar far-side single crater	Plotted
1044-1206	3° N, 143° E (approximate center of sequence)	Near-vertical sequence of lunar far-side single crater	Plotted
1207-1273	3° N, 132° E (approximate center of sequence)	Near-vertical sequence of lunar far-side single crater	Plotted
1274-1338	4° N, 120° E (approximate center of sequence)	Near-vertical sequence of lunar far-side single crater	Plotted
1339-1676	Not located	Earthrise; poor condition of scene	Not plotted
1677-1687		Overexposure; no scene	Not plotted
1688-2213	Not located	Far-side scene near subsolar; poor condition	Not plotted
		Start of roll	
2214-2225		Roll; no scene	Not plotted
2226-5341	Sequence from 51° E to 23° E	Continuous near-vertical sequence from Sea of Fertility across Sea of Tranquility, south of site 2	Plotted

Magazine G, film SO-368

Frames	Location	Description	Remarks
1-5342	Sequence from 62° E to 21° E	Continuous sequence starting with lunar far-side scene at edge of Sea of Waves and Foaming Sea, continuing to front side over Sea of Fertility, and ending in Sea of Tranquility; passes south of site 2	Plotted

Magazine H, film SO–368			
1–5021	Sequence starts at 124° E and ends at 77° E	Sequence contains near vertical, low, and high obliques of lunar far-side scenes, Smyth's Sea, and earthrise	Plotted
Magazine I, film SO–368			
1–5462	Sequence starts at 171° E and ends at 128° E	High to low oblique of lunar far-side scene; features not named	Plotted
Magazine J, film SO–168			
		Overexposed; reentry—underexposed; chutes out	Not plotted
Magazine K, film SO–368			
1–162		LM photography of CSM only	Not plotted
163–2790	Sequence from 115° E to 74° E	LM photography of CSM with lunar far-side scene in background	Plotted; location questionable
2791–3970	Sequence from 38° E to 22° E	LM photography of CSM with lunar front-side scene in background; sequence over site 2	Plotted
3971–4207		Blank	Not plotted
4208–4360	6° N, 119° E (approximate center of sequence)	Oblique sequence of lunar far-side single crater (no. 211)	Plotted
4361–5058	2° S, 80° E (approximate center of sequence)	High-oblique sequence of earthrise over Smyth's Sea; poor scene rendition	Plotted
Magazine L, film SO–168			
1–929		IVA	Not plotted
930–1955	Sequence from 22° E to 9° E	Continuous sequence of high to low obliques from Sabine and Ritter to Godin	Plotted
1956–2234		LM photography of CSM	Not plotted

TABLE A–II.—*Apollo 10 Sequence Photography (16 mm)*—Concluded

Frames	Location	Description	Remarks
		Magazine V, film SO–368	
1–2104	Earth	Earth view	Unplottable
2105–2625	Not located	High to low obliques from LM; overlapping sequence of lunar far-side scene	Not plotted
2626–2682	1° N, 45° E (approximate center of sequence)	Low- to near-vertical sequence taken from LM; partial overlap of lunar front-side scene; Messier, Messier A, and Secchi are predominant craters	Plotted
2683–2862	16° S, 30° E (approximate center of sequence)	High obliques taken near terminator; Theophilus, Madler, and Isidorus are predominant craters	Plotted
2863–3240	10° N, 103° E (approximate center of sequence)	High obliques of lunar far-side scene; craters not named: nos. 197, 198, 199	Plotted
3241–3329	12° N, 85° E (approximate center of sequence)	High obliques of lunar far-side scene; Neper, Goddard, and the Border Sea are predominant features	Plotted
		Magazine W, film SO–368	
1–977	Sequence starts at 43° E and ends at 4° W	Sequence starts with high obliques at edge of Sea of Fertility and passes over Maskelyne, site 2, Sabine and Ritter, and site 3	Plotted
977–end		Panoramic high obliques of Tsiolkovsky; quarter, half, and full Moon, and Earth	Not plottable at map scale
		Magazine Y, film SO–368	
1–1492	Not located	Docking; far-side scene in background	Not plotted
1493–2050	Sequence from 164° E to 144° E	Continuous high- to low-oblique sequences of lunar far-side scene; features not named	Plotted

2051–3603	Not located	Broken series of frames of hand-held telephoto panoramic shots of lunar far-side scene; mostly low obliques and near vertical; locations questionable	Not plotted
3604–5614	Sequence from 44° E to 26° E	High-altitude continuous, low-oblique to near-vertical sequence from edge of Sea of Fertility over Censorinus into Sea of Tranquility	Plotted

APPENDIX B

Glossary

aa—Rough, scoriaceous lava.

albedo—The ratio of reflected to incident light.

chit area—An area approximately 200 by 200 m subjected to computer analysis to determine landing suitability.

dike—A hardened, tabular mass of igneous rock that has been forced into a fissure while in a melted state.

earthflow—A landslide consisting of unconsolidated surface material that flows down a slope.

earthshine—Sunlight reflected from the Earth. Earthshine on the Moon is usually much brighter than moonlight on Earth.

ejecta—Material ejected from craters during their formation.

gamma—The slope or gradient of the relatively straightline region of the curve that is the plot of density (ordinate axis) versus the logarithm of exposure (abscissa).

groundtrack—The vertical projection of the spacecraft trajectory on the lunar surface.

halo—A bright ring around a feature on the Moon (see **nimbus**). A bright ring around the spacecraft shadow on the Moon (see **heiligenschein**).

heiligenschein—A bright area around the zero-phase (spacecraft shadow) point.

highland—Elevated or mountainous land.

isodensitracer—A device for measuring and recording areas of equal photographic density.

limb—The edge of the Moon as viewed from Earth.

mare, pl **maria**—Large area on the lunar surface that is darker in color and of lower elevation and generally smoother than surrounding terra. The maria are generally circular in plan.

mass wasting—The slow, downslope movement of debris under the influence of gravity.

nadir point—The point vertically below the observer or 180° from the zenith.

nimbus, pl **nimbi**—Patch of lighter material around a crater.

oblique photography—Photography taken with the camera axis directed between the horizontal and the vertical. Low-oblique photographs are those that do not contain the horizon. Those photographs in which the horizon appears are called high obliques.

orbit—The path of a spacecraft or other satellite around a larger body.

pahoehoe—Cooled hard lava marked by a smooth, often billowy, shiny surface.

pass—A part of a revolution when a particular operation is being performed; i.e., a photo pass or landmark tracking pass.

phase angle—The angle at the point of intersection formed by the vectors from the source (Sun) and the observer or camera.

photoclinometry—The technique for extracting slope information from an image brightness distribution.

photometry—That science dealing with the measure of the intensity and direction of light.

ray, ray system, rayed craters—A deposit of high-albedo material of unknown composition ejected from craters. The ejecta may either intensify cratering or smooth a previously cratered surface. The albedo is believed to decrease with age. The ray system is a group of narrow, linear, sometimes interrupted rays radiating from a crater. A rayed crater is the source of these linear rays.

rev, revolution—360° of travel in an orbit.

rille—A long, narrow trench or valley on the lunar surface.

sequence camera—A 16-mm camera that can be set to expose 1, 4, 8, 12, or 24 frames per second.

solar corona—The outer atmosphere of the Sun. The temperature is 1 to 2 million degrees Kelvin. The light—having an intensity about one-half that of the full Moon—is mainly due to sunlight scattered by free electrons.

solifluction—The slow creeping of fragmental material down a slope, sometimes resulting in the formation of terraces.

stereo, stereoscopic strip—Photography taken so that sufficient forward overlap exists to permit stereoscopic (three dimensional) viewing and reconstruction of the surface area photographed (see **strip photography**).

stereopair, stereoscopic pair—Two photographs that include a portion of the same object (see **stereoscopic strip**).

strip photography—Photography taken in a systematic manner, with a constant amount of forward overlap, that covers a strip of surface below the

spacecraft trajectory (see **stereo, stereoscopic strip**).

subsolar point—That point on a planetary body at which the Sun is in the zenith.

Sun angle—The angle formed, in a vertical plane, between the incident Sun rays and the local horizontal.

talus—A sloping pile of rock fragments at the foot of a cliff.

terminator—The boundary between the illuminated and unilluminated portion of the lunar surface. The lunar terminator advances approximately 13° each 24 hr.

terra—An area on the lunar surface which is relatively higher in elevation and lighter in color than the maria. The terra is characterized by a rough texture formed by intersecting or overlapping large craters.

transearth insertion—The propulsive maneuver that increases spacecraft velocity to allow it to return to Earth.

translunar injection—The propulsive maneuver that increases spacecraft velocity to allow it to escape the Earth's gravitational field.

vertical photography—Photography taken with the optical axis alined, as nearly as possible, with the local vertical.

washout—See **heiligenschein.**

zero phase—The condition when the vectors from the source (Sun) and the observer are colinear.

zero-phase photography—Photography that includes the image of zero phase.

APPENDIX C

Author Affiliation

NASA Manned Spacecraft Center
James H. Sasser
Thomas P. Stafford
Eugene A. Cernan
John W. Young

U.S. Geological Survey
Richard J. Pike
Keith Howard
H. J. Moore
Don E. Wilhelms
B. K. Lucchitta
Robert L. Wildey
Howard A. Pohn
N. J. Trask
Sherman S. C. Wu

Smithsonian Astrophysical Observatory
Edward H. Jentsch

University of Arizona
R. G. Strom
E. A. Whitaker

Bellcomm, Inc.
Farouk El-Baz

PHOTOGRAPHIC MAGAZINES

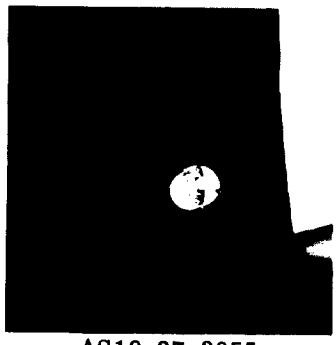
AS10-27-3855

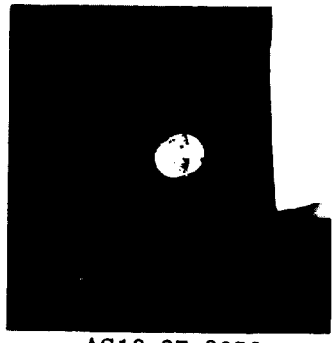
AS10-27-3856

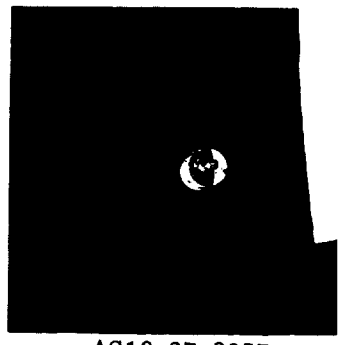
AS10-27-3857

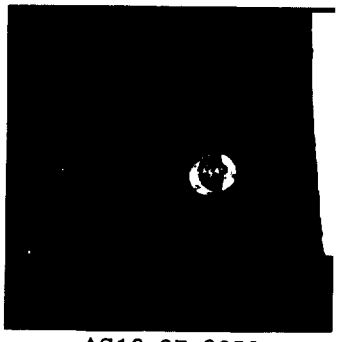
AS10-27-3858


AS10-27-3859

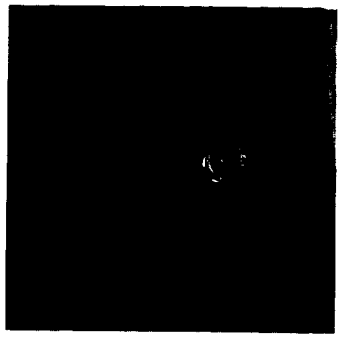
AS10-27-3860

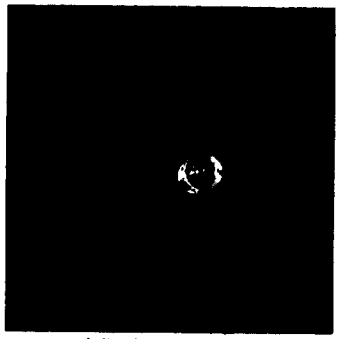
AS10-27-3861

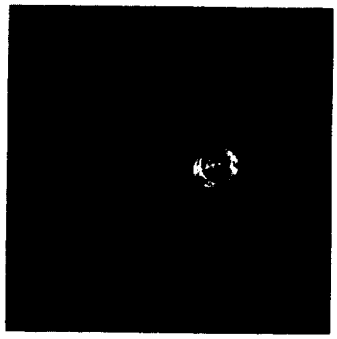
AS10-27-3862

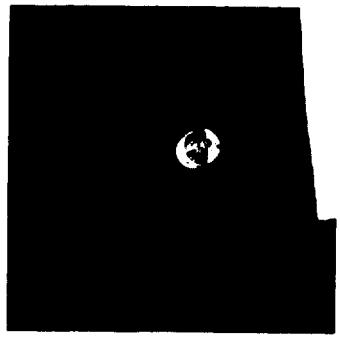
AS10-27-3863

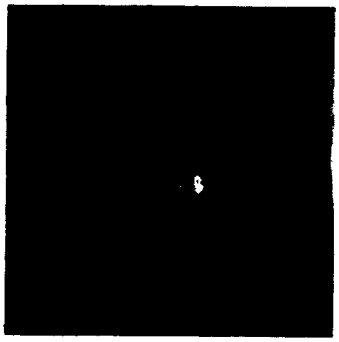
AS10-27-3864

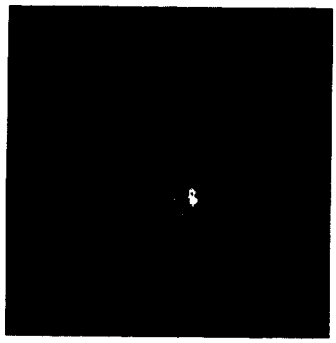
AS10-27-3865

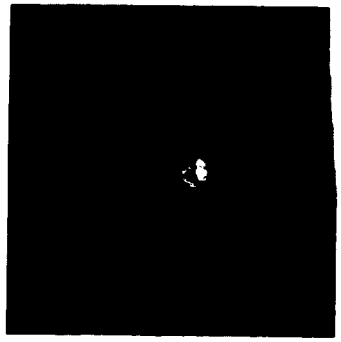
AS10-27-3866

(Available in color.)

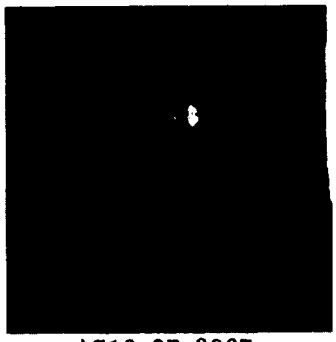
AS10-27-3867

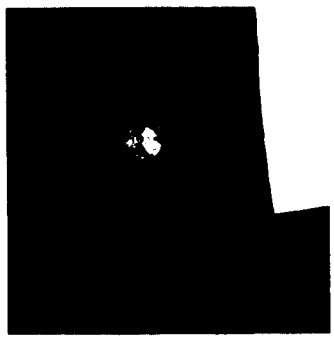
AS10-27-3868

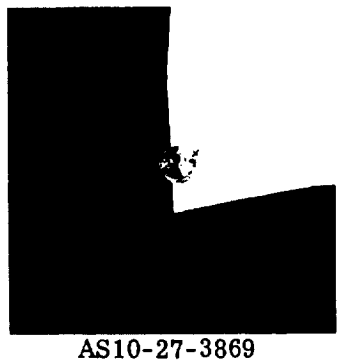
AS10-27-3869

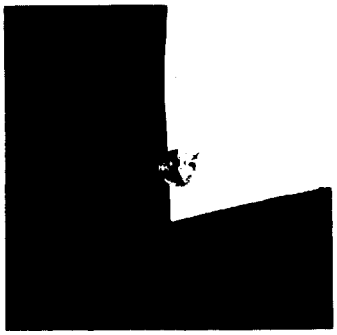
AS10-27-3870


AS10-27-3871

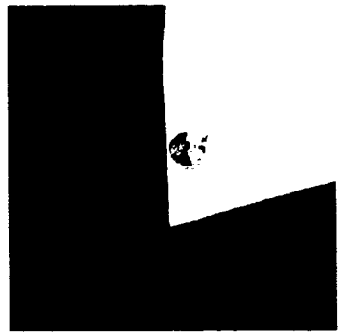
AS10-27-3872

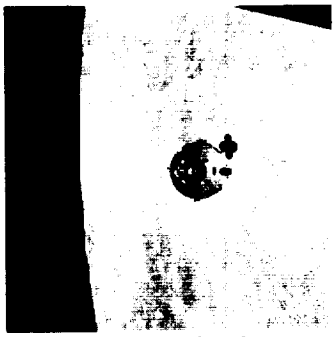
AS10-27-3873

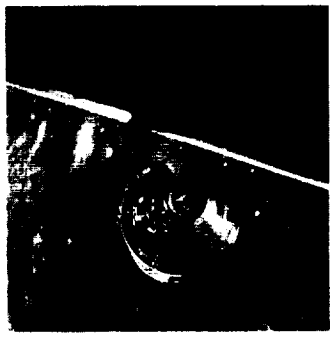
AS10-27-3874


AS10-27-3875

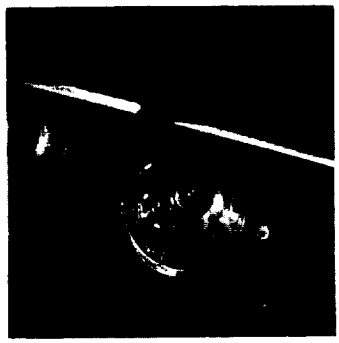
AS10-27-3876

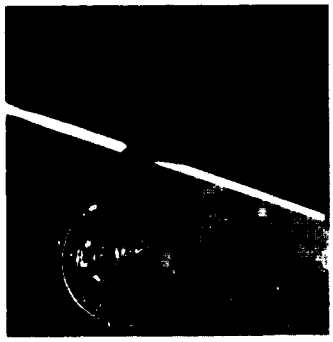
AS10-27-3877


AS10-27-3878

(Available in color.)

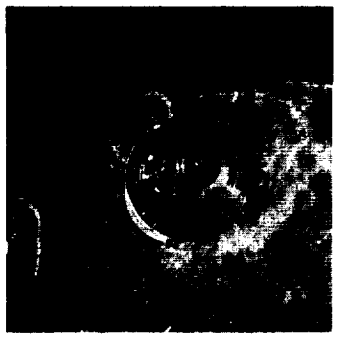
AS10-27-3879


AS10-27-3880

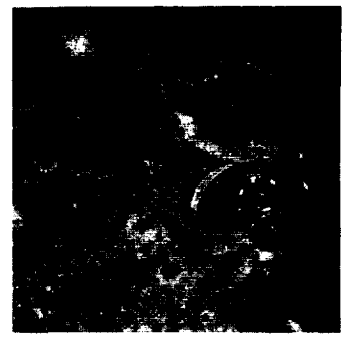
AS10-27-3881


AS10-27-3882


AS10-27-3883

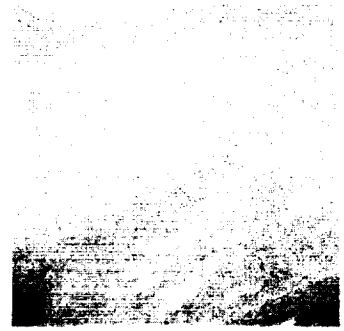
AS10-27-3884

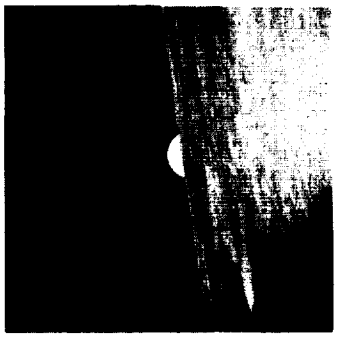
AS10-27-3885


AS10-27-3886

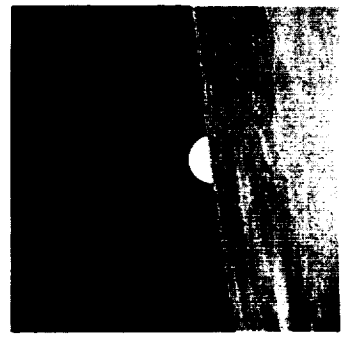
AS10-27-3887

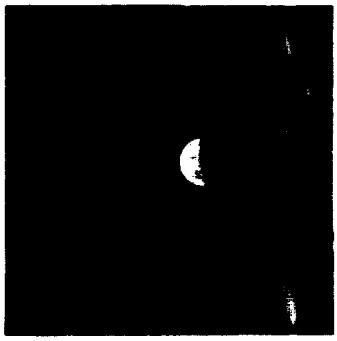
AS10-27-3888

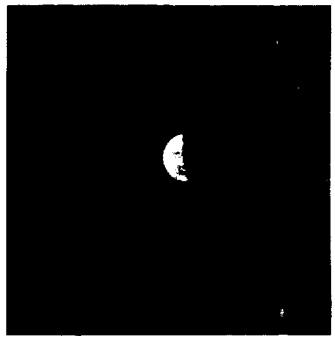
AS10-27-3889

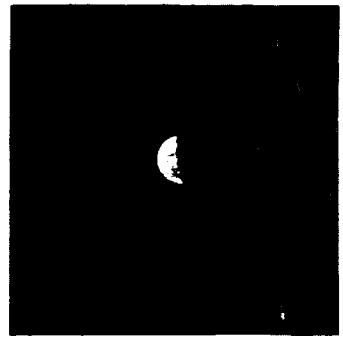
AS10-27-3890

(Available in color.)

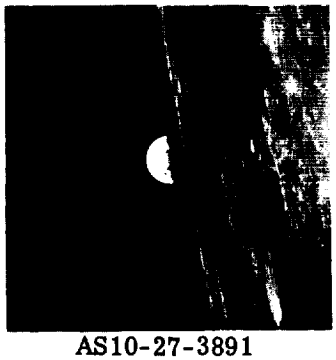
AS10-27-3891


AS10-27-3892

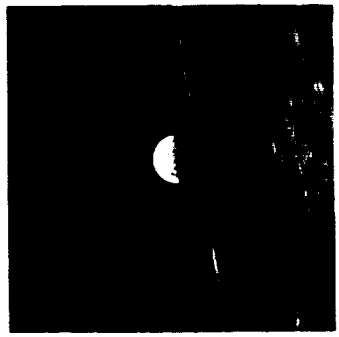
AS10-27-3893


AS10-27-3894


AS10-27-3895


AS10-27-3896


AS10-27-3897

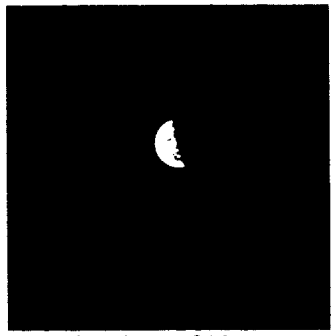
AS10-27-3898

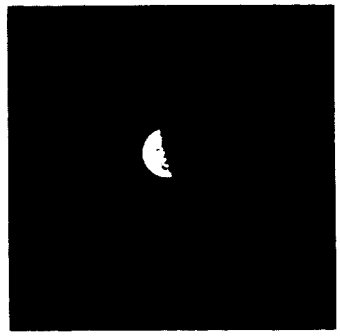
AS10-27-3899

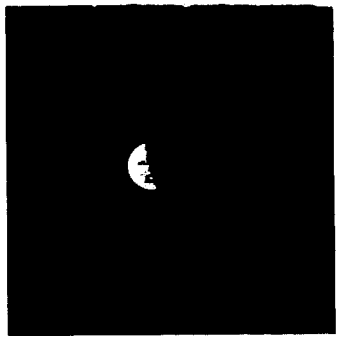
AS10-27-3900

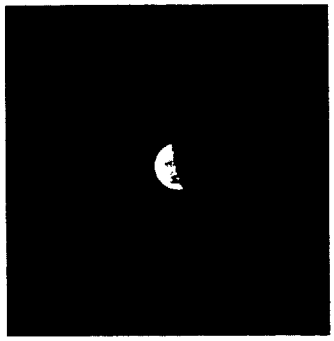
AS10-27-3901

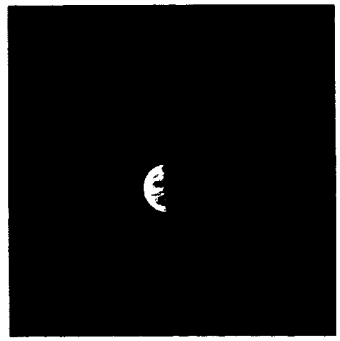
AS10-27-3902

(Available in color.)


AS10-27-3903

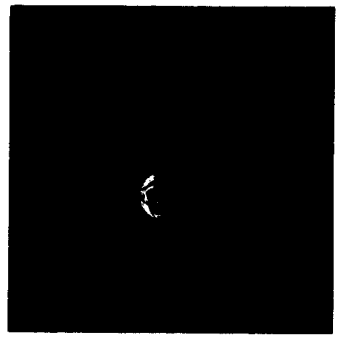
AS10-27-3904


AS10-27-3905


AS10-27-3906

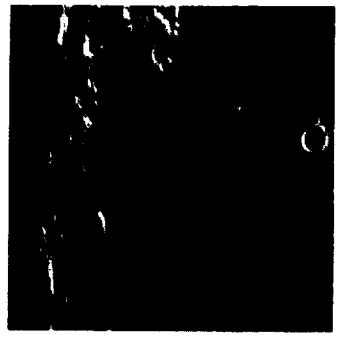
AS10-27-3907


AS10-27-3908

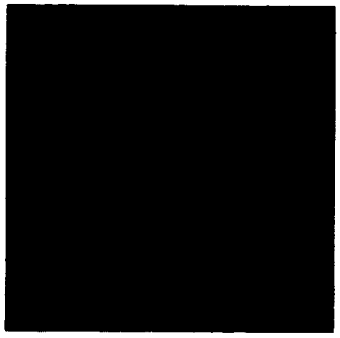
AS10-27-3909


AS10-27-3910


AS10-27-3911

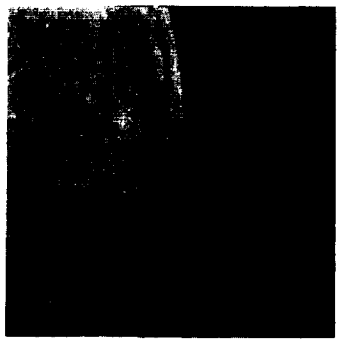
AS10-27-3912

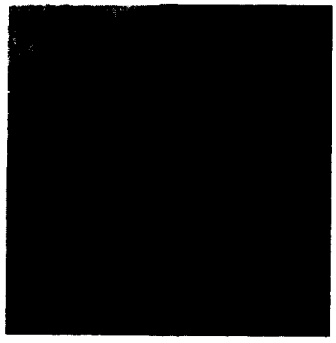
AS10-27-3913

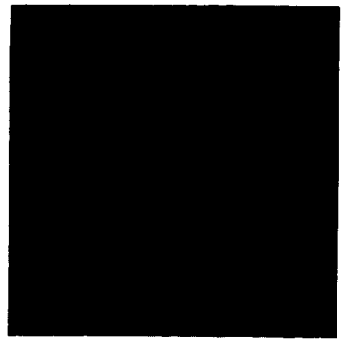
AS10-27-3914

(Available in color.)

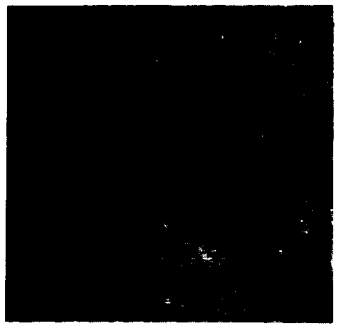
AS10-27-3915


AS10-27-3916


AS10-27-3917


AS10-27-3918


AS10-27-3919

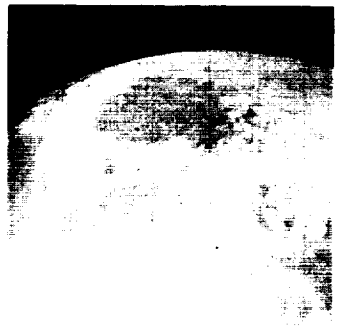
AS10-27-3920

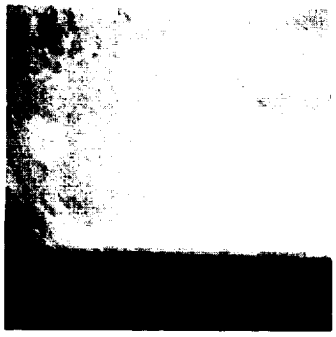
AS10-27-3921

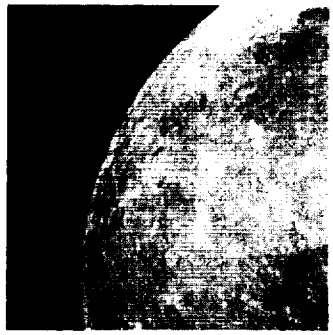
AS10-27-3922


AS10-27-3923


AS10-27-3924

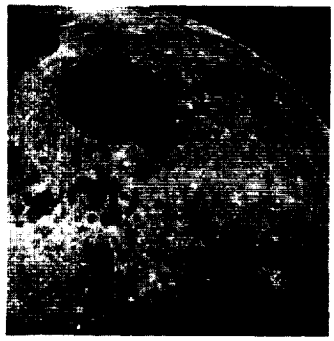
AS10-27-3925


AS10-27-3926

(Available in color.)

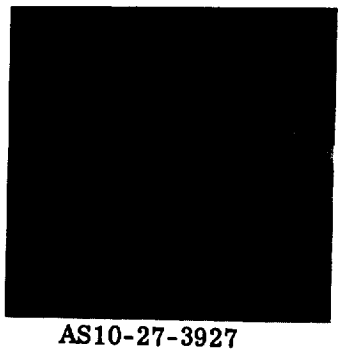
AS10-27-3927

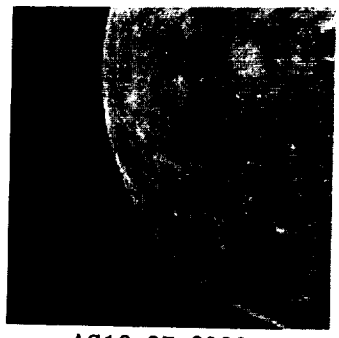
AS10-27-3928

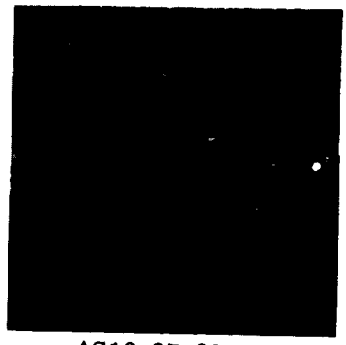
AS10-27-3929

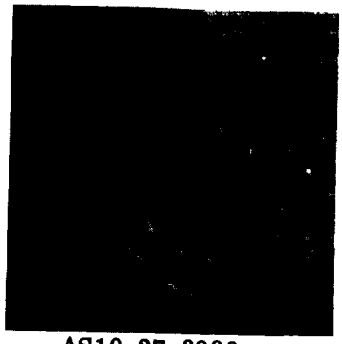
AS10-27-3930

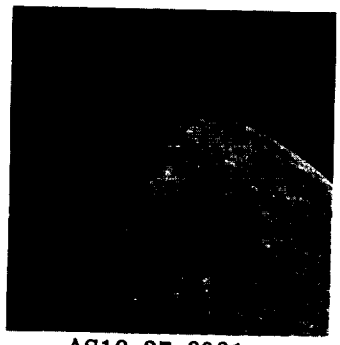
AS10-27-3931

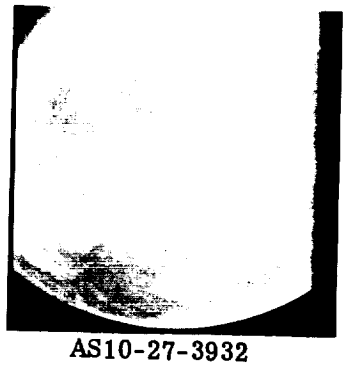
AS10-27-3932

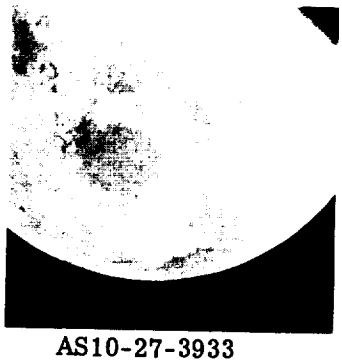
AS10-27-3933

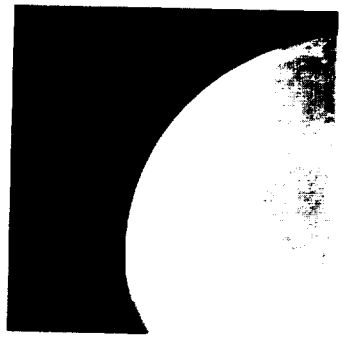
AS10-27-3934

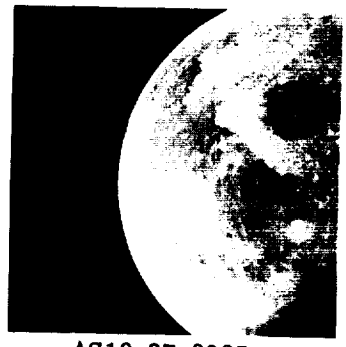
AS10-27-3935

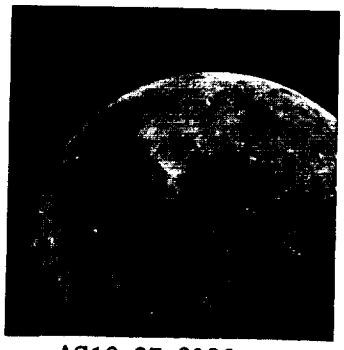
AS10-27-3936


AS10-27-3937


AS10-27-3938

(Available in color.)

AS10-27-3939

AS10-27-3940

AS10-27-3941

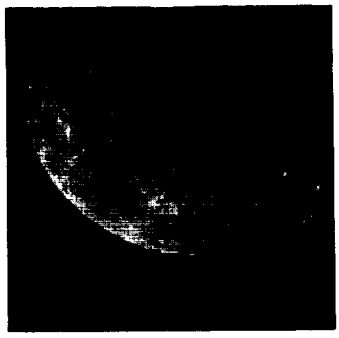

AS10-27-3942

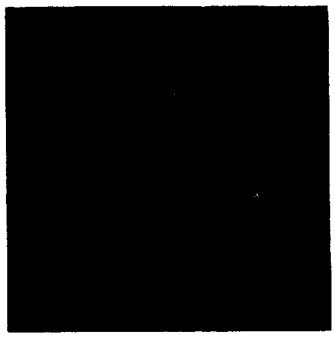

AS10-27-3943

AS10-27-3944

AS10-27-3945

AS10-27-3946

AS10-27-3947

AS10-27-3948

AS10-27-3949

AS10-27-3950

(Available in color.)

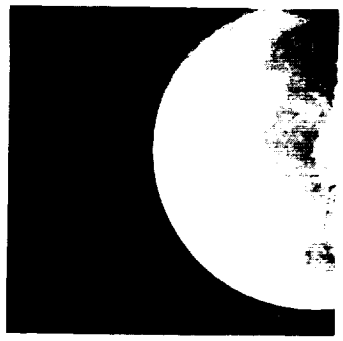
AS10-27-3951

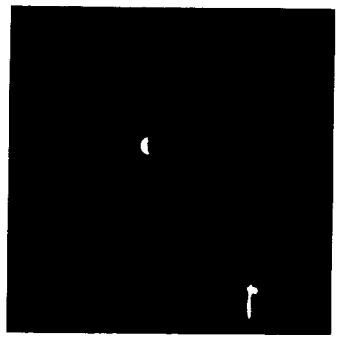
AS10-27-3952

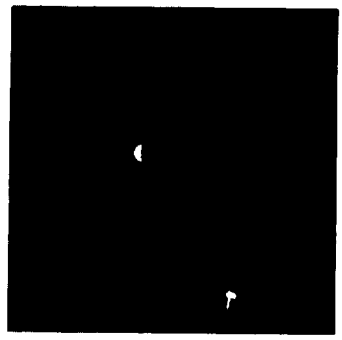
AS10-27-3953

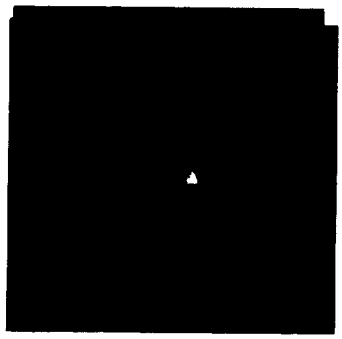
AS10-27-3954

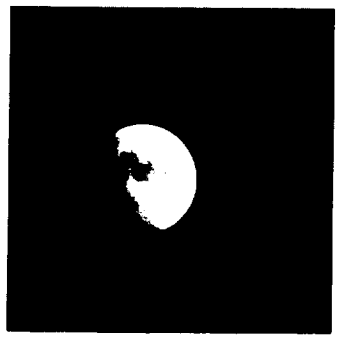
AS10-27-3955

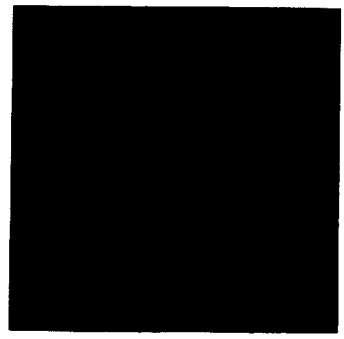
AS10-27-3956

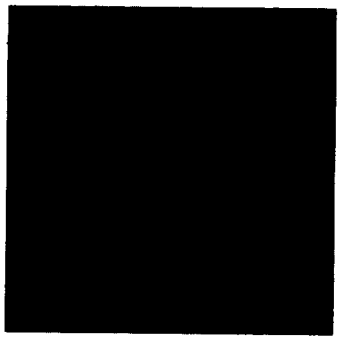
AS10-27-3957

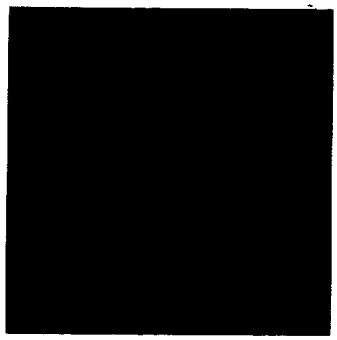
AS10-27-3958

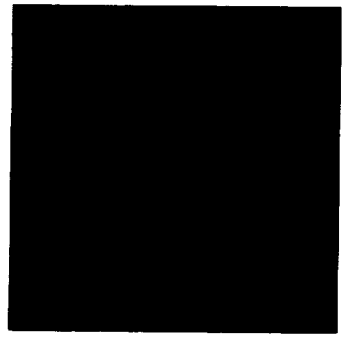
AS10-27-3959

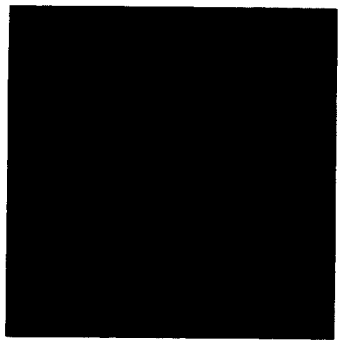
AS10-27-3960


AS10-27-3961


AS10-27-3962

(Available in color.)


AS10-27-3963


AS10-27-3964


AS10-27-3965

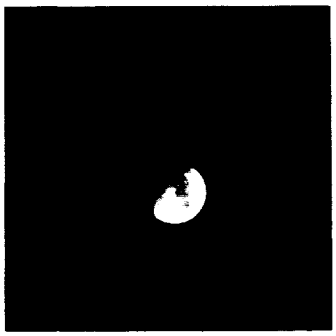
AS10-27-3966

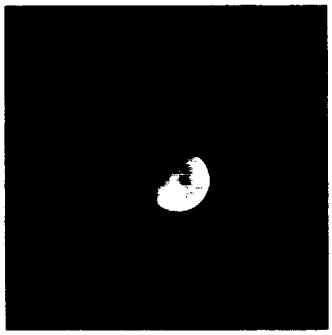
AS10-27-3967

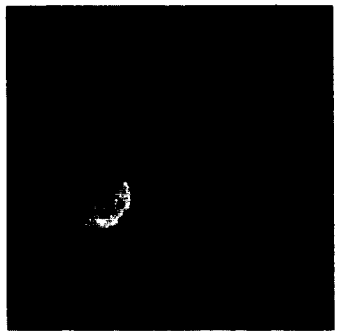
AS10-27-3968


AS10-27-3969

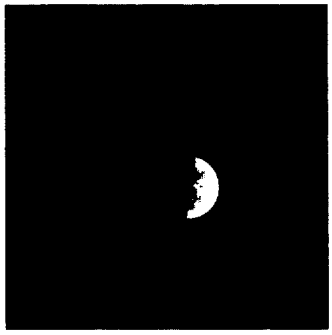
AS10-27-3970

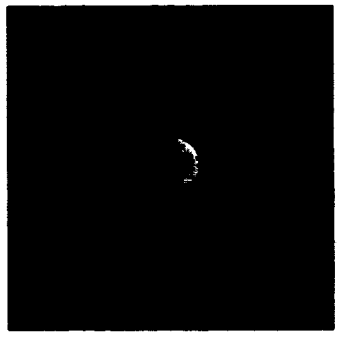
AS10-27-3971


AS10-27-3972


AS10-27-3973


AS10-27-3974

(Available in color.)

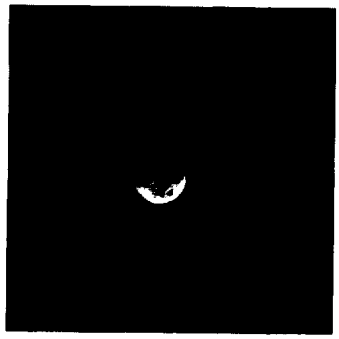

AS10-27-3975

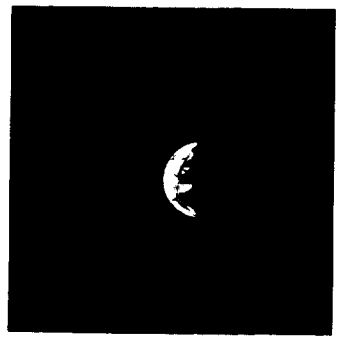

AS10-27-3976

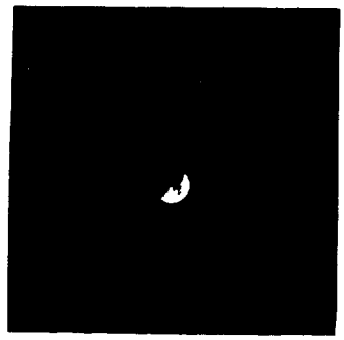

AS10-27-3977

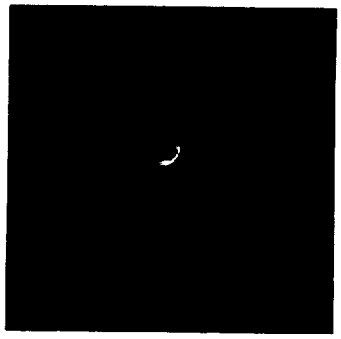

AS10-27-3978

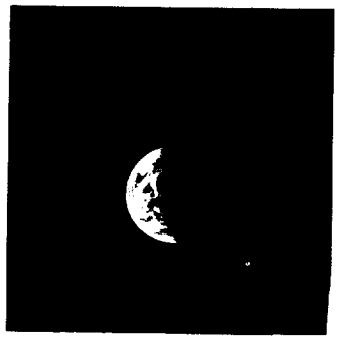

AS10-27-3979

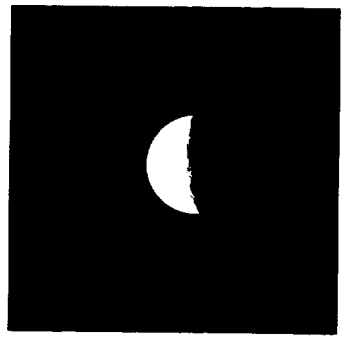

AS10-27-3980

AS10-27-3981

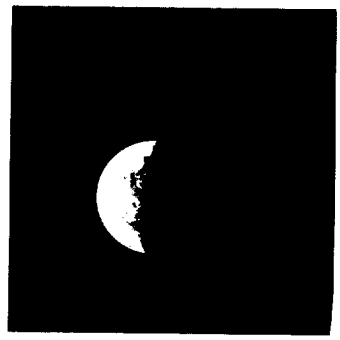

AS10-27-3982

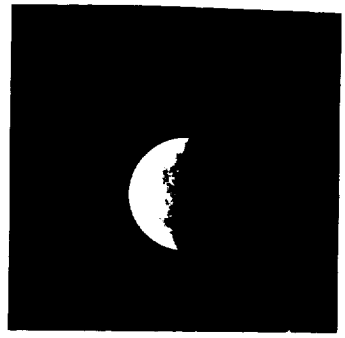

AS10-27-3983

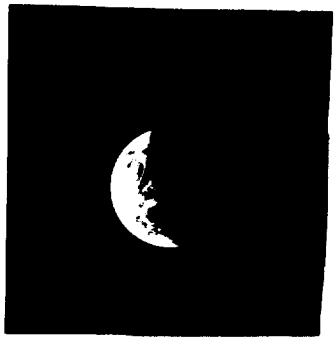

AS10-27-3984

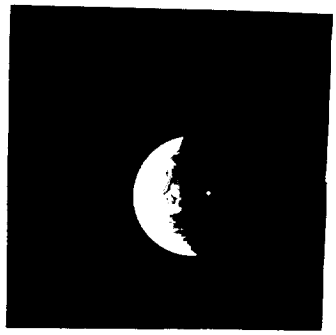

AS10-27-3985

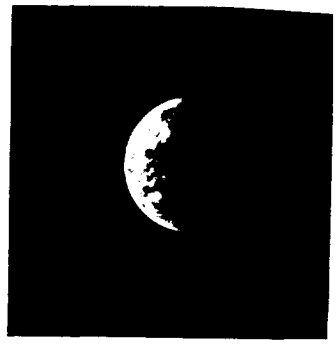

AS10-27-3986

(Available in color.)

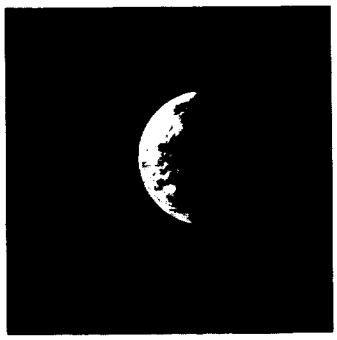

AS10-27-3987

AS10-28-3988

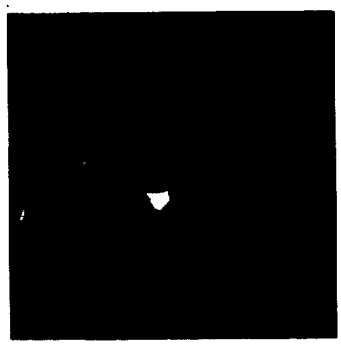

AS10-28-3989

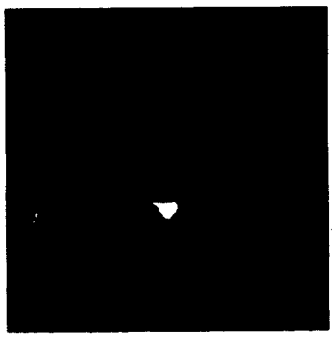

AS10-28-3990

AS10-28-3991

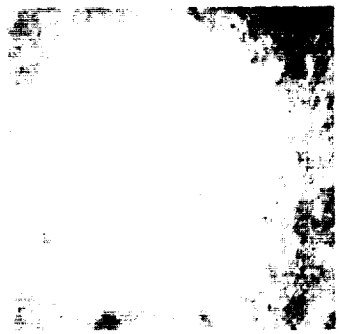

AS10-28-3992

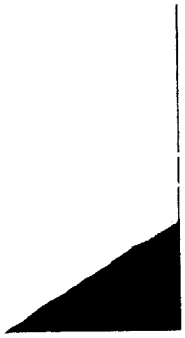

AS10-28-3993

AS10-28-3994

AS10-28-3995

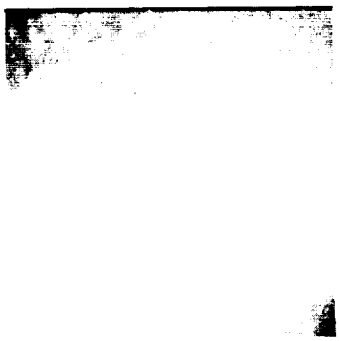

AS10-28-3996

AS10-28-3997

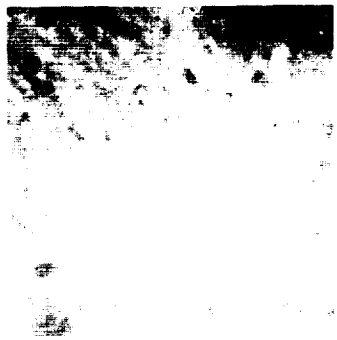

AS10-28-3998

(Available in color.)


AS10-28-3999

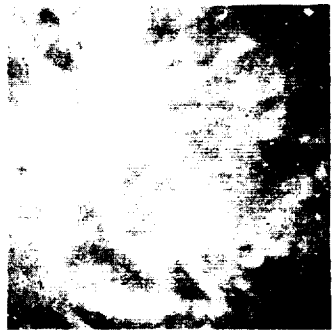
AS10-28-4000

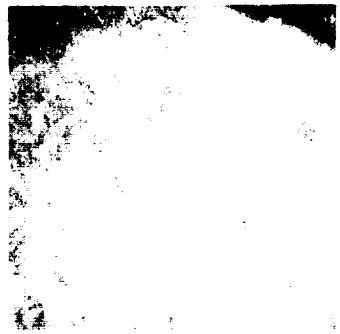
AS10-28-4001


AS10-28-4002

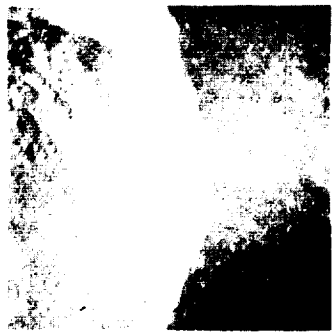
AS10-28-4003

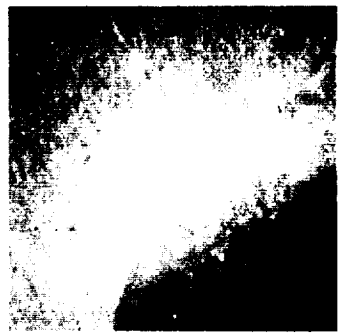
AS10-28-4004


AS10-28-4005

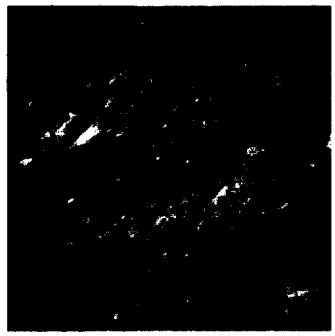
AS10-28-4006


AS10-28-4007

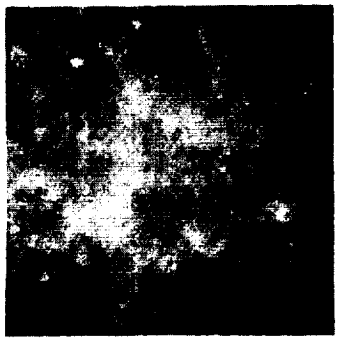
AS10-28-4008

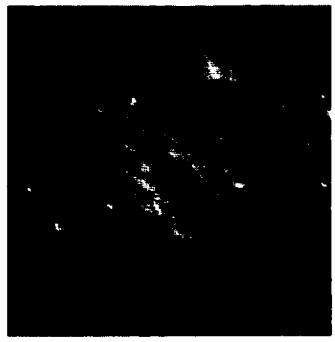
AS10-28-4009


AS10-28-4010


AS10-28-4011


AS10-28-4012


AS10-28-4013

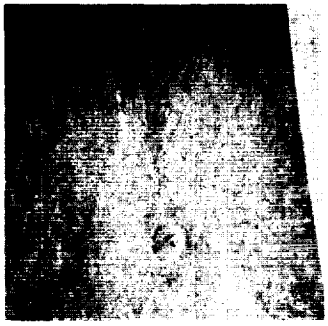
AS10-28-4014

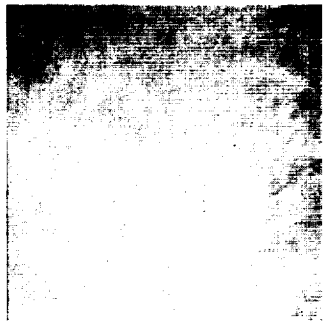
AS10-28-4015

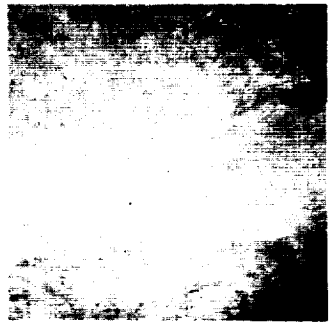
AS10-28-4016


AS10-28-4017

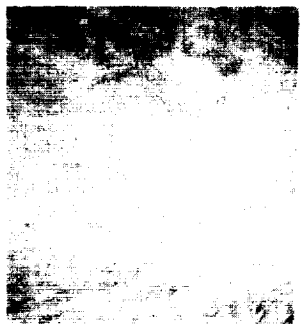
AS10-28-4018

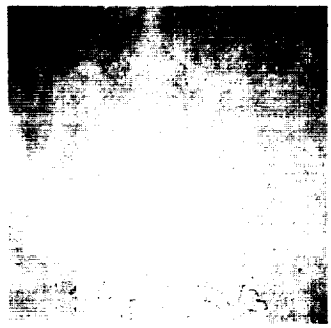
AS10-28-4019


AS10-28-4020


AS10-28-4021

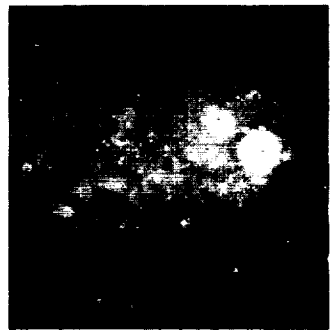
AS10-28-4022

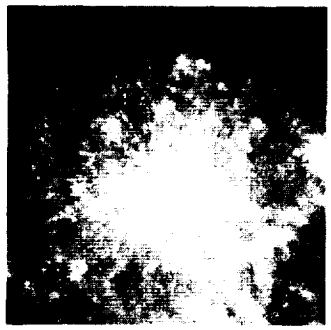
AS10-28-4023

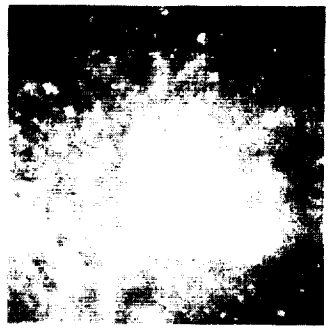
AS10-28-4024


AS10-28-4025

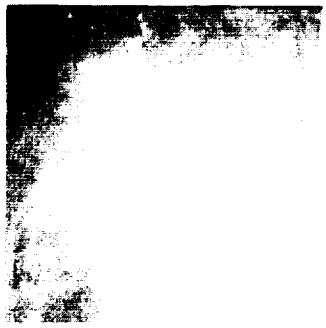
AS10-28-4026

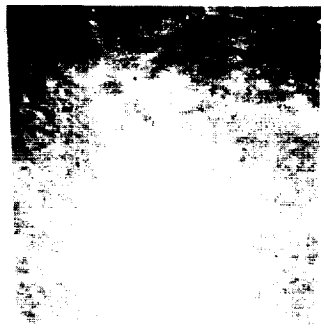
AS10-28-4027


AS10-28-4028


AS10-28-4029


AS10-28-4030

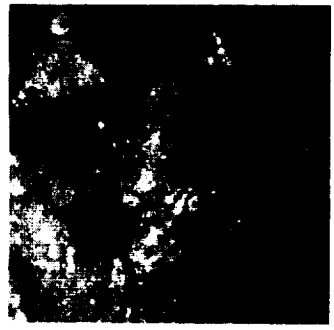
AS10-28-4031


AS10-28-4032


AS10-28-4033


AS10-28-4034


AS10-28-4035


AS10-28-4036


AS10-28-4037

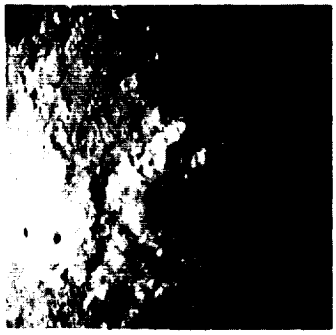
AS10-28-4038

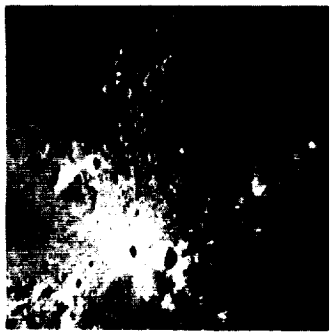
AS10-28-4039


AS10-28-4040

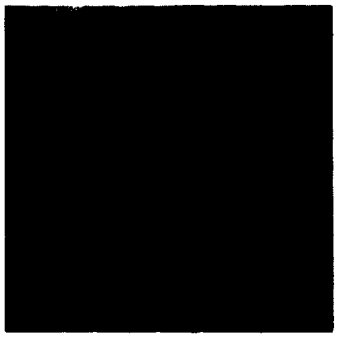
AS10-28-4041

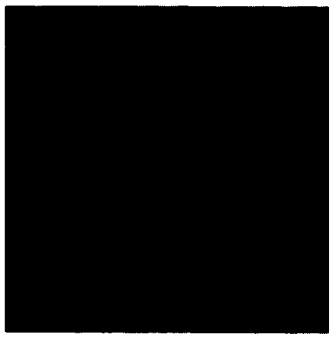
AS10-28-4042

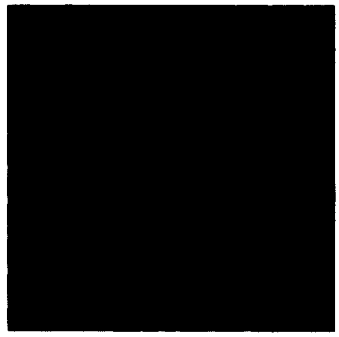
AS10-28-4043

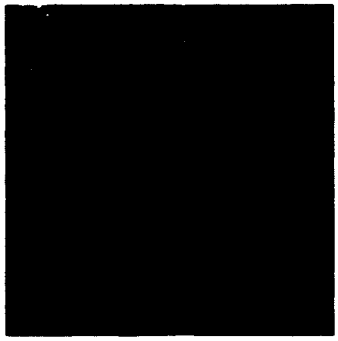
AS10-28-4044

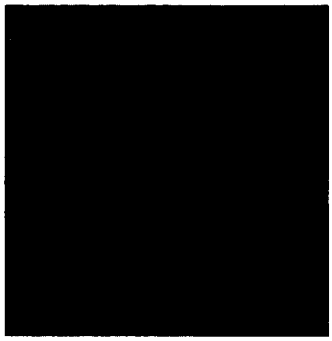
AS10-28-4045

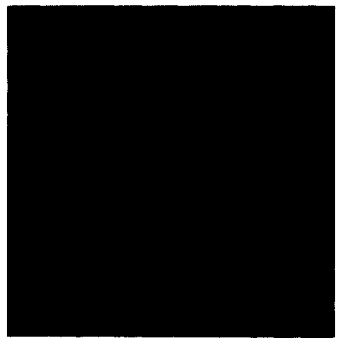
AS10-28-4046

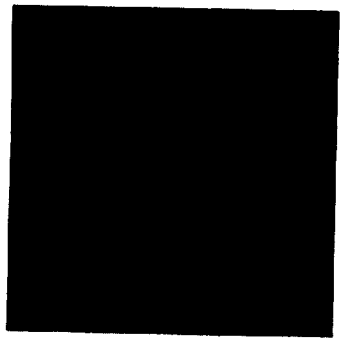

AS10-28-4047

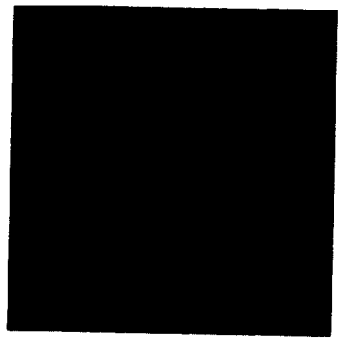

AS10-28-4048

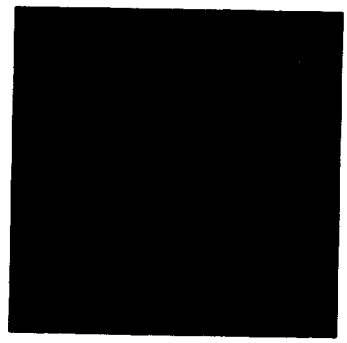

AS10-28-4049

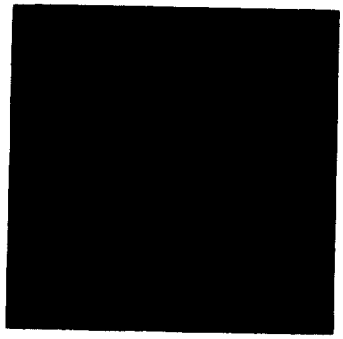

AS10-28-4050

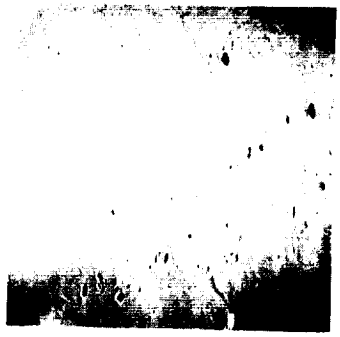

AS10-28-4051

AS10-28-4052

AS10-28-4053

AS10-28-4054

AS10-28-4055

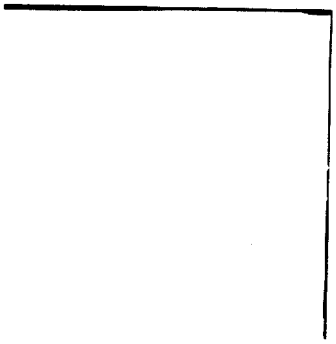

AS10-28-4056

AS10-28-4057

AS10-28-4058


AS10-28-4059

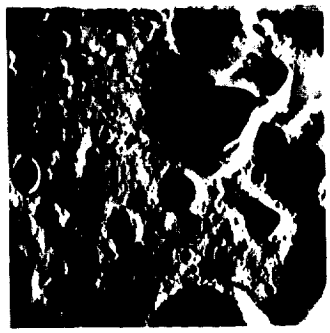
AS10-28-4060


AS10-28-4061

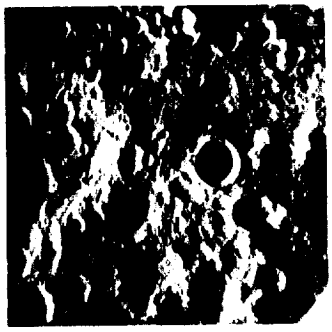
AS10-28-4062

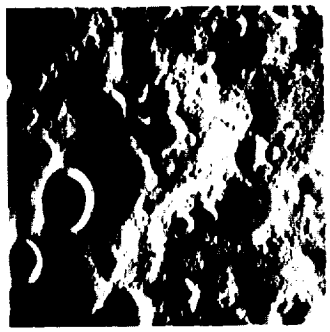
AS10-28-4063


AS10-28-4064

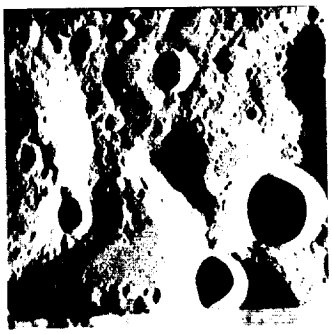
AS10-28-4065

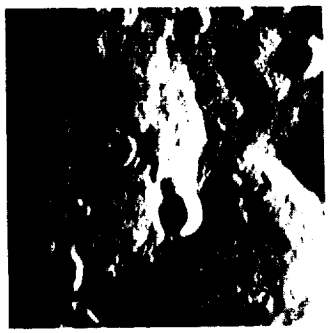
AS10-28-4066

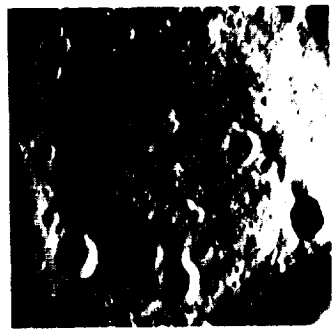
AS10-28-4067


AS10-28-4068


AS10-28-4069

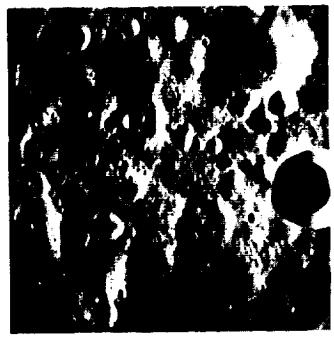
AS10-28-4070


AS10-28-4071


AS10-28-4072

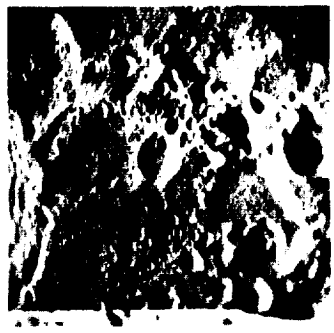
AS10-28-4073


AS10-28-4074


AS10-28-4075


AS10-28-4076


AS10-28-4077

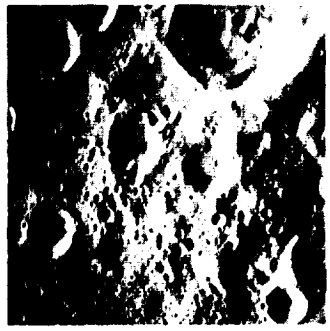
AS10-28-4078

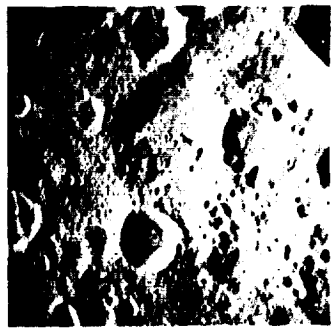
AS10-28-4079


AS10-28-4080

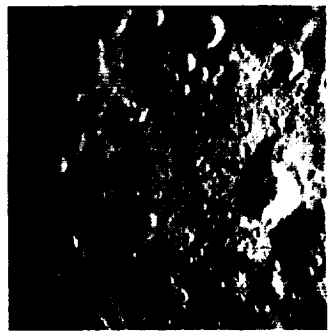
AS10-28-4081

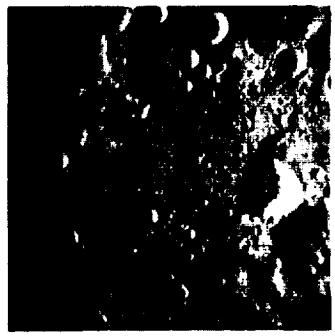
AS10-28-4082

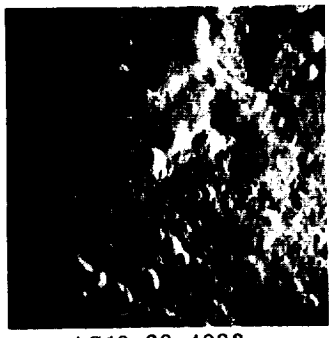
AS10-28-4083

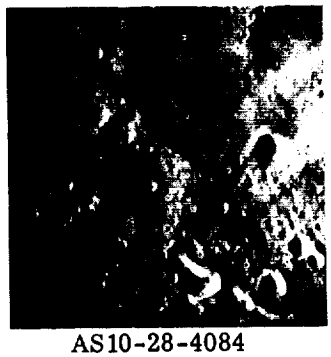
AS10-28-4084

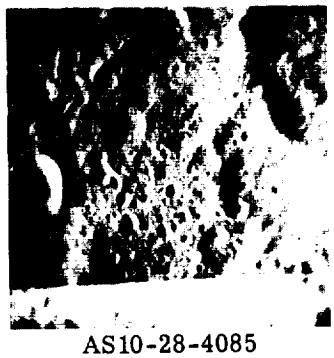
AS10-28-4085

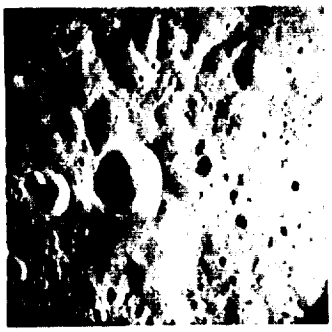
AS10-28-4086

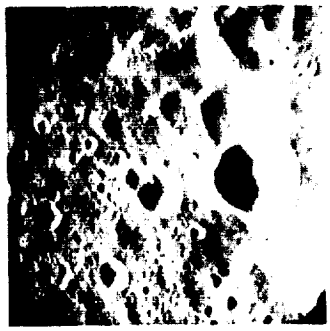
AS10-28-4087


AS10-28-4088

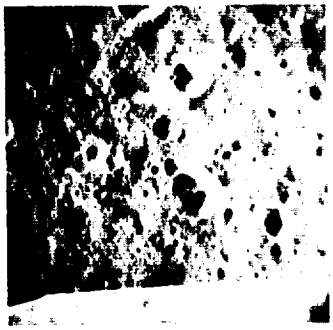
AS10-28-4089

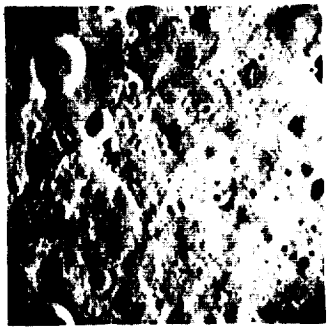
AS10-28-4090

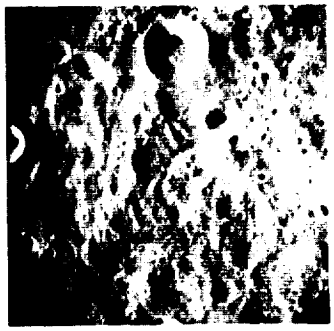
AS10-28-4091


AS10-28-4092

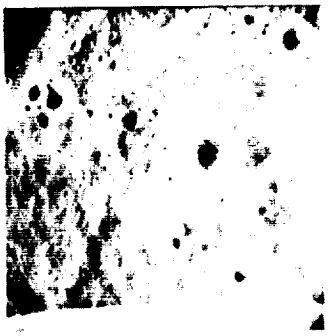
AS10-28-4093

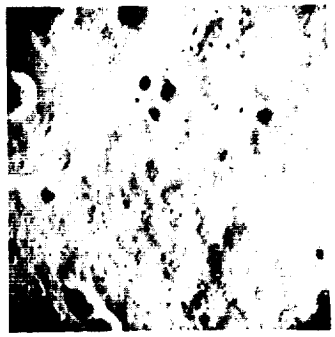
AS10-28-4094

AS10-28-4095

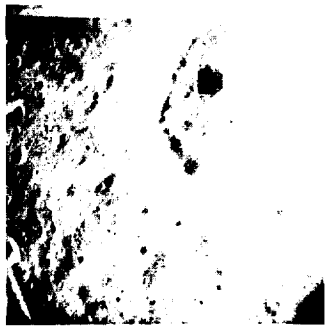

AS10-28-4096

AS10-28-4097

AS10-28-4098

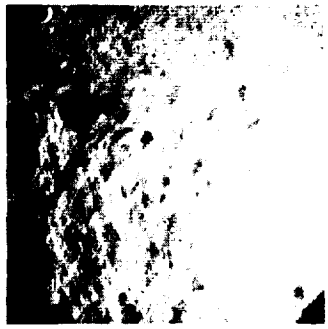

AS10-28-4099

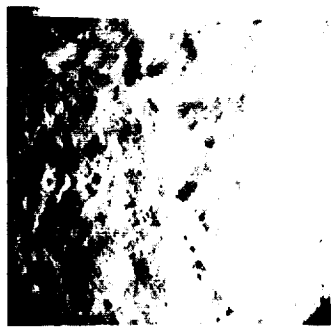

AS10-28-4100

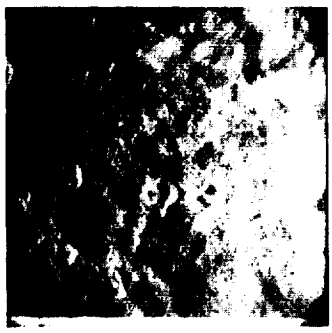

AS10-28-4101

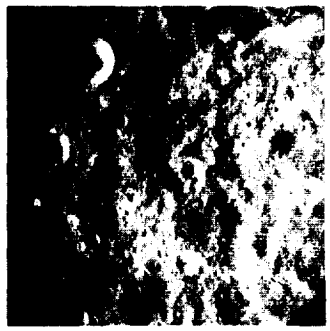

AS10-28-4102

AS10-28-4103

AS10-28-4104

AS10-28-4105

AS10-28-4106


AS10-28-4107

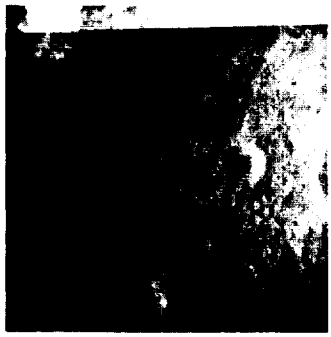
AS10-28-4108


AS10-28-4109

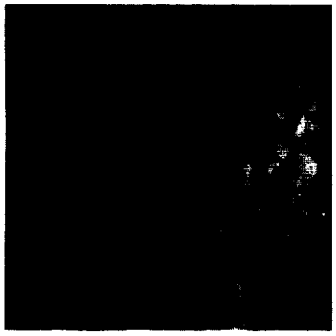
AS10-28-4110

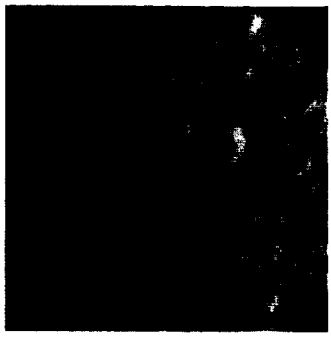
AS10-28-4111

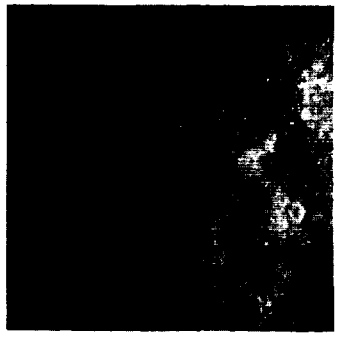
AS10-28-4112


AS10-28-4113


AS10-28-4114

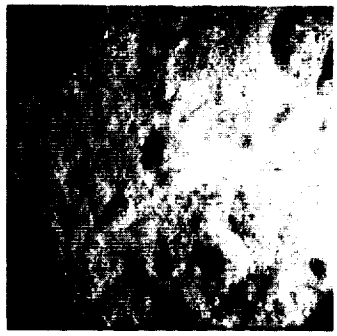
AS10-28-4115

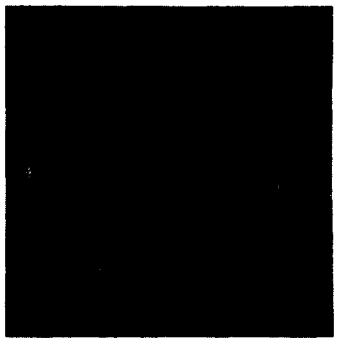
AS10-28-4116

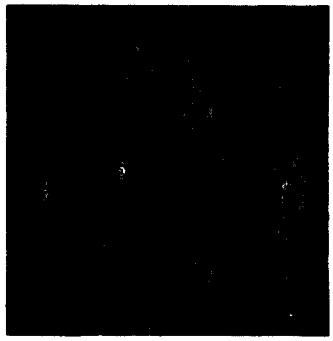
AS10-28-4117


AS10-28-4118

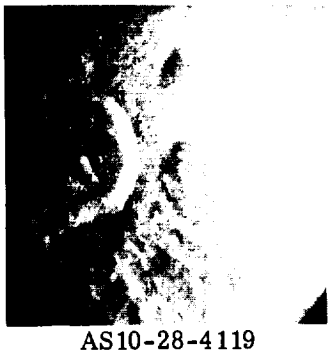
AS10-28-4119


AS10-28-4120

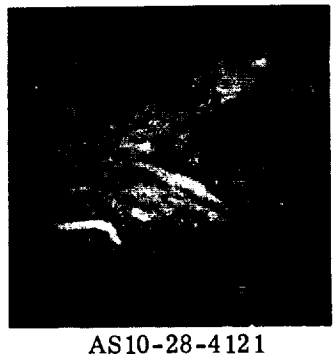
AS10-28-4121

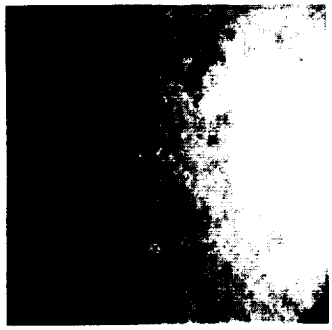
AS10-28-4122

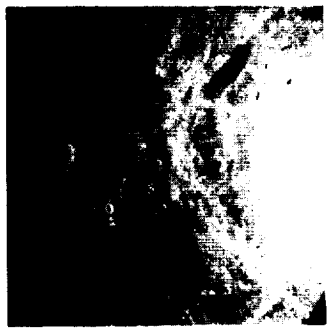
AS10-28-4123

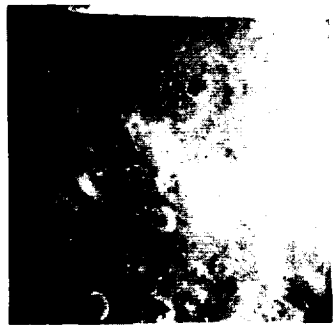
AS10-28-4124

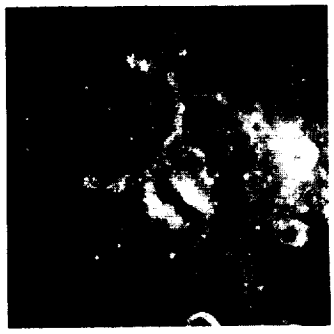
AS10-28-4125


AS10-28-4126


AS10-28-4127


AS10-28-4128

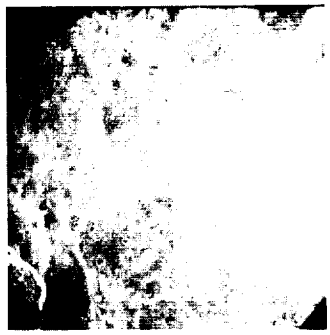
AS10-28-4129

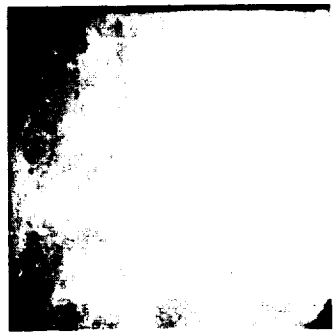
AS10-28-4130


AS10-28-4131

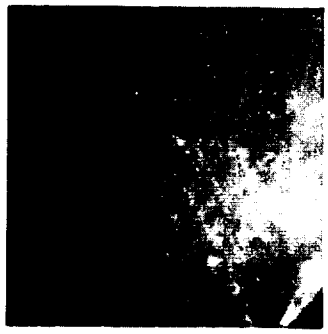
AS10-28-4132

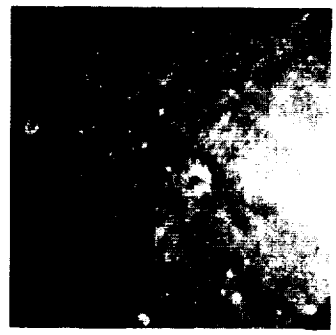
AS10-29-4133

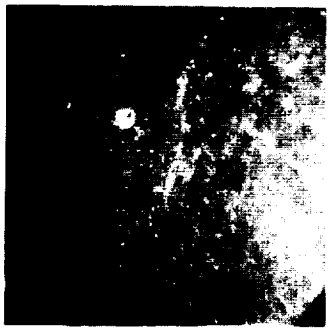
AS10-28-4134

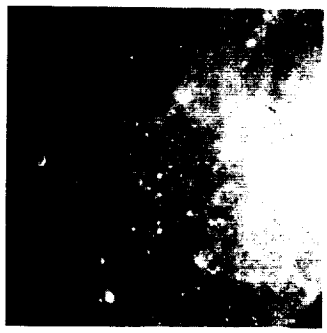
AS10-28-4135

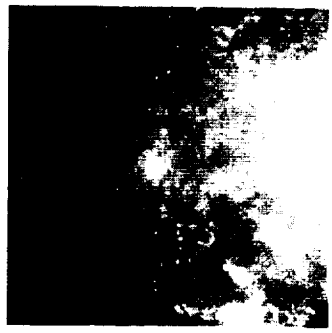
AS10-28-4136


AS10-28-4137

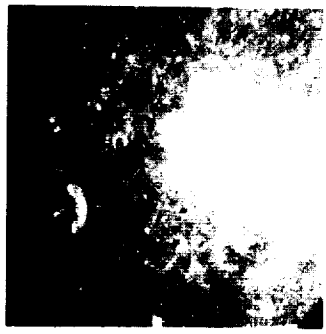
AS10-28-4138

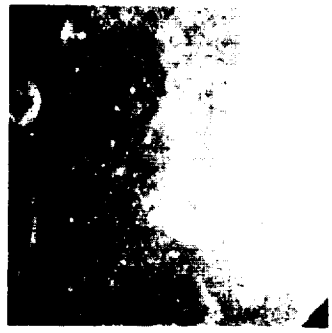
AS10-28-4139


AS10-28-4140

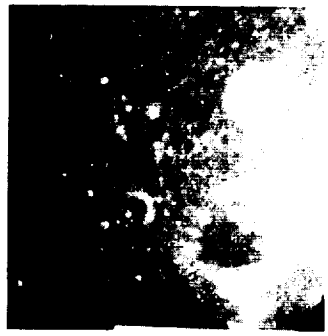
AS10-28-4141

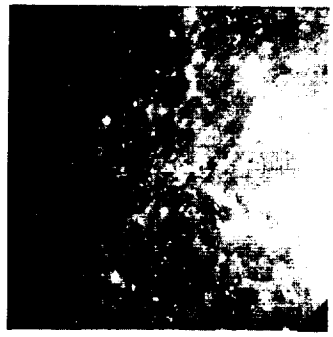
AS10-28-4142


AS10-28-4143

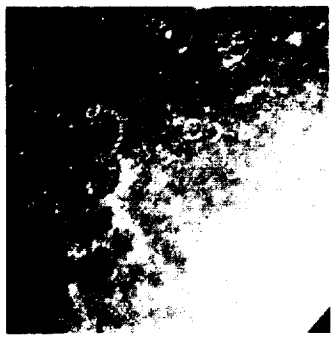
AS10-28-4144


AS10-28-4145

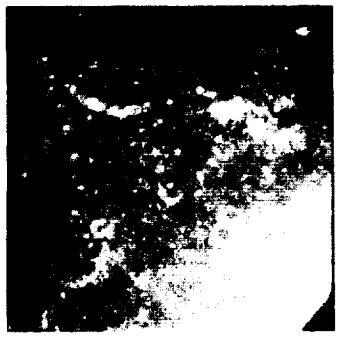
AS10-28-4146

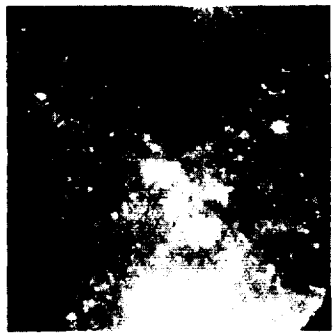
AS10-28-4147


AS10-28-4148


AS10-28-4149

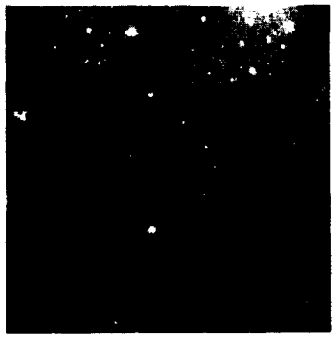
AS10-28-4150


AS10-28-4151

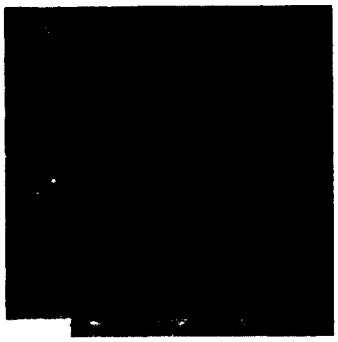
AS10-28-4152

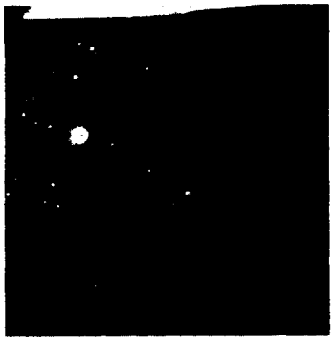
AS10-28-4153


AS10-28-4154


AS10-28-4155

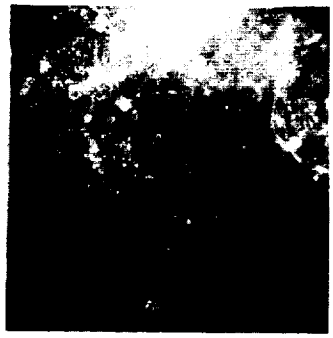
AS10-28-4156


AS10-29-4157


AS10-29-4158


AS10-29-4159


AS10-29-4160


AS10-29-4161

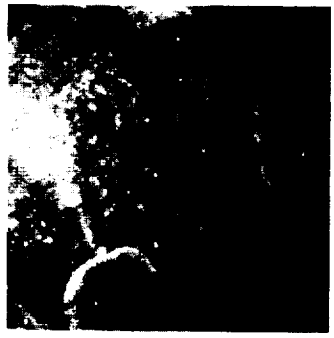
AS10-29-4162

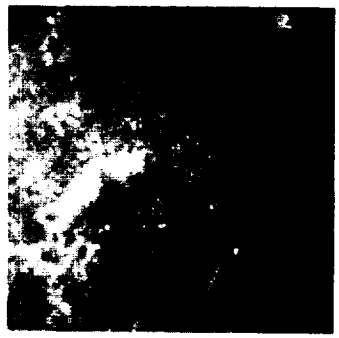
AS10-29-4163

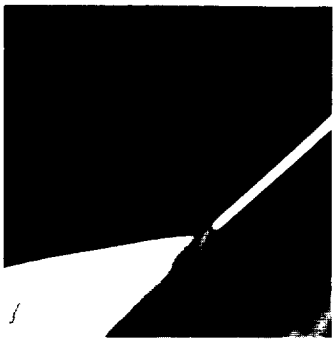
AS10-29-4164

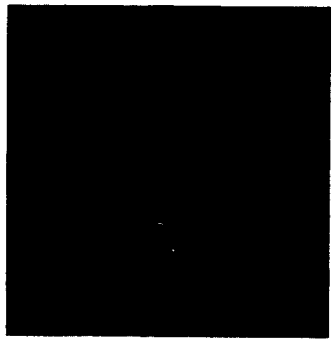
AS10-29-4165

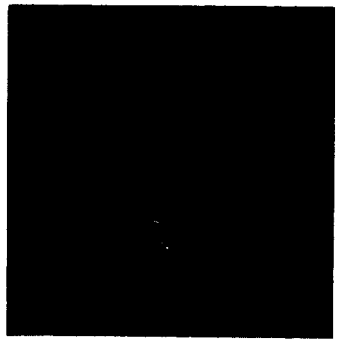
AS10-29-4166

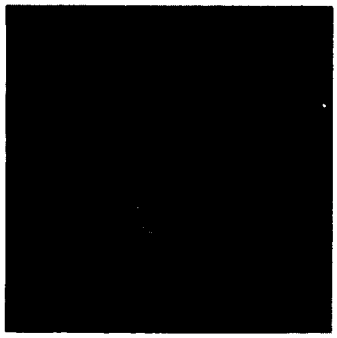
AS10-29-4167

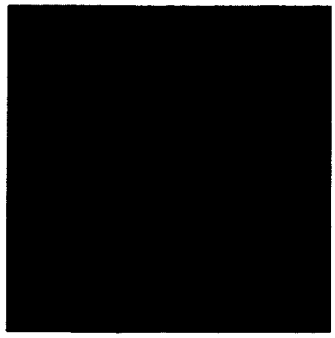
AS10-29-4168

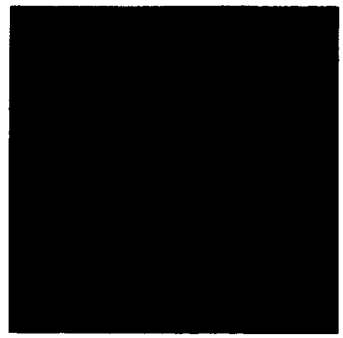
AS10-29-4169

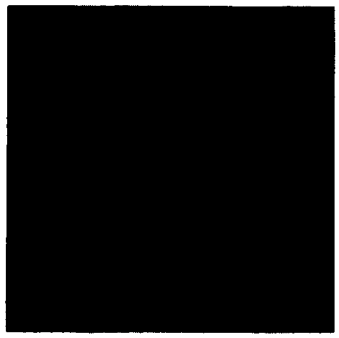
AS10-29-4170

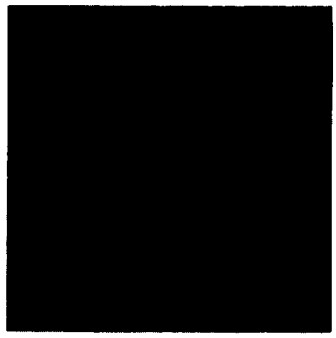
AS10-29-4171

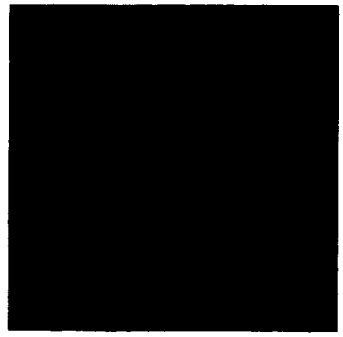
AS10-29-4172

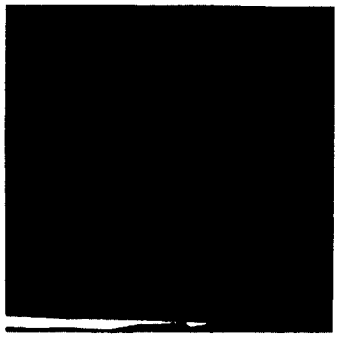
AS10-29-4173

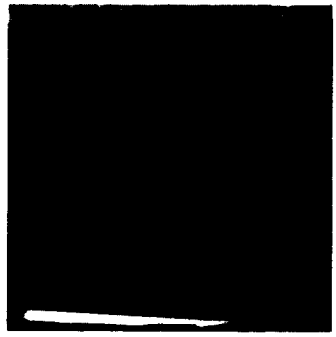
AS10-29-4174


AS10-29-4175


AS10-29-4176


AS10-29-4177

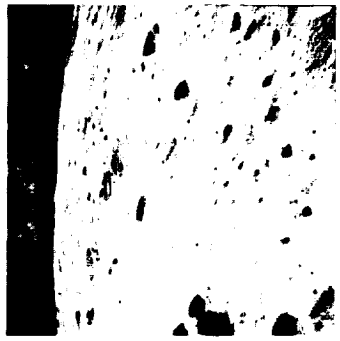
AS10-29-4178

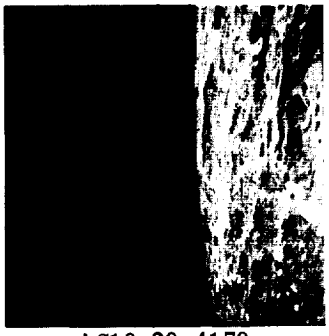
AS10-29-4179


AS10-29-4180


AS10-29-4181


AS10-29-4182


AS10-29-4183

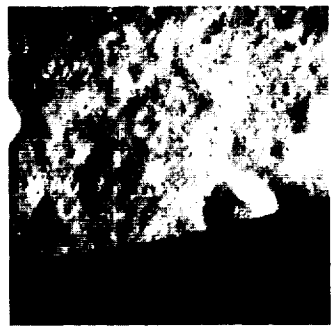
AS10-29-4184


AS10-29-4185


AS10-29-4186


AS10-29-4187


AS10-29-4188


AS10-29-4189

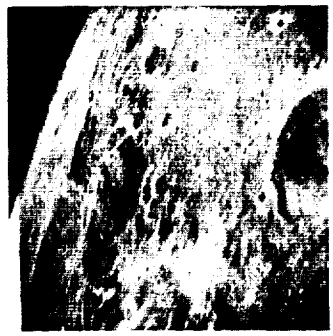
AS10-29-4190


AS10-29-4191

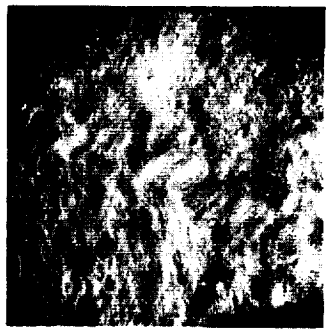
AS10-29-4192

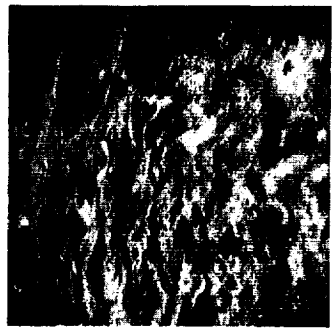
AS10-29-4193

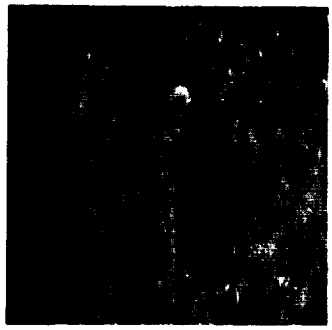
AS10-29-4194

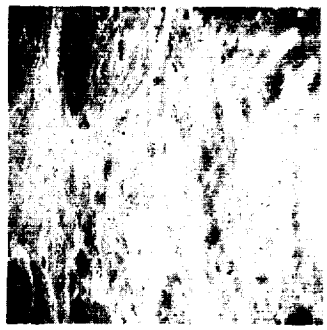
AS10-29-4195

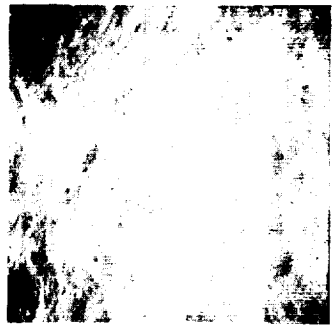
AS10-29-4196


AS10-29-4197

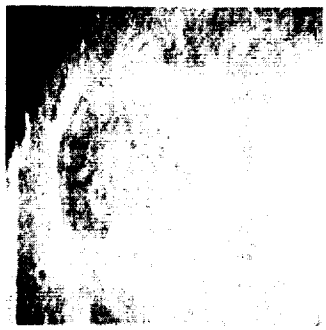
AS10-29-4198

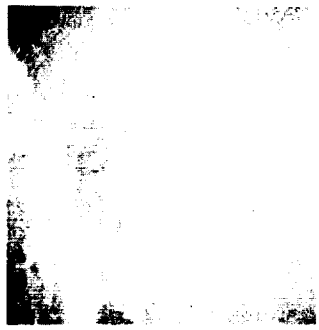
AS10-29-4199


AS10-29-4200

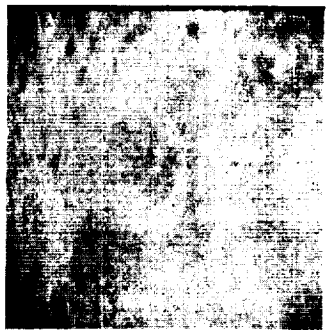
AS10-29-4201


AS10-29-4202


AS10-29-4203


AS10-29-4204

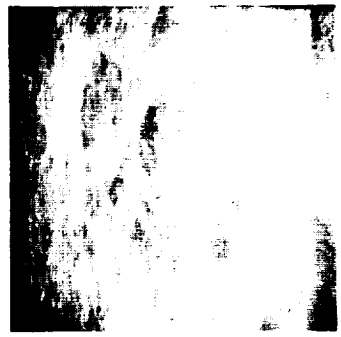
AS10-29-4205

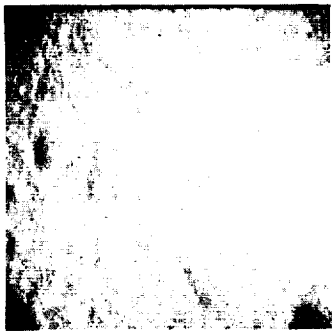
AS10-29-4206

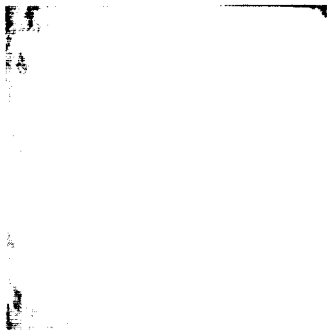
AS10-29-4207

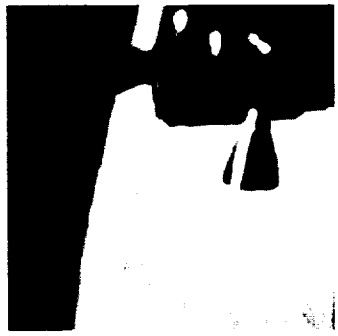
AS10-29-4208

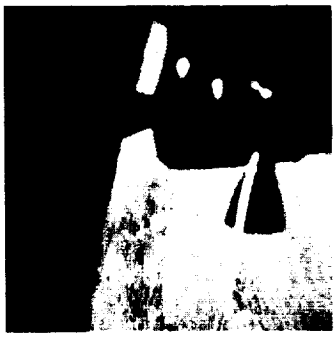
AS10-29-4209


AS10-29-4210

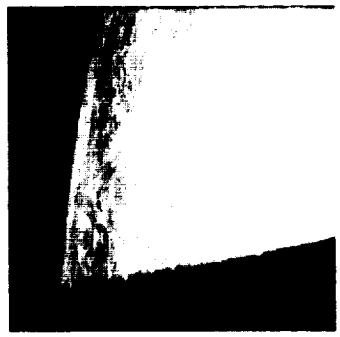
AS10-29-4211


AS10-29-4212


AS10-29-4213

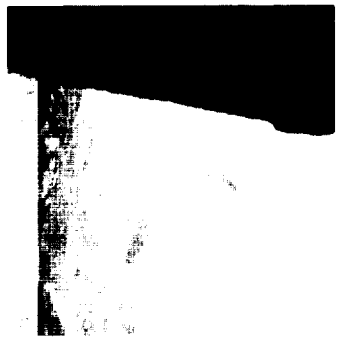
AS10-29-4214


AS10-29-4215


AS10-29-4216

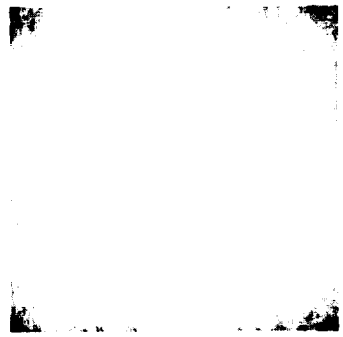
AS10-29-4217

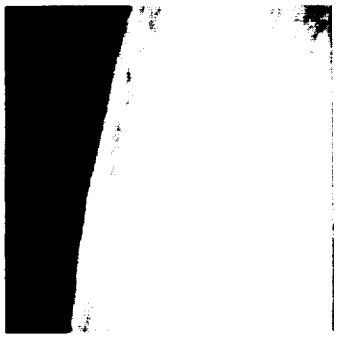
AS10-29-4218

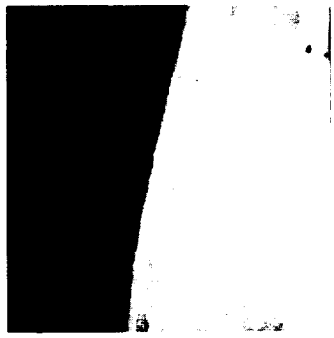
AS10-29-4219


AS10-29-4220

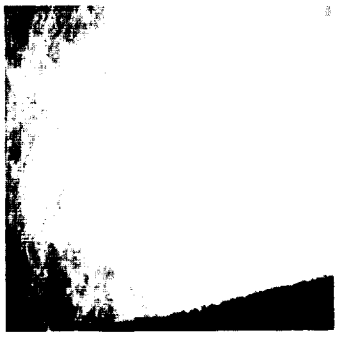
AS10-29-4221


AS10-29-4222


AS10-29-4223


AS10-29-4224


AS10-29-4225

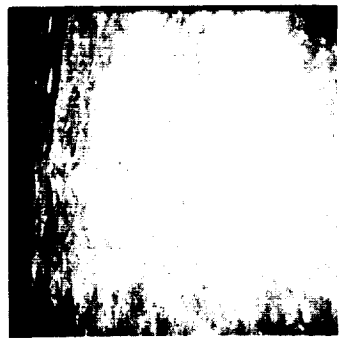
AS10-29-4226

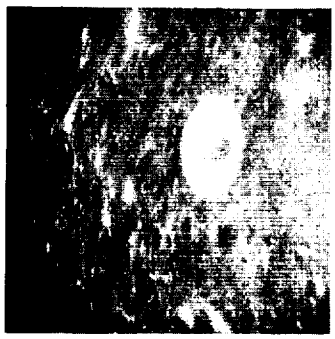
AS10-29-4227


AS10-29-4228


AS10-29-4229

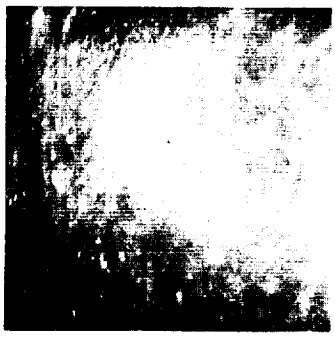
AS10-29-4230

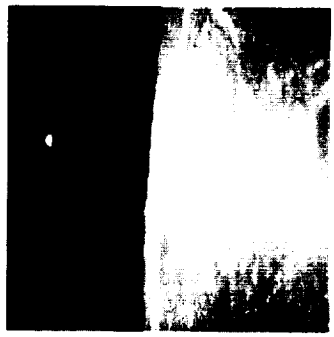
AS10-29-4231


AS10-29-4232

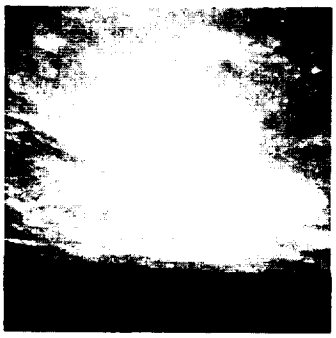
AS10-29-4233


AS10-29-4234

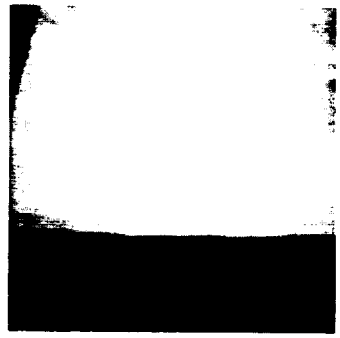
AS10-29-4235

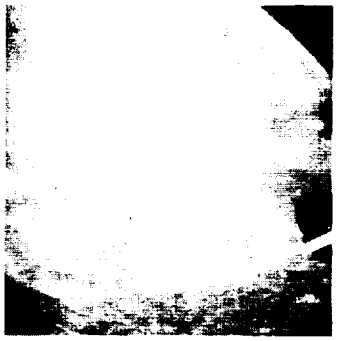
AS10-29-4236

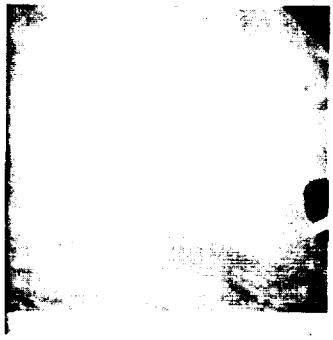
AS10-29-4237

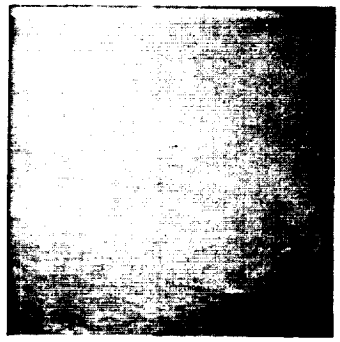
AS10-29-4238

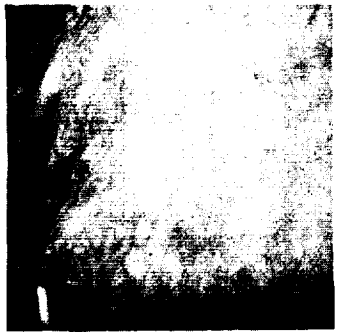
AS10-29-4239


AS10-29-4240

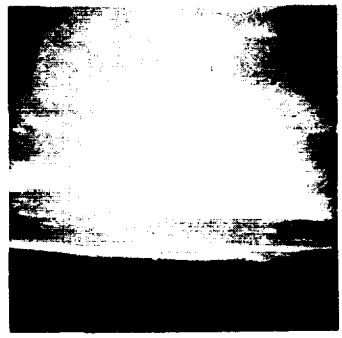
AS10-29-4241


AS10-29-4242


AS10-29-4243


AS10-29-4244

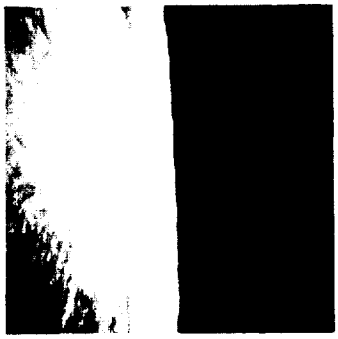
AS10-29-4245


AS10-29-4246

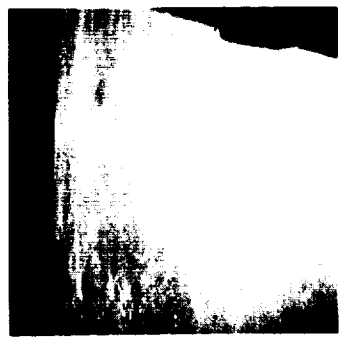
AS10-29-4247


AS10-29-4248

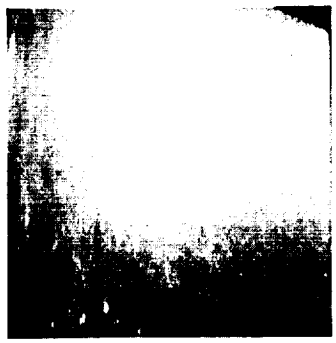
AS10-29-4249


AS10-29-4250


AS10-29-4251


AS10-29-4252


AS10-29-4253


AS10-29-4254

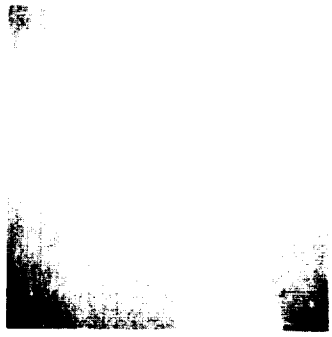
AS10-29-4255


AS10-29-4256


AS10-29-4257


AS10-29-4258


AS10-29-4259


AS10-29-4260

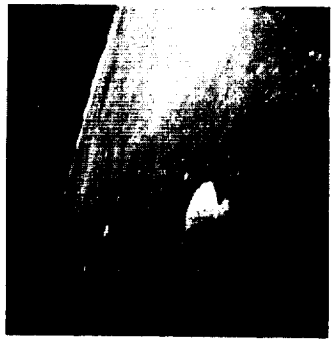
AS10-29-4261

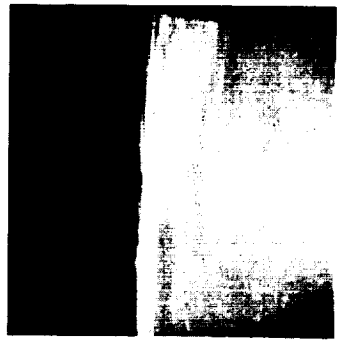
AS10-29-4262


AS10-29-4263


AS10-29-4264


AS10-29-4265


AS10-29-4266

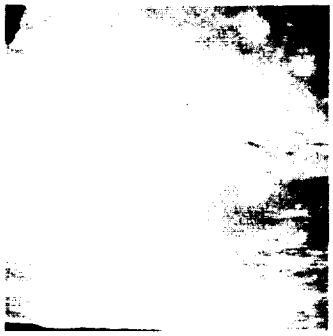
AS10-29-4267

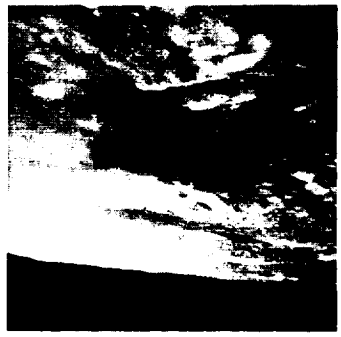
AS10-29-4268

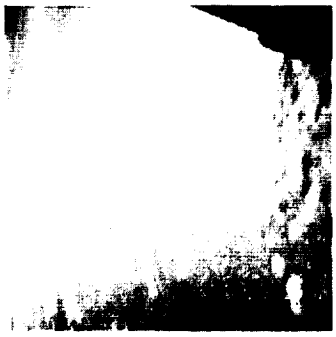
AS10-29-4269

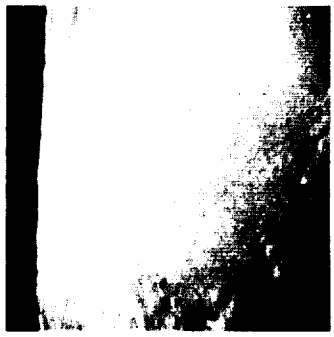
AS10-29-4270

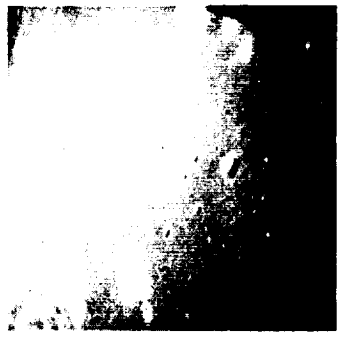
AS10-29-4271


AS10-29-4272

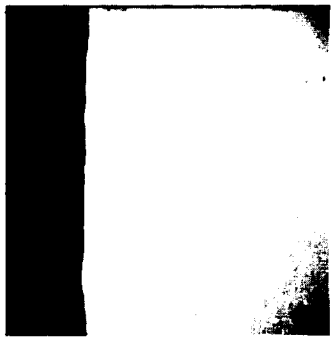
AS10-29-4273


AS10-29-4274


AS10-29-4275


AS10-29-4276


AS10-29-4277


AS10-29-4278

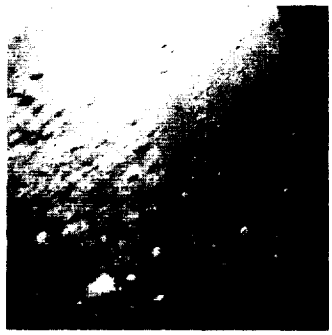
AS10-29-4279

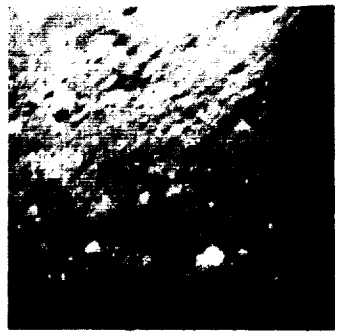
AS10-29-4280


AS10-29-4281


AS10-29-4282


AS10-29-4283


AS10-29-4284


AS10-29-4285


AS10-29-4286


AS10-29-4287


AS10-29-4288


AS10-29-4289


AS10-29-4290

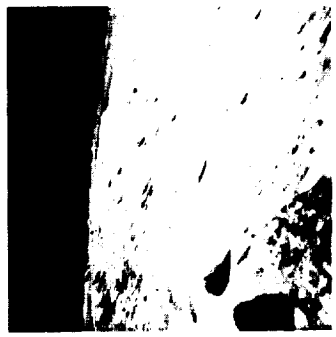
AS10-29-4291


AS10-29-4292


AS10-29-4293

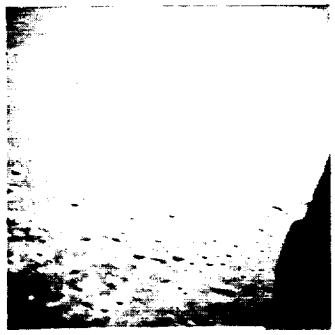
AS10-29-4294

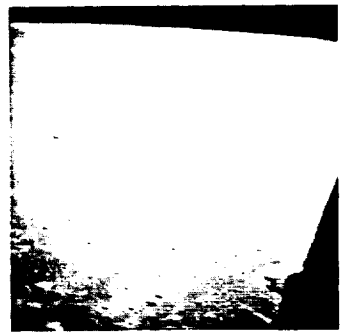
AS10-29-4295


AS10-29-4296

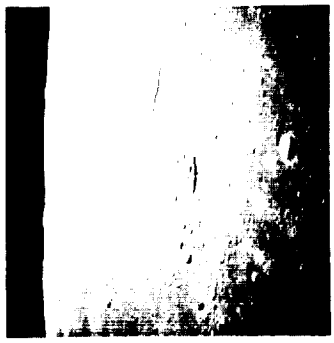
AS10-29-4297


AS10-29-4298


AS10-29-4299


AS10-29-4300


AS10-29-4301


AS10-29-4302


AS10-29-4303


AS10-29-4304

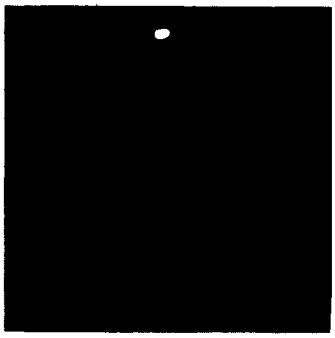
AS10-29-4305

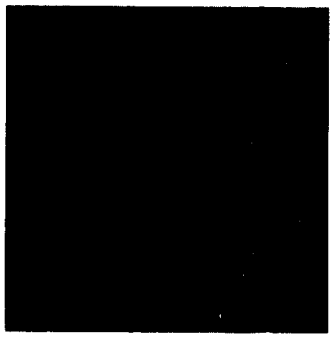
AS10-29-4306


AS10-29-4307


AS10-29-4308

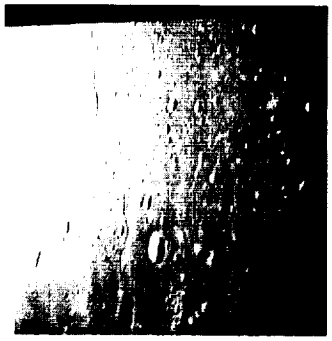
AS10-29-4309


AS10-29-4310


AS10-29-4311

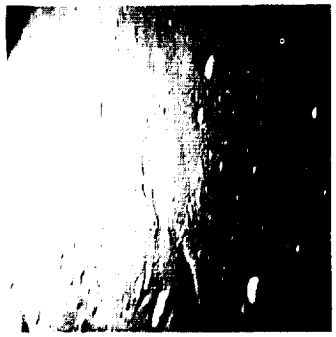
AS10-29-4312

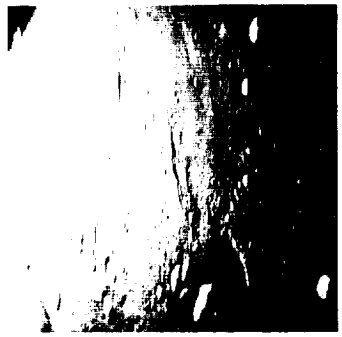
AS10-29-4313


AS10-29-4314


AS10-29-4315


AS10-29-4316


AS10-29-4317

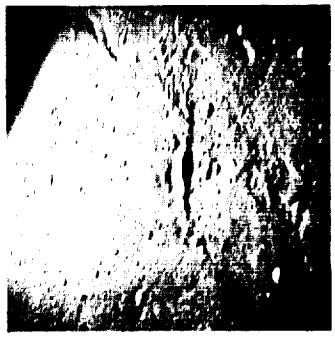
AS10-29-4318

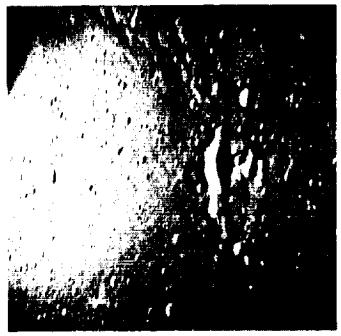
AS10-29-4319


AS10-29-4320

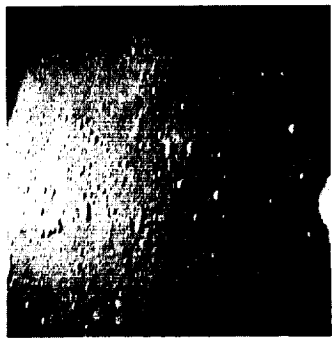
AS10-29-4321


AS10-29-4322

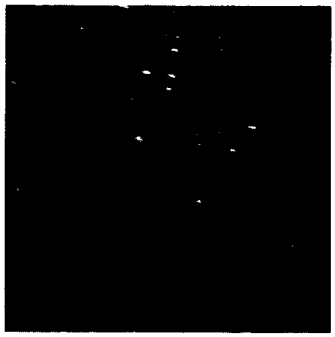
AS10-29-4323


AS10-29-4324


AS10-29-4325


AS10-29-4326


AS10-29-4327


AS10-29-4328

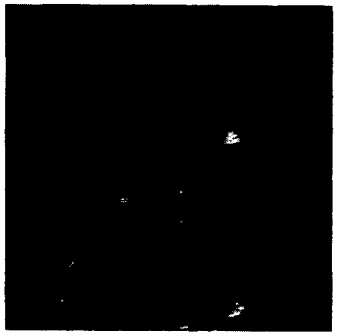
AS10-29-4329


AS10-29-4330


AS10-30-4331

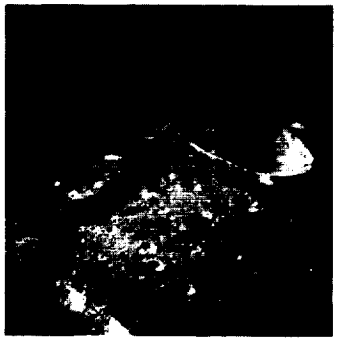
AS10-30-4332


AS10-30-4333

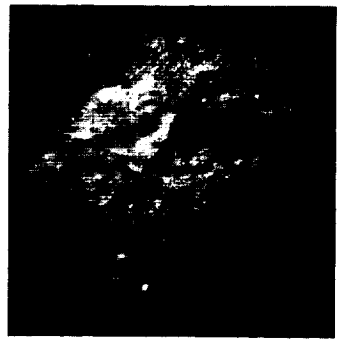
AS10-30-4334

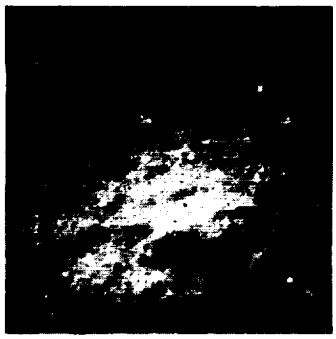
AS10-30-4335


AS10-30-4336

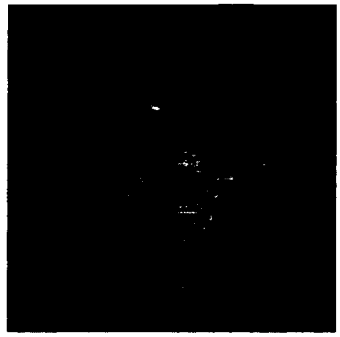
AS10-30-4337


AS10-30-4338


AS10-30-4339


AS10-30-4340


AS10-30-4341


AS10-30-4342

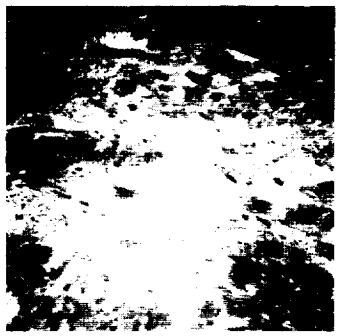
AS10-30-4343

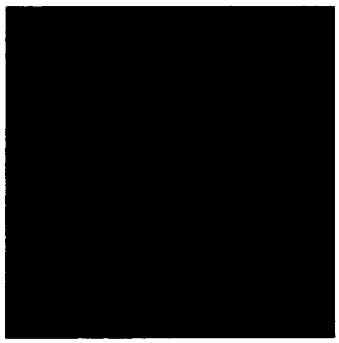
AS10-30-4344

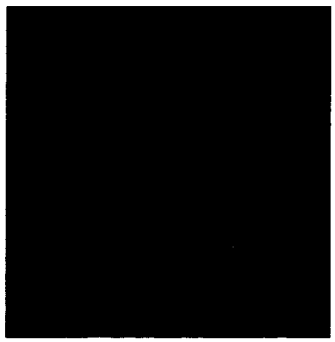
AS10-30-4345

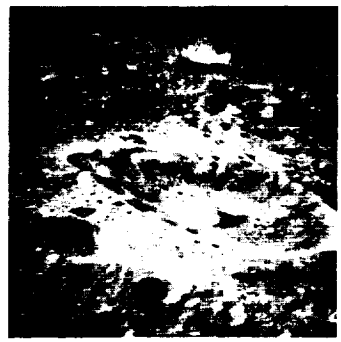
AS10-30-4346


AS10-30-4347


AS10-30-4348

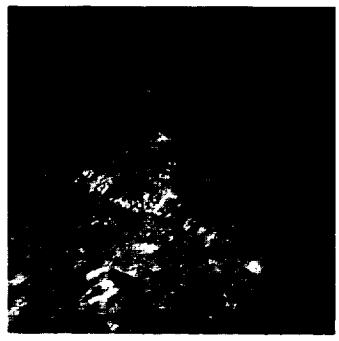
AS10-30-4349

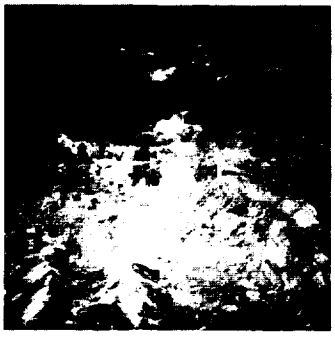
AS10-30-4350


AS10-30-4351


AS10-30-4352


AS10-30-4353

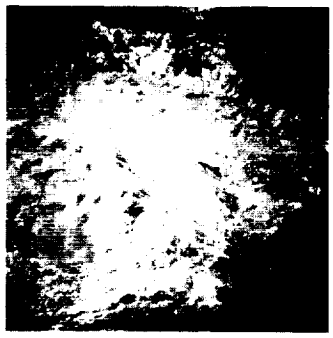
AS10-30-4354


AS10-30-4355

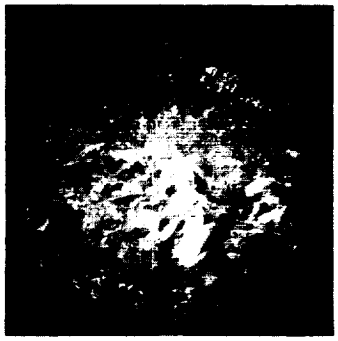
AS10-30-4356


AS10-30-4357

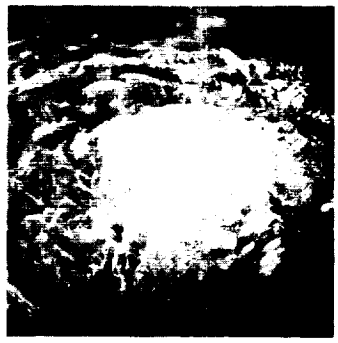
AS10-30-4358

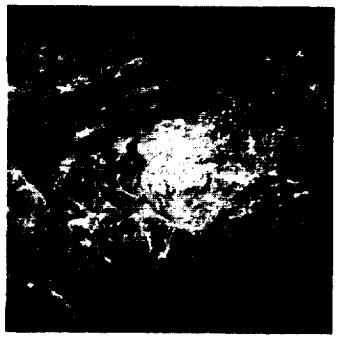
AS10-30-4359

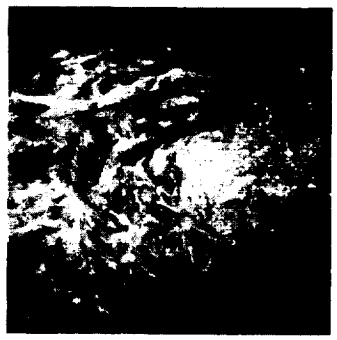
AS10-30-4360


AS10-30-4361


AS10-30-4362


AS10-30-4363


AS10-30-4364


AS10-30-4365

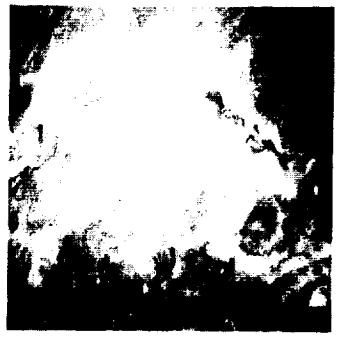
AS10-30-4366

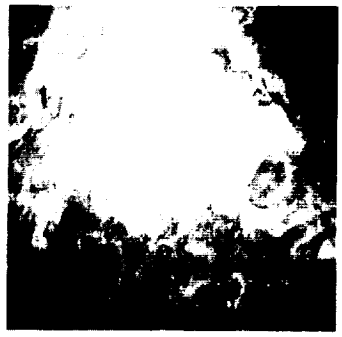
AS10-30-4367


AS10-30-4368


AS10-30-4369


AS10-30-4370


AS10-30-4371

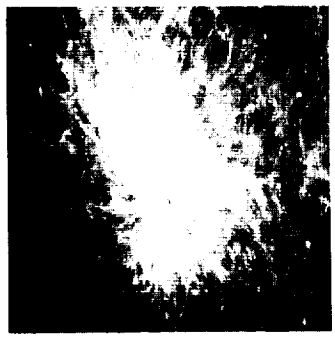
AS10-30-4372


AS10-30-4373

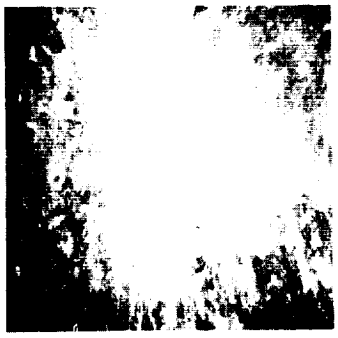
AS10-30-4374


AS10-30-4375


AS10-30-4376

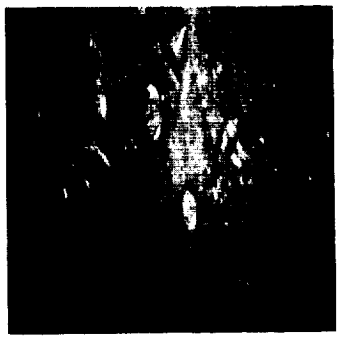
AS10-30-4377


AS10-30-4378


AS10-30-4379


AS10-30-4380

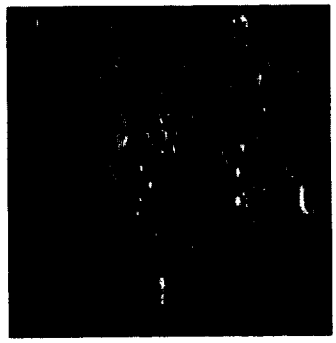
AS10-30-4381

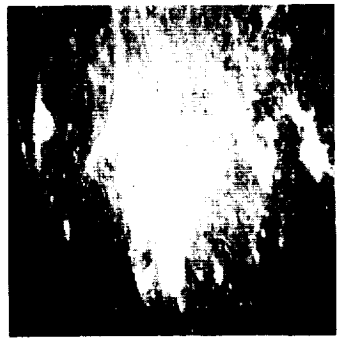
AS10-30-4382


AS10-30-4383


AS10-30-4384


AS10-30-4385


AS10-30-4386


AS10-30-4387


AS10-30-4388


AS10-30-4389

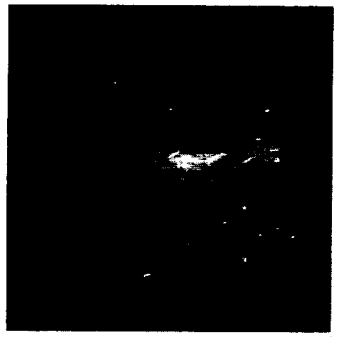
AS10-30-4390


AS10-30-4391


AS10-30-4392


AS10-30-4393


AS10-30-4394


AS10-30-4395


AS10-30-4396


AS10-30-4397


AS10-30-4398


AS10-30-4399

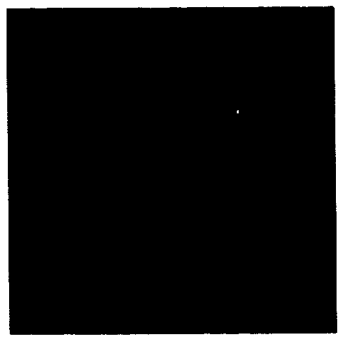
AS10-30-4400

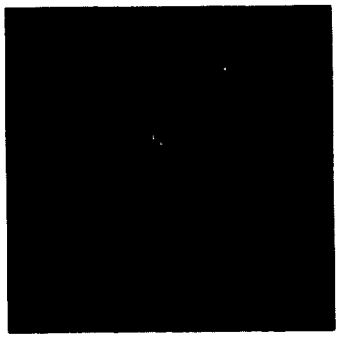
AS10-30-4401

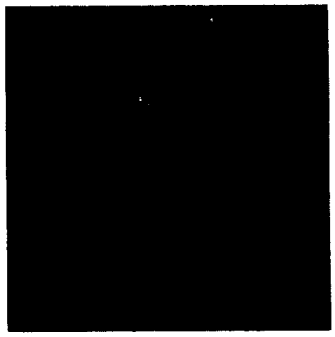
AS10-30-4402


AS10-30-4403


AS10-30-4404


AS10-30-4405


AS10-30-4406


AS10-30-4407


AS10-30-4408


AS10-30-4409


AS10-30-4410

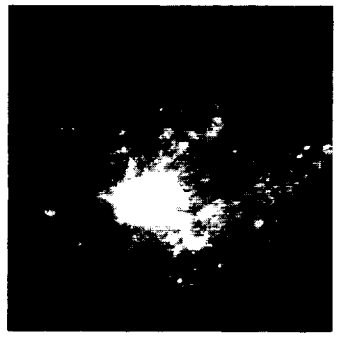
AS10-30-4411

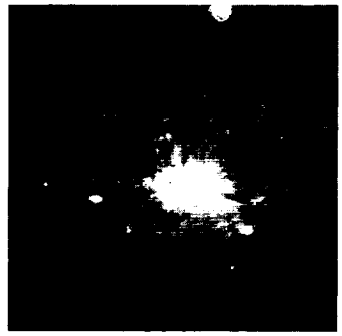
AS10-30-4412

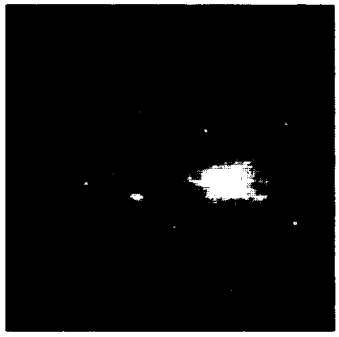
AS10-30-4413


AS10-30-4414


AS10-30-4415


AS10-30-4416

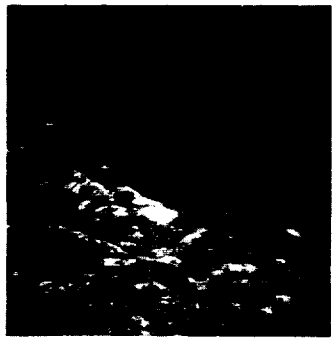
AS10-30-4417


AS10-30-4418

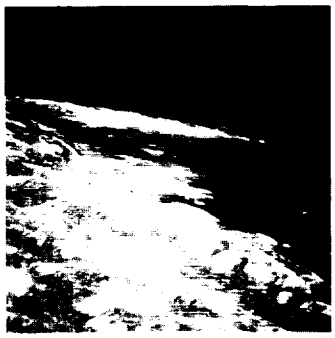
AS10-30-4419


AS10-30-4420

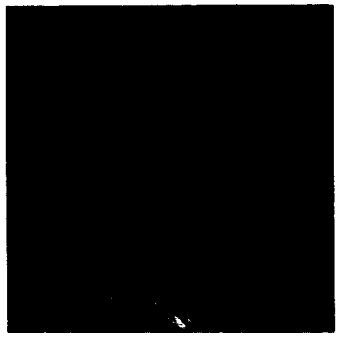
AS10-30-4421


AS10-30-4422

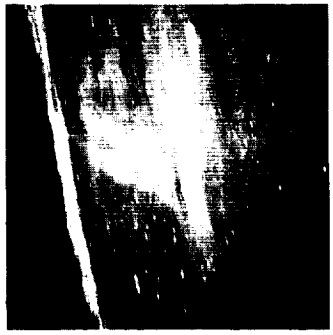
AS10-30-4423


AS10-30-4424

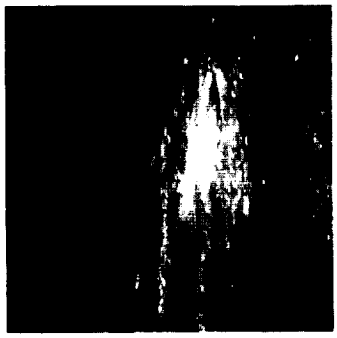
AS10-30-4425


AS10-30-4426

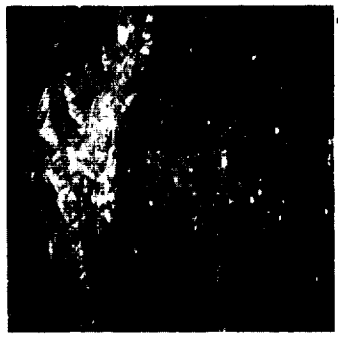
AS10-30-4427


AS10-30-4428

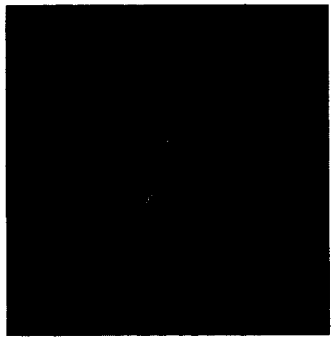
AS10-30-4429


AS10-30-4430


AS10-30-4431

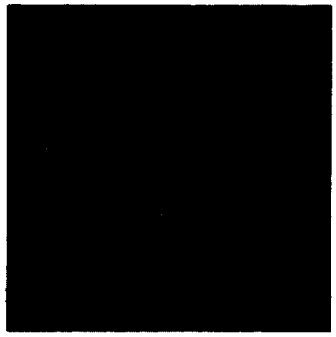
AS10-30-4432

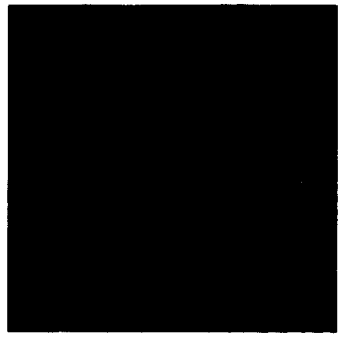
AS10-30-4433


AS10-30-4434


AS10-30-4435


AS10-30-4436

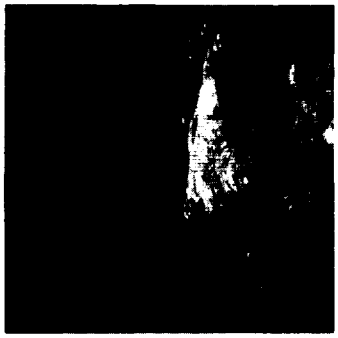
AS10-30-4437

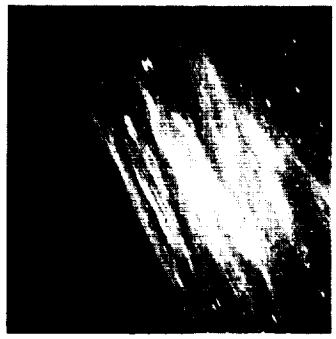
AS10-30-4438


AS10-30-4439


AS10-30-4440


AS10-30-4441


AS10-30-4442

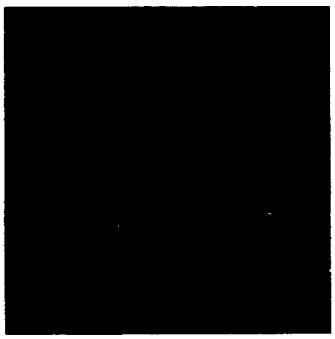
AS10-30-4443

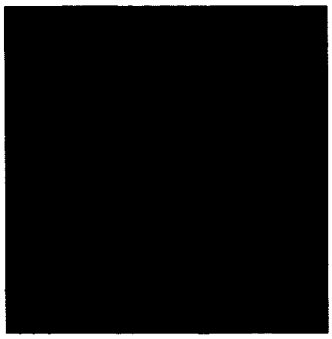
AS10-30-4444


AS10-30-4445

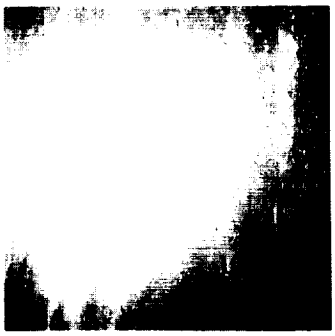
AS10-30-4446

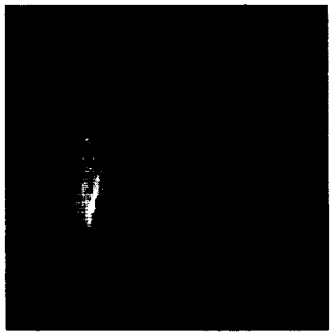
AS10-30-4447

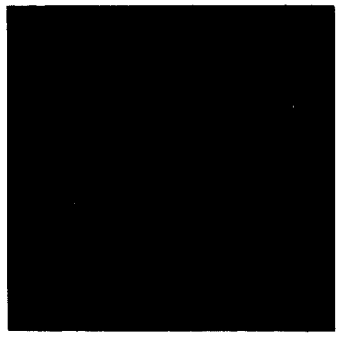
AS10-30-4448


AS10-30-4449

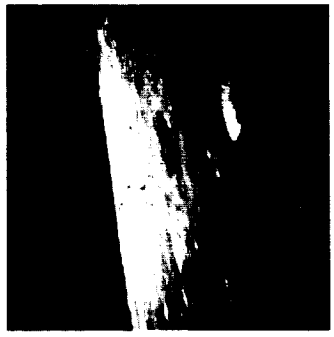
AS10-30-4450


AS10-30-4451


AS10-30-4452

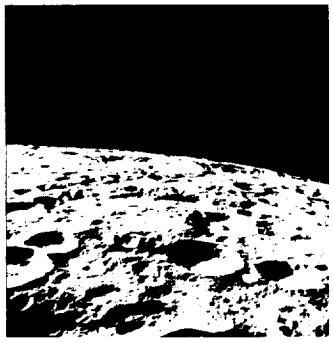
AS10-30-4453

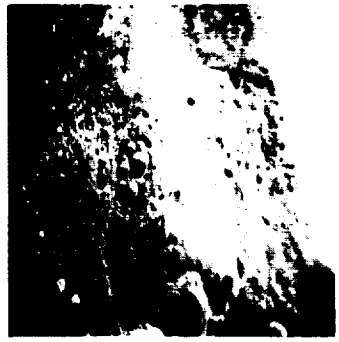
AS10-30-4454


AS10-30-4455


AS10-30-4456


AS10-30-4457


AS10-30-4458


AS10-30-4459


AS10-30-4460


AS10-30-4461


AS10-30-4462


AS10-30-4463


AS10-30-4464


AS10-30-4465


AS10-30-4466


AS10-30-4467


AS10-30-4468

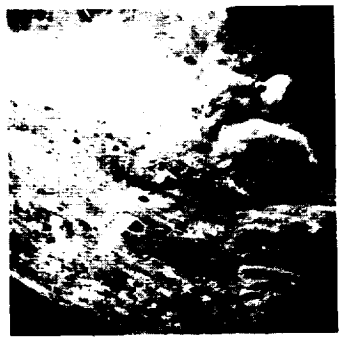
AS10-30-4469


AS10-30-4470

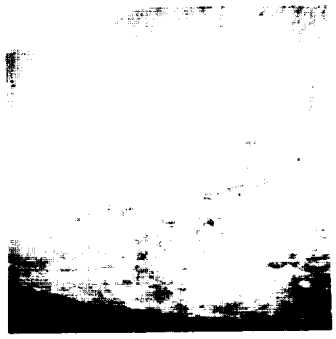
AS10-30-4471

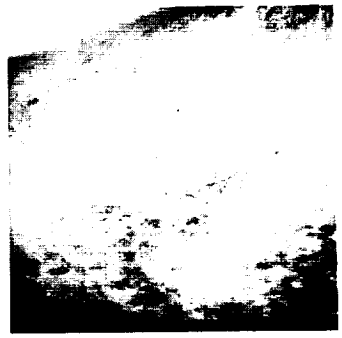
AS10-30-4472


AS10-30-4473


AS10-30-4474


AS10-30-4475


AS10-30-4476

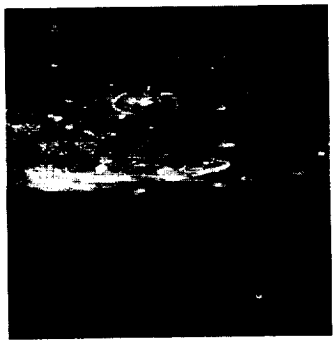
AS10-30-4477


AS10-30-4478


AS10-30-4479


AS10-30-4480

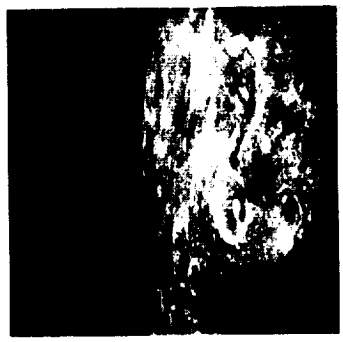
AS10-30-4481


AS10-30-4482


AS10-30-4483


AS10-30-4484


AS10-30-4485

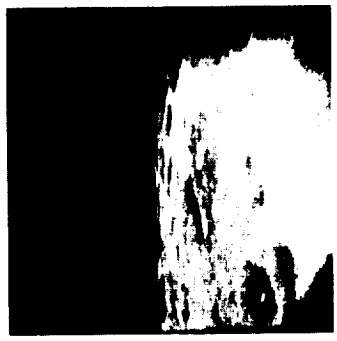
AS10-30-4486

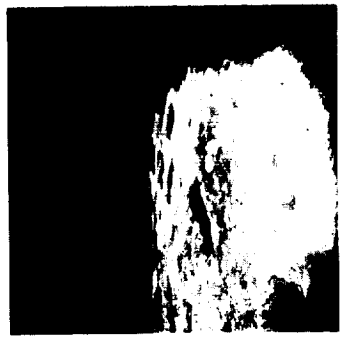
AS10-30-4487


AS10-30-4488


AS10-30-4489


AS10-30-4490


AS10-30-4491


AS10-30-4492


AS10-30-4493


AS10-30-4494


AS10-30-4495


AS10-30-4496


AS10-30-4497


AS10-30-4498


AS10-30-4499

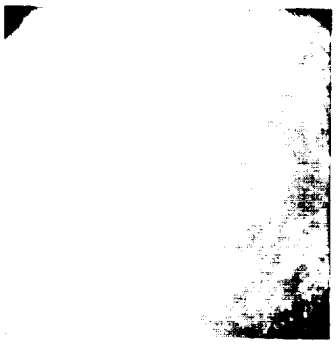
AS10-31-4500


AS10-31-4501

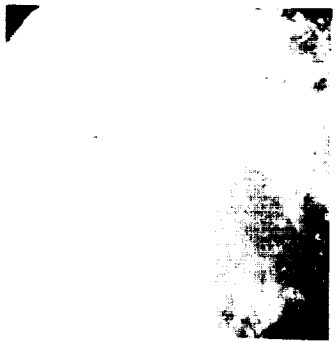
AS10-31-4502

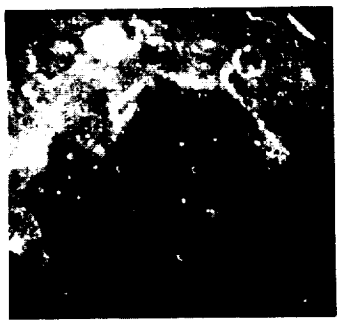

AS10-31-4503

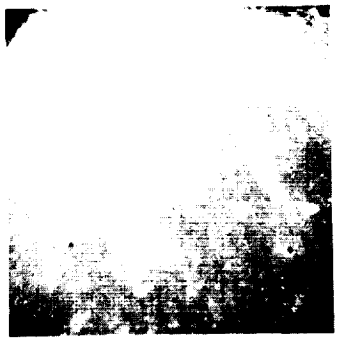

AS10-31-4504

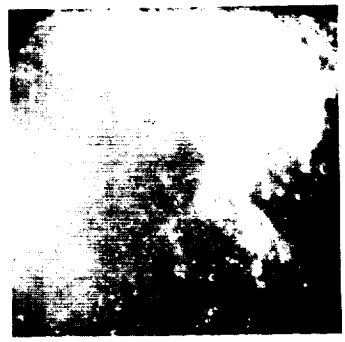

AS10-31-4505

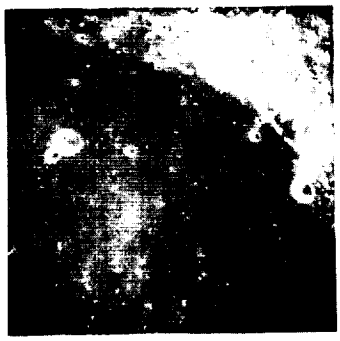

AS10-31-4506

AS10-31-4507

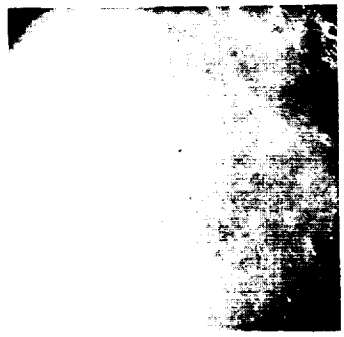

AS10-31-4508

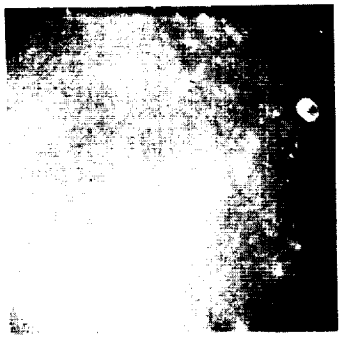

AS10-31-4509

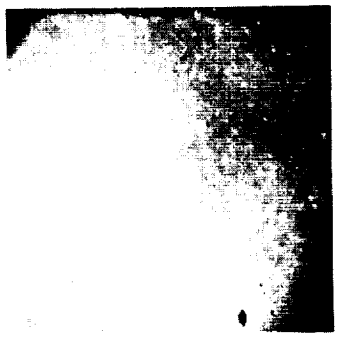

AS10-31-4510

AS10-31-4511

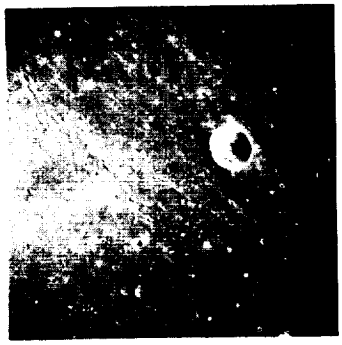

AS10-31-4512

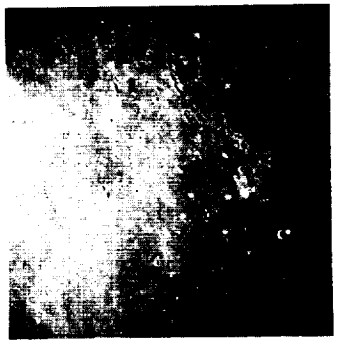

AS10-31-4513

AS10-31-4514


AS10-31-4515

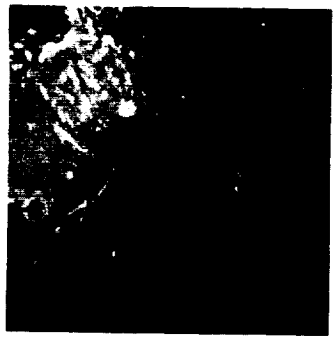
AS10-31-4516


AS10-31-4517


AS10-31-4518

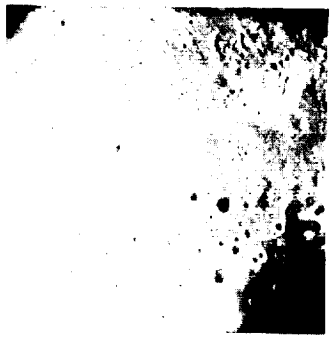
AS10-31-4519


AS10-31-4520

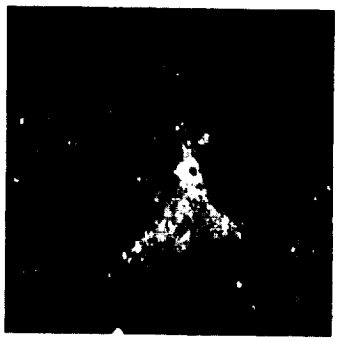
AS10-31-4521


AS10-31-4522


AS10-31-4523

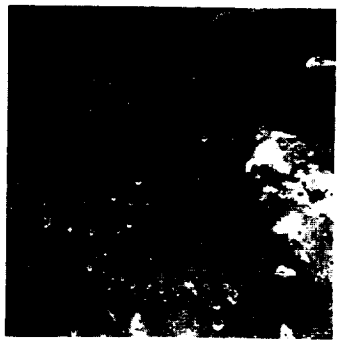
AS10-31-4524

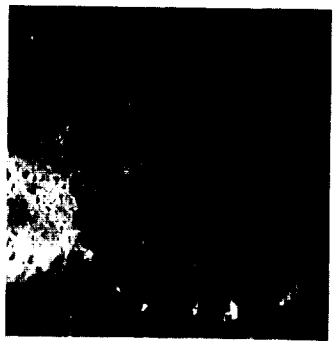
AS10-31-4525

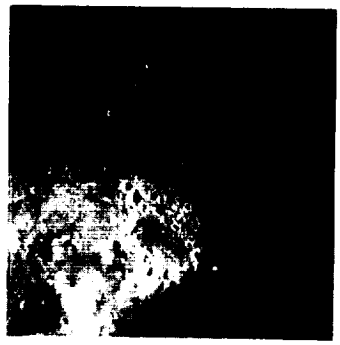
AS10-31-4526

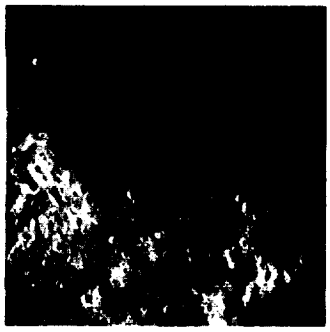
AS10-31-4527


AS10-31-4528


AS10-31-4529

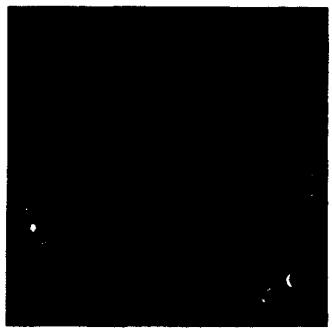
AS10-31-4530

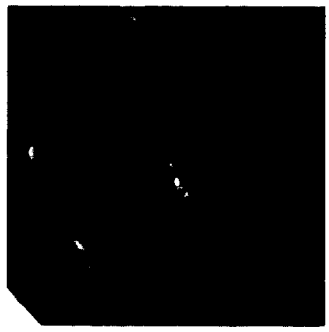
AS10-31-4531


AS10-31-4532


AS10-31-4533

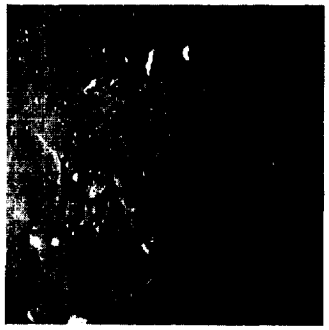
AS10-31-4534


AS10-31-4535

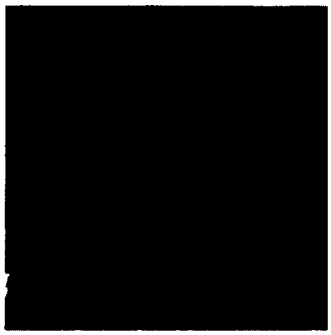
AS10-31-4536

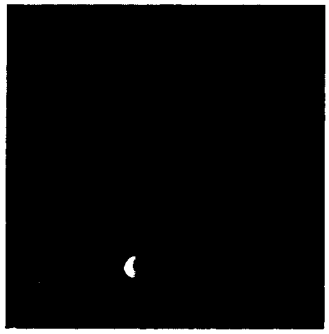
AS10-31-4537

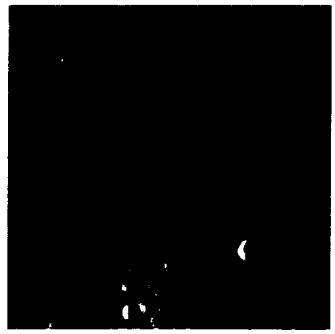
AS10-31-4538


AS10-31-4539

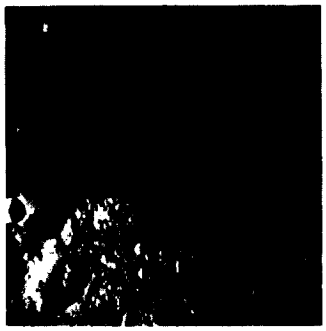
AS10-31-4540


AS10-31-4541


AS10-31-4542

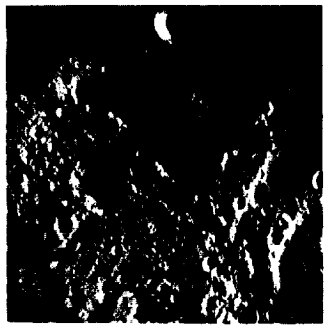
AS10-31-4543


AS10-31-4544


AS10-31-4545


AS10-31-4546


AS10-31-4547


AS10-31-4548


AS10-31-4549


AS10-31-4550

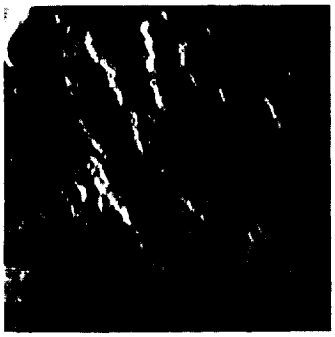
AS10-31-4551

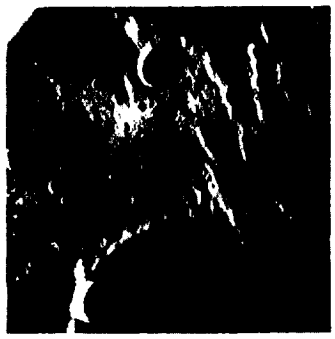
AS10-31-4552

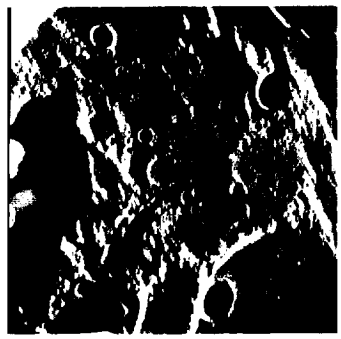
AS10-31-4553

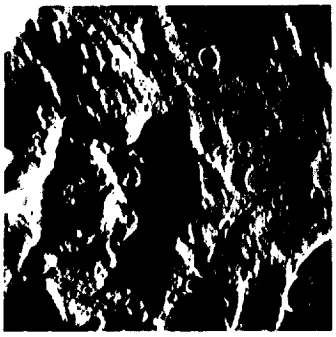
AS10-31-4554

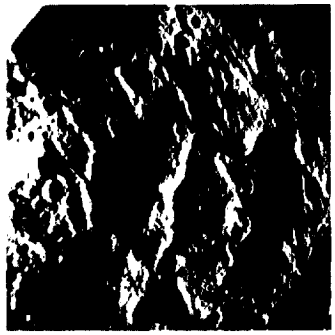
AS10-31-4555

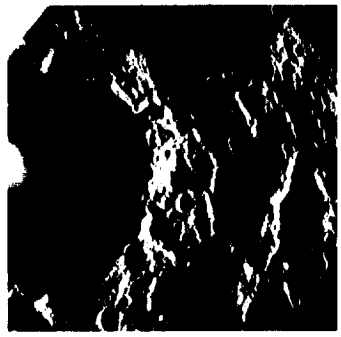
AS10-31-4556

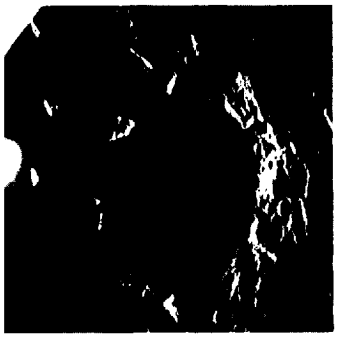
AS10-31-4557


AS10-31-4558


AS10-31-4559

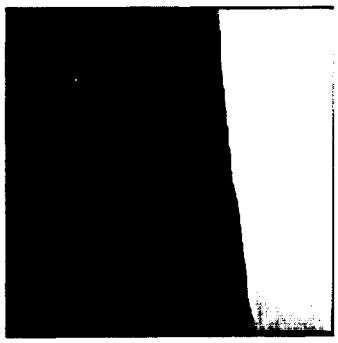
AS10-31-4560

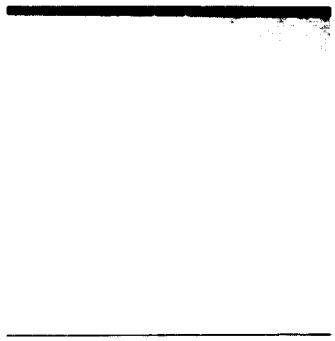
AS10-31-4561


AS10-31-4562

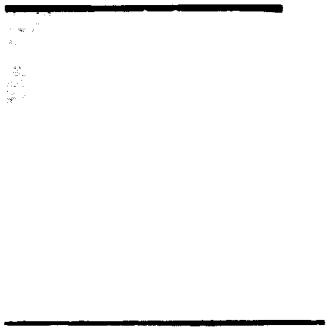
AS10-31-4563


AS10-31-4564


AS10-31-4565


AS10-31-4566

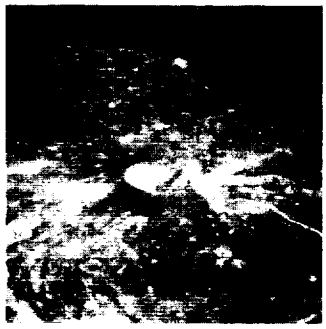
AS10-31-4567


AS10-31-4568


AS10-31-4569

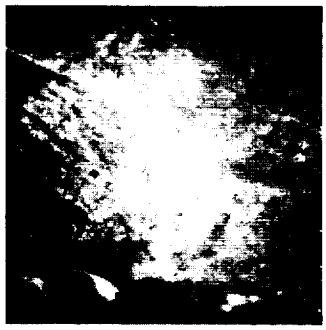
AS10-31-4570


AS10-31-4571


AS10-31-4572

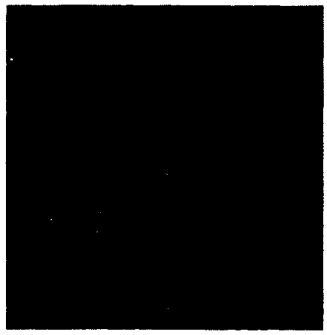
AS10-31-4573


AS10-31-4574

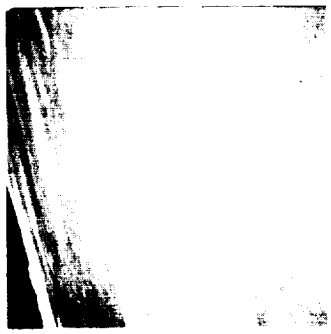
AS10-31-4575

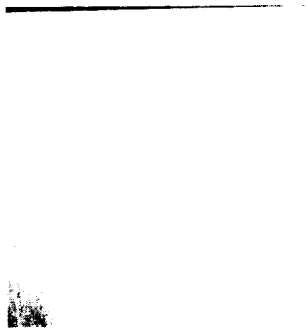
AS10-31-4576


AS10-31-4577


AS10-31-4578

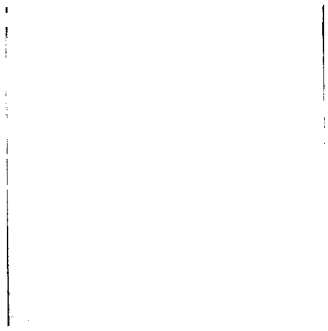
AS10-31-4579


AS10-31-4580

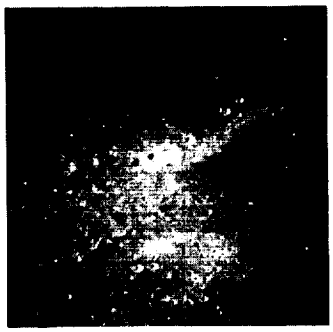
AS10-31-4581


AS10-31-4582

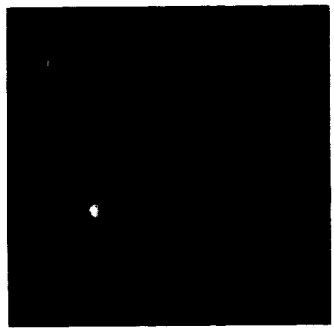
AS10-31-4583

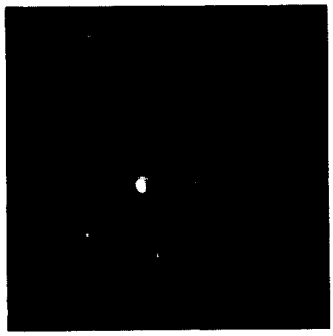
AS10-31-4584

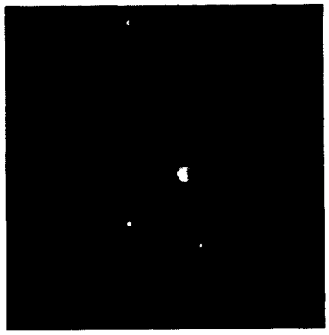
AS10-31-4585


AS10-31-4586

AS10-31-4587

AS10-31-4588

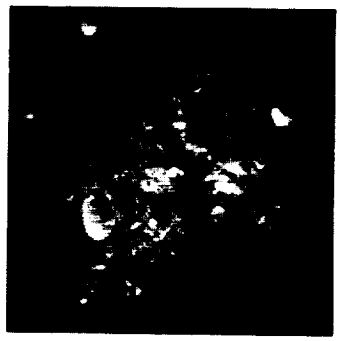

AS10-31-4589

AS10-31-4590

AS10-31-4591

AS10-31-4592

AS10-31-4593

AS10-31-4594

AS10-31-4595

AS10-31-4596

AS10-31-4597

AS10-31-4598

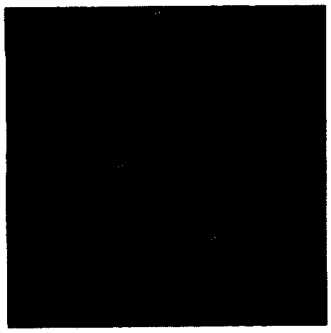
AS10-31-4599

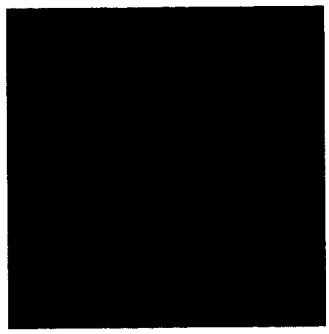
AS10-31-4600


AS10-31-4601


AS10-31-4602


AS10-31-4603


AS10-31-4604

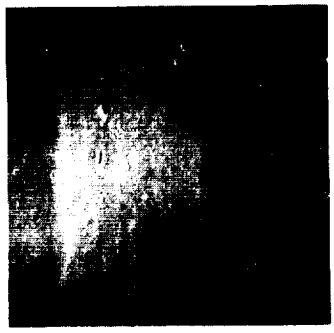
AS10-31-4605

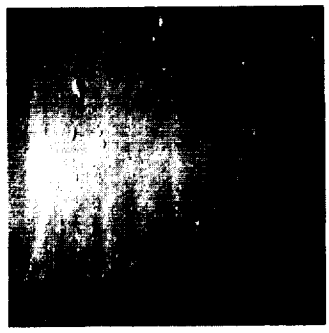
AS10-31-4606


AS10-31-4607

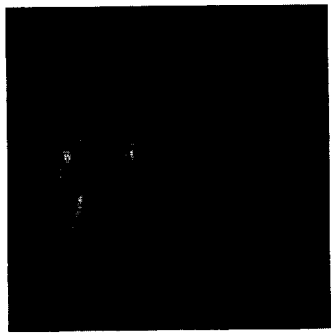
AS10-31-4608

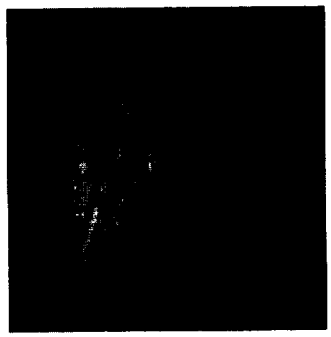
AS10-31-4609

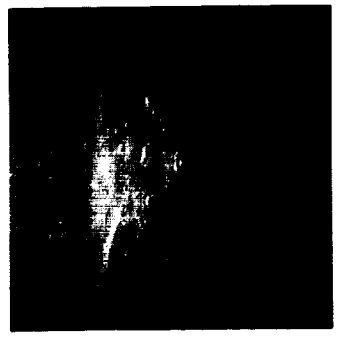
AS10-31-4610

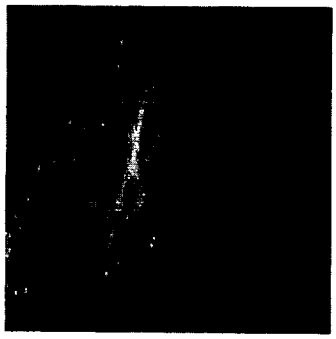
AS10-31-4611


AS10-31-4612

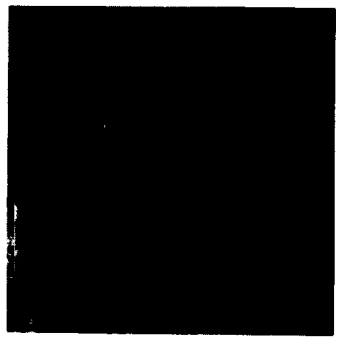
AS10-31-4613

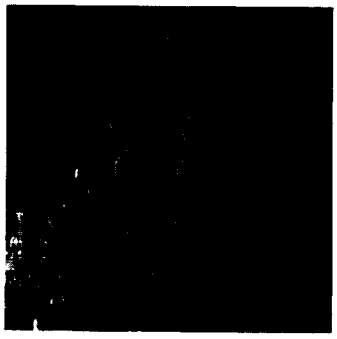
AS10-31-4614

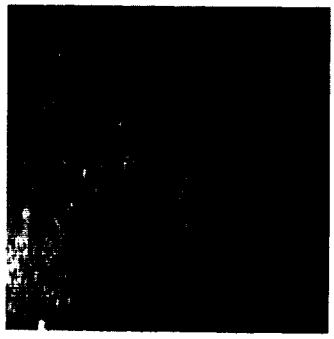
AS10-31-4615


AS10-31-4616


AS10-31-4617


AS10-31-4618


AS10-31-4619


AS10-31-4620

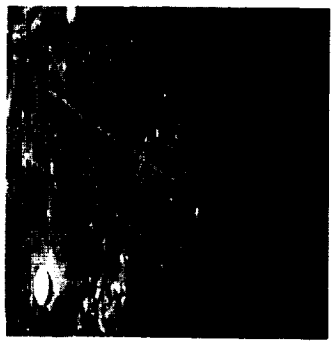
AS10-31-4621


AS10-31-4622

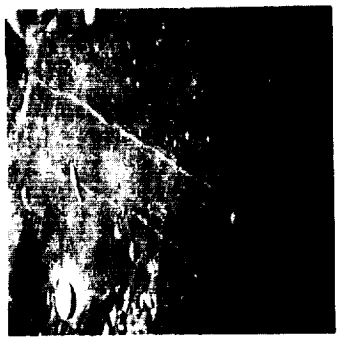
AS10-31-4623


AS10-31-4624


AS10-31-4625

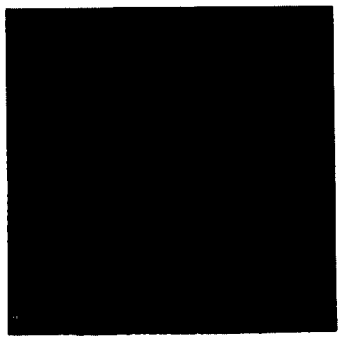
AS10-31-4626

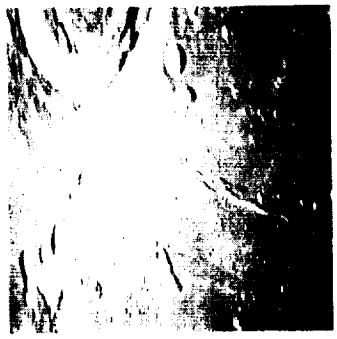
AS10-31-4627

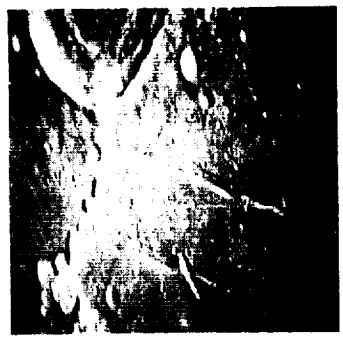
AS10-31-4628


AS10-31-4629


AS10-31-4630

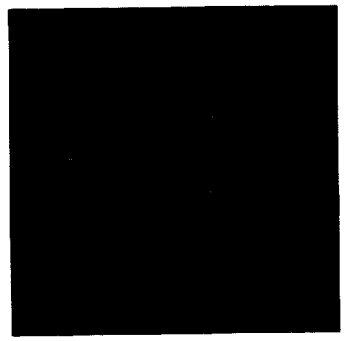
AS10-31-4631

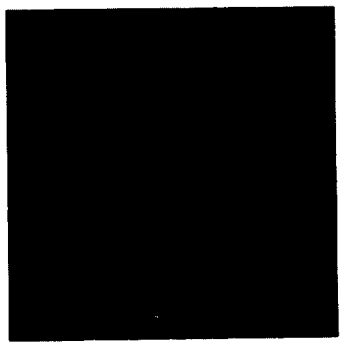
AS10-31-4632

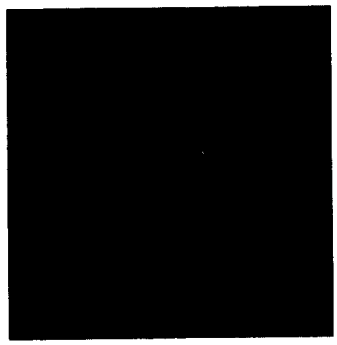
AS10-31-4633

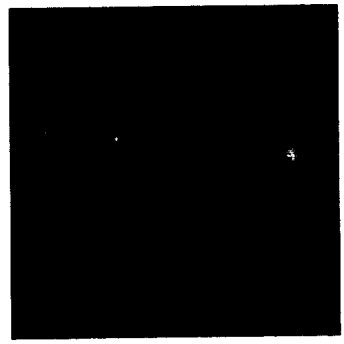
AS10-31-4634

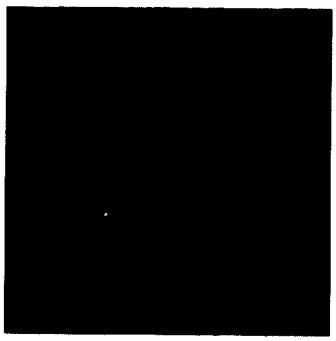
AS10-31-4635


AS10-31-4636

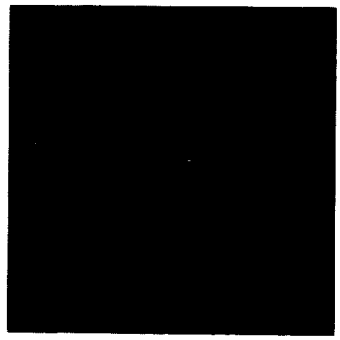
AS10-31-4637


AS10-31-4638


AS10-31-4639


AS10-31-4640

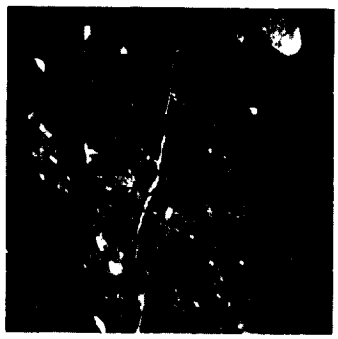
AS10-31-4641

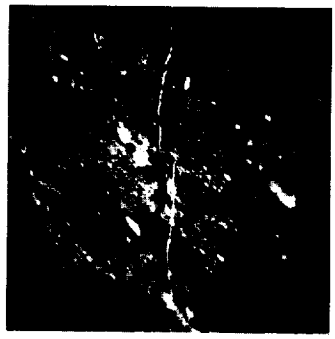
AS10-31-4642


AS10-31-4643

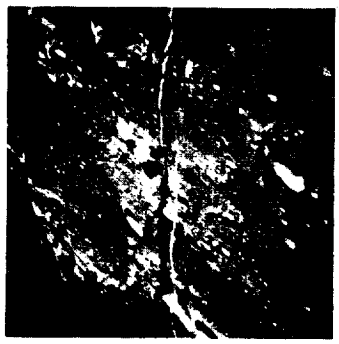
AS10-31-4644


AS10-31-4645


AS10-31-4646


AS10-31-4647


AS10-31-4648


AS10-31-4649


AS10-31-4650


AS10-31-4651


AS10-31-4652


AS10-31-4653


AS10-31-4654


AS10-31-4655


AS10-31-4656


AS10-31-4657


AS10-31-4658


AS10-31-4659


AS10-31-4660


AS10-31-4661


AS10-31-4662


AS10-31-4663


AS10-31-4664


AS10-31-4665


AS10-31-4666


AS10-31-4667

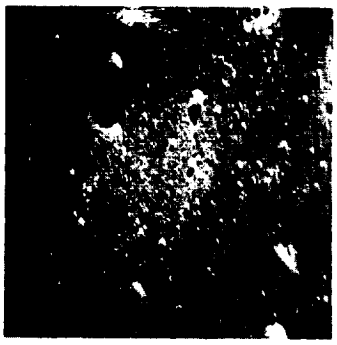
AS10-31-4668


AS10-31-4669


AS10-31-4670


AS10-31-4671


AS10-31-4672

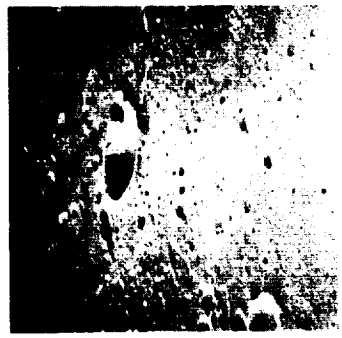
AS10-31-4673


AS10-31-4674


AS10-32-4675


AS10-32-4676


AS10-32-4677


AS10-32-4678


AS10-32-4679


AS10-32-4680


AS10-32-4681


AS10-32-4682


AS10-32-4683

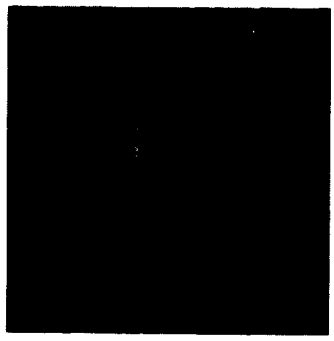
AS10-32-4684


AS10-32-4685


AS10-32-4686


AS10-32-4687


AS10-32-4688

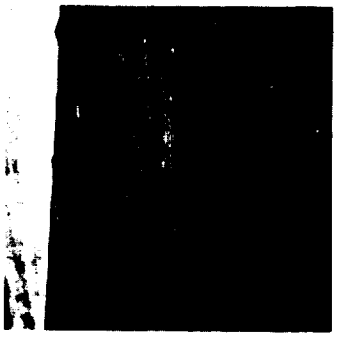
AS10-32-4689


AS10-32-4690


AS10-32-4691


AS10-32-4692


AS10-32-4693


AS10-32-4694

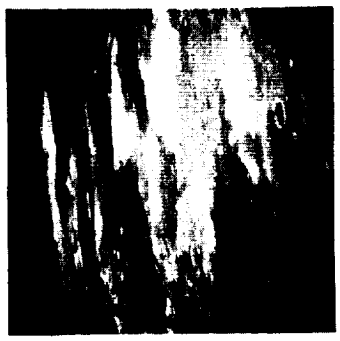
AS10-32-4695


AS10-32-4696


AS10-32-4697


AS10-32-4698


AS10-32-4699


AS10-32-4700


AS10-32-4701


AS10-32-4702


AS10-32-4703


AS10-32-4704


AS10-32-4705


AS10-32-4706


AS10-32-4707


AS10-32-4708


AS10-32-4709

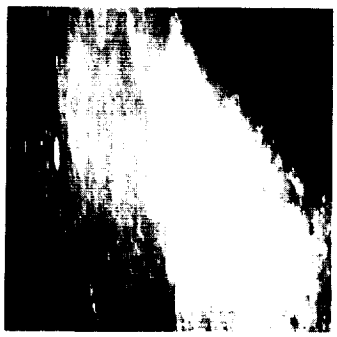
AS10-32-4710


AS10-32-4711

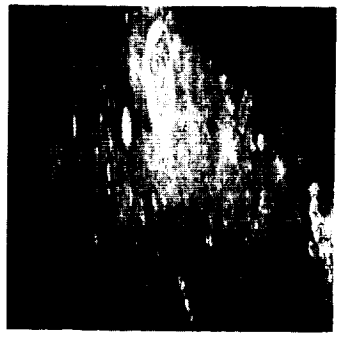
AS10-32-4712


AS10-32-4713


AS10-32-4714


AS10-32-4715

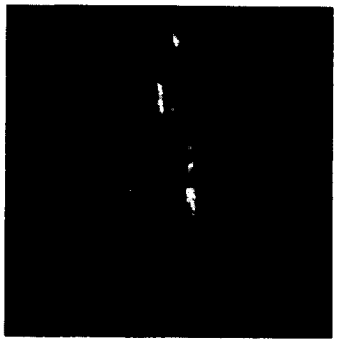
AS10-32-4716

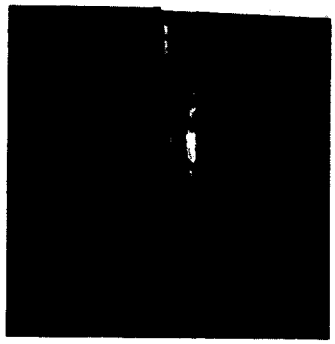
AS10-32-4717


AS10-32-4718

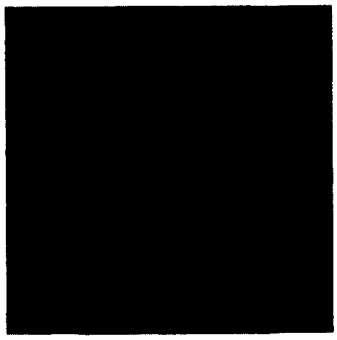
AS10-32-4719

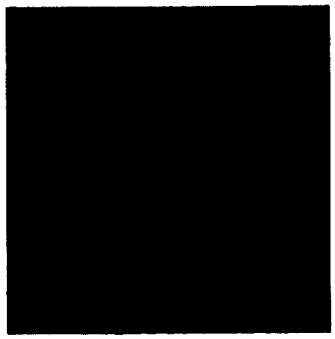
AS10-32-4720

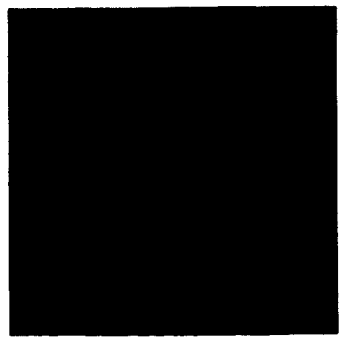
AS10-32-4721

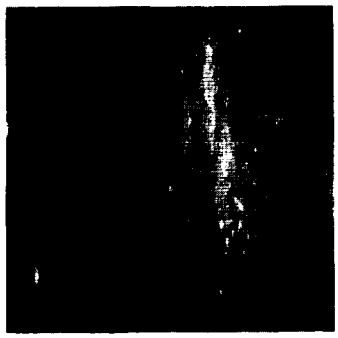
AS10-32-4722

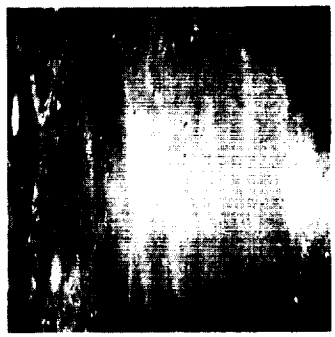
AS10-32-4723


AS10-32-4724


AS10-32-4725

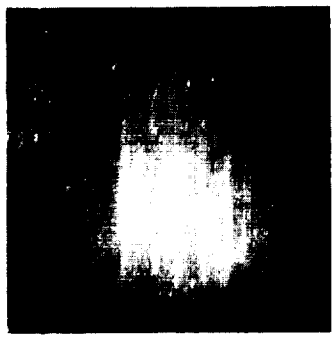
AS10-32-4726

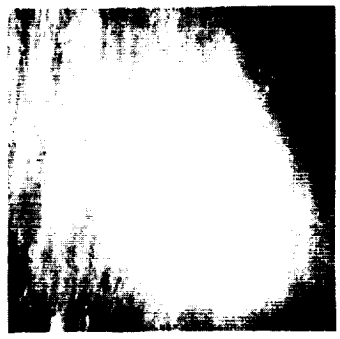
AS10-32-4727


AS10-32-4728

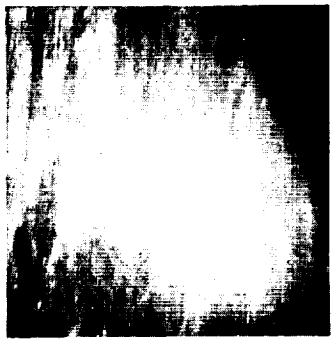
AS10-32-4729


AS10-32-4730

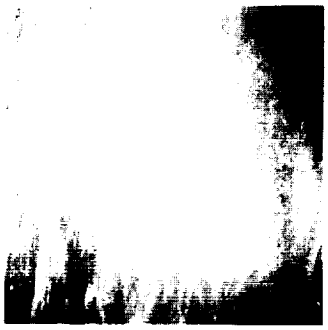
AS10-32-4731


AS10-32-4732


AS10-32-4733


AS10-32-4734

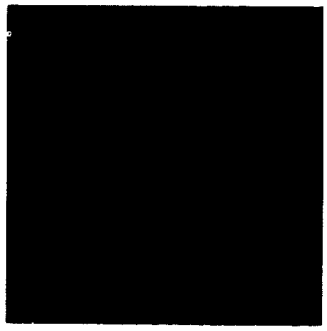
AS10-32-4735


AS10-32-4736


AS10-32-4737

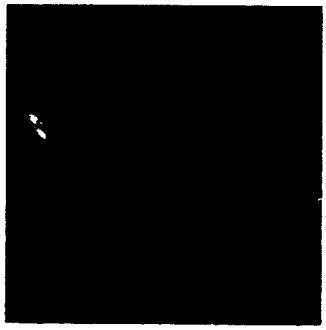
AS10-32-4738


AS10-32-4739

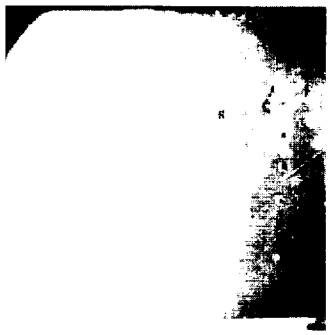
AS10-32-4740


AS10-32-4741

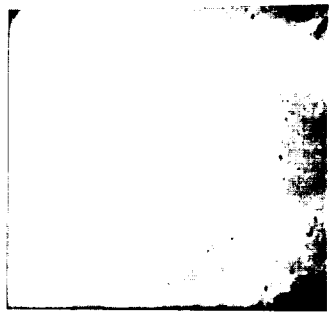
AS10-32-4742


AS10-32-4743

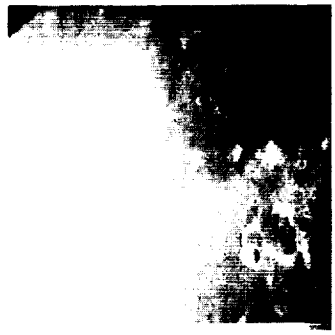
AS10-32-4744


AS10-32-4745


AS10-32-4746


AS10-32-4747


AS10-32-4748


AS10-32-4749

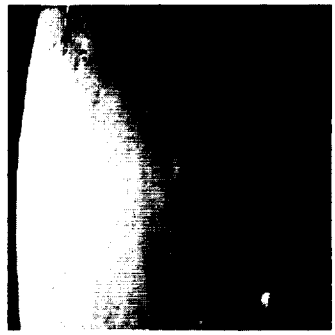
AS10-32-4750


AS10-32-4751

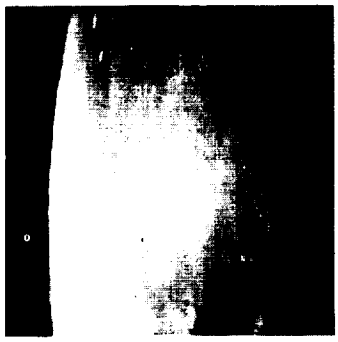
AS10-32-4752

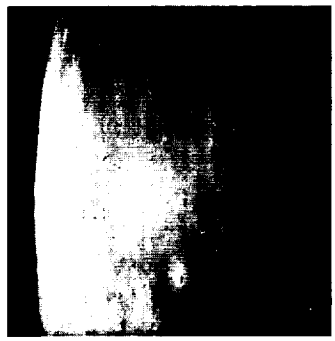
AS10-32-4753

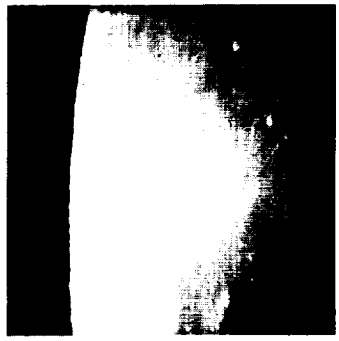
AS10-32-4754

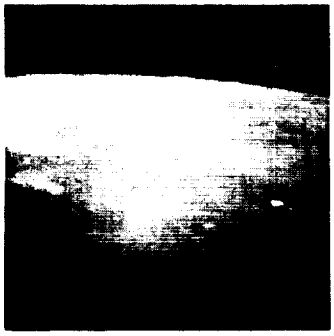
AS10-32-4755

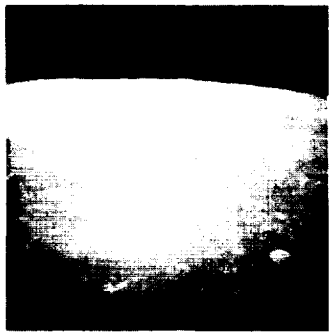
AS10-32-4756

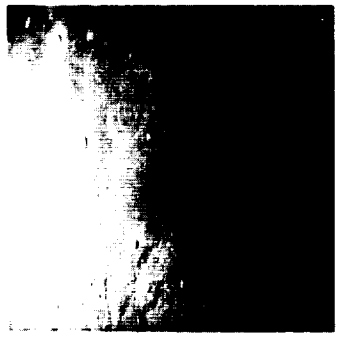
AS10-32-4757


AS10-32-4758

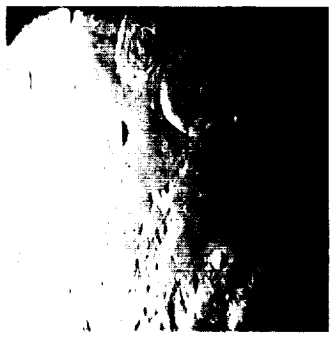
AS10-32-4759


AS10-32-4760

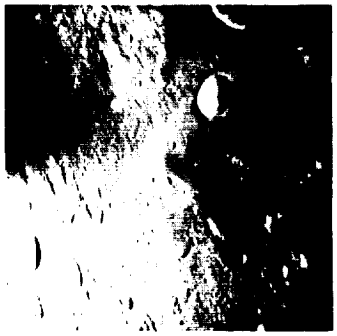
AS10-32-4761

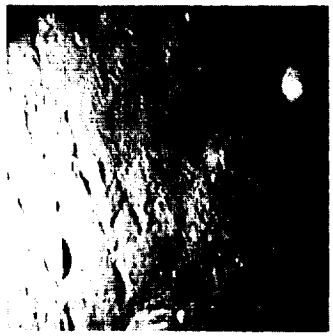
AS10-32-4762

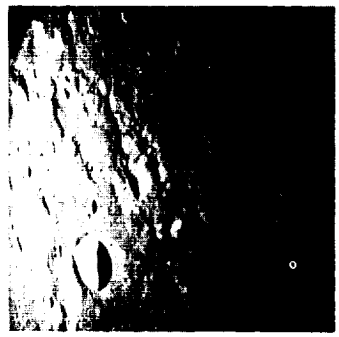
AS10-32-4763

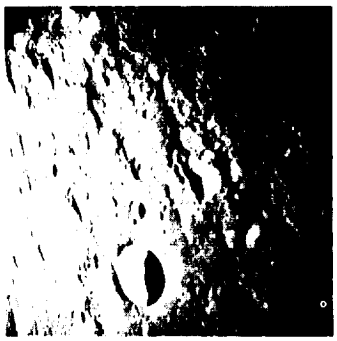
AS10-32-4764

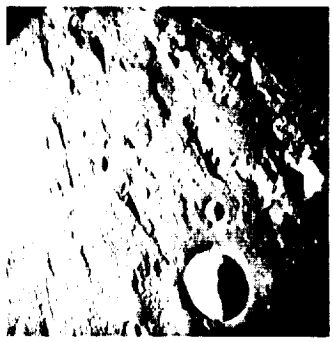
AS10-32-4765

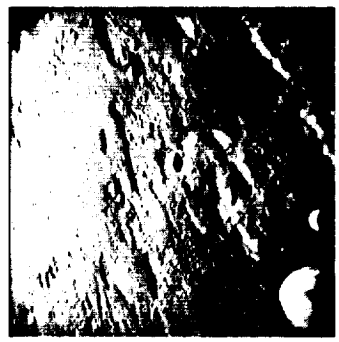
AS10-32-4766

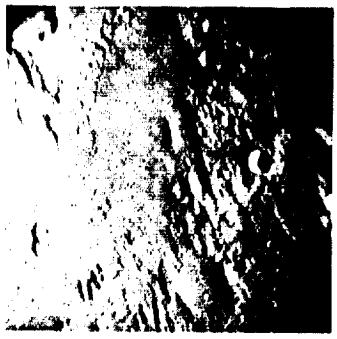
AS10-32-4767

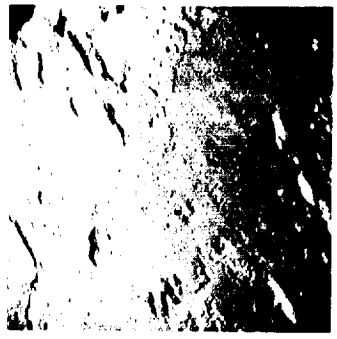
AS10-32-4768


AS10-32-4769

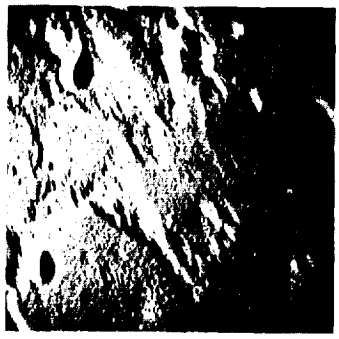
AS10-32-4770

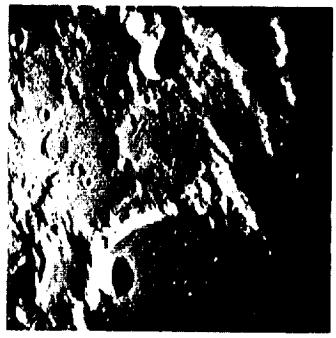
AS10-32-4771

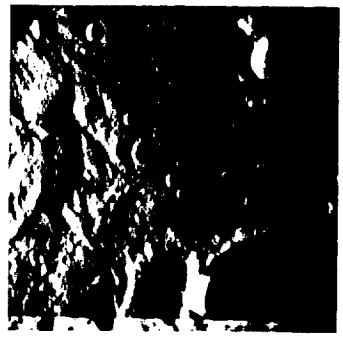
AS10-32-4772

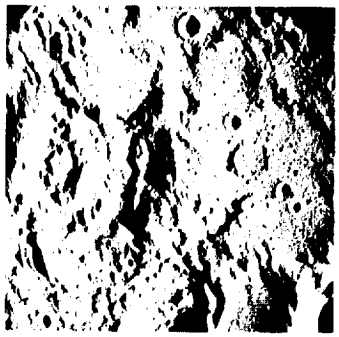
AS10-32-4773


AS10-32-4774


AS10-32-4775

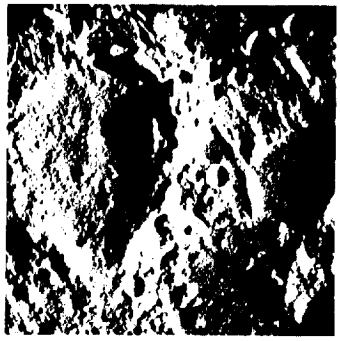
AS10-32-4776

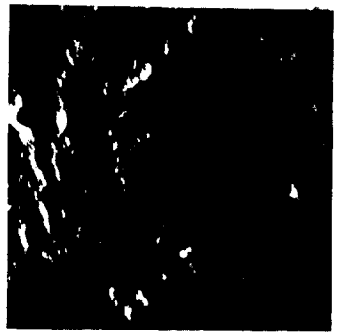
AS10-32-4777


AS10-32-4778


AS10-32-4779


AS10-32-4780


AS10-32-4781


AS10-32-4782


AS10-32-4783


AS10-32-4784


AS10-32-4785

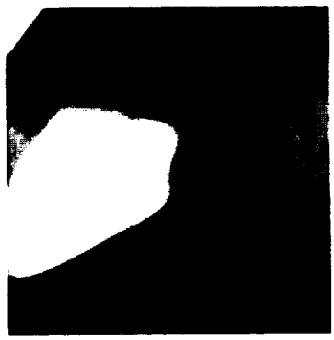
AS10-32-4786

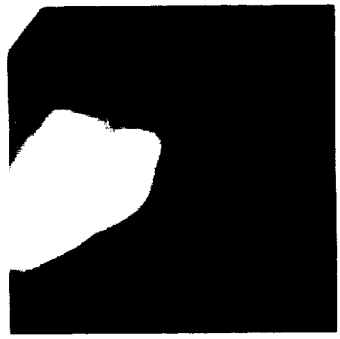
AS10-32-4787

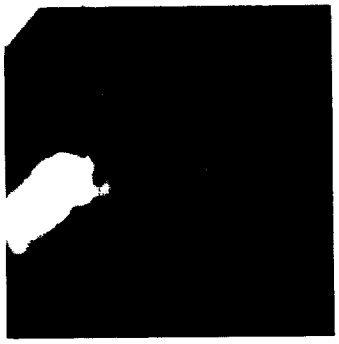
AS10-32-4788

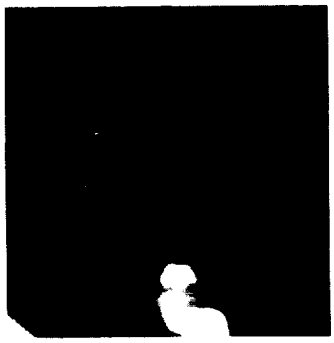
AS10-32-4789


AS10-32-4790


AS10-32-4791


AS10-32-4792

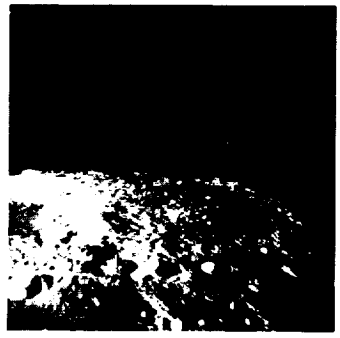
AS10-32-4793


AS10-32-4794

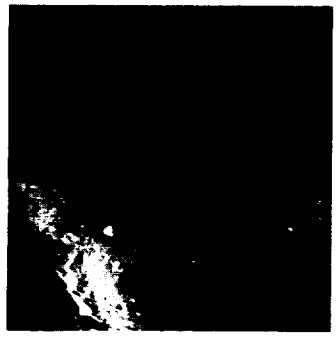
AS10-32-4795


AS10-32-4796

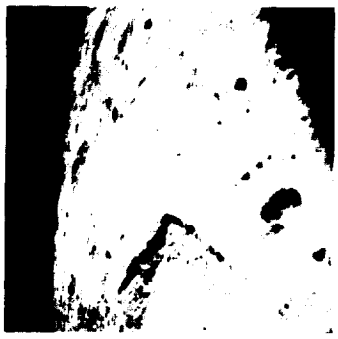
AS10-32-4797


AS10-32-4798

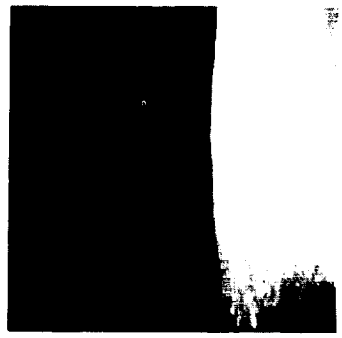
AS10-32-4799


AS10-32-4800


AS10-32-4801

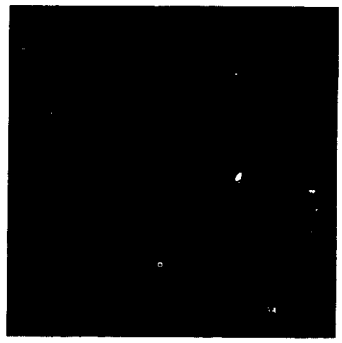
AS10-32-4802

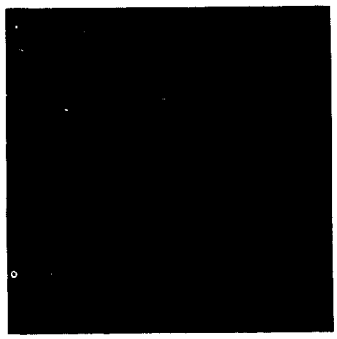
AS10-32-4803

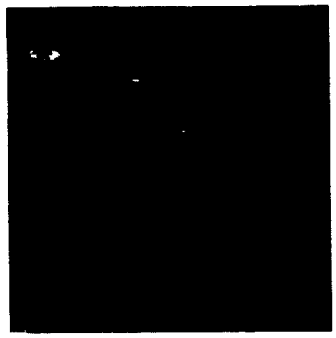
AS10-32-4804

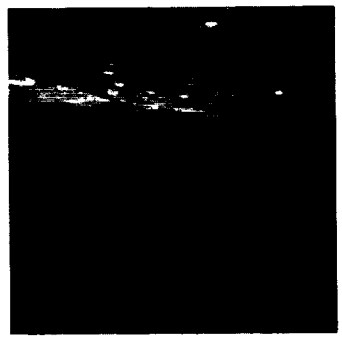
AS10-32-4805

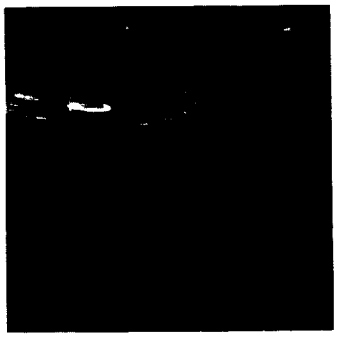
AS10-32-4806


AS10-32-4807


AS10-32-4808


AS10-32-4809

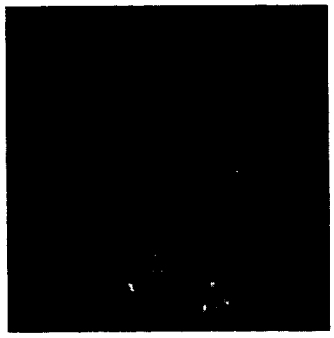
AS10-32-4810

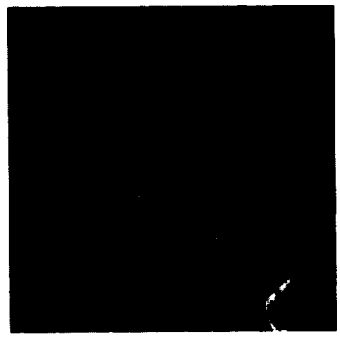
AS10-32-4811

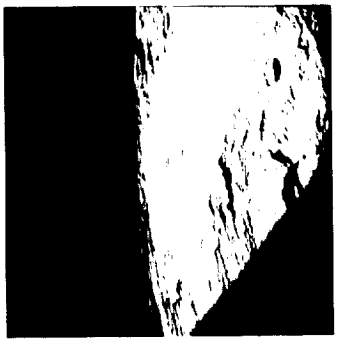
AS10-32-4812


AS10-32-4813

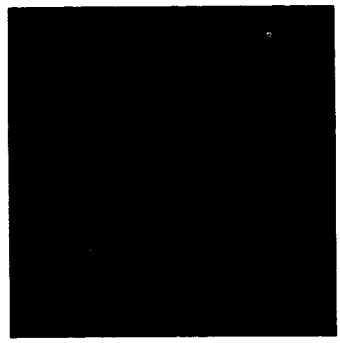
AS10-32-4814

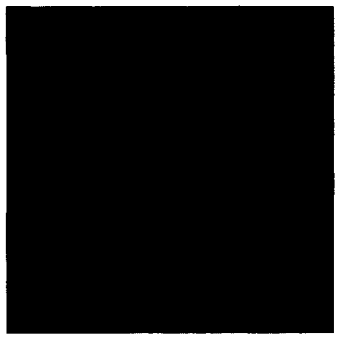
AS10-32-4815


AS10-32-4816

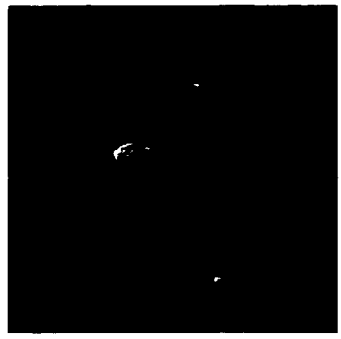
AS10-32-4817


AS10-32-4818


AS10-32-4819


AS10-32-4820


AS10-32-4821

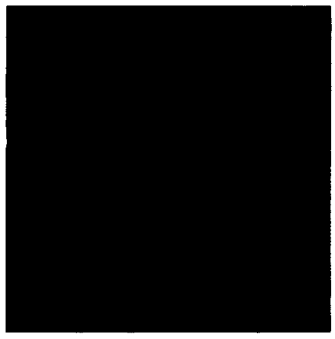
AS10-32-4822


AS10-32-4823


AS10-32-4824


AS10-32-4825

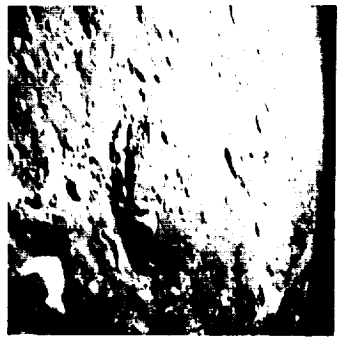
AS10-32-4826

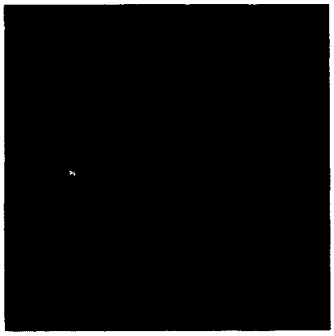
AS10-32-4827

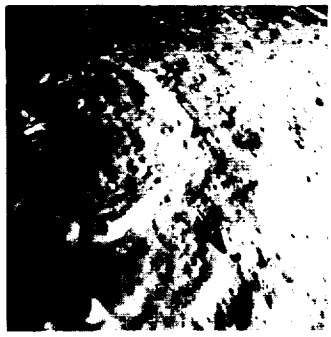
AS10-32-4828

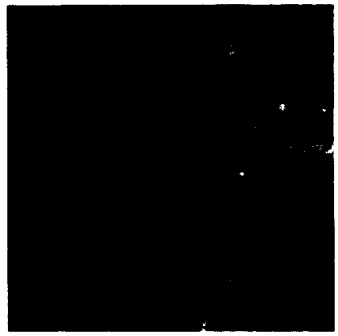
AS10-32-4829

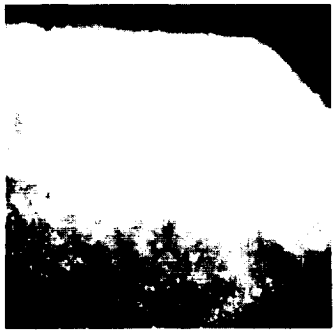
AS10-32-4830


AS10-32-4831


AS10-32-4832

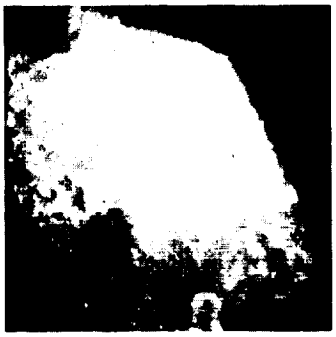
AS10-32-4833

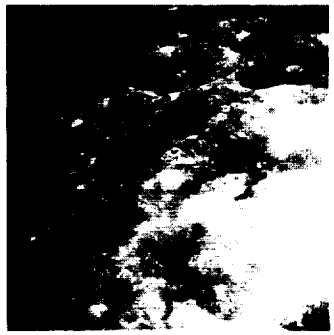
AS10-32-4834

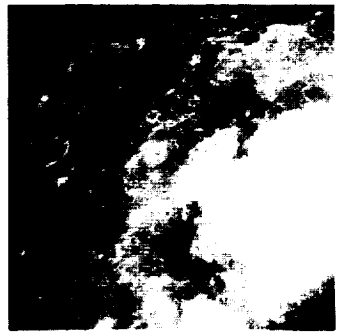
AS10-32-4835

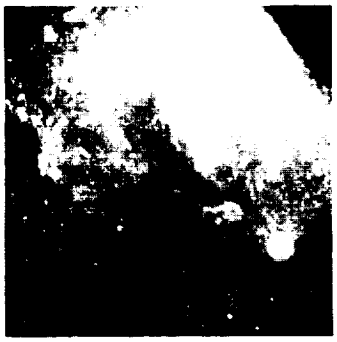
AS10-32-4836

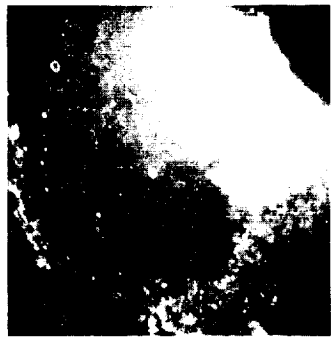
AS10-32-4837

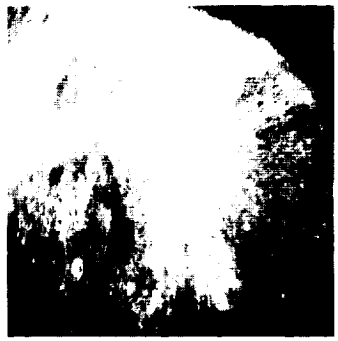
AS10-32-4838

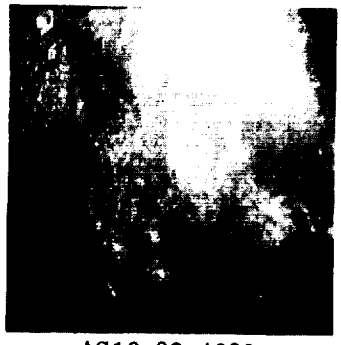
AS10-32-4839

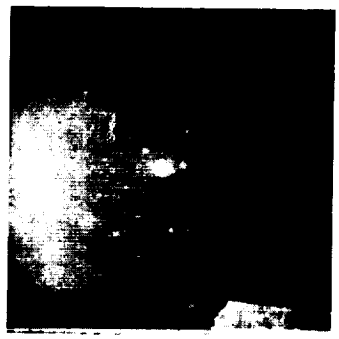
AS10-32-4840


AS10-32-4841


AS10-32-4842


AS10-32-4843


AS10-32-4844

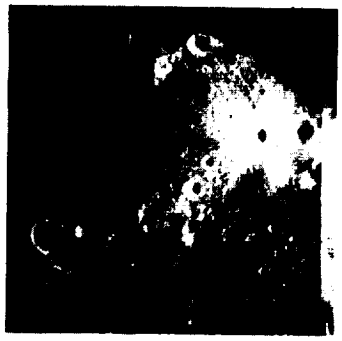
AS10-32-4845

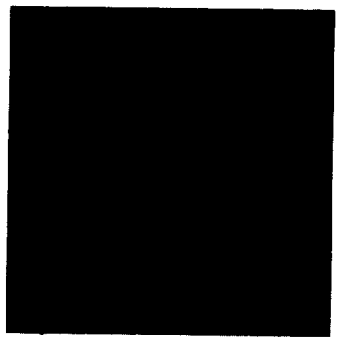
AS10-32-4846


AS10-32-4847


AS10-32-4848

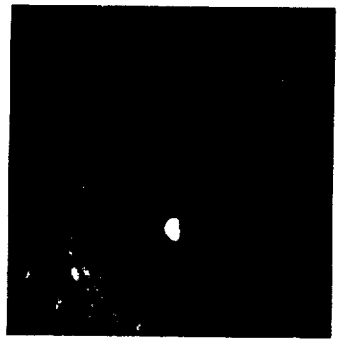
AS10-32-4849

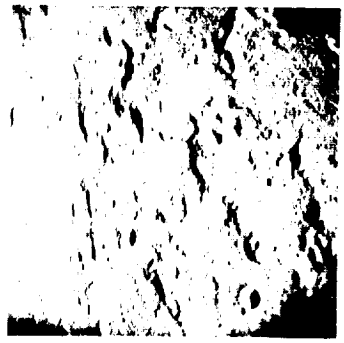
AS10-32-4850

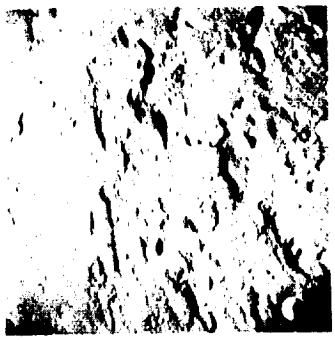
AS10-32-4851

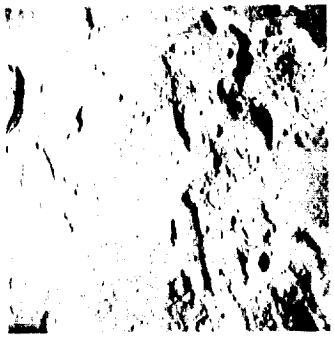
AS10-32-4852

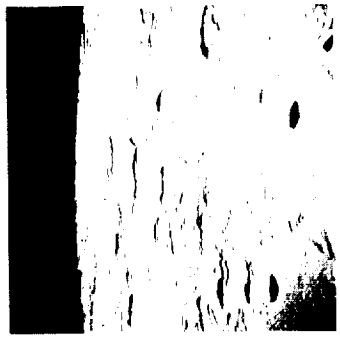
AS10-32-4853

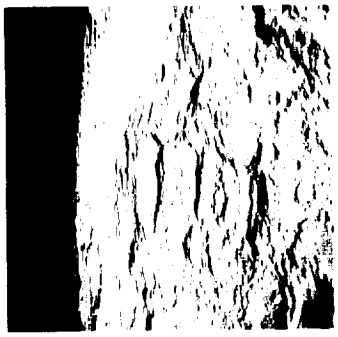
AS10-32-4854

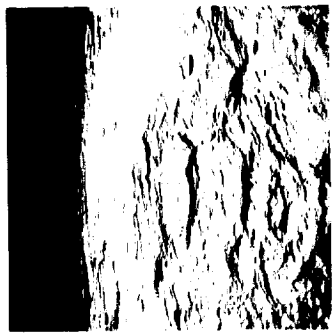
AS10-32-4855


AS10-32-4856


AS10-33-4857


AS10-33-4858


AS10-33-4859


AS10-33-4860

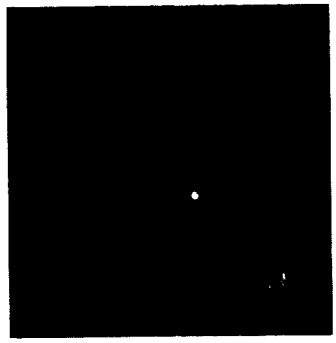
AS10-33-4861

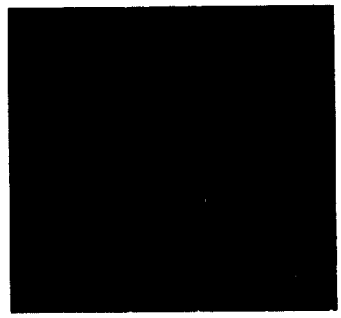
AS10-33-4862

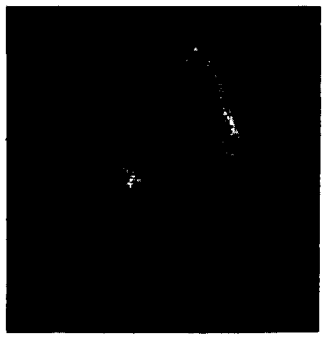
AS10-33-4863

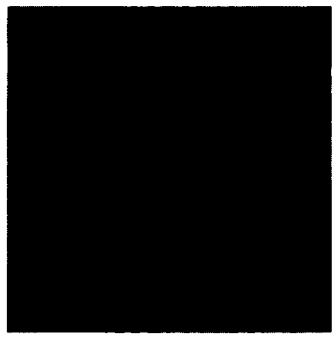
AS10-33-4864


AS10-33-4865


AS10-33-4866

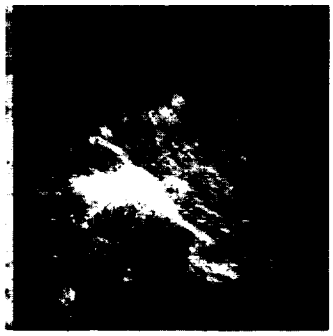
AS10-33-4867

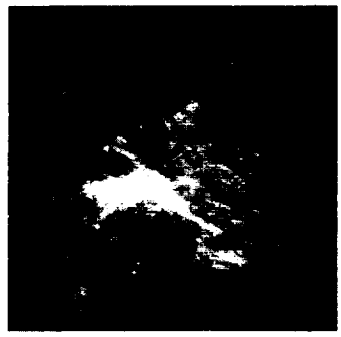
AS10-33-4868

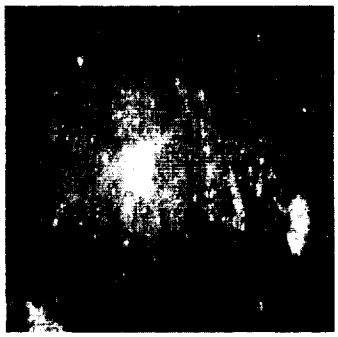
AS10-33-4869


AS10-33-4870


AS10-33-4871


AS10-33-4872


AS10-33-4873


AS10-33-4874


AS10-33-4875

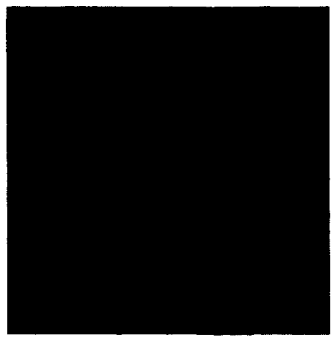
AS10-33-4876

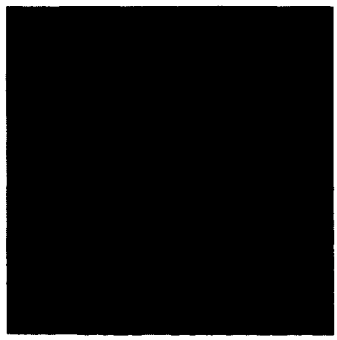
AS10-33-4877

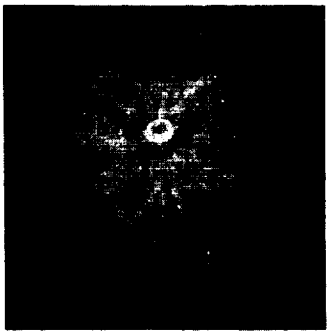
AS10-33-4878


AS10-33-4879

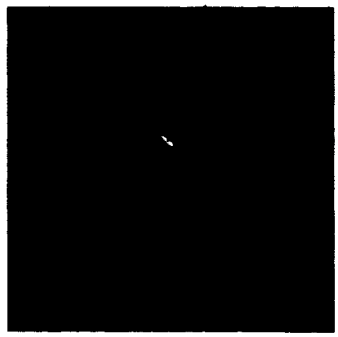
AS10-33-4880

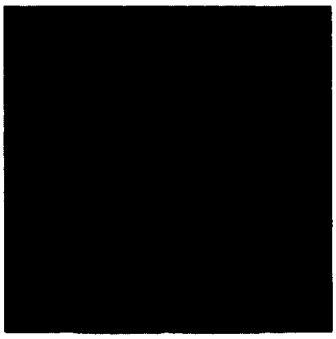
AS10-33-4881


AS10-33-4882


AS10-33-4883

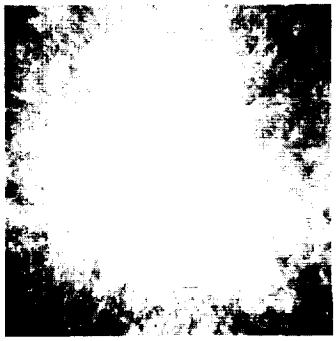
AS10-33-4884

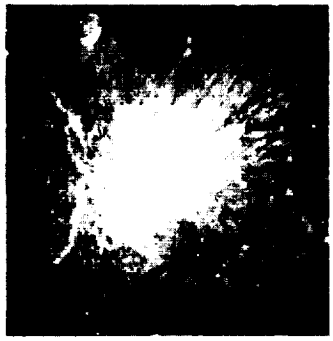
AS10-33-4885


AS10-33-4886

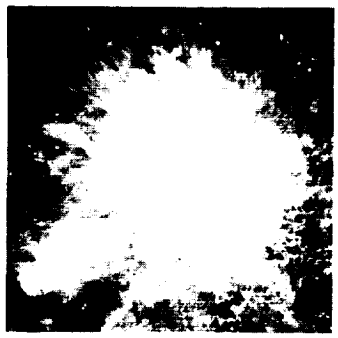
AS10-33-4887

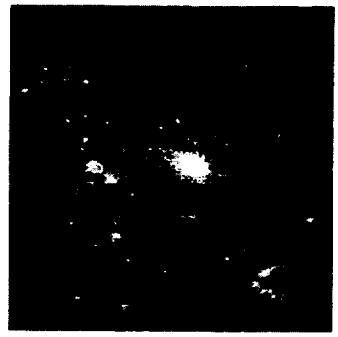
AS10-33-4888

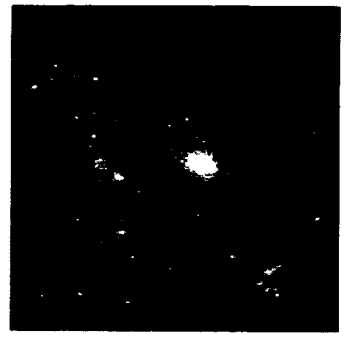
AS10-33-4889

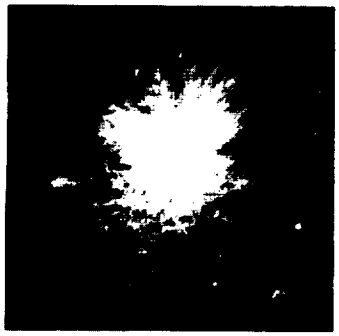
AS10-33-4890


AS10-33-4891

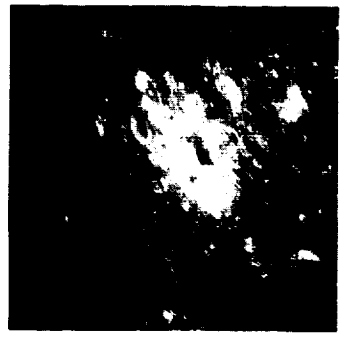
AS10-33-4892


AS10-33-4893

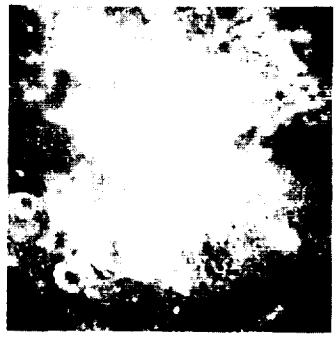
AS10-33-4894

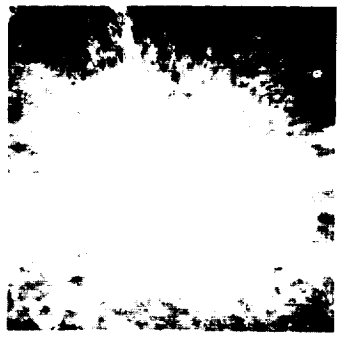
AS10-33-4895

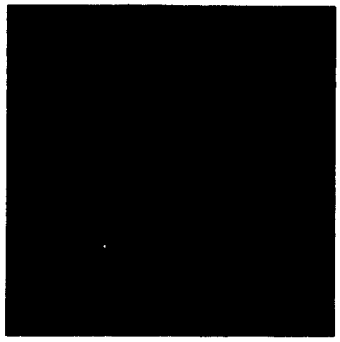
AS10-33-4896

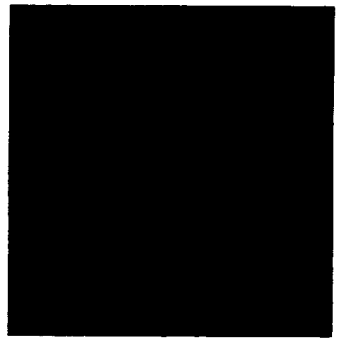
AS10-33-4897

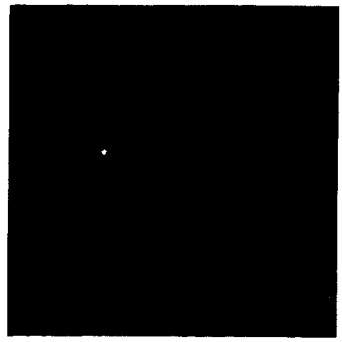
AS10-33-4898

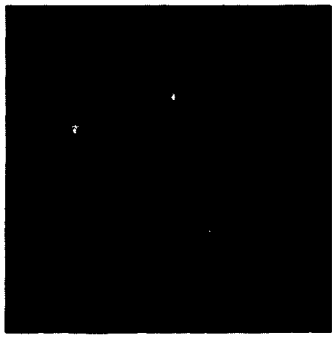
AS10-33-4899

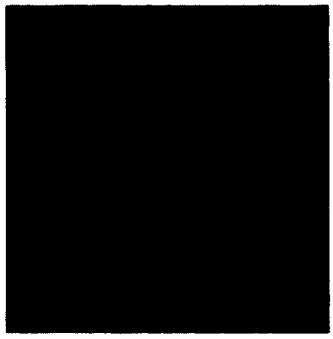
AS10-33-4900

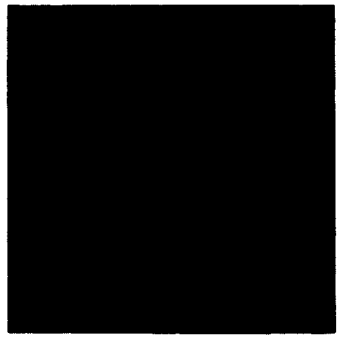
AS10-33-4901

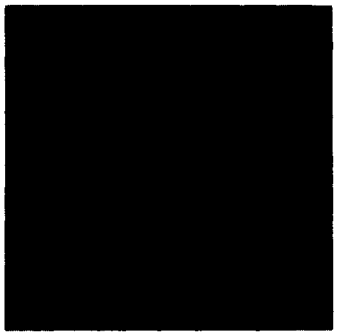
AS10-33-4902

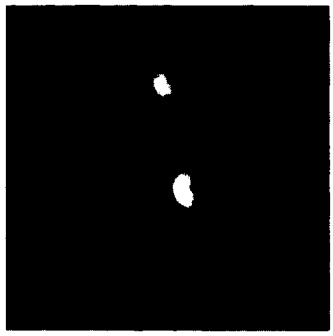
AS10-33-4903

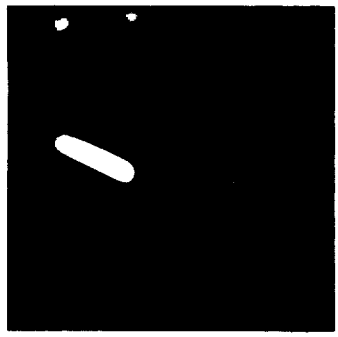
AS10-33-4904

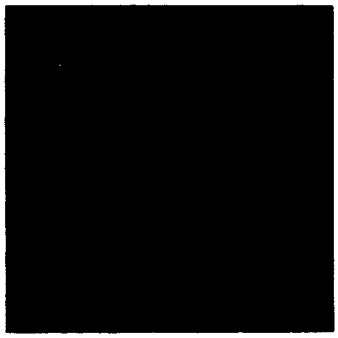
AS10-33-4905

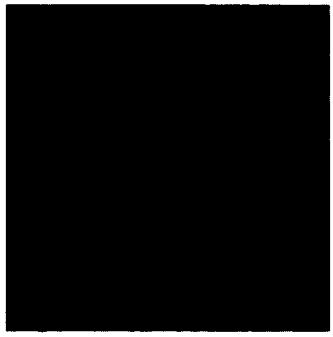
AS10-33-4906


AS10-33-4907

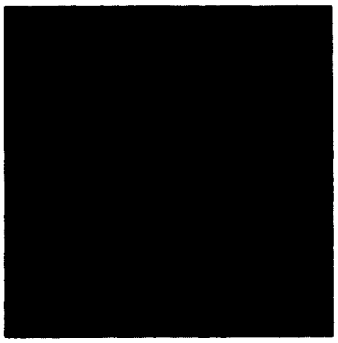
AS10-33-4908

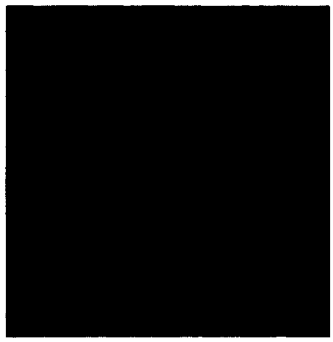
AS10-33-4909

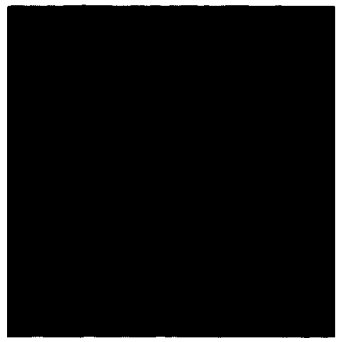
AS10-33-4910

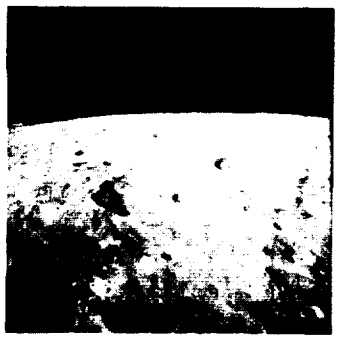
AS10-33-4911

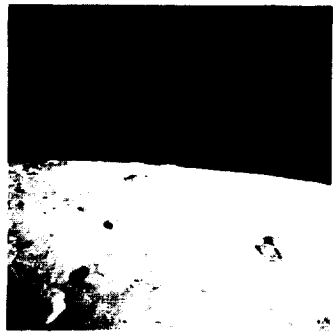
AS10-33-4912

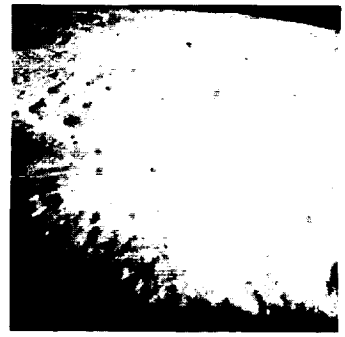
AS10-33-4913


AS10-33-4914

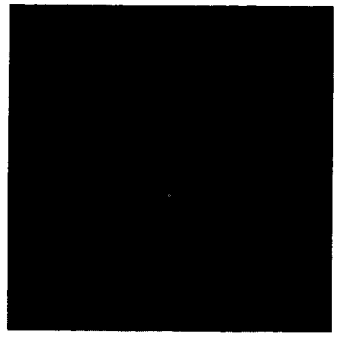
AS10-33-4915

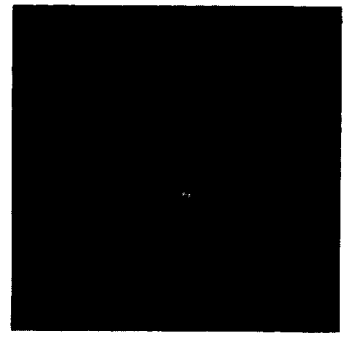
AS10-33-4916

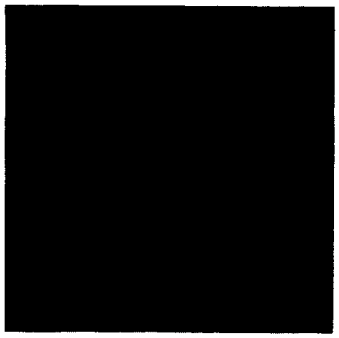
AS10-33-4917

AS10-33-4918

AS10-33-4919

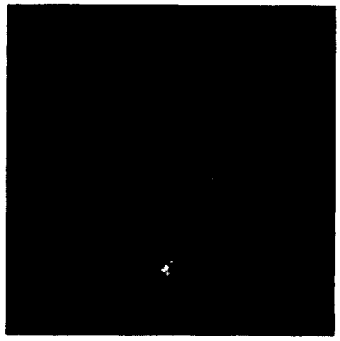
AS10-33-4920


AS10-33-4921


AS10-33-4922


AS10-33-4923


AS10-33-4924


AS10-33-4925


AS10-33-4926


AS10-33-4927


AS10-33-4928


AS10-33-4929


AS10-33-4930


AS10-33-4931


AS10-33-4932

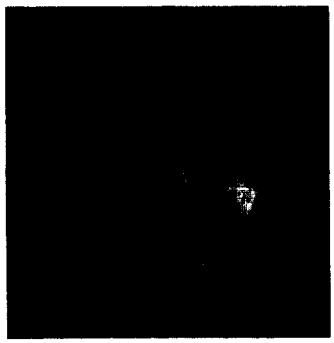
AS10-33-4933


AS10-33-4934


AS10-33-4935


AS10-33-4936

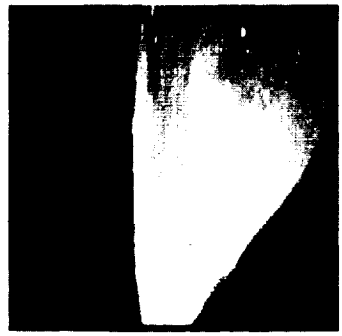
AS10-33-4937


AS10-33-4938


AS10-33-4939

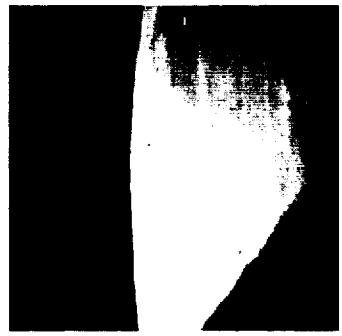
AS10-33-4940

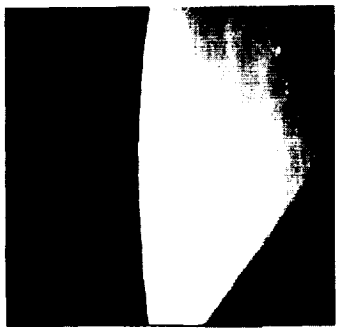
AS10-33-4941


AS10-33-4942


AS10-33-4943


AS10-33-4944


AS10-33-4945

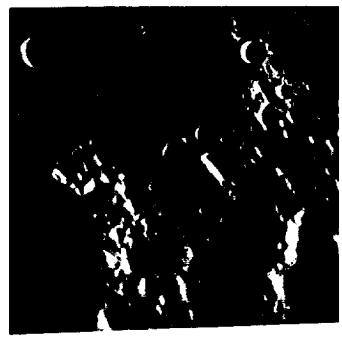
AS10-33-4946

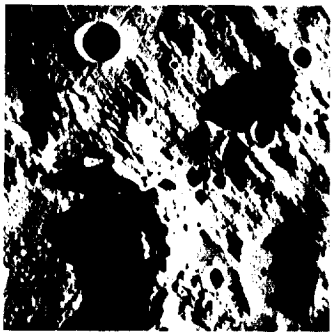
AS10-33-4947


AS10-33-4948


AS10-33-4949

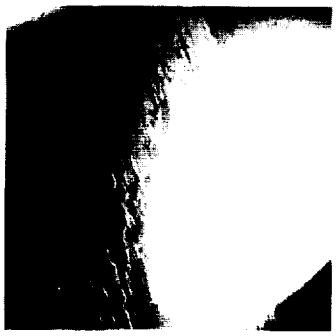
AS10-33-4950

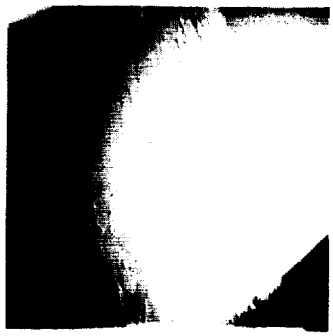
AS10-33-4951

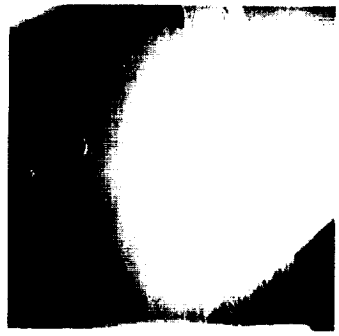
AS10-33-4952

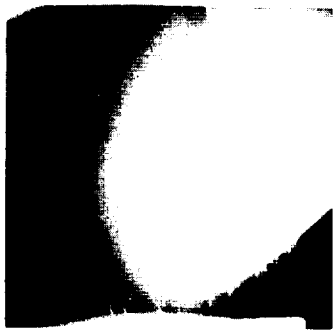
AS10-33-4953


AS10-33-4954


AS10-33-4955


AS10-33-4956


AS10-33-4957

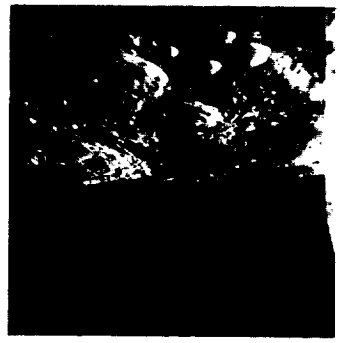
AS10-33-4958


AS10-33-4959

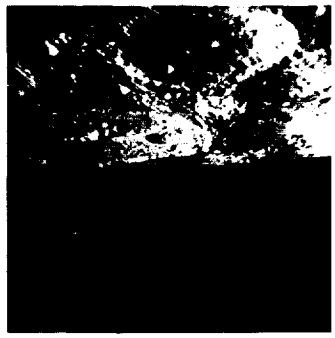
AS10-33-4960

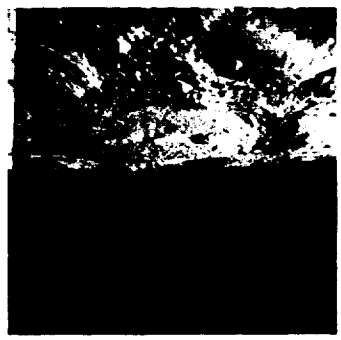
AS10-33-4961

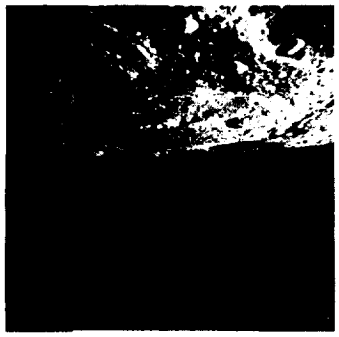
AS10-33-4962


AS10-33-4963

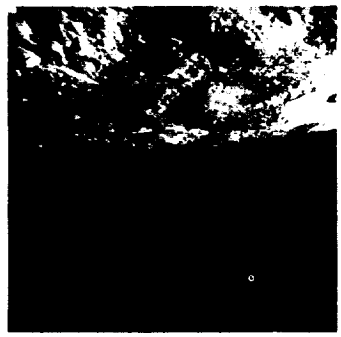
AS10-33-4964

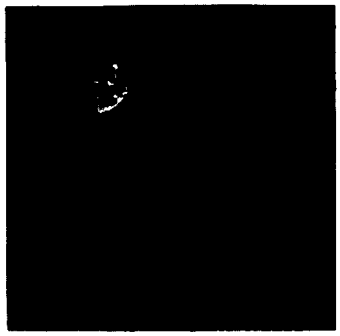
AS10-33-4965

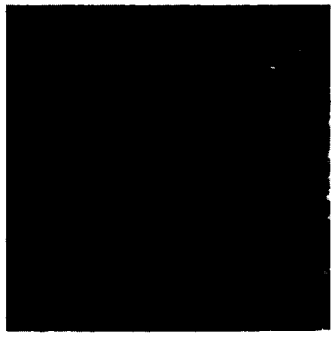
AS10-33-4966

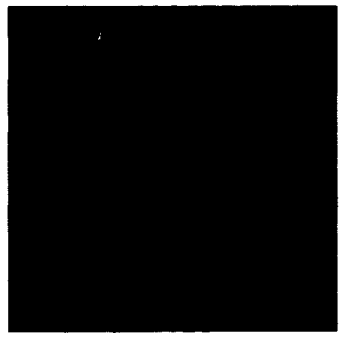
AS10-33-4967

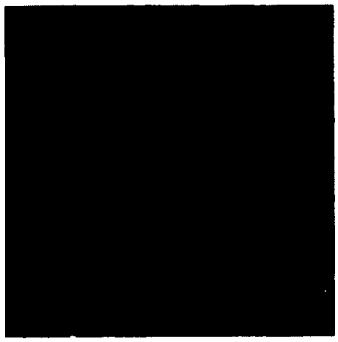
AS10-33-4968

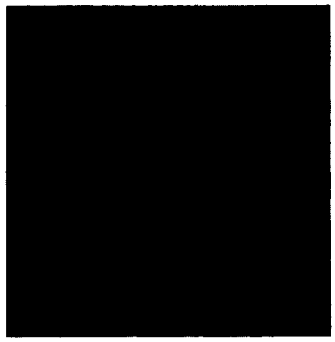
AS10-33-4969

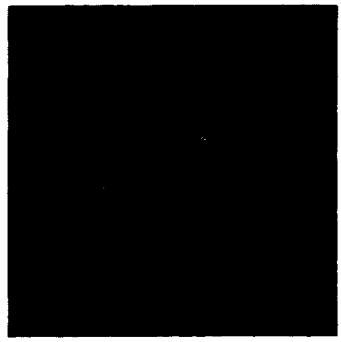
AS10-33-4970

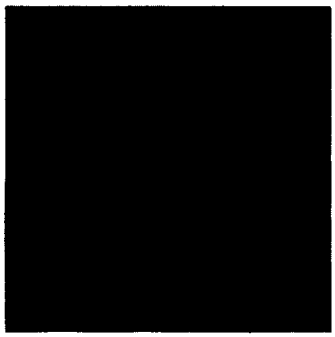
AS10-33-4971

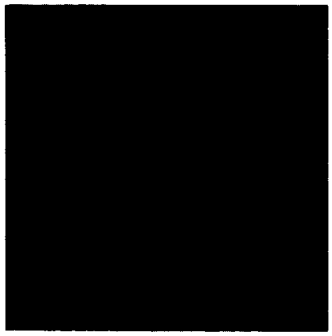
AS10-33-4972

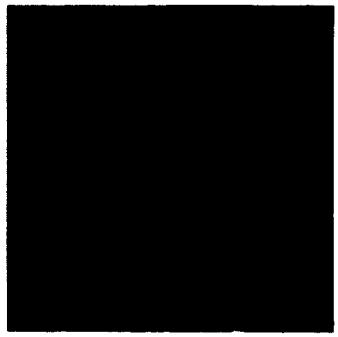
AS10-33-4973


AS10-33-4974


AS10-33-4975


AS10-33-4976


AS10-33-4977

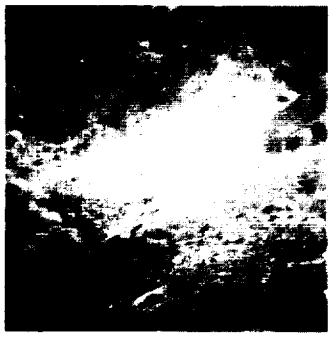
AS10-33-4978


AS10-33-4979

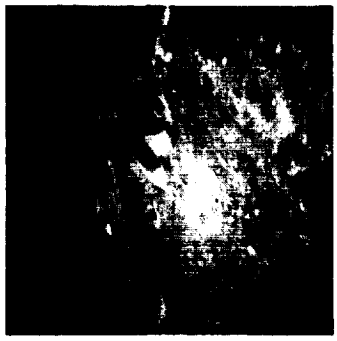
AS10-33-4980


AS10-33-4981


AS10-33-4982

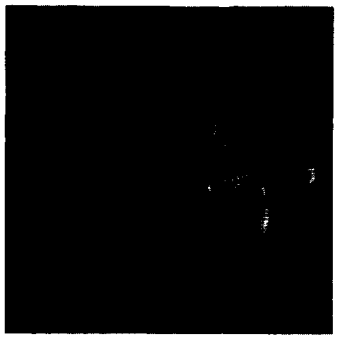
AS10-33-4983


AS10-33-4984

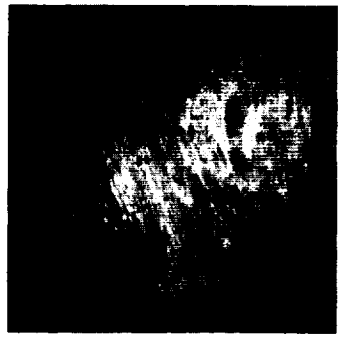
AS10-33-4985

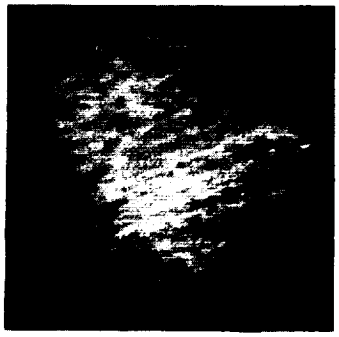
AS10-33-4986

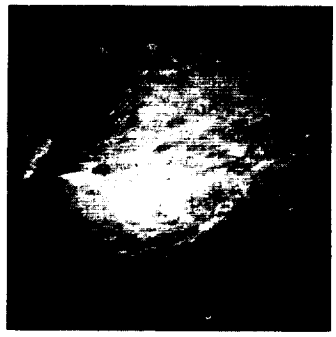
AS10-33-4987


AS10-33-4988


AS10-33-4989

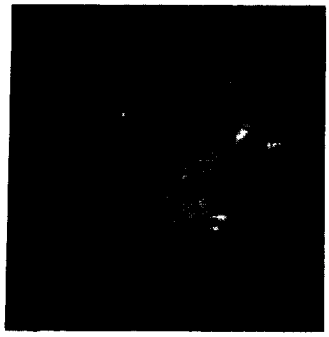
AS10-33-4990

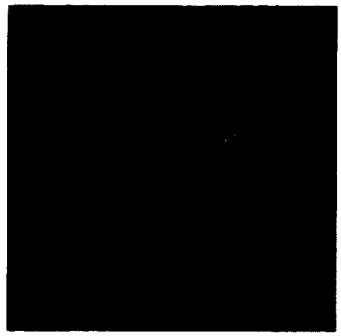
AS10-33-4991

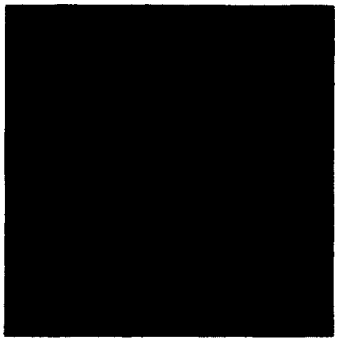
AS10-33-4992

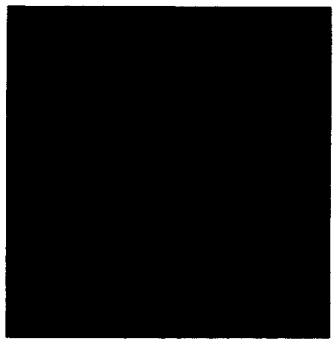
AS10-33-4993

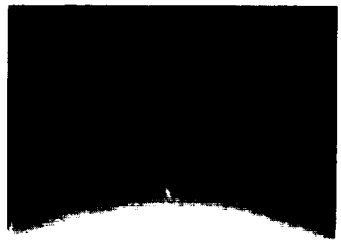
AS10-33-4994

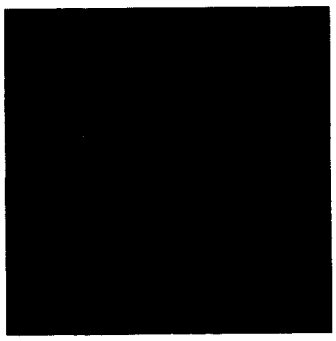
AS10-33-4995

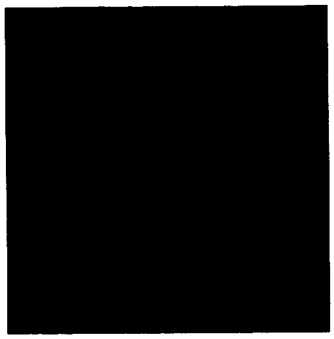
AS10-33-4996


AS10-33-4997

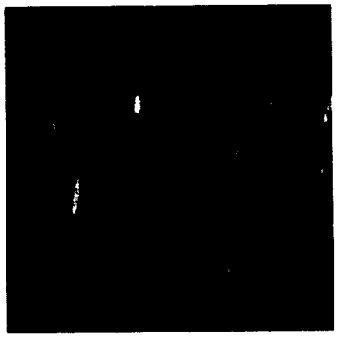
AS10-33-4998

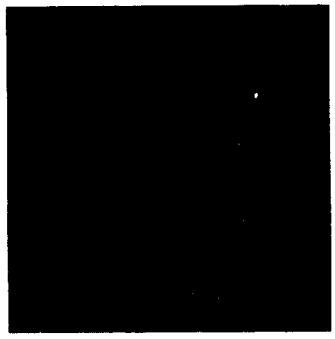
AS10-33-4999


AS10-33-5000


AS10-33-5001

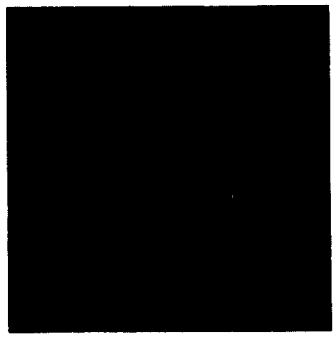
AS10-33-5002

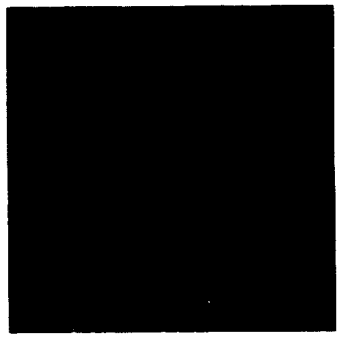
AS10-33-5003

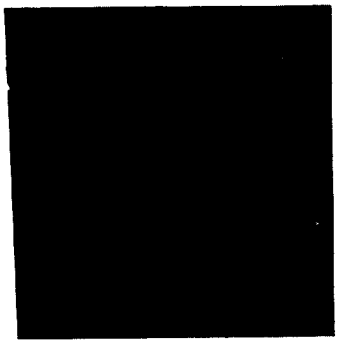
AS10-33-5004


AS10-33-5005


AS10-33-5006

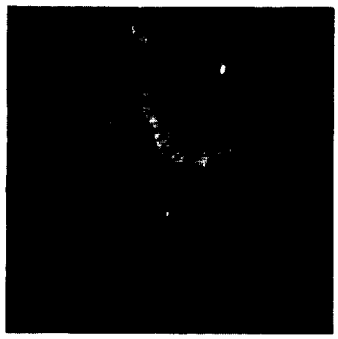

AS10-33-5007

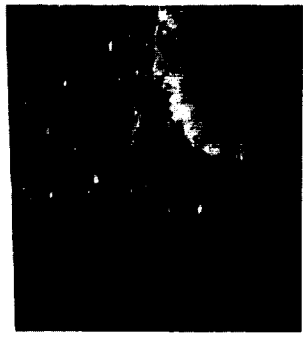

AS10-33-5008

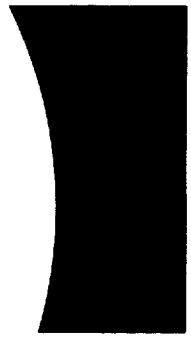

AS10-34-5009

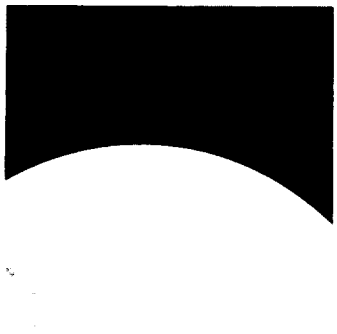

AS10-34-5010

AS10-34-5011

AS10-34-5012

AS10-34-5013

AS10-34-5014

AS10-34-5015

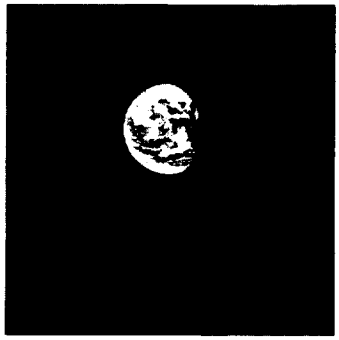

AS10-34-5016

AS10-34-5017

AS10-34-5018

(Available in color.)

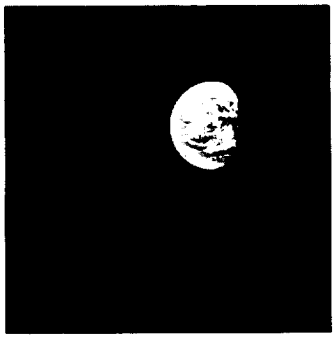

AS10-34-5019

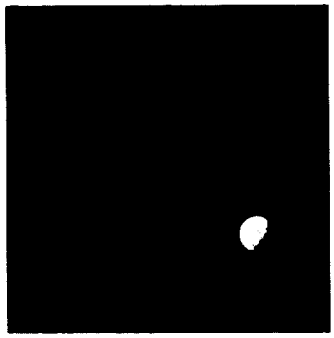

AS10-34-5020

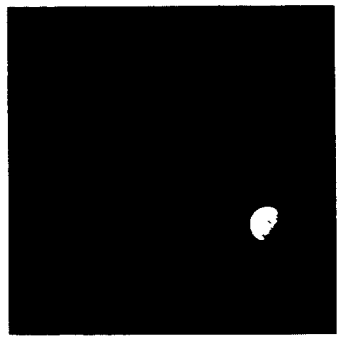

AS10-34-5021

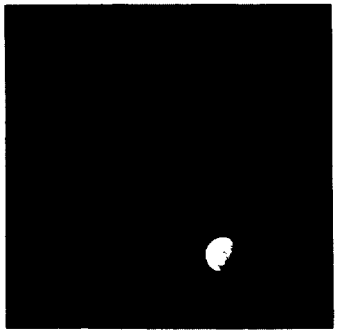

AS10-34-5022

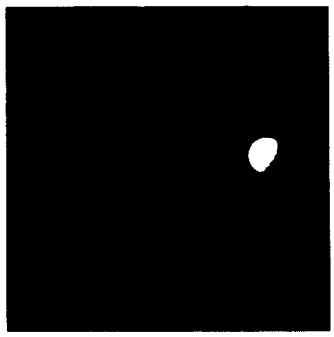

AS10-34-5023

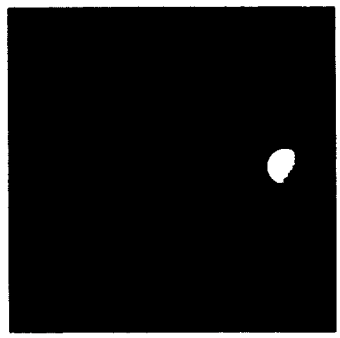

AS10-34-5024

AS10-34-5026

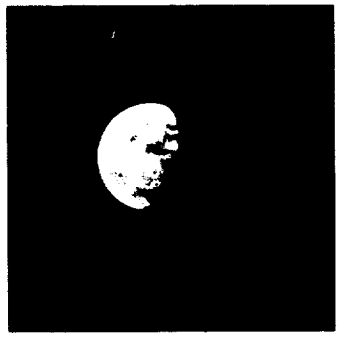

AS10-34-5027

AS10-34-5025

AS10-34-5028

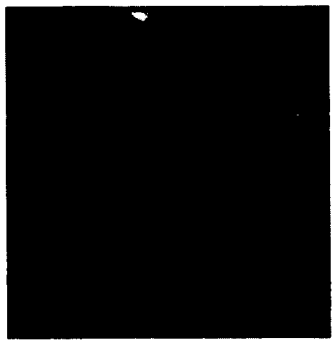

AS10-34-5029

AS10-34-5030

(Available in color.)


AS10-34-5031


AS10-34-5032


AS10-34-5033

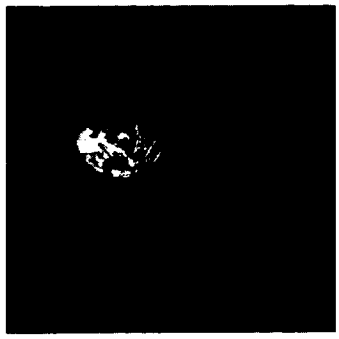
AS10-34-5034


AS10-34-5035

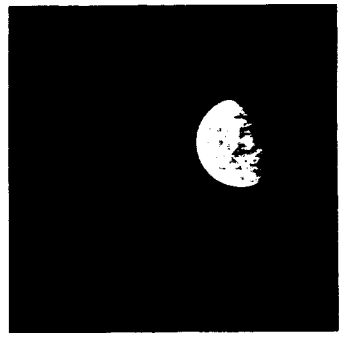
AS10-34-5036

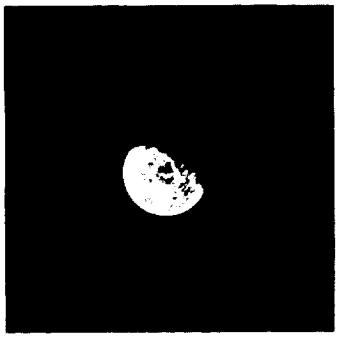
AS10-34-5037


AS10-34-5038


AS10-34-5039


AS10-34-5040

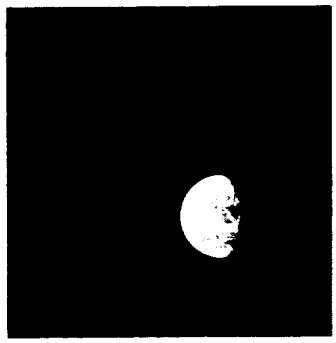
AS10-34-5041


AS10-34-5042

(Available in color.)

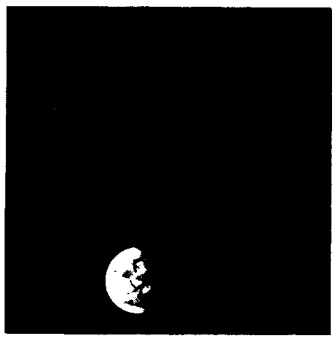
AS10-34-5043

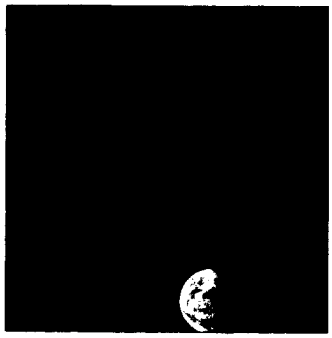
AS10-34-5044

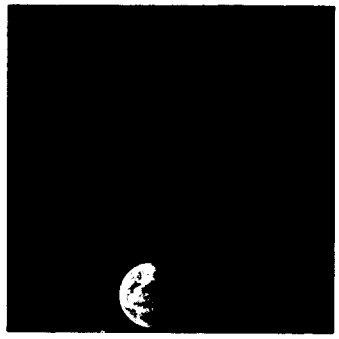
AS10-34-5045

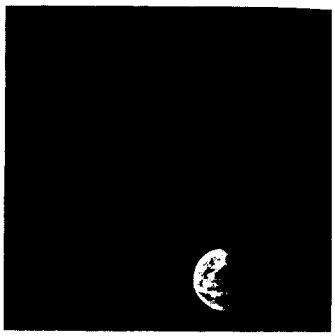
AS10-34-5046

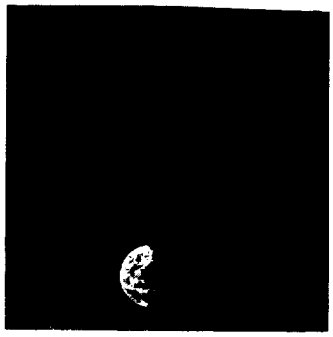
AS10-34-5047

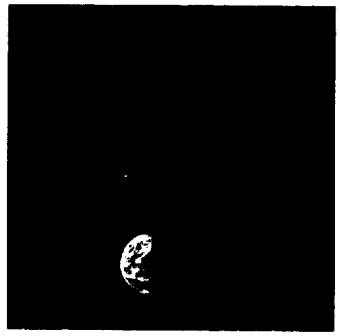
AS10-34-5048


AS10-34-5049


AS10-34-5050


AS10-34-5051


AS10-34-5052


AS10-34-5053

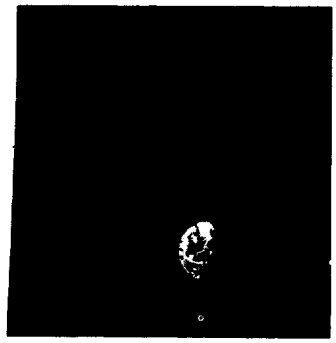
AS10-34-5054

(Available in color.)

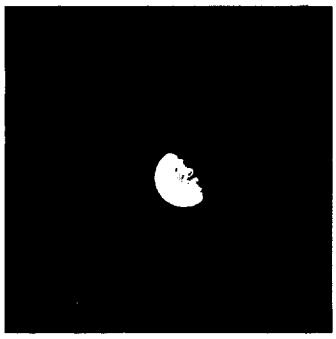
AS10-34-5055


AS10-34-5056


AS10-34-5057


AS10-34-5058

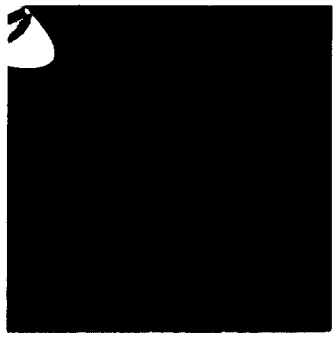
AS10-34-5059


AS10-34-5060


AS10-34-5061


AS10-34-5062


AS10-34-5063


AS10-34-5064


AS10-34-5065


AS10-34-5066

(Available in color.)


AS10-34-5067


AS10-34-5068


AS10-34-5069


AS10-34-5070


AS10-34-5071

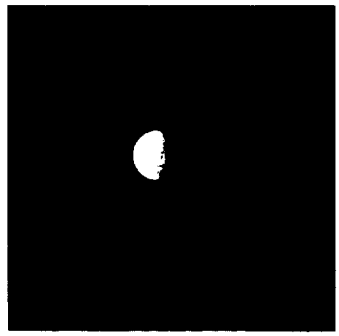
AS10-34-5072


AS10-34-5073

AS10-34-5074

AS10-34-5075

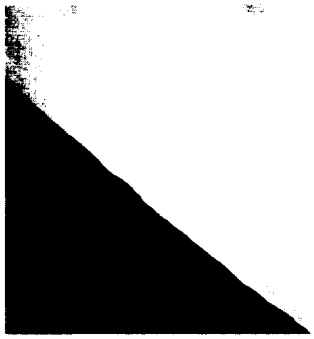
AS10-34-5076


AS10-34-5077

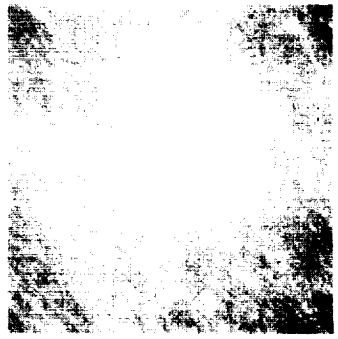
AS10-34-5078

(Available in color.)

AS10-34-5079

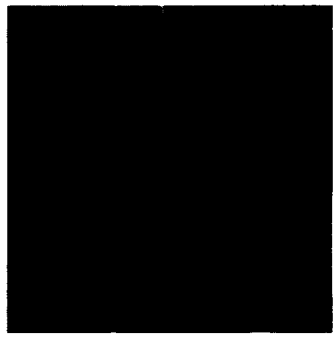

AS10-34-5080

AS10-34-5081

AS10-34-5082

AS10-34-5083

AS10-34-5084

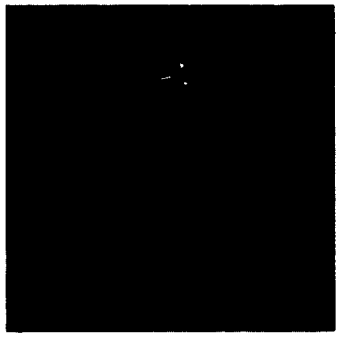

AS10-34-5085

AS10-34-5086

AS10-34-5087

AS10-34-5088

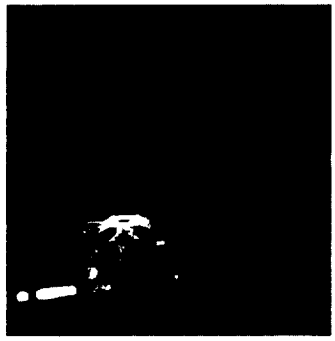

AS10-34-5089

AS10-34-5090

(Available in color.)


AS10-34-5091


AS10-34-5092

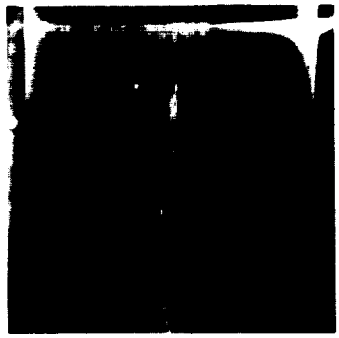
AS10-34-5093

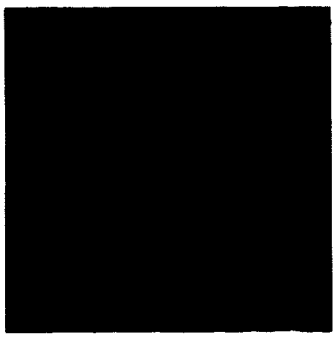
AS10-34-5094

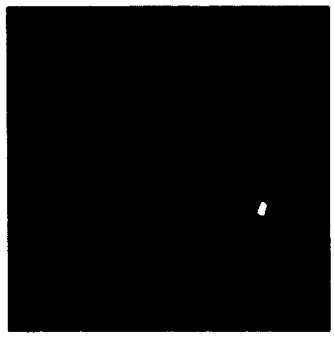
AS10-34-5095

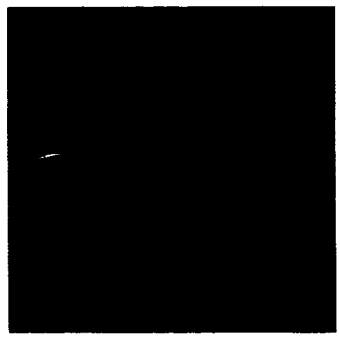
AS10-34-5096

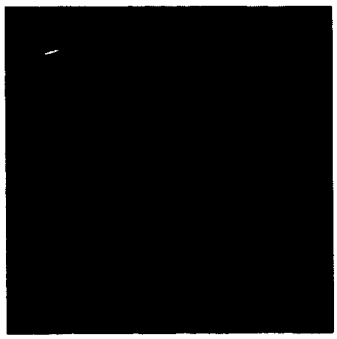
AS10-34-5097

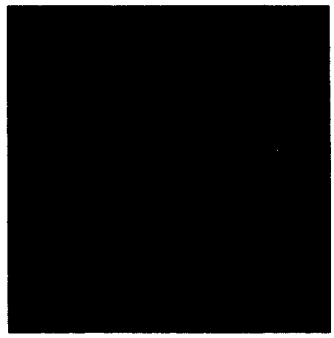
AS10-34-5098

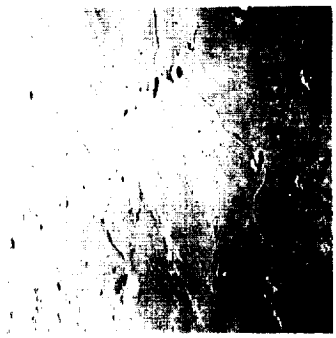
AS10-34-5099

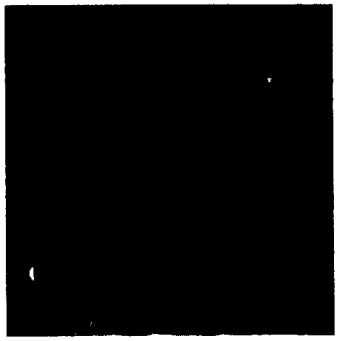
AS10-34-5100


AS10-34-5101


AS10-34-5102

(Available in color.)

AS10-34-5103

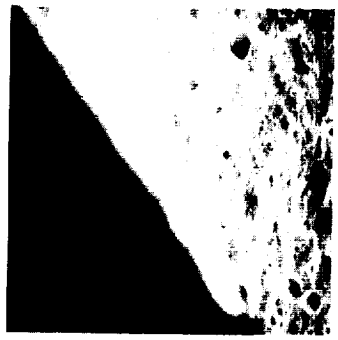

AS10-34-5104

AS10-34-5105

AS10-34-5106

AS10-34-5107

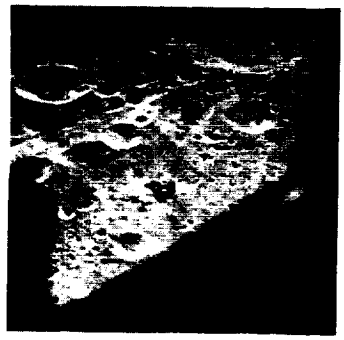

AS10-34-5108

AS10-34-5109

AS10-34-5110

AS10-34-5111

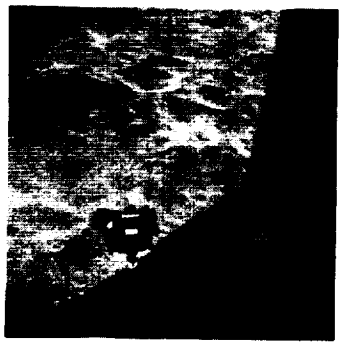

AS10-34-5112

AS10-34-5113

AS10-34-5114

AS10-34-5115

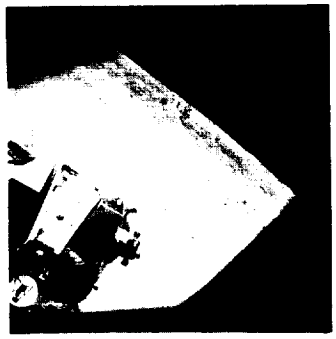

AS10-34-5116

AS10-34-5117

AS10-34-5118

AS10-34-5119

AS10-34-5120

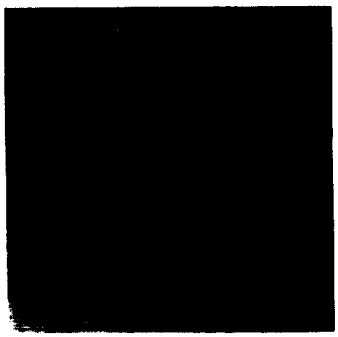

AS10-34-5121

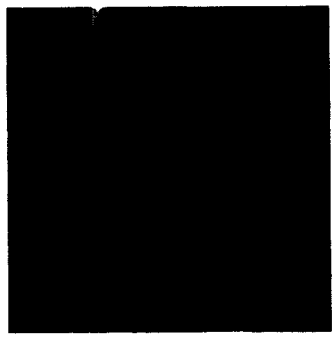

AS10-34-5122

AS10-34-5123

AS10-34-5124

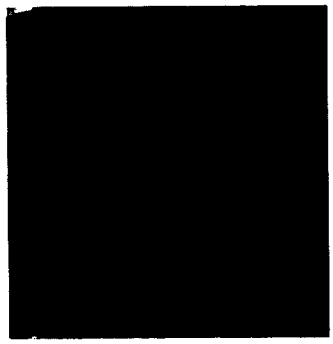

AS10-34-5125

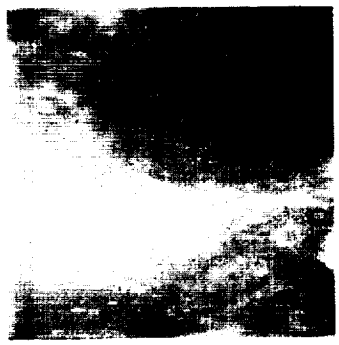

AS10-34-5126

(Available in color.)


AS10-34-5127


AS10-34-5128


AS10-34-5129

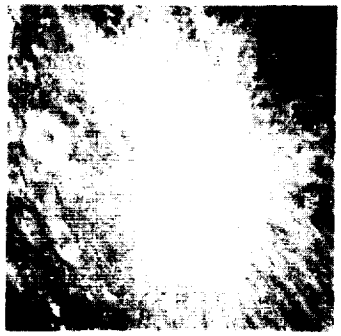
AS10-34-5130


AS10-34-5131

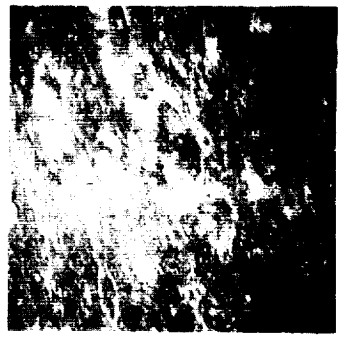
AS10-34-5132


AS10-34-5133


AS10-34-5134


AS10-34-5135

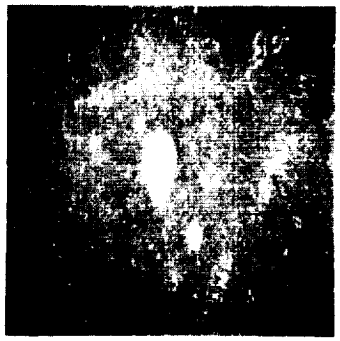
AS10-34-5136


AS10-34-5137


AS10-34-5138

(Available in color.)


AS10-34-5139


AS10-34-5140


AS10-34-5141

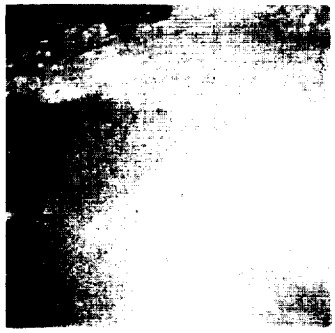
AS10-34-5142


AS10-34-5143


AS10-34-5144

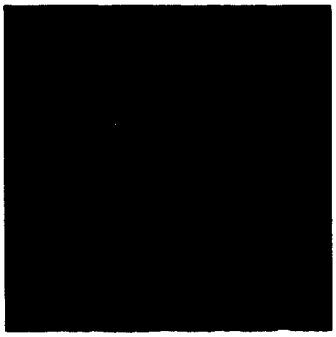
AS10-34-5145

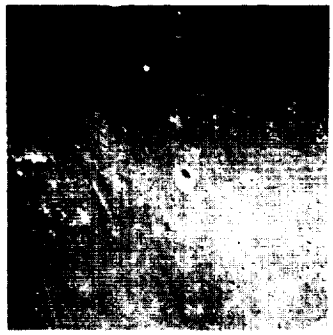
AS10-34-5146


AS10-34-5147

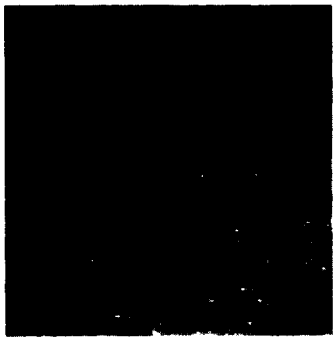
AS10-34-5148

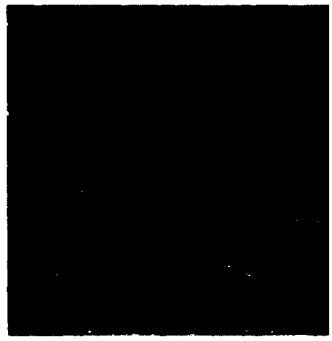
AS10-34-5149


AS10-34-5150

(Available in color.)

AS10-34-5151

AS10-34-5152

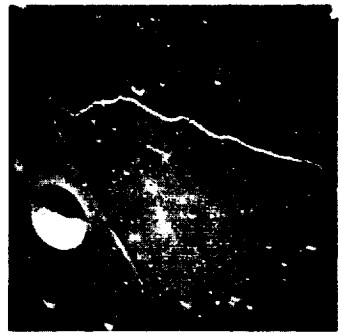

AS10-34-5153

AS10-34-5154

AS10-34-5155

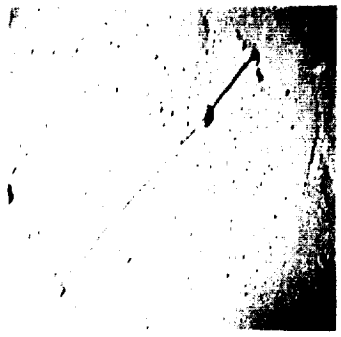

AS10-34-5156

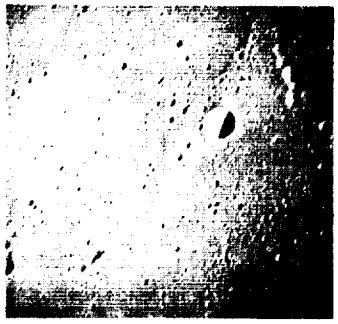

AS10-34-5157

AS10-34-5158

AS10-34-5159

AS10-34-5160

AS10-34-5161

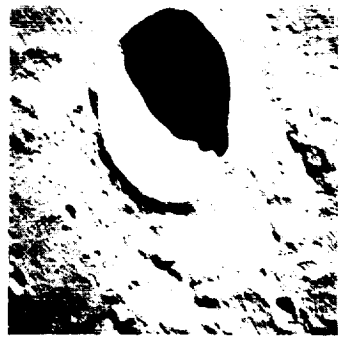

AS10-34-5162

(Available in color.)

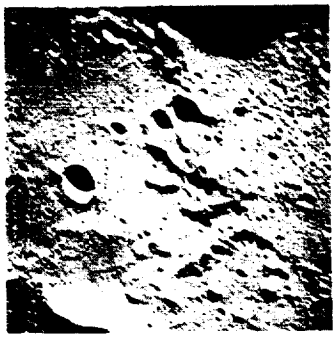
AS10-34-5163

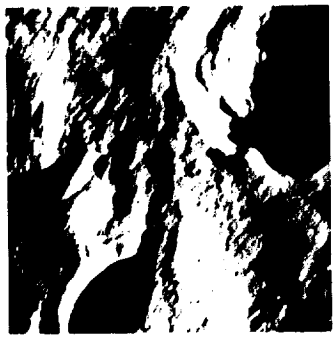
AS10-34-5164


AS10-34-5165

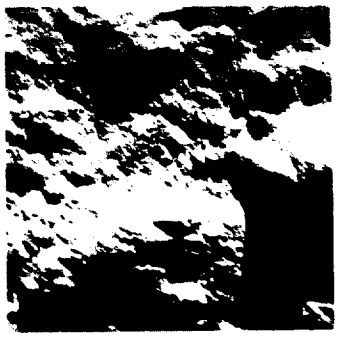
AS10-34-5166

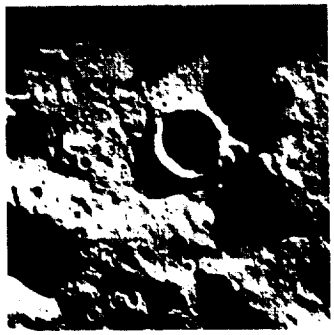
AS10-34-5167


AS10-34-5168

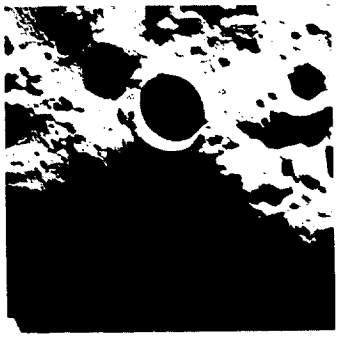
AS10-34-5169


AS10-34-5170

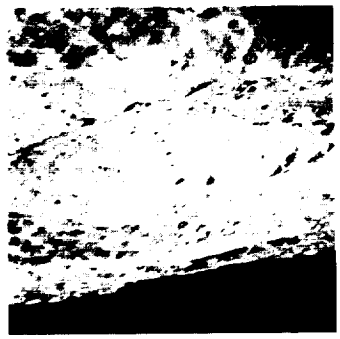
AS10-34-5171

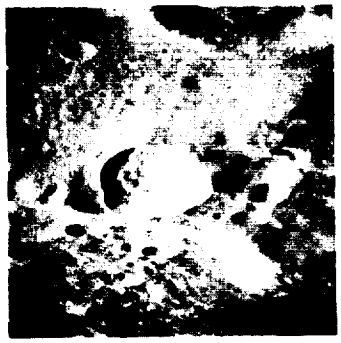
AS10-34-5172

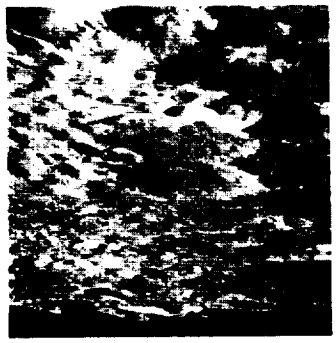
AS10-34-5173

(Available in color.)